DYSREGULATED PATHWAYS IN SPINOCEREBELLAR ATAXIA TYPE 2 AND ATAXIA TELANGECTASIA

DISSERTATION
ZUR ERLANGUNG DES DOKTORGRADES
DER NATURWISSENSCHAFTEN

VORGELEGT BEIM FACHBEREICH BIOWISSENSCHAFTEN
DER JOHANN WOLFGANG GOETHE -UNIVERSITÄT
IN FRANKFURT AM MAIN

VON JÚLIA CANET-PONS
AUS CIUTADELLA DE MENORCA

FRANKFURT AM MAIN, 2019
(D30)

Vom Fachbereich Biowissenschaften (15) der Johann Wolfgang Goethe Universität als Dissertation angenommen.

Dekan: Prof. Dr. rer. nat. Sven Klimpel

Gutachter: Prof. Dr. rer. nat. Amparo Acker-Palmer

Prof. Dr. med. Georg Auburger

Datum der Disputation: 11 Dezember 2019

Nothing in Biology makes sense except in the light of evolution

Theodosius Dobzhansky, 1973

Table of contents

1 INTRODUCTION

1.1 Degeneration of the cerebellum: cerebellar ataxias

Cerebellar ataxias are a group of neurodegenerative disorders primarily affecting the cerebellum in addition to other areas such as the basal ganglia and cerebral cortex. Imbalance and coordination problems are broader symptoms exhibited by patients (Akbar & Ashizawa 2015). There is currently no cure for ataxias and although mutations in several genes have been identified as causative, there is a lack of understanding of why some neurons are more sensitive than others. For example affecting more severely the cerebellum over other areas of the central nervous system (CNS).

Deciphering the mechanisms through which certain neuron populations are affected is important for not only understanding ataxias, but also neurodegenerative disorders in general. A lot of effort has been dedicated to elucidating pathological mechanisms with little success in understanding and developing treatment for this type of diseases. Continued research into the most fundamental neurological, genetic, and molecular mechanisms is crucial given the debilitating and life-shortening nature of neurodegenerative disorders.

1.2 The cerebellum

The cerebellum (CB) is a well-organized, evolutionary conserved structure that controls smooth and skillful movements, and is involved in higher cognitive and emotional functions(Lee et al 2015, Rodriguez et al 2005). Functional and anatomical abnormalities of the cerebellum have been linked to psychological disorders like autism (Sathyanesan et al 2019), while pathological defects, such as spinocerebellar ataxias, cause abnormal motor coordination (Zoghbi 2000).

The different neuronal types in the CB are classified based on their excitatory or inhibitory function. The excitatory glutamatergic neurons are the granule cells (GC), unipolar brush cells, and the deep cerebellar neurons. The inhibitory

GABAergic neurons, which use γ-aminobutyric acid or glycine as neurotransmitters, are Purkinje neurons (PN), Golgi cells, stellate cells, and basket cells.

There are two major afferent fibers to the cerebellum; climbing fibers that originate from the inferior olive, and the mossy fibers that originate from the pontine nuclei, spinal cord, and vestibular system (Figure 1.1).

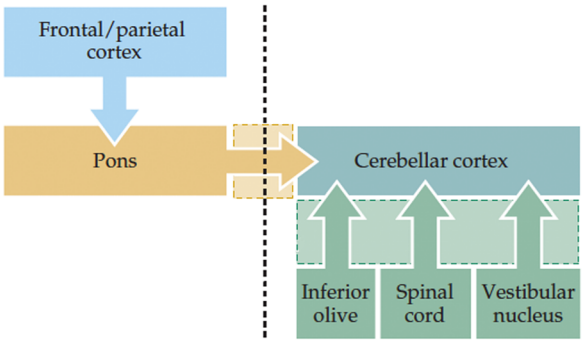

Figure 1.1. Diagram of the major inputs to the cerebellum. Modified from (Purves 2004).

Mossy fibers form synapses on the GC layer. GC have specialized axons called parallel fibers, which ascend to the molecular layer and make excitatory synapses onto the distal domain of the dendritic tree of the PN. In contrast, climbing fibers innervate the proximal domain of PN dendrites (Figure 1.2). Therefore, PN are the final destination of the afferent pathways to the CB (Purves 2004), receiving numerous inputs from parallel fibers and input from a single climbing fiber.

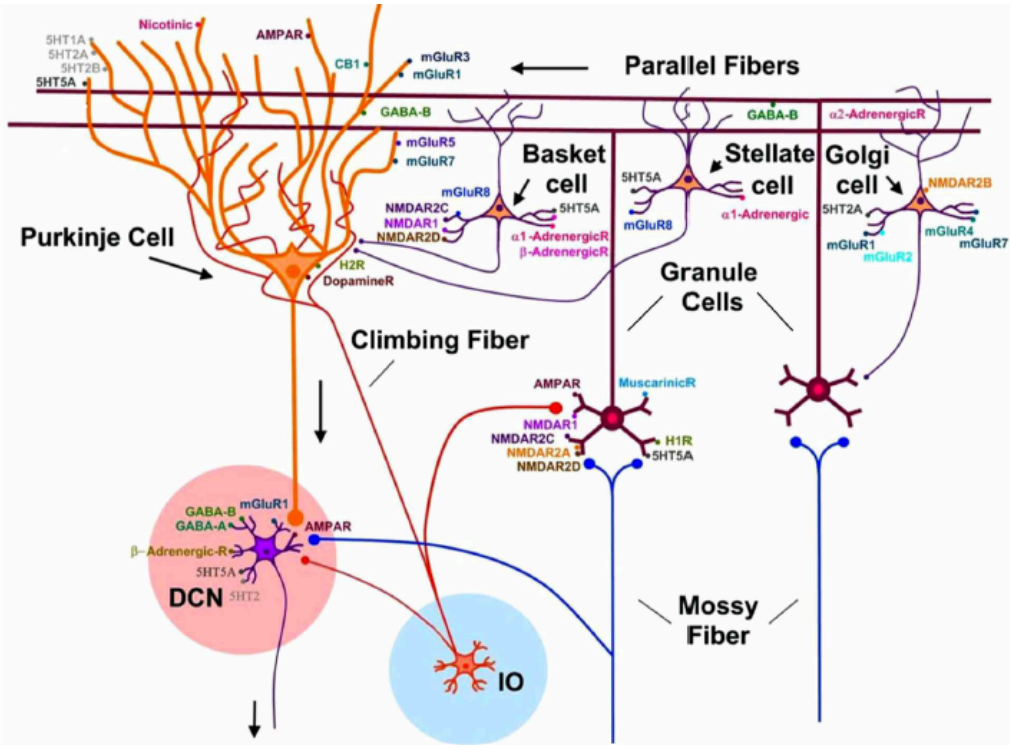

Figure 1.2. Representation of connectivity of cerebellar neurons and expression of receptors. Two categories of inputs reach the cerebellar cortex: (1) the mossy fibers targeting granule cells and cerebellar nuclei (DCN), and (2) the climbing fibers originating from the inferior olivary complex (IO) and projecting to cerebellar nuclei and Purkinje neurons. Granule cells give rise to parallel fibers, which make numerous synapses with dendritic spines of Purkinje cells. Inhibitory interneurons of the cerebellar cortex include basket cells, stellate cells and Golgi cells (Marmolino & Manto 2010).

Purkinje neurons are the sole output of the cerebellar cortex projecting to the deep cerebellar nuclei, being wholly inhibitory. Deep cerebellar nuclei also receive excitatory input from collaterals of mossy and climbing fibers (Figure 1.2), therefore the inhibitory output of PN serves to modulate the level of this excitation.

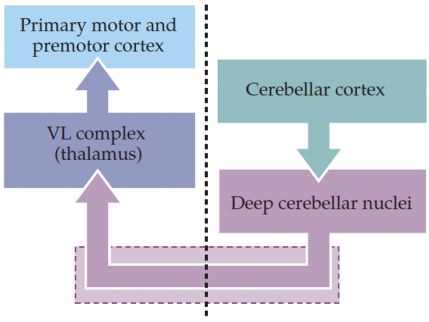

Figure 1.3. Functional organization of the outputs from the cerebellum to the cerebral cortex. The axons of the deep cerebellar nuclei cross in the midbrain before reaching the thalamus. Modified from (Purves 2004).

The deep cerebellar nuclei projects to the thalamic nuclei, which directly projects to the primary motor and premotor cortices. The cerebellum signals to the upper motor neurons to coordinate voluntary movements through this pathway.

1.3 Classification of cerebellar ataxias

Cerebellar ataxias can be acquired, inherited or sporadic (without defined genetic cause or acquired etiology). Common causes of acquired ataxias are a result of vascular insults, tumors, traumas, or demyelinating diseases like multiple sclerosis. Inherited ataxias, those with a defined genetic cause, can be classified in four different categories: dominant ataxias, recessive ataxias, mitochondrial ataxias, and X-linked ataxias (Figure 1.4).

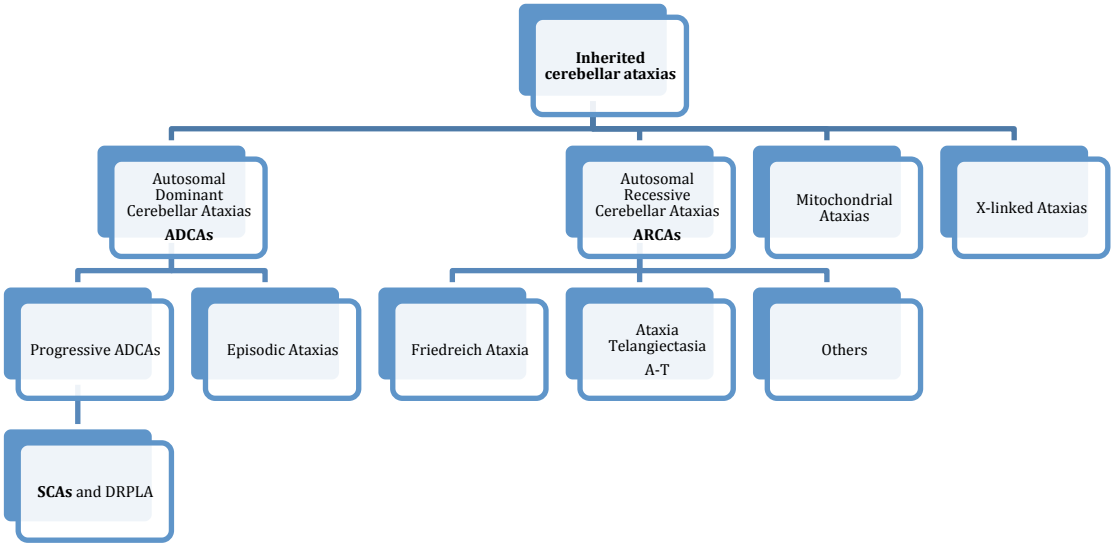

Figure 1.4 Classification of the inherited cerebellar ataxias. They can be divided into autosomal dominant, recessive dominant, X-linked, and mitochondrial ataxias. The most common autosomal dominant ataxias are the Spinocerebellar ataxias (SCAs). DRPLA stands for Dentatorubral-pallidoluysian atrophy.

1.4 Autosomal dominant cerebellar ataxias

Autosomal dominant cerebellar ataxias (ADCAs) are a type of dominantly inherited ataxias that develop during adulthood. There are three types of ADCAs: Spinocerebellar ataxias (SCAs), Denatorubral-pallidoluysian atrophy (DRPLA), and episodic autosomal dominant ataxias. Once symptoms appear they worsen over time with the exception of episodic ataxias.

1.4.1 Spinocerebellar ataxias

Spinocerebellar ataxias (SCAs) are a group of neurodegenerative disorders causing motor deficits due to cerebellar dysfunction. It is a group of genetically heterogeneous disorders and, so far, 48 different types have been described (Kuo 2019, Matilla-Duenas et al 2014). Despite the existence of so many genetic variations, patients show common symptoms of ataxic gait, poor coordination, speech and eye affected movements; all caused by pathological defects in the cerebellar circuits (Matilla-Duenas et al 2014). Cerebellar dysfunction results in an altered cerebellar output pointing to an impairment of the sole cerebellar output, the Purkinje neurons. This can be caused by the direct affection of the PN, by the alteration of the input that they are receiving, or by a combination of both. Disease onset is usually between 30 and 50 years of age, although early onset in childhood (Mao et al 2002) and onset after 60 years of age have been reported (Duenas et al 2006). Nine SCA subtypes, including SCA 1, 2, 3, 6, 7, 8, 10, 17 and DRPLA, are associated with repeat expansion sequences in coding regions (Table 1.1).

SCA subtype	Protein	Expansion	Reference
SCA 1	Ataxin 1	CAG	(Orr et al 1993)
SCA 2	Ataxin 2	CAG	(Imbert et al 1996, Pulst et al 1996, Sanpei et al 1996)
SCA 3	Ataxin 3	CAG	(Kawaguchi et al 1994)
SCA 6	CACNA1A[a]	CAG	(Zhuchenko et al 1997)
SCA 7	Ataxin 7	CAG	(David et al 1997)
SCA8	ATXN8[b] and ATXN8OS[c]	CTG	(Ikeda et al 2008, Koob et al 1999)
SCA10	Ataxin 10	ATTCT	(Grewal et al 1998, Zu et al 1999)
SCA 17	TATA box binding protein	CAG	(Nakamura et al 2001)
DRPLA	Atrophin 1	CAG	(Koide et al 1994)

Table 1.1. Summary of SCAs and DRPLA caused by CAG expansion sequences in coding regions. [a]CACNA1A stands for 1A-voltage-dependent calcium channel. [b]ATXN8 stands for Ataxin 8. [c]ATXN8OS stands for Ataxin 8 Opposite Strand.

Seven of the previous disorders are caused by exonic CAG repeats (coding for glutamine) and are referred to as polyglutamine (polyQ) disorders (SCA 1,2,3, 6,17 and DRPLA). These SCAs show common features like progressive

neurodegeneration of distinct brain areas, and formation of nuclear or cytoplasmic poly-glutamine-containing protein aggregates (Zoghbi & Orr 2000). However affected proteins do not share similar structure or motif homologies. Moreover, the critical length of the CAG repeats varies among them.

Two other neurological disorders that are part of the polyQ disorders are Huntington's disease (HD) (Walker et al 1981) and Spinal and bulbar muscular atrophy (SBMA) (La Spada et al 1991), caused by mutations in the protein huntingtin (HTT) and the androgen receptor (AR) respectively.

1.4.2 Spinocerebellar ataxia type 2

Spinocerebellar ataxia type 2 (SCA2) is caused by repeat expansion mutations in the *ATXN2* gene, which encodes the protein Ataxin2 (ATXN2) (Table 1.1). Three independent labs identified the genetic cause of SCA2 in 1996 (Imbert et al 1996, Pulst et al 1996, Sanpei et al 1996). A polyglutamine (polyQ) tract consisting of CAG repeats interrupted by CAA was identified at exon 1 of *ATXN2*. Healthy individuals have between 22 and 23 glutamines (Qs), with a sequence of $(CAG)_8CAA(CAG)_4CAA(CAG)_8$, while expansions longer than 33 CAG repeats cause SCA2 (Fernandez et al 2000). A strong correlation between age of onset and CAG repeat length has been described (Figure 1.5) (Pulst et al 2005, Velazquez-Perez et al 2014). Moreover, CAG repeat length in other polyQ proteins like CACNA1A and ATXN7 affects SCA2 onset (Pulst et al 2005, Tezenas du Montcel et al 2014). Intermediate expansions of the polyQ tract have been associated with autosomal-dominant Parkinson's disease (PD) (Gwinn-Hardy et al 2000, Sen et al 2016) and expansions between 27-33 Qs were linked to amyotrophic lateral sclerosis (ALS) (Elden et al 2010, Gispert et al 2012, Ross et al 2011).

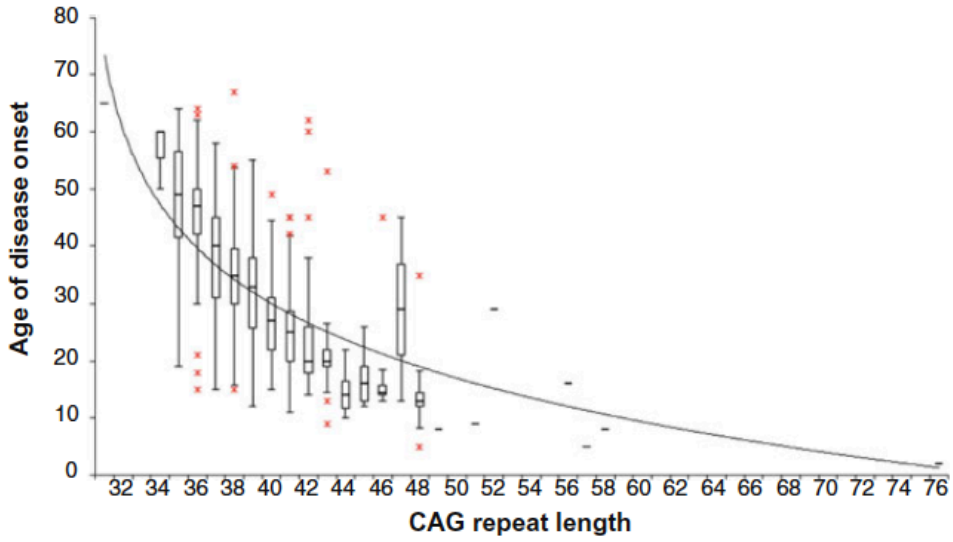

Figure 1.5. Age at onset and CAG repeat length are inversely related. SCA2 age of onset is negatively correlated with *ATXN2* CAG repeat length (Pulst et al 2005).

The most noticeable symptom that SCA2 patients show is ataxic gait; however they also show cerebellar dysarthria, dysdiadochokinesia, and ocular dysmetria caused by the progressive cerebellar degeneration. Slow or absent saccade velocity is one predominant ocular symptom from SCA2 patients due to degeneration of the oculomotor brainstem. Apart from the cerebellar and oculomotor symptoms, patients also suffer from areflexia of the upper and lower limbs (peripheral neuropathy) and some cases show fasciculations and amyotrophy (involvement of motor neurons) (Auburger 2012, Lastres-Becker et al 2008b, Velazquez-Perez et al 2011). Histological analysis of *post-mortem* samples from SCA2 patients showed a general reduction of the brain size with significant atrophy of the cerebellum, brainstem, and frontal lobe. A reduction of the cerebral and cerebellar white matter was also detected (Estrada et al 1999). Further studies of spinal cord samples showed severe and widespread neurodegeneration of the central somatosensory system (Rub et al 2007).

1.4.3 Ataxin 2

Ataxin 2 (ATXN2) is an evolutionary conserved RNA binding protein (RBP) (Jiménez-López & Guzmán 2014). All vertebrates, except birds, have two ATNX2 homologs (ATXN2 and ATXN2-like), probably generated by gene duplication (Zu et al 1999). ATXN2 is a member of the Like-Sm (LSm) protein family, having RNA processing and metabolism roles (Tharun 2009, Wilusz & Wilusz 2005).

Figure 1.6. Structure of ATXN2 and its conserved domains in *Mus musculus* and *Homo sapiens*. ATSS stands for alternative translational start site. Modified from Ostrowski et al 2017.

Downstream of the polyQ tract, at the N-terminal region, ATXN2 presents an LSm domain and an LSm-associated domain (LSmAD) (Figure 1.6) responsible for its physical interaction with RNAs (Yokoshi et al 2014). Moreover, the LSm and LSm-AD domains are sufficient to interact with DDX6 and LSM12 and carry ATXN2 posttranscriptional activity (Lee et al 2017, Nonhoff et al 2007). Towards the C-terminal there are two more conserved domains, a proline-rich domain and a PAM2 domain (Figure 1.6), mediating the interaction with poly(A)-binding protein 1 (PABP1) (Kozlov et al 2010, Mangus et al 1998). PABP1 is an RBP important for poly-A tailing, translation, and mRNA decay (Xie et al 2014). The proline-rich domain has been described to mediate the association of ATXN2 with the receptor endocytosis apparatus and influence the trophic state of the cells (Drost et al 2013, Nonis et al 2008).

1.4.4 Molecular functions of Ataxin2: RNA metabolism

ATXN2 has been linked to several RNA processing roles based on experimental studies in *Saccharomyces cerevisiae* (yeast), *Caenorhabditis elegans* (worms), *Drosophila melanogaster* (flies), mouse models and humans.

As previously mentioned, ATXN2 interacts with PABP1 through its PAM2 domain. Based on studies with *S. cerevisiae*, PBP1 (Pab1-binding protein 1; ATXN2 ortholog in yeast) promotes mRNA stability and protein production influencing RNA polyadenylation (Mangus et al 1998, Ralser et al 2005). Although the 3' end of pre-mRNA were found to be properly cleaved, Pbp1 knock-out yeast cells show shorten polyadenylated (poly(A)) tails (Mangus et al 1998). Moreover, ATXN2 can bind to uridine-rich elements (AU-rich element,

ARE) at the 3'UTRs of its mRNA targets through the LSm domain, thereby stabilizing the mRNA targets (Yokoshi et al 2014). Based on PAR-CLIP (photoactivatable-ribonucleoside-enhanced crosslinking and immunoprecipitation) experiments, ATXN2 was found to up-regulate proteins involved in RNA splicing, polyadenylation and 3' end processing (Yokoshi et al 2014). In the same publication, the authors showed how the deletion of the polyQ domain affected ATXN2 role in mRNA stabilization while the absence of the PAM2 domain did not alter its role significantly (Yokoshi et al 2014). Furthermore, the *Atxn2*-KO mouse model showed a global reduction in protein synthesis, supporting the role of ATXN2 in general translation (Fittschen et al 2015). In *C. elegans* experiments, the ATXN2 ortholog ATX2, was shown to play a role in regulation of translation (Ciosk et al 2004). The ATX2 loss elevated the protein levels of GLD1 (defective in germ line development; ortholog of human QKI) and MEX3 (muscle Excess; ortholog of human MEX3B) without affecting their mRNA level, both of them containing KH-domains (RNA recognition domain). Through studies in *D. melanogaster*, dATX2 (ATXN2 ortholog in flies) was shown to be necessary for regulating synapse-specific plasticity via microRNA-mediated translational repression (McCann et al 2011, Sudhakaran et al 2014). Human ATXN2 and dATX2 had been shown to physically assemble with polyribosomes being part of the messenger ribonucleoproetien (mRNP) complexes (Satterfield & Pallanck 2006). The domains responsible for direct assembly with polyribosomes are the Lsm and LsmAD. The PAM2 domain in dATX2 was shown to be necessary to bind to polysome-bound dPABP1 in *D. melanogaster* (Satterfield & Pallanck 2006). Based on all these data, the promotion of RNA stability and translation by Ataxin2 seems to be evolutionarily conserved among species.

In periods of cellular stress such as a decreasing source of energy, the translation has to be stalled until favourable conditions return. Stress granules (SG) and processing bodies (P-bodies) are two distinct conserved cytoplasmic mRNP (messenger ribonucleoproteins) granules rich in untranslating mRNA (Buchan & Parker 2009, Kedersha et al 2013). SG contain mRNA stalled at the translation initiation step, 40S ribosomal subunits, various translation initiation factors,

RBPs, and many non-RNA-binding proteins (Buchan & Parker 2009, Jain et al 2016, Protter & Parker 2016). SG are formed as a response to cellular stress when the translation initiation is inhibited (Anderson & Kedersha 2009). On the contrary, P-bodies contain mRNA associated with translational repressors and the mRNA decay machinery. These mRNAs can be targeted for decapping and degradation (Aizer et al 2014, Parker & Sheth 2007). SG and P-bodies are dynamic structures that can exchange components and are functionally linked (Buchan & Parker 2009, Kedersha et al 2005) (Figure 1.7).

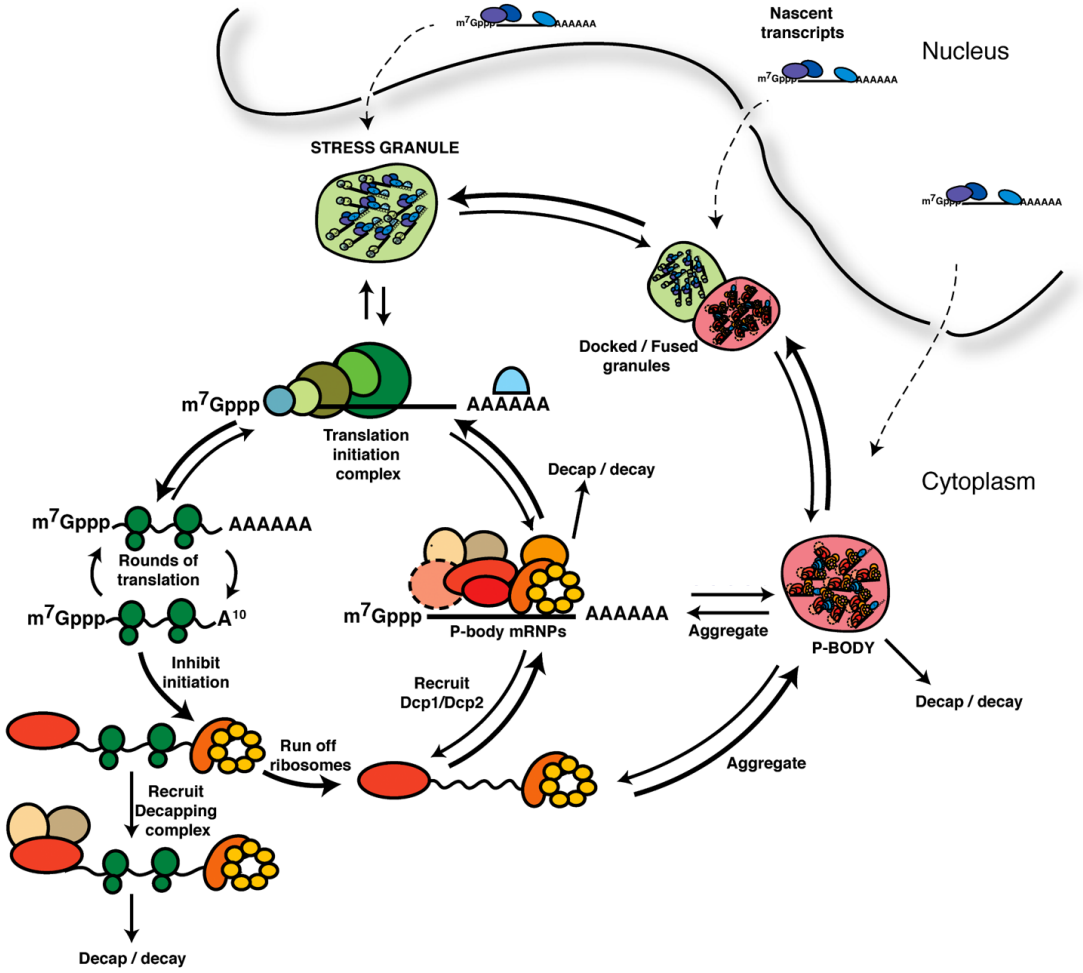

Figure 1.7. Model integrating Stress Granules and P-bodies into an mRNP cycle. Proposed model for mRNP transitions, particularly during stress. Dashed arrows indicate possible destination of exported nascent transcripts. Modified from Buchan & Parker 2009.

An increasing number of RBPs have been described to localize in SG and/or P-bodies (Nunes et al 2019) one of them being ATXN2. There is extensive evidence that ATXN2 acts as a stress response factor in different models (Nonhoff et al 2007, Ralser et al 2005) localizing to SG together with other RBPs, such as

PABP1 and TIA1 (Kedersha et al 1999, Ralser et al 2005, Swisher & Parker 2010). Nonhoff and colleagues showed that the absence of ATXN2 leads to an impairment of SG formation and a higher level of PABP1 (a key protein in mRNA translation and stability) while P-bodies are not affected. In contrast, overexpression of ATXN2 leads to a reduced number of P-bodies, no effect on SG assembly, and lower levels of PABP1 (Nonhoff et al 2007). The effect of reduced numbers of P-bodies in the presence of high levels of ATXN2 seems to be mediated by the Lsm and LsmAD domains interacting with the conserved DEAD/H-box RNA helicase DDX6, an important component of P-bodies involved in mRNA decay (Coller et al 2001, Cougot et al 2004, Fischer & Weis 2002). Therefore, ATXN2 and its ortholog seem to act as stress response factors promoting the assembly of SG formation and influencing components of the P-bodies. Since ATXN2 levels are altered in a number of diseases such as neurodegenerative disorders and cancer, its dysregulation might contribute to the disruption of mRNP granules underling some of these pathologies.

1.4.5 Physiological functions of Ataxin2: metabolism and circadian rhythm

Ataxin2 has been implicated in numerous physiological processes such as embryonic development (Kiehl et al 2000), apoptosis (Wiedemeyer et al 2003), cellular proliferation (Drost et al 2013), and various metabolic processes (Carmo-Silva et al 2017). Its role in these processes may be a result of its molecular functions, for example through stabilizing some of its mRNA targets.

Increase in body weight, insulin sensitivity, and reduced fertility were reported from the two *Atxn2*-KO mouse mutants (Kiehl et al 2006, Lastres-Becker et al 2008a). A similar effect in body weight and growth increase was observed in *C. elegans* when Atx2 was knocked-down (Bar et al 2016). In contrast, the A*txn2*-CAG42 and BAC-72 SCA2 mouse models (described in the *Mouse models of SCA2* section) showed reduced body weight compared to wild-type (WT) mice (Damrath et al 2012, Dansithong et al 2015). Moreover, the *Atxn2*-KO mice showed dyslipidemia, increased serum cholesterol levels, and down-regulation of ACADS (acetyl-CoA dehydrogenase, implicated in fatty acid β-oxidation),

suggesting that the absence of *Atxn2* leads to a lipid metabolism dysregulation (Lastres-Becker et al 2008a, Meierhofer et al 2016). Several studies in SCA2 patients corroborate the lipid pathology including apolipoproteins C-II and C-III down-regulation (Abdel-Aleem & Zaki 2008, Dominiczak & Caslake 2011, Swarup et al 2013).

The mTOR (mammalian target of rapamycin protein kinase) signaling cascade is the best-described pathway for nutrient sensing in the cell. There are two different mTOR complexes: complex 1 and complex 2 (mTORC1/2) (Wullschleger et al 2006). Evidence points to a conserved inhibition of mTOR by ATXN2 (Bar et al 2016, DeMille et al 2015, DeMille et al 2014, Lastres-Becker et al 2016, Takahara & Maeda 2012). During heat stress, which promotes the formation of SG, TORC1 is inhibited via sequestration within SG in yeast. The same happens when overexpressing *PBP1* (ATXN2 ortholog in yeast); TORC1 activity is reduced, and both PBP1 and TORC1 localize into SG (Takahara & Maeda 2012). Further experiments in yeast showed that a signaling cascade up-stream of TORC1, including nutrient-sensing kinases AMPK/SNF1 and PSK1 (yeast ortholog of PAS kinase), is implicated in the PBP1-dependent inhibition of TORC1 (DeMille et al 2014). Adverse growth conditions in yeast promote the phosphorylation of PSK1 by AMPK/SNF1, which then enhances TORC1 sequestration via PBP1 (DeMille et al 2015). In addition, MEFs (mouse embryonic fibroblasts) from *Atxn2*-KO mice exhibited increased phosphorylation of RPS6 (ribosomal protein 6) and 4E-BP (eukaryotic initiation factor 4E-binding protein), both of which are substrates of the mTORC1 complex (Lastres-Becker et al 2016). Mice lacking RPS6 and 4E-BP show hypoinsulinemia, glucose intolerance, and reduction of adipose tissue (Ruvinsky et al 2005, Tsukiyama-Kohara et al 2001). Experiments in the SH-SY5Y neuroblastoma cell line showed how under starvation and in the presence of rapamycin (mTOR inhibitor), *ATXN2* mRNA levels are increased (Lastres-Becker et al 2016). These suggest that ATXN2 could act as a metabolic sensor either directly or through SG modulating the mTOR pathway (Figure 1.8).

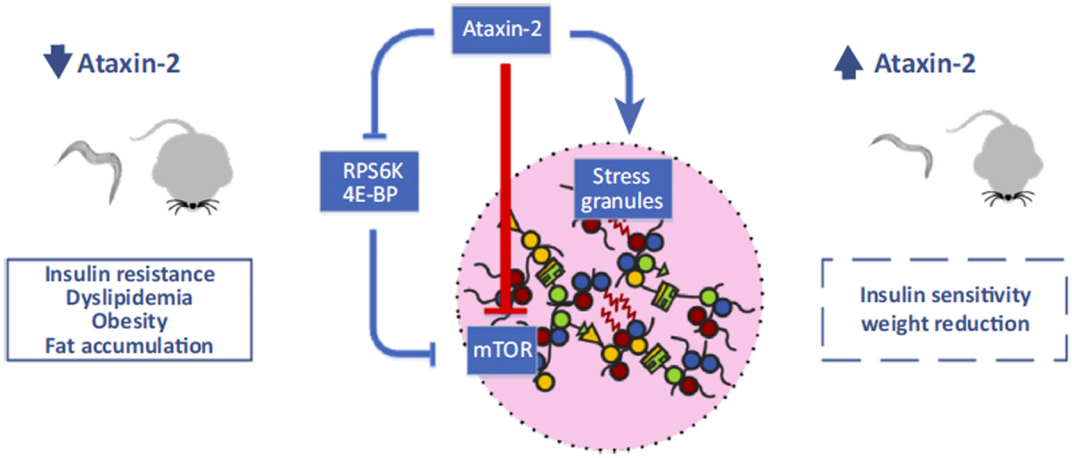

Figure 1.8. Ataxin2 as a metabolic modulator. Ataxin2 deficiency has been linked to metabolic dysfunction in mice and worms leading to fat accumulation and obesity. ATXN2 has been reported to modulate mTOR pathway. ATXN2 is influenced by nutritional status of the cell and could be blocking mTOR via promoting reduced phosphorylation of RPS6 (ribosomal protein S6) and 4E-BP (eukaryotic initiation factor 4E-binding protein). On the other hand, mTOR RNA may be sequestered into SG blocking its translation. As a consequence, an up-regulation of ATXN2 might be the cause of weight reduction in SCA2 patients through mTOR pathway (Carmo-Silva et al 2017).

Ataxin2 also plays a role in the function of the circadian clock; it modulates the expression of intrinsic timekeepers genes that oscillate through a 24 hour light-dark period determining the timing for functions such as behaviour and photosynthesis (Salmela & Weinig 2019). Circadian rhythm is important to maintain optimal functions in organisms: circadian sleep-wake disruptions or chronic alterations often lead to psychiatric and neurodegenerative disorders (Wahl et al 2019). Two independent groups showed the requirement of dATXN2 for Period mRNA translation (Lim & Allada 2013, Zhang et al 2013b). Period (dPER in flies) is a key component of the circadian pacemaker in *Drosophila* which is regulated at multiple levels (Kozlov & Nagoshi 2019). Lower levels of dPER were detected when *dAtxn2* was knocked-down causing longer period of constant darkness behaviour in the flies (Lim & Allada 2013, Zhang et al 2013b). *Atxn2*-KO mice showed longer period of re-adjusting after transient dysregulation of the circadian cycle compared to WT, although no effects on PER (PER1 and PER2) expression levels were detected (Pfeffer et al 2017). Moreover, SCA2 patients suffer from sleep disorders and disturbed REM (rapid eye movement) sleep, regulated by the circadian clock, which can be detected before

the onset of ataxia symptoms (Lastres-Becker et al 2008b, Tuin et al 2006, Velazquez-Perez et al 2011).

1.4.6 Ataxin2 role in other neurodegenerative disorders: Amyotrophic lateral sclerosis

ALS is a fatal neurodegenerative disease where the motor neurons in the brain and spinal cord degenerate. Only 10% of ALS cases are genetically transmitted, with high penetrance (Taylor et al 2016). *SOD1* (superoxide dismutase) was the first ALS gene identified (Rosen et al 1993) and since then more than 50 potential ALS genes have been published. ATXN2 has been shown to interact with some of these gene products such as C9ORF72 (chromosome 9 open reading frame 72), FUS (fused in sarcoma), and TDP43 (TAR DNA-binding protein 43) (Vucic et al 2014).

Heterozygous hexanucleotide expanded repeat (HRE) mutations located in the intronic region between exons 1a and 1b of the C9ORF72 gene were identified as a genetic cause in families with autosomal dominant frontotemporal dementia (FTD) and/or ALS (DeJesus-Hernandez et al 2011, Renton et al 2011). The function of the C9ORF72 gene product is unknown but so far it is the most commonly affected gene in familial ALS and FTD. Studies in French and Indian cohorts showed co-occurrence for ATXN2 intermediate poly(Q) expansions and C9ORF72 HRE in both ALS and FTD-ALS patients (Lattante et al 2014, Narain et al 2017). At the molecular level, loss of C9ORF72 function dysregulates autophagy in animal and cellular models (Ji et al 2017, Ugolino et al 2016) and it synergizes with intermediate poly(Q) expanded ATXN2 (Ciura et al 2016, Sellier et al 2016). Sellier *et al* showed how the motor neuron dysfunction and neuronal cell death was more significant in C9ORF72 deficiency together with ALS-linked expanded ATXN2 rather than only loss of C9ORF72 (Sellier et al 2016). Moreover, ATXN2 has been linked to cell death and SCA2-poly(Q) expansion caused apoptosis and caspase-3 activation in primate and rat cell lines (Huynh et al 2003).

Fused in sarcoma (FUS) is a nucleoprotein involved in DNA and RNA metabolism such as DNA repair, RNA splicing, and export to the cytoplasm. FUS gene was identified in 1993 as part of a fusion gene with the transcript factor gene CHOP

in tumor tissue from liposarcoma (Rabbitts et al 1993). Later on, several mutations in FUS were linked to ALS (Corrado et al 2010, Kwiatkowski et al 2009, Vance et al 2009). Intermediate poly(Q) expansions in ATXN2 were shown to interact with *wildtype* FUS, and more strongly with FUS containing R521C (arginine 521 to cysteine) or R521H (arginine 521 to histidine) mutations (Farg et al 2013). This interaction increased cytoplasmic FUS levels, ER stress, Golgi fragmentation, and apoptosis (Farg et al 2013). FUS with ALS-linked mutations were found to localize in cytoplasmic SG and interact with PABPC1 in an RNA-dependent manner while *wildtype* FUS was not detected (Vance et al 2013).

TAR DNA-binding protein 43 (TDP43) is an RNA/DNA-binding protein with important roles in RNA processing and metabolism. TDP43 is able to shuttle between the nuclei and the cytoplasm and during cellular stress localizes in SG (Birsa et al 2019). Several dominant mutations in the TDP43 gene have been linked to ALS (Buratti & Baralle 2010), potentially leading to an abnormal accumulation of TDP43 forming pathologic cytoplasmic inclusions (Neumann et al 2006). These inclusions were found to contain a hyperphosphorylated, ubiquitinated, and cleaved form of TDP43 (pathologic TDP43) in neurons, and glia, from both ALS and FTLD patients (Arai et al 2006, Neumann et al 2006). Ataxin2 is a potent modifier of TDP43 toxicity based on animal and cellular models of ALS (Elden et al 2010). ATXN2 and TDP43 can interact in an RNA-dependent manner, and up-regulation of ATXN2 increases toxicity of TDP43 shortening the life span of flies and yeast models (Elden et al 2010). It was also shown how intermediate poly(Q) expansions enhanced the ATXN2 stability and promote its association with TDP43 (Elden et al 2010). In addition, ATXN2 has been involved in Caspase3 (CASP3) activation and increased cleavage of TDP43 leading to pathological accumulation of cleaved fragments (Hart & Gitler 2012). Hart *et al* showed a lower caspase activation threshold in presence of intermediate poly(Q) expansions in ATXN2, causing aberrant TDP43 cleavage leading to neuronal death (Hart & Gitler 2012). Recent research using TDP43 overexpression mice showed that reducing ATXN2 could rescue the mouse phenotype and extend their life span (Becker et al 2017).

Ataxin2 has also been implicated in other neurodegenerative disorders such as Parkinson's disease (Sen et al 2016), Spinocerebellar ataxia type 1 (Al-Ramahi et

al 2007, Lim et al 2006), and Machado-Joseph disease (also known as SCA3) (Ding et al 2016, Nobrega et al 2015).

1.4.7 Mouse models of SCA2

Until recently, five mouse models for SCA2 have been described; four of which are transgenic and only one *Knock-in* (KIN) (Alves-Cruzeiro et al 2016). The first model was reported in 2000 and this SCA2 mouse model overexpressed a full length cDNA of human *ATXN2* with 58 CAG repeats (Huynh et al 2000). The introduced cDNA is under control of the Pcp2 promoter (Purkinje cell protein 2) limiting the expression of the transgene to the PN. This model showed a late-onset progressive motor phenotype and, around 12 months of age, shrinkage of the molecular layer and reduction of calbindin staining. The next SCA2 mouse model generated was a transgenic overexpression line with the full-length human *ATXN2* gene without expansion, including the promoter region (Aguiar et al 2006). Compared to the previous mouse model, this model achieved ubiquitous expression of the transgene in the entire animal. In 2012, the first report of a KIN mouse model of SCA2 was published (Damrath et al 2012). This mutant mouse was generated via homologous recombination in embryonic stem cells in order to introduce 42 CAG repeats in the murine *Atxn2* gene, *Atxn2*-CAG42. A reduction in the weight of these animals compared to the *wild type* (WT) was detected starting at the age of 10 days and the locomotor behaviour characterization showed significant deficits on the accelerating rotarod at the age of 18 months. Following the same idea as the first mouse model described (Huynh et al 2000), the third transgenic SCA2 mouse model was generated introducing a longer CAG repeat expansion (127 CAGs) into the overexpressed human *ATXN2* cDNA under control of the Pcp2 promoter (Hansen et al 2013). They aimed to generate a model with a stronger phenotype and an earlier degenerative onset than the first model (with 58 CAG repeats). In 2015, Dansithong and colleagues generated the most recent transgenic mouse model of SCA2 (Dansithong et al 2015), the BAC-72Q. They used the bacterial artificial chromosomes (BACs) approach to overexpress the entire *ATXN2* human gene (with 72 CAG repeats) including introns and regulatory regions within the mouse genome. A total of four copies of the *ATXN2* transgene were integrated in

a tandem manner. The ATXN2-72CAG protein was detected in the CB, spinal cord, brain, heart, and liver of this mouse model.

Although the previously described mouse models have been highly relevant in the field of SCA2, there are some limitations. For example, the random integration of the BAC approach that could affect the endogenous expression of other genes or the fact that overexpression of Ataxin2 will mask the relevance of partial ATXN2 loss-of-function effects for the disease mechanisms. To overcome some of these limitations, we generated a new mouse model where 100 CAG repeats were introduced in the mouse *Atxn2* gene as previously described for the *Atxn2*-CAG42 (Damrath et al 2012), which showed ataxic phenotype at the old age of 18 months. Increasing the CAG expansion caused an early and more severe phenotype without the risk of affecting other gene expression, a limiting factor in the BAC-72Q, and without altering the expression pattern of the *Atxn2* gene (Sen et al 2019).

Two other important mouse mutants for the field are the two *Atxn2*-Knock-out mouse lines independently generated in Los Angeles and in Frankfurt (*Atxn2*-KO) (Kiehl et al 2006, Lastres-Becker et al 2008a). These two KO models have been useful to get a better understanding of the functions and pathways of ATXN2, like its role in insulin resistance and obesity (Auburger et al 2014), or translation rate (Fittschen et al 2015).

1.5 Autosomal Recessive Cerebellar Ataxias

Autosomal Recessive Cerebellar Ataxias (ARCAs) are autosomal recessive inherited disorders with an early onset typically occurring before the age of 20. ARCAs are characterized by degeneration or abnormal development of the cerebellum and spinal cord (Palau & Espinos 2006). Although there is not a unique classification for ARCAs, they can be divided into three categories based on their neuropathy characteristics: 1) cerebellar ataxias with predominant sensory neuronopathy (Table 1.2); 2) with sensorimotor axonal neuropathy (Table 1.3); and 3) without sensory neuropathy (Table 1.4) (Kuo 2019).

Disease	Gene mutated	Age of Onset	References
Friedreich ataxia	*FXN*	Childhood – 30s	(Chamberlain et al 1988)
SANDO[a]	*POLG*	20-60s	(Van Goethem et al 2003)

Table 1.2. Common causes of cerebellar ataxia with predominant sensory neuropathy. [a]SANDO stands for Sensory ataxic neuropathy, dysarthria, and ophthalmoparesis.

The most common recessive ataxia is Friedreich ataxia (FRDA) occurring in approximately 1 in 50.000 individuals. It is characterized by progressive gait and limb ataxia with limb muscle weakness, absence of lower limb reflexes, dysarthria, and decreased vibratory sense and proprioception (Delatycki et al 2000). FRDA is caused by a GAA trinucleotide repeat expansion in intron 1 of the Frataxin gene (*FXN*) (~98% of cases) or by point mutations (~2% of cases), leading to a reduction of FXN levels (Delatycki et al 1999, Lodi et al 1999).

Disease	Gene mutated	Age of Onset	References
A-T[a]	*ATM*	<5 years	(Gatti et al 1988)
AOA1[b]	*APTX*	<20 years	(Date et al 2001, Moreira et al 2001)
AOA2[c]	*SETX*	Childhood-30s	(Moreira et al 2004)
CTX[d]	*CYP27*	Childhood	(Cali et al 1991)

Table 1.3. Common causes of cerebellar ataxia with sensorimotor axonal neuropathy. [a]AOA1 stands for Ataxia with oculomotor apraxia type1. [b]AOA2 stands for Ataxia with oculomotor apraxia type 2. [c]CTX stands for Cerebrotendinous xanthomatosis

Disease	Gene mutated	Age of Onset	References
ARCA1/SCAR8[a]	*SYNE1*	20-30s	(Gros-Louis et al 2007)
ARCA2/SCAR9[b]	*ADCK3*	Childhood	(Lagier-Tourenne et al 2008, Mollet et al 2008)
NPC[c]	*NPC1* and *NPC2*	20-30s	(Carstea et al 1997, Naureckiene et al 2000)

Table 1.4. Common causes of cerebellar ataxia without sensory neuropathy. [a]ARCA1 stands for Autosomal recessive cerebellar ataxia type 1; SCAR8 stands for Spinocerebellar ataxia autosomal recessive type 8. [b]ARCA2 stands for Autosomal recessive cerebellar ataxia type 2; SCAR9 stands for Spinocerebellar ataxia autosomal recessive type 9. [c]NPC stands for Niemann-Pick disease type C.

1.5.1 Ataxia Telangiectasia

Ataxia-telangiectasia (A-T) is an autosomal recessive disorder with childhood onset. A-T patients show severe cerebellar atrophy manifesting as ataxia when the child starts to walk and symptoms generally plateau at 2 to 5 years of age

(Chun & Gatti 2004). Other movement symptoms are hypotonia, dystonia, myoclonus, choreoathetosis, tremor, and Parkinsonism (Boder & Sedgwick 1958, Meneret et al 2014, Nissenkorn & Ben-Zeev 2015, Perlman et al 2012, Shaikh et al 2013). A-T patients show systemic and neurological features like dilatation of blood vessels (telangiectasia), oculomotor apraxia (Nissenkorn & Ben-Zeev 2015), dysarthria (Lohmann et al 2015), axonal sensorimotor neuropathy (Woods & Taylor 1992), immune defects (Carbonari et al 1990), predisposition to malignancies (Bigbee et al 1989), and hypersensitivity to radiotherapy. Patients also show endocrine abnormalities including growth retardation, gonadal atrophy, delayed pubertal development and insulin resistant diabetes (Nissenkorn et al 2016). In 1972, it was shown that the levels of alpha-fetoprotein (AFP), which probably originate from the liver (Ishiguro et al 1986), were elevated in A-T patients' blood (Waldmann & McIntire 1972) and increasing over time (Stray-Pedersen et al 2007). AFP blood levels can be used to follow the progression of the disease (Rothblum-Oviatt et al 2016).

1.5.2 Ataxia Telangiectasia mutated

The genetic cause of A-T are loss-of-function-mutations in the Ataxia Telangiectasia Mutated gene (*ATM*) (Gatti et al 1988, Savitsky et al 1995). ATM protein is a 370 kDa Serine/Threonine kinase with the kinase domain located at the C-terminus, exhibiting homology to the phosphatidylinositol3 (PI3) family of lipid kinases (PI3Ks). In contrast to the other PI3K-like protein kinases (PIKKs), ATM does not phosphorylate phosphatidylinositol (Jung et al 1997). Several enzymes involved in DNA damage response (DDR) are part of the PIKKs family: ATM, ataxia-telangiectasia and Rad3-related (ATR), and DNA-dependent protein kinase catalytic subunit (DNA-PKcs). These three factors are associated directly with DNA-damaged regions. Members of this family also include the mammalian target of rapamycin (mTor) protein kinase, the suppressor of morphogenesis in genitalia 1 (SMG1), and the kinase-dead adaptor protein TRRAP (transformation/transcription domain-associated protein) (Abraham 2004) (Figure 1.9).

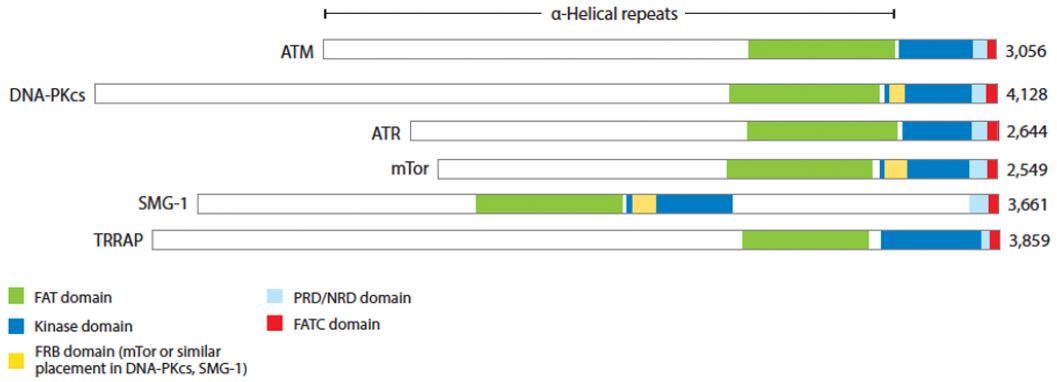

Figure 1.9. PIKK enzymes. Numerals refer to amino acids. Green represents the FAT domain (FRAP-ATM-TRAP transformation/transcription domain-associated protein); blue, the kinase domain; yellow, insertions in kinase domain (FKBP12/rapamycin-binding (FRB) in mTor; unknown function in DNA-PKcs and SMG-1); and red the FATC (FAT C-terminal) domain. Light blue represents the sequence between the kinase domain and the FATC domain, also known as the PIKK regulatory domain (PRD) or the negative regulatory domain (NRD) (Paull 2015).

The FRAP-ATM-TRRAP domain (FAT) and the FAT C-terminal (FATC) are closely intertwined with the Kinase domain (KD). Mutations in these domains are associated with effects on the catalytic activity of the kinase (Awasthi et al 2015). This FAT-KD-FATC structure is exclusive to the PIKKs family, while the FAT and FATC domains haven't been identified in other protein families (Baretic et al 2019).

Two general attributes are shared between PI3K enzymes and the PIKKs family. First, the PI3K enzymes in resting state are strongly and redundantly autoinhibited. In absence of stimulus, they are inactive and located in the cytoplasm. Second, PI3K enzymes require re-localization for their full activation. Similarly, ATM is found in an inactive resting state but can be rapidly activated and re-located to DNA damage sites (Blackford & Jackson 2017, Paull 2015).

1.5.3 ATM in DNA damage response and oxidative stress

Damage to DNA caused by endogenous or exogenous agents such as ionizing radiation (IR), ultraviolet radiation (UVR), pathogens, reactive oxygen species (ROS), and others can lead to alterations of the genetic code (Burger et al 2019a). DNA double-strand breaks (DSBs) are one of the most cytotoxic lesions, which impair DNA replication, impair RNA synthesis, and can lead to cell death (Jackson & Bartek 2009). Two major types of repair pathways have evolved in

order to maintain genome stability: homologous recombination (HR) (Her & Bunting 2018) and non-homologous end joining (NHEJ) (Hnizda & Blundell 2019). ATM is involved in DNA damage response (DDR), together with ATR and DNA-PK, being necessary to initiate a cascade of kinase-dependent phosphorylation in the DSB signaling (Burger et al 2019a, Paull 2015).

ATM is generally found in the nuclei in the form of a noncovalent inactive homodimer (Bakkenist & Kastan 2003). In case of DNA damage, ATM can quickly convert to its monomeric active form and phosphorylate a large number of substrates involved in cell-cycle checkpoints, DNA repair, and other cellular processes (Bensimon et al 2010, Matsuoka et al 2007). Autophosphorylation of ATM was one of the first steps described together with monomerization and activation in response to DNA damage (Bakkenist & Kastan 2003). To date, several autophosphorylation sites in ATM have been identified and their role in optimal ATM-mediated response demonstrated (Bensimon et al 2010, Graham et al 2017). The highly conserved MRN complex (Mre11, Rad50 and Nbs1), which plays a key role in DSB repair, can also activate ATM in response to DNA damage recruiting it to the affected site (Lee & Paull 2005). Moreover, activated ATM has been shown to localize at the DSBs in a protein complex with FOXO3a and KAT5/Tip60. This complex relies on MRN complex for proper substrate recognition (Adamowicz et al 2016). Other factors such as Mdc1 have been identified as necessary for the localization of ATM to the DNA damage site, a key event for its activation (Lou et al 2006). Therefore, the activation of ATM seems to be crucial in maintaining genomic stability and depends on the interaction with other complexes (Her & Bunting 2018, Jackson & Bartek 2009, Paull 2015).

Interestingly, ATM was found to localize mainly in the cytoplasm of postmitotic neurons, PN, and SH-SY5Y cells (Barlow et al 2000, Boehrs et al 2007, Oka & Takashima 1998). Fractions of ATM were also found to associate with organelles and proteins involved in vesicle trafficking (Lim et al 1998). Therefore, it is accepted that ATM has separate functions between the nuclei and the cytoplasm, and it has been shown to be via genetically separable pathways (Lee et al 2018).

The respiratory chain in the mitochondria is responsible to produce the majority of ROS. In addition to causing DNA damage, ROS can also damage lipids and proteins. Studies in A-T patients' fibroblasts demonstrate their higher sensitivity

to oxidative damage caused by hydrogen peroxide than normal cells (Ward et al 1994, Yi et al 1990). Several tissues from *Atm*-/- were also found to suffer from oxidative damage (Barlow et al 1999). Guo and colleagues showed for the first time how hydrogen peroxide and oxidant agents directly activate ATM in absence of DNA DSBs and the MRN complex (Guo et al 2010). They also showed how mutations in the cysteine 2991 at the FATC domain impaired ATM response to oxidative stress, but not its response to DSBs (Guo et al 2010). Therefore, ATM can be dually activated either for oxidative stress or DNA damage response. Recent experimental results managed to delineate which activities of ATM are specific to its activation by oxidation, or to DNA damage related functions (Lee et al 2018). The platelet-derived growth factor receptor β (PDGFRB) has been implicated in a neuronal survival-signaling pathway linking ATM to the transcription factor ATBF1 during of oxidative stress (Kim et al 2010). Inhibitors of PDGFRB suppressed the activation of ATM under oxidative stress but did not alter ATM activation by X-ray irradiation (Kim et al 2010). Based on their results, the authors suggested ATM has a role in autophagy in protection of neurons and elimination of damaged organelles (Kim et al 2010).

1.5.4 Implication of ATM in mTOR pathway, insulin resistance, and autophagy

The mTOR Serine/Threonine kinase is also a member of the PIKK family as ATM, and it has been implicated in cellular growth. Environmental stresses such as hypoxia, DNA damage, and nutrient availability, can affect cellular growth and viability (Reiling & Sabatini 2006, Wullschleger et al 2006). The mTOR complex 1 (mTORC1) activity inhibits autophagy; a process necessary to eliminate damaged organelles and recover nutrients. In response to oxidative stress, ATM has been indirectly implicated in down-regulation of mTORC1 activity. ATM activates TSC2 (tuberous sclerosis2) tumor suppressor in the cytoplasm in response to elevated ROS and repress mTORC1 to induce autophagy (Alexander et al 2010). Under hypoxic conditions, ATM also seems to inhibit mTORC1 activity indirectly. REDD1 (regulated in development and DNA-damage response 1) protein is a negative regulator of mTORC1 (Cam et al 2010) under the transcription factor HIF-1α. Under hypoxic conditions, HIF-1α dimerizes with HIF-β and translocates

to the nucleus to induce the expression of hypoxia-inducible genes, including *REDD1* (Majmundar et al 2010). ATM is activated under hypoxic conditions (Bencokova et al 2009) in a DNA-damage independent manner. Hypoxia-activated ATM stabilizes HIF-1α via phosphorylation (Cam et al 2010). On the contrary, ATM deficient cells showed a significantly impaired translocation of HIF-1α to the nucleus and reduced *REDD1* transcript levels (Cam et al 2010).

A-T patients have an increased risk of developing insulin resistance and diabetes type 2 (Nissenkorn et al 2016). ATM has been shown to participate in insulin signaling through phosphorylation of 4E-BP1 (eIF-4E-binding protein 1) (Yang & Kastan 2000). Cells lacking ATM kinase activity exhibit a significant down-regulation of the insulin-induced dissociation of 4E-BP1 from eIF-4E, a critical step during response to insulin (Yang & Kastan 2000). Moreover, studies in muscle cells demonstrate the ATM mediated activation of Akt and regulation of the GLUT4 (glucose transporter 4) translocation during insulin signaling (Halaby et al 2008). Muscle cells from insulin resistant rats had reduced ATM levels and decreased AKT phosphorylation in comparison to WT (Halaby et al 2008). Further experiments with mouse embryonic fibroblast (MEF) *Atm-/-* and WT confirmed the role of ATM in activating Akt (Halaby et al 2008). The translocation of GLUT4 to the cell surface was markedly inhibited in transfected cells with kinase-dead ATM (Halaby et al 2008).

Autophagy is a regulated mechanism through which the cell can degrade and recycle unnecessary or damaged components/organelles (Klionsky 2008, Kobayashi 2015). Basal levels of autophagy are necessary to maintain cell homeostasis under normal conditions (Anding & Baehrecke 2017). It is also an important process during of cellular stress such as starvation (Wei et al 2015), hypoxia (Choi et al 2016), oxidative stress (Alexander et al 2010, Tripathi et al 2013), and others. Since ATM can be activated to respond to the previous mentioned stimuli, it is not surprising that ATM plays a role in autophagy (Alexander et al 2010, Liu et al 2013, Mahemuti et al 2018). Although autophagy has been considered as non-selective process, increasing number of studies have pointed to a more selective type (Rogov et al 2014). Selective autophagy can degrade specific cellular components into membrane vesicles even under nutrient-rich conditions in a selective manner (Rogov et al 2014). Several

selective autophagy receptors such as SQSTM1 (sequestosome1, also known as p62), linking the cargo to the autophagic machinery, have been characterized (Johansen & Lamark 2011) (Figure 1.10).

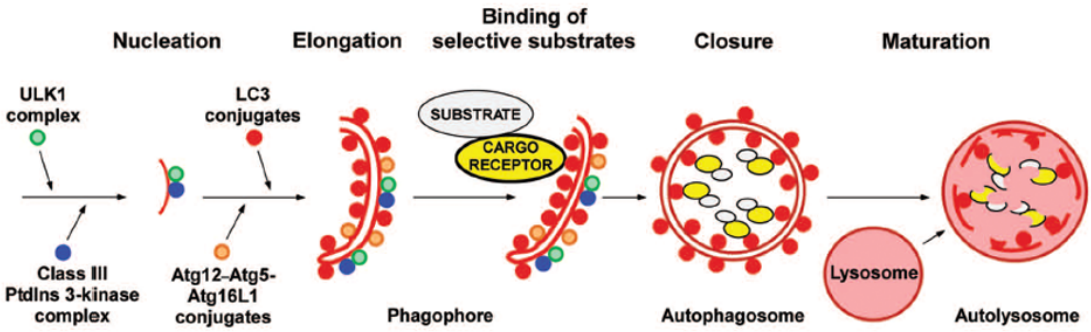

Figure 1.10. Model for selective autophagy in mammalian cells. Briefly, selective autophagy depends on binding of substrates to the inner surface of the growing phagophore, and this can be achieved by cargo receptors associated to both substrate and with ATG8 family proteins anchored to the phagophore. Closure results in the formation of a double-membrane autophagosome. The maturation step (fusion with lysosome) is required for the formation of the autolysosomes where the substrates are degraded (Johansen & Lamark 2011).

Selective autophagy can be classified into multiple categories depending on the location in which it occurs: mitophagy (monitoring the quantity and quality of mitochondria; further discussed), pexophagy (selective removal/degradation of excess and damaged peroxisomes), lipophagy (related to lipid metabolism), lysophagy (Figure 1.11), and others (Klionsky et al 2016).

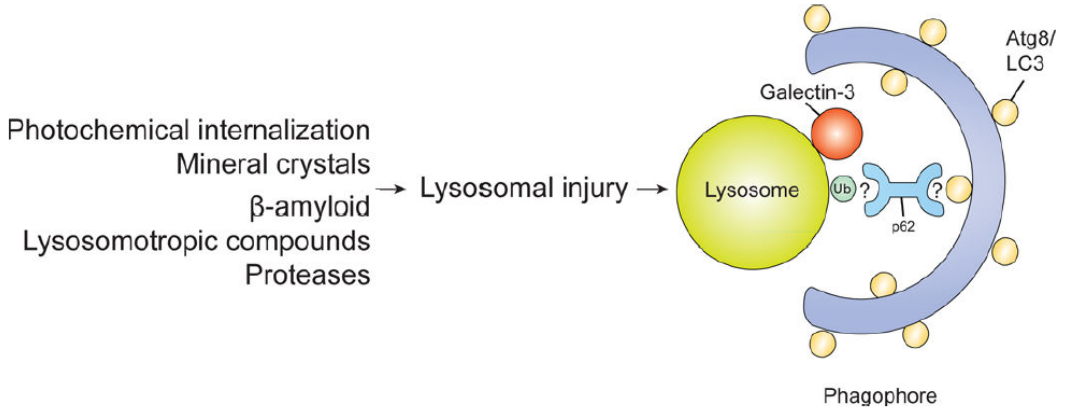

Figure 1.11. Model of lysophagy in mammalian cells. Lysophagy can be induced by a variety of stimuli that can lead to lysosome damage. Upon injury, lysosomal membranes are ubiquitinated and co-localize with p62. The exact mechanisms of lysophagy regulation are still unclear (Anding & Baehrecke 2017).

ATM was found to localize in the peroxisomes when activated by ROS (Watters et al 1999, Zhang et al 2015). Peroxisomes are organelles that can be degraded via proteases, autolysis, or pexophagy (selective removal) (Zhang et al 2015). In front of ROS, ATM is activated and phosphorylates the peroxisomal import receptor protein PEX5. Ubiquitination of PEX5 by SQSTM1 is the next step to signal for degradation (Zhang et al 2015). Therefore, ATM plays an important role in pexophagy, however more research in the exact mechanisms is needed.

1.5.5 Mitochondrial functions and mitophagy regulation by ATM

Mitochondria are double-membrane organelles found in eukaryotic organisms. They are responsible for generating most of the cell energy in form of ATP (adenosine triphosphate) through the electron transport chain/oxidative phosphorylation system (ETC/OXPHOS system) (Henze & Martin 2003). This process seems to be inefficient and can generate endogenous ROS. Moreover, mitochondrial dysfunction leads to an excessive production of ROS and is believed to contribute to diseases such as diabetes, many progressive neurodegenerative disorders, and cancer (de Moura et al 2010).

Based on data from ATM-deficient cells and *Atm-/-* mice, mitochondrial functions were found to be abnormal and the mitochondria-specific superoxide dismutase (MnSOD) was elevated (Kamsler et al 2001). Mitochondrial respiration was also reported to be abnormal in *Atm-/-* mice, pointing to an overall diminished mitochondrial respiratory activity in A-T and implicating ATM in the regulation of mitochondrial function (Ambrose et al 2007, Blignaut et al 2019, Stern et al 2002). Recent work from Zhang *et al* demonstrates ATM activation by mitochondria-derived hydrogen peroxide via dimerization, and ATM relocalization to the nuclei in HeLa cells (Zhang et al 2018). The authors also suggest that mitochondrial dysfunction and oxidative stress in A-T are due to the loss-of-function mutations in *ATM* linked to the loss of the redox-sensing function of ATM (Zhang et al 2018).

ATM has also been implicated in mitochondrial homeostasis by negatively regulating mitophagy (Valentin-Vega & Kastan 2012). Analysis of thymocytes from *Atm-/-* mice revealed altered mitochondrial homeostasis as a result of abnormal mitophagy engagement (Valentin-Vega & Kastan 2012). Additionally,

spermidine treatment (a polyamine) induced ATM-dependent mitophagy via PINK1/Parkin pathway in human fibroblasts (Qi et al 2016). The formation of mitophagosomes and mitolysosomes were blocked by the ATM kinase inhibitor KU55933 (Qi et al 2016). Lead (Plumbum) toxicity was also reported to induce mithopgay on an ATM-dependent manner via PINK1/Parkin pathway (Gu et al 2018). Although ATM seemingly has a role in mitophagy, the exact mechanisms need further research.

1.5.6 ATM and synaptic function

Neurons show significant amounts of ATM in their cytoplasm rather than in the nuclei, as is typical in other cell types. Moreover, ATM was found to associate with organelles and proteins involved in vesicle trafficking (Barlow et al 2000, Lim et al 1998, Oka & Takashima 1998, Watters et al 1999). Using primary neuronal cultures from *Atm-/-* mice, biochemical and physical relationship were demonstrated among ATM, ATR, VAMP2 (synaptobrevin) and synapsin-I, coupled with defects in LTP and spontaneous dye release (Li et al 2009). This association of ATM with synaptic function pointed to a new explanation for the neurological symptoms in A-T, where neurons seem to be subjected to synaptic dystrophy on top of cellular loss (Li et al 2009). Follow up work on ATM and ATR role in synaptic function showed a complementary role for these two kinases in maintaining the excitatory/inhibitory balance in the nervous system (Cheng et al 2018). Superresolution microscopy and coimmunoprecipitation experiments showed an exclusive association of ATM with excitatory (VGLUT1 positive) vesicles while ATR associated only with inhibitory (VGAT positive) vesicles suggesting a role in maintaining the excitatory/inhibitory (E/I) balance. Levels of ATM and ATR were also found to respond to each other meaning that when ATM is deficient, ATR levels rise (Cheng et al 2018). Epilepsy, anxiety disorders, and memory impairment have been linked to E/I imbalance and neuronal network dysfunction (Bateup et al 2013, Foerster et al 2013, Rudenko et al 2015). Cheng *et al* propose a model where both proteins have an important function in synaptic vesicle trafficking and potentially in vesicle endocytosis (Figure 1.12). ATM and ATR complementary roles may provide new neurological insights into A-T and perhaps other neurodegenerative diseases (Shen et al 2016).

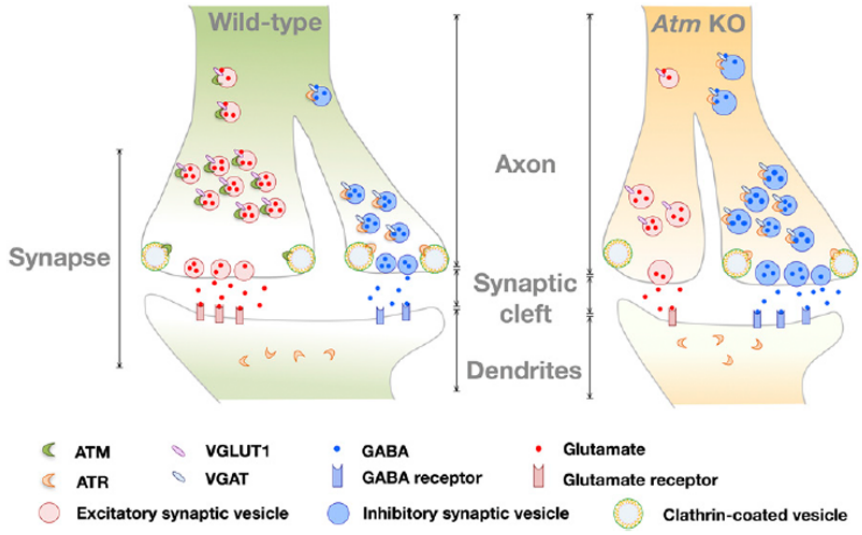

Figure 1.12.Diagram of the vesicle trafficking model of WT and *Atm*-KO synapses. This model proposes that in synapses, ATM protein localizes predominately in presynaptic terminals, while ATR localizes on both sides of the synapse. ATM binds exclusively to VGLUT1⁺ vesicles, while ATR localizes only to VGAT⁺ vesicles. Compared with WT, *Atm*-KO (*Atm -/-*) neurons show decreased E/I balance, impaired clathrin-mediated synaptic vesicle endocytosis, increased ATR protein levels, and larger vesicle size (Cheng et al 2018).

1.5.7 Mouse models for A-T

Three mouse models for A-T were generated in 1996 following different strategies to cause loss-of-function. All showed growth retardation, infertility, T-cell maturation defects, and sensitivity to gamma irradiation (Barlow et al 1996, Elson et al 1996, Xu & Baltimore 1996).

Further characterization of the A-T mouse model generated by Barlow and colleagues (Barlow et al 1996) showed oxidative damage in several target organs (Barlow et al 1999) and the requirement of ATM to prevent lysosomal accumulation in the mouse brain (Barlow et al 2000). Defects in calcium spikes and calcium currents were also detected in PN of this ATM-deficient mouse model (Chiesa et al 2000). No gross behavioural abnormalities were detected in this mouse model, nor loss of PN at histological level, probably due to thymic lymphomas limiting the life span of these mice to 4-6 months. In order to detect neuronal loss in the cerebellum, the life span of these animals had to be extended by bone marrow transplantation (Pietzner et al 2013).

Many more studies using these A-T mouse models have helped to define the function of ATM but still there isn't a therapeutic strategy to resolve or ameliorate the neurological symptoms of A-T patients.

1.6 Aim of the thesis

Despite all the efforts to elucidate the pathomechanisms implicated in ataxia there is still no cure or therapy to palliate the symptoms and improve the life standards of the patients. Therefore further research has to be done in the field.
In the framework of this thesis two different inherited ataxias have been analyzed: the autosomal dominantly inherited spinocerebellar ataxia type 2 and the autosomal recessively inherited ataxia telangiectasia.

The first aim of the thesis was to characterize the newly generated mouse model *Atxn2*-CAG100-KIN to determine its usefulness in the SCA2 research field and application in other neurodegenerative disorders such as ALS where ATXN2 has been implicated. Further questions rose during the characterization of this mouse model such as:

- How is the spinal cord pathology observed in the *Atxn2*-CAG100-KIN animals characterized?
- Does this pathology implicate the ALS linked protein TDP43 and other RBP?

Based on the strategy followed to generate this mouse model, conserving the exon-intron structure and intact murine promoter, the expanded ATXN2 preserves its native expression regulation. Thus, this model will allow understanding the implication of other non-neuronal cell types in the pathology. Moreover, neuroinflammation has been long implicated in several neurodegenerative disorders and more recently TDP43 depletion has been shown to alter microglia phagocytic functions. Therefore we aimed to answer the following questions:

- Are other non-neuronal cell types such as microglia and astrocytes implicated in the pathology seen in the *Atxn2*-CAG100-KIN mice?
- Could manipulating glia response help ameliorate the symptomatology?

After characterizing similar affection of the cerebellum and the spinal cord and following the generation of the transcriptome data sets, we aimed to define common and early affected pathways.

- Cholesterol metabolism alteration was identified as an early and common event. How are these alterations characterized at transcript level?
- Could the altered factors become reliable biomarkers for the progression of the disease?

The second part of this work was focused on a recessive form of ataxia, Ataxia Telangiectasia. In collaboration with Prof. Dr. Ralf Schubert's Lab, the second aim of this thesis was to analyze and gain deeper insight in the cerebellar pathology of A-T using proteomics data generated from patients' CSF and the cerebellar tissue from the *Atm-/-* mouse model. We aimed to:

- Define novel biomarkers, which would allow following the neurodegeneration in extracellular fluid.
- Using the *Atm-/-* mouse model, we further validate the results obtained in the patients' CSF proteome data in order to define altered pathways before the ataxic symptoms appear.

One general characteristic observed in A-T murine models is the short life span due to lymphomas, so they die before showing any behaviour alteration. Therefore, the cerebellar degeneration has not being studied in depth. Using bone marrow transplantation surgery, the life span of *Atm-/-* animals could be extended and a transcriptomics data set was generated from 12-month-old cerebellar samples. Based on the data obtained the following questions rose:

- Which other known ataxia genes are implicated in the cerebellar degeneration based on the transcript evaluation?
- Which pathways are also altered in young pre-ataxic *Atm-/-* animals?
- Could we define further blood biomarkers correlating with the neurologic affection observed in A-T patients?

2 MATERIALS AND METHODS

2.1 Animals

2.1.1 Housing and breeding

Atxn2-CAG100-Knock-in (*Atxn2*-CAG100-KIN), *Atxn2*-Knock-out (*Atxn2*-KO) and *Atm*-Knock-out (*Atm* -/-) animals were housed at the Central Animal Facility (ZFE) of the Goethe University Medical School, Frankfurt am Main Germany, a FELASA-certified facility. They were kept in individually ventilated cages in a 12-hour light / 12-hour dark cycle under routine health monitoring and fed *ad libitum.* The cages were supplemented with bedding and paper chipping and were cleaned weekly. Breeding took place in heterozygous matings for both lines. All procedures were in accordance with the German Animal Welfare Act, the Council Directive of 24th November 1986 (86/609/EWG), Annex II and the ETS123 (European Convention for the Protection of Vertebrate Animals).

2.1.2 Genotyping – DNA extraction and PCR

Ear punches were taken when the pups were between 10 and 12 days old, collected in 1.5mL tubes and immediately processed or frozen at -20ºC. A tail sample was also collected after each dissection in order to verify the genotype.
For the DNA extraction, 500 µL of Proteinase K buffer (10 mM Tris-HCl, 100 mM NaCl, 10 mM EDTA, 0.5% SDS, pH8.0) mixed with 25 µL of Proteinase K were used per sample and incubated at 55ºC in a thermoshaker at 450 rpm overnight to ensure the digestion of the tissue. Next day, 250 µL of 6M NaCl were added to the samples to remove the proteins bound to the DNA, incubated on ice for 10 min and centrifuged at 5000 rpm for 10 min. 500 µL of the supernatant was transferred to a fresh 1.5 mL tube and the DNA was precipitated adding 1 mL of 100% ethanol (EtOH). In order to improve the precipitation, the samples were incubated at -80ºC for 10 min before centrifuging at maximum speed for 10 min at room temperature (RT). The pellet was then washed with 1 mL of 70% EtOH,

centrifuged at 8000 rpm for 5 min, dried at RT for no more than 5 min and resuspended in 200 µL of DNase/RNase free water.

For the *Atxn2*-CAG100-KIN mouse line, the polymerase TAKARA La Taq® was used to amplify the flanking region of the Neo-excised *Atxn2* locus that still contains a FRT (flippase recognition target) and a loxP (locus of X-over P1) site in the mutant animals.

Reaction		**Condition**			
10x LA Buffer	2.5 µL	Step	Temperature	Time	Cycles
dNTPs (2.5 mM)	1 µL each	Initial denat.	94ºC	3 min	1
Primers	0.1 µL	Denaturation	94 ºC	30 sec	35
LA Taq	0.25 µL	Annealing	68ºC	30 sec	
DNA	20-50 ng	Elongation	68ºC	50 sec	
Final volume	25 µL	Final elongation	68ºC	7 min	1

Table 2.1. PCR conditions for La Taq® used to genotype the *Atxn2*-CAG100-KIN mouse line.

Name	**Sequence**	**Genotype**	**Product size**
Primer K	TGAGTTGACTCCACAGGGAGGTGAGC	WT	793 bp
Primer H	CCATCTCGCCAGCCCGTAAGATTC	KIN	984 bp

Table 2.2. Sequence of the primers used to genotype the *Atxn2*-CAG100-KIN mouse line.

To genotype the *Atxn2*-KO line, the Ampli-Taq-DNA Polymerase was used together with pink juice (2 mM Cresol, 12.5% 10x PE buffer, 2 mM dNTPs, 15% Sucrose), primers (Atxn2 F2, Atxn2 R3 and Atxn2 R4) and DNA as specified in the Table 2.3.

Reaction		**Condition**			
Pink juice	16 µL	Step	Temperature	Time	Cycles
Primer	1 µL each	Initial denat.	95ºC	3 min	1
AmpliTaq	0.1 µL	Denaturation	94 ºC	30 sec	35
DNA	20-50 ng	Annealing	57ºC	30 sec	
Final volume	20 µL	Elongation	72ºC	50 sec	
		Final elongation	72ºC	7 min	1

Table 2.3. PCR conditions for Ampli-Taq-DNA Polymerase used to genotype the *Atxn2*-KO mouse line.

Name	Gene position	Sequence	Genotype	Product size
Atxn2 F2	14381	CATGTGCCATAACCAGGGG		
Atxn2 R3	14854	GAACTGGGTGATGGGGTCTC	WT	474 bp
Atxn2 R4	18512	CAGGCCCAGAAGTGAAAGAC	KO	229 bp

Table 2.4. Sequence of the primers used to genotype the *Atxn2*-KO mouse line.

Genotyping of the *Atm* -/- animals was performed by members of Prof. Dr. Ralf Schubert's laboratory.

2.1.3 Ageing and behavioral tests

After genotyping, the animals were aged in pairs of mutant and WT of the same sex in order to reduce variation. After reaching the desired age, they were tested in different behavioral tests; no distinction between males or females was done. All tests were done in a separated and ventilated room at the same animal facility.

2.1.3.1 Rotarod

To evaluate the motor performance a Rotarod (model 7650 Robert & Jones, Ugo Basile, Comerio) was used. Wild type and mutant animals aged in the same cage were evaluated together. During the acceleration of the rotarod from 4-40 rpm, every mouse had four consecutive 6 min trials interrupted by at least 10 min of break, without previous training. The latency to fall was recorded for each trial; the mean value of the four trails was calculated and used for statistical analysis.

2.1.3.2 Open field

Open field arena (Versamax, Omnitech, Columbus, Ohio) was used to record the spontaneous activity. The arena consists of a 20 cm by 20 cm with infrared beams at each side therefore; vertical and horizontal movements were recorded.

2.1.3.3 Paw print

Paw prints were evaluated by painting the forepaws and hind limbs with a non-toxic red and blue ink, respectively. The mice were placed at one end of a dark tunnel, so that their walk to the other end would leave paw prints on the white paper that covers the floor (tunnel 6cm high x 9cm wide x 40cm long).

2.1.3.4 Grip strength

Grip strength was assessed by measuring the peak force of the fore limbs in 10 trials per mouse on an electronic grip strength meter (TSE, Bad Homburg). The average of the 10 trials was used for further statistical analyzes using GraphPad Prism version 7.02.

2.1.4 Fresh tissue - sample collection

After the behavioral tests or at the predetermined age, animals were sacrificed via cervical dislocation and the brain was dissected together with other tissues. The cerebellum, remainder of the brain, spinal cord, liver, heart, and skeletal muscle were collected in 1,5 mL tubes, immediately snap frozen in liquid nitrogen and kept at -80ºC until further use.

2.1.5 Material used in Animals section

2.1.5.1 Mouse models

Mouse model	Mutation	Background	Reference
Atxn2-Knock-out	Excision of *Atxn2* exon 1	C57BL/6J	Lastres-Becker et al., 2008
Atxn2-CAG100-Knock-in	Insertion of 100 CAG in the exon 1 of *Atxn2*	C57BL/6J	Sen, Canet-Pons, Halbach et al., 2019
Atm-Knock-out	Insertion of truncation mutation at gene position 5790	129SvEv	Barlow et al., 1996

Table 2.5. Mouse models used.

2.1.5.2 Chemicals and reagents used for DNA extraction and genotyping

Chemicals/Reagents	Cat. No.	Company
Agarose	A9539	Sigma-Aldrich
Ampli-Taq-DNA Polymerase	P/N1000204	AB
Cresol Red sodium salt	50100	Sigma-Aldrich
DNase/RNase free water	10977-035	Invitrogen
dNTP set 100 mM (dATP, dCTP, dGTP, dTTP)	R0181	Thermo Scientific
Ethidium bromide	2218.1	ROTH
Ethylenediamine tetraacetic acid (EDTA,	E5134-1KG	Sigma-Aldrich

$C_{10}H_{16}N_2O_8$)		
Ethanol (C_2H_6OH)	32221-1L-M	Sigma-Aldrich
Proteinase K	25530-015	Life Technologies
SDS pellets	CN30.2	ROTH
Sodium Cloride (NaCl)	31434-1KG-M	Sigma-Aldrich
Sucrose ($C_{12}H_{22}O_{11}$)	84100	Sigma-Aldrich
TAKARA La Taq®	RR002M	Takara
Tracklt™ 1Kb DNA Ladder	10488-072	Life Technologies
Trizma® base ($C_4H_{11}NO_3$)	T1503-1KG	Sigma-Aldrich

Table 2.6. Chemicals and reagents used for DNA extraction and genotyping.

2.1.5.3 Instruments used for behavioral tests

Instrument	Company
Grip strength	TSE
Rotarod 7650	Ugo Basile
Versamax Animal Activity Monitoring System	Accuscan Instruments

Table 2.7. Instruments used for the behavioral tests performed.

2.2 RNA work

All RNA work was performed after cleaning the work area, pipets and other necessary instruments with RNaseZap wipes. All reagents used were RNase/DNase free.

2.2.1 RNA extraction and quantification

The RNA extraction was performed using the phenol-chloroform extraction protocol. A total of 50 – 100 mg of tissue were homogenized in 300 µL of TRI Reagent and 700 µL more were added to a final volume of 1 mL. Samples were incubated at RT for 5 min, 200 µL of chloroform were added and were vigorously shacken for 15 sec. To allow the phases to start separating, the samples were kept at RT for 10 min before centrifuging them at 12000 xG for 15 min in a cooled centrifuge at 4ºC. Three phases could be identified: a lower red phase (phenol-chloroform, DNA), a white interphase (proteins) and a transparent aqueous upper phase containing the RNA. In order to precipitate the RNA, the first step was to transfer the aqueous phase into a fresh 1,5 mL tube where 500 µL of isopropanol were added. Samples were then mixed by inversion, incubated at RT for 10 min, and centrifuged at 12000 xG for 10 min at 4ºC. Sometimes a

white pellet could be visualized corresponding to the precipitated RNA. The supernatant was then discarded and the RNA was washed with at least 1 mL of freshly prepared 75% EtOH, briefly vortex, and centrifuged at no more than 7500 xG for 5 min at 4ºC. The supernatant was again discarded and the pellet dried at RT for maximum 10 min. RNA was re-dissolved in RNase free water by pipetting several times and incubated at 55ºC for 10 min in order to ensure its complete dissolution.

In case of extracting RNA from cells, the pellet from a 6-well plate was re-suspended in 1 mL of TRI Reagent and the protocol was followed as described for tissue samples.

A total of 2 µL of RNA sample were used to determine its quantity and quality with the TECAN Spark. After that, the samples were used for RT-PCR or stored at -80ºC.

2.2.2 Reverse transcription PCR

Reverse transcription polymerase chain reaction (RT-PCR) was performed using the SuperScript IV VILO Master Mix following the manufacturer's protocol. The samples were kept on ice all the time and were spun down after the addition of each reagent. For the reaction, 1 µg of RNA was used in a final volume of 8 µL with DNase/RNase free water; 2 µL of a mix 1 to 1 of ezDNase enzyme and 10x ezDNase buffer were mixed with the samples in order to degrade any residual DNA present. The samples were incubated at 37ºC for 2 min in a thermocycler, moved to 4ºC, and 10 µL of Vilo IV master mix diluted in water (2:3) were added. The final reaction was carried out in the same thermocycler and consisted of an annealing step (10 min at 25ºC), reverse transcription step (10 min at 50ºC), and enzyme inactivation step (5 min at 85ºC). After that, the samples were moved to 4ºC, 180 µL of RNase free water were added and the samples were kept at -80ºC until used.

2.2.3 Quantitative-PCR and data analysis

In order to evaluate differences in gene expression, quantitative PCR (Q-PCR) was performed from 20 ng of cDNA in a 96-well optical plate with a StepOnePlus

Real-Time PCR system. Replicates from each sample were included per assay. The reaction mix per sample consisted of 10 ng of cDNA, 0.5 µL 20× TaqMan gene expression assay, 5 µL of 2× FastStart Universal Probe Master, and 2.5 µL DNAse/RNAse-free water. The Q-PCR conditions were 50ºC 2 min, 95ºC 10 min, 40 x (95ºC 15 sec, 60ºC 1 min). The data obtained from the StepOnePlus machine was processed following the $2^{-\Delta\Delta Ct}$ method (Schmittgen & Livak 2008) and the statistical analysis and graphics were done with GraphPad Prism version 7.02. *Tbp* was used as housekeeping gene for murine samples and HPRT1 for human cell lines.

2.2.4 Transcriptomics – Clariom D microarray and data analysis

1 µg of RNA was pre-treated with DNase amplification grade (Invitrogen) as recommended. The Gene Chip™ WT PLUS Reagent Kit (Appliedbiosystems) was used to generate single-stranded cDNA (ss-cDNA) following the manufacturer's instructions. The ss-cDNA was fragmented and labeled right before the hybridization to a Clariom D Array (Thermo Fisher). The arrays were scanned with the Affymetrix Gene Chip Scanner and the data was processed with the Transcriptome Analysis Console (TAC) 4.0.1 (Appliedbiosystems) using default algorithm parameters.

2.2.5 Material used for RNA work

2.2.5.1 Reagents used for RNA extraction, cDNA synthesis and Q-PCR

Reagents	Cat.No.	Company
Chloroform	A3633.0500	AppliChem
Ethanol (C_2H_6OH)	32221-1L-M	Sigma-Aldrich
FastStart Universal Probe Master (ROX)	04914058001	Roche
Isopropanol	P/7500/15	Fisher Chemical
SuperScript IV VILO Master Mix	11766050	Thermo Fisher
Tri Reagent	T-9424	Sigma-Aldrich
Water DNAse/RNase free	10977-035	Invitrogen

Table 2.8. Reagents used for RNA extraction, cDNA synthesis and Q-PCR.

2.2.5.2 Materials and instruments used for RNA extraction and quantification

Material	Cat. No.	Company
Pellet pestles polypropylene	Z359947	Sigma-Aldrich
RNaseZap wipes	AM9786	Invitrogen
TECAN Spark		TECAN
KontesTM Pellet Pestle™ Cordless Motor		Sigma-Aldrich

Table 2.9. Materials and instruments used for RNA extraction and quantification.

2.2.5.3 TaqMan® assays

Gene	Assay ID	Gene	Assay ID
Aar2	Mm00503287_m1	*Gsr*	Mm00439154_m1
Abca1	Mm00442646_m1	*Gss*	Mm00515065_m1
Abcg1	Mm00437390_m1	*Gstp1*	Mm04213618_gH
Ahnak	Mm00613028_m1	*Hmgcs1*	Mm01304569_m1
Ahnak2	Mm03015444_s1	*Hnrnpa1b2*	Mm01332941_m1
Aif1	Mm00479862_g1	*Hnrnpd*	Mm01201314_m1
Als2	Mm00511896_m1	*Hnrnpk*	Mm04409831_s1
Anapc5	Mm01194479_m1	*Hnrnpu*	Mm00469329_m1
Anxa2	Mm01150673_m1	*Homer2*	Mm01314936_m1
Apob	Mm01545150_m1	*Homer3*	Mm00803747_m1
Apoc3	Mm00445670_m1	*Hsd11b1*	Mm00476182_m1
Apod	Mm01342307_m1	*Ighm*	Mm01718955_g1
Apoe	Mm00437573_m1	*Inpp5a*	Mm00805812_m1
Apoer2	Mm00474030_m1	*Insig1*	Mm00463389_m1
Apoh	Mm00496516_m1	*Irak1*	Mm01193538_m1
Apoj (Clu)	Mm00442773_m1	*Irak4*	Mm00459443_m1
App	Mm01344172_m1	*Itpka*	Mm00525139_m1
Atm	Mm01177457_m1	*Itpr1*	Mm00439907_m1
Atp2a2	Mm01201431_m1	*Kcna1*	Mm00439977_s1
Atp2b2	Mm00437640_m1	*Lamp1*	Mm00495262_m1
Atr	Mm01223626_m1	*Lamp2*	Mm00495267_m1
Atxn2	Mm01199902_m1	*Lcat*	Mm01247340_m1
Atxn2L	Mm00805548_m1	*Ldlr*	Mm01177349_m1
Blmh	Mm00724434_m1	*Lrp1*	Mm00464608_m1
C1qa	Mm00432142_m1	*Lrp1b*	Mm00466712_m1
C1qb	Mm01179619_m1	*Lrp2*	Mm01328171_m1
C1qc	Mm00776126_m1	*Lrp6*	Mm00999795_m1
C3	Mm01232779_m1	*Lrp8*	Mm00474030_m1
Cacna1a	Mm00432190_m1	*Lrp8 (exon 19)*	Mm01257937_m1
Cadps2	Mm00462577_m1	*Lsm1*	Mm01600253_m1
Calb1	Mm04886647_m1	*Lyn*	Mm01217488_m1
Calm1	Mm01336281_g1	*M6pr*	Mm04208409_gH
Camk2a	Mm00437967_m1	*M6prbp1*	Mm00482206_m1

Car15	Mm00472660_m1	*Msmo1*	Mm00499390_m1
Car8	Mm00801469_m1	*Mtcl1*	Mm01226260_m1
Casp3	Mm01195085_m1	*Npc1*	Mm00435300_m1
Cbln1	Mm01247194_g1	*Npc2*	Mm00499230_m1
Cbln2	Mm01261557_g1	*Nr1h2 (LXRβ)*	Mm00437262_m1
Cbln3	Mm00490772_g1	*Nr1h3 (LXRa)*	Mm00443451_m1
Cbln4	Mm00558663_m1	*Nr4a1*	Mm00439358_m1
Cdr1	Mm04178856_s1	*Nr4a2*	Mm00443060_m1
Celf3	Mm00549809_m1	*Nr4a3*	Mm00450074_m1
Cirbp	Mm00483336_g1	*Pabpc1*	Mm00849569_s1
Cntn2	Mm00516138_m1	*Pafah1b1*	Mm00443070_m1
Cyba	Mm00514478_m1	*Pafah1b2*	Mm00476594_m1
Cybb	Mm01287743_m1	*Pafah1b3*	Mm01177179_m1
Cyp46a1	Mm00487306_m1	*Pcbp1*	Mm00478712_s1
Cyp51	Mm00490968_m1	*Pcbp2*	Mm01296174_g1
Dab1	Mm00438366_m1	*Pcbp3*	Mm01149750_m1
Dab2	Mm01307290_m1	*Pcbp4*	Mm00451991_g1
Dag1	Mm00802400_m1	*Pms2*	Mm01200871_m1
Dcp1a	Mm00460131_m1	*Por*	Mm01208218_m1
Dcp1b	Mm01183995_m1	*Ppp1cb*	Mm01209998_m1
Dcp2	Mm01264061_m1	*Ppp1r17*	Mm00495458_m1
Dcps	Mm00510029_m1	*Prkcg*	Mm00440861_m1
Ddx1	Mm00506205_m1	*Prpf19*	Mm01208295_m1
Ddx26b	Mm00555431_m1	*Ptbp1*	Mm01731480_gH
Ddx6	Mm00619326_m1	*Pten*	Mm00477208_m1
Dhcr24	Mm00519071_m1	*Puf60*	Mm00505017_m1
Dhx15	Mm00492113_m1	*Pura*	Mm01158049_s1
Efemp1	Mm01295779_m1	*Reelin*	Mm00465200_m1
Eif2a	Mm01289723_m1	*Ripk1*	Mm00436354_m1
Eif3a	Mm00468721_m1	*Rnaset2a/b*	Mm02601904_m1
Eif4e	Mm00725633_s1	*Rora*	Mm01173766_m1
Eif5a2	Mm00812570_g1	*Scg2*	Mm04207690_m1
Eif5b	Mm01227247_m1	*Sema7a*	Mm00441361_m1
Eif6	Mm00550245_m1	*Sf3a1*	Mm00470710_m1
Ephb2	Mm01181021_m1	*Sf3a2*	Mm00449720_m1
Fan1	Mm00625959_m1	*Sgk1*	Mm00441387_g1
Fat2	Mm01295779_m1	*Slc17a6*	Mm00499876_m1
Fgf14	Mm00438914_m1	*Slc17a7*	Mm00812886_m1
Fgfr1	Mm00438930_m1	*Slc1a6*	Mm01173279_m1
Fmr1	Mm01339582_m1	*Slc44a5*	Mm01317372_m1
Fos	Mm00487425_m1	*Smad2*	Mm00487530_m1
Fyn	Mm00433373_m1	*Smad3*	Mm00489637_m1
Gfap	Mm01253033_m1	*Src*	Mm00436783_m1
Gpnmb	Mm01328587_m1	*Srrm2*	Mm00613771_m1
Grb2	Mm03023989_g1	*Srsf1*	Mm01152449_g1
Gria1	Mm00433753_m1	*Srsf2*	Mm00448705_m1

Gria2	Mm00442822_m1	*Ssb*	Mm00447374_m1
Gria3	Mm00497506_m1	*Stat1*	Mm01257286_m1
Gria4	Mm00444754_m1	*Stxbp5l*	Mm00552492_m1
Grid2	Mm00515053_m1	*Syne1*	Mm04238399_m1
Grik2 (Grm6)	Mm00599860_m1	*Tacr1*	Mm00436892_m1
Grin1	Mm00433800_m1	*Tardbp*	Mm00523866_m1
Grin2a	Mm00433802_m1	*Tcfeb*	Mm00448968_m1
Grin2b	Mm00433820_m1	*Tharp3*	Mm01181269_g1
Grin2c	Mm00439180_m1	*Tlr3*	Mm01207404_m1
Grin3a	Mm01341722_m1	*Tlr7*	Mm00446590_m1
Grin3b	Mm00504568_m1	*Tlr9*	Mm00446193_m1
Grind2d	Mm00433822_m1	*Tpr*	Mm00460177_m1
Grm1	Mm00810219_m1	*Trem2*	Mm00451744_m1
Grm3	Mm00725298_m1	*Tyrobp*	Mm00449152_m1
Grm4	Mm01306128_m1	*Tyw5*	Mm01254171_m1
Grm5	Mm00690332_m1	*U2af2*	Mm01330812_g2
Grm7	Mm01189424_m1	*Vamp1*	Mm01185107_g1
Grm8	Mm00433840_m1	*Vldlr*	Mm00443298_m1
Grn	Mm00433848_m1	*Ybx1*	Mm00850878_g1
Gsk3b	Mm00444911_m1	*Zic4*	Mm00657066_m1

Table 2.10. Taqman assays used with murine samples.

Gene	Assay ID
AHNAK	Hs01102463_m1

Table 2.11. Taqman assay used with human cell line samples.

2.3 Protein work

2.3.1 Protein extraction – RIPA and SDS fraction

Protein extraction from tissue was performed homogenizing each sample in approximately 5-10 v/v of RIPA buffer (50 mM Tris-HCl pH8, 150 mM NaCl, 1% NP-40, 0.5% Sodium Deoxycholate, 0.1% SDS, 2 mM EDTA, 1 tablet of Proteinase inhibitor per 10 mL) using a pellet pestle. Samples were then incubated for 30 min at 4ºC in a tube rotator to ensure a complete membrane disruption and centrifuged at 14000 xG for 15 min using a cooled centrifuge at 4ºC. The supernatant (RIPA fraction) was then transferred to a fresh tube and the pellet was then re-suspended in 100-250 µL of SDS lysis buffer (137 mM Tris-HCl pH6.8, 4% SDS, 20% Glycerol, 1 tablet of Proteinase inhibitor per 10 mL). At this point, samples were normally quite viscous due to the release of DNA from the nuclei. To avoid problems during further experiments, the samples were

sonicated three times for 10 sec. After quantification (see section below), they were stored at -80ºC.

The procedure to extract protein from cell cultures was similar to the one described above. Cells were grown in 6-well plates; 1 mL of DPBS was used to detach them from the plate and they were transferred to a 1.5 mL tube. Samples were then centrifuged at 1000 xG for 5 min, the supernatant was aspirated, and the pellet was re-suspended in 100-150 µL of RIPA buffer. Samples were kept at 4ºC rotating and were then centrifuged at 14000 xG for 15 min at 4ºC; the supernatant was transferred to a fresh tube. After quantification, the samples were stored at -80ºC.

2.3.2 Protein Quantification

After the protein extractions, samples were quantified using the Pierce BCA Assay Kit. In a 96 well flat bottom plate, 150 µL of 0.9% NaCl were pipetted per well, 3 µL from each sample or standard curve and 150 µL BCA-mix (1:8 ratio of reagent A and B) were added. The plate was then incubated at 37ºC for 30-45 min and the absorption at 560 nm was measured with the TECAN reader. The results were then compared to the standard curve and the final quantification was extrapolated.

2.3.3 SDS-PAGE

SDS-PAGE (sodium dodecyl sulphate-polyacrylamide gel electrophoresis) was used to separate the extracted proteins by size. 20 µg of total protein were mixed with 2x loading buffer (250 mM Tris-HCl pH6.9, 20% Glycerol, 4% SDS, 10% Mercaptoethanol, 0.01% Bromophenolblue, 5% MilliQ water), boiled at 90ºC for 5 min and loaded onto the gel. Each gel contained two parts, an upper stacking gel (12.92% Acrylamide/Bisacrylamide-30%, 24.8% 0.5M Tris-HCl pH6.9, 0.99% SDS-10%, 0.5% APS-10%, 0.1% TEMED) and a lower running gel (27.6%-50% Acrylamide/Bisacrylamide-30%, 25% 1.5M Tris-HCl pH8.9, 1% SDS-10%, 0.33% APS-10%, 0.07% TEMED). The percentage of AA/BA depends on the size of your protein of interest, higher percentage of AA/BA resolves smaller proteins and

vice versa. The gels ran at 100 V for 15 min until the samples entered the running gel, and then at 120 V for another 50-60 min.

2.3.4 Western blot

Once proteins were separated by size, they were transferred to a 0.2 μm nitrocellulose membrane using a wet blot system in order to make them accessible to antibody detection. Each stack was composed of two sponges, 4 Whatman papers, the gel, and the membrane. The transfer was run at 50 V for 90 min, or at 20 V overnight at 4ºC for bigger proteins. Membranes were blocked in 5% BSA in TBS-T buffer (20 mM Tris-HCl pH7.5, 150mM NaCl, 0.1% Tween20) for at least one hour at RT and incubated overnight with the primary antibody at 4ºC. The next day, membranes were washed three times for 5 min each with TBS-T and incubated with the corresponding fluorescent-labeled secondary antibody for one hour at room temperature protected from the light. Membranes were washed again 3 times and scanned with LI-COR.

2.3.5 Analysis

Image Studio Lite Version 5.2.5 software was used to analyze the images obtained from LI-COR. The signal intensity of the band corresponding to the protein of interest was normalized against the Actin beta (ACTB) signal from the same sample. Again, the statistical analysis was done with GraphPad Prism version 7.02.

2.3.6 Material used for Protein work

2.3.6.1 Chemicals and reagents used for protein extraction, quantification and western blot

Chemicals/Reagents	Cat. No.	Company
Acrylamide/Bisacrylamide 30%	A0951.0500	PanReac AppliChem
Albumin Fraction V 98% (BSA)	8076.2	ROTH
Ammonium persulfate (APS)	9592.2	ROTH
Beta-Mercaptoethanol	A1108.0100	AppliChem
Bromophenolblue	B6131	Sigma-Aldrich
Protease inhibitor cocktail tablets	11836170001	Roche
Ethylenediamine tetraacetic acid (EDTA)	E5134	Sigma-Aldrich

Glycerol	G8773	Sigma-Aldrich
Glycine	10119CU	VWR Chemical
Methanol	M/4000/PC17	Fisher Chemical
NP-40 IGEPAL	198596	Biomedicals
Pierce BCA Protein Assay Kit	23227	Thermo Scientific
SDS pellets	CN30.2	ROTH
Sodium Chloride	31434-1KG-M	Sigma-Aldrich
Sodium Deoxycholate	D5670	Sigma-Aldrich
TEMED	2367.3	ROTH
Trizma® base ($C_4H_{11}NO_3$)	T1503-1KG	Sigma-Aldrich
Tween® 20 ($C_{58}H_{114}O_{26}$)	A1389	Applichem

Table 2.12. Chemicals and reagents used for protein extraction, quantification and western blot.

2.3.6.2 Materials used for protein extraction, quantification and western blot

Material	Cat. No.	Company
96 well flat bottom transparent plate	655101	Greiner BioOne
KontesTM Pellet Pestle™ Cordless Motor		Sigma-Aldrich
Lids for 96 well plate	656190	Greiner BioOne
Nitrocellulose membrane 0.2 µm	1620112	BIORAD
Pellet pestles polypropylene	Z359947	Sigma-Aldrich
SONOPLUS	HD2070	BANDELIN
TECAN Spark		TECAN

Table 2.13. Materials used for protein extraction, quantification and western blot.

2.3.6.3 Primary antibodies used for Western blot

Antibody	Cat. No.	Company	Dilution	Predicted size
ACTB	A5441	Sigma	1:10000	42 kDa
ApoB	ab20737	Abcam	1:250	500 kDa
ApoE	ab1906	Abcam	1:500	36 kDa
ApoER2	ab108208	Abcam	1:500	110 kDa
ApoJ (CLU)	AF2747_SP	Novus	1:500	52 kDa
ATXN2	21776-1-AP	Proteintech	1:500	150 kDa
CALB1	13176	Cell Signaling	1:1000	30 kDa
CASP3	9665	Cell Signaling	1:1000	31.5 kDa
GFAP	ZO334	Dako	1:2000	50 kDa
GPNMB	AF 2330	Biotechne	1:500	64 kDa
IBA1	019-19741	Wako	1:2000	17 kDa
NeuN	ABN78	Millipore	1:1000	41 kDa
PCBP1	14523-1-AP	Proteintech	1:250	37.5 kDa
PCBP2	PA5-22350	Thermo Scientific	1:250	39 kDa
PGRN	AF 2557	Biotechne	1:250	63.5 kDa
PQBP1	A302-802A-M	Biomol	1:500	38 kDa

PTBP1	32-4800	Thermofisher	1:250	56 kDa
PURA	ab79936	Abcam	1:250	35 kDa
RELN	ab78540	Abcam	1:500	387 kDa
RIPK1	3493S	Cell Signaling	1:500	75 kDa
TDP43	ab41881	Abcam	1:1000	45 kDa
VGLUT1	135 011	Synaptic Systems	1:5000	62 kDa
VLDLR	AF2258	R&D Systems	1:500	96 kDa
YBX1	ab12148	Abcam	1:500	36 kDa

Table 2.14. Primary antibodies used for western blot and their predicted size.

2.3.6.4 Secondary antibodies for western blot

Antibody	Cat.No.	Company	Dilution
IRDye 680RD goat anti-mouse	926-32220	LI-COR	1:10000
IRDye 800CW donkey anti-goat	926-32214	LI-COR	1:5000
IRDye 800CW goat anti-mouse	926-32210	LI-COR	1:10000
IRDye 800CW goat anti-rabbit	926-32211	LI-COR	1:10000

Table 2.15. Secondary antibodies used for western blot.

2.4 Immunohistochemistry and Immunocytochemistry

2.4.1 Perfusion and tissue processing

Mice were anesthetized with an overdose of Ketaset (300 mg/kg) and Domitor (3 mg/kg) by an intraperitoneal injection. To assess the anesthetic depth the withdrawal reflex was monitored. Intracardial perfusion was done with PBS (137 mM NaCl, 2.7 mM KCl, 10 mM Na_2HPO_4, 1.8 mM KH_2PO_4) followed by 4% paraformaldehyde (PFA) in 0.1 M PBS for at least 5 min each. The brain, cerebellum, spinal cord and liver were dissected and post-fixed overnight in 4% PFA at 4ºC. Samples were then immersed in 30% sucrose until they sank, frozen, cut with a cryostat in 30-µm-thick slices, and kept in cryoprotection solution (30% ethylene glycol, 25% glycerin, 0,01% sodium azide in 0.1 M PBS) at -20 °C until used.

2.4.2 Staining – Immunohistochemistry and Immunocytochemistry

All immunohistochemistry was done in free-floating 30 µm sections. The selected tissue sections from WT and mutant animals were washed three times for 5 min each in PBS, blocked in blocking buffer (5% Goat Serum 0.03% Triton X-100 in PBS) at RT for 1 hour, and incubated with primary antibodies overnight

at 4ºC with soft shaking. The next morning, the samples were washed three times in PBS and incubated with the corresponding secondary antibodies and DAPI at RT for one hour protected from the light. Last step was a series of three 5 min washing steps in PBS followed by mounting the samples on SuperFrost Plus slides with Mountant PermaFluor mounting media and storage at 4ºC.

The protocol to stain organotypic cell cultures (OTC) was similar to the one followed for tissue. In this case, the slices were growing on milli-cell membranes and, after fixing with cold 4% PFA and washing three times with PBS, the membranes were cut around the tissue and the resulting pieces were moved to a 12-well plate. The samples were then permeabilized and blocked overnight at 4ºC (~12 hours) with 0.5% Triton X-100, 20% BSA, PBS. The next day, using blocking buffer (5% BSA in PBS), primary antibodies were diluted and the samples were again incubated overnight at 4ºC. They were washed three times for 5 min each with cold PBS and incubated with the corresponding secondary antibodies at room temperature for 3 hours. Three more washing steps were performed using cold PBS and samples were mounted carefully on SuperFrost Plus slides with Mountant PermaFluor mounting media and kept at 4ºC.

Finally, immunocytochemistry was performed with fixed cells grown on poly-D-lysine (0.1 mg/mL) treated glass slides. Cells were fixed with 4% PFA at RT for 20 min, washed 3 times with DPBS, permeabilized with 0.1% Triton X-100 and blocked with 5% BSA for 30 min at RT. Primary antibodies were diluted in blocking solution and samples were incubated overnight at 4ºC with soft shaking. The next day, the slides were washed three times with 1x PBS and incubated with the corresponding secondary antibodies and DAPI for 1 hour at RT protected from the light. Samples were washed three times, mounted using Mountant PermaFluor mounting media, and kept at 4ºC.

2.4.3 Imaging and image processing

Images from the different staining were done with a Nikon Eclipse TE200-E confocal microscope. In all cases, Z-stacks were done and processed with FiJi (Schindelin et al 2012). Photoshop CS5.1 was used to generate the final figures and compositions.

2.4.4 Material used for Immunohistochemistry and Immunocytochemistry

2.4.4.1 Reagents and chemicals used for perfusion, processing of the tissue and immunohistochemistry

Reagent/Chemical	Cat. No.	Company
4 ',6-diamidino-2-phenylindol (DAPI)	D9542-5mg	Sigma-Aldrich
di-Potassium hydrogen phosphate (KH_2PO_4)	A3620	Applichem
di-Sodium hydrogen phosphate (Na_2HPO_4)	106559	Merck
Domitor (1 mg/mL)	779-376	Orion Pharma
Ethylenglycol ($C_2H_6O_2$)	A1643,1000	Applichem
Glycerin ($C_3H_8O_3$)	G8773	Sigma-Aldrich
Ketaset (100 mg/mL)	5841328	Zoetis
Mountant, PermaFluor	TA-030-FM	Thermo sicentific
Normal goat serum	G9023 - 10ml	SIGMA
Paraformaldehyde	16005	Sigma-Aldrich
Potassium chloride (KCl)	A2939	Applichem
Sodium azide (NaN_3)	S8032	Sigma-Aldrich
Sodium chloride (NaCl)	31434	Sigma-Aldrich
Sucrose ($C_{12}H_{22}O_{11}$)	84100	Sigma-Aldrich
Triton® X-100 ($C_{30}H_{60}O_9$)	282103	Sigma-Aldrich

Table 2.16. Reagents and chemicals used for perfusion, tissue processing and immunohistochemistry

2.4.4.2 Material and instruments used for processing the tissue and imaging

Material	Cat. No.	Company
Cryostat	CM3050 S	Leica
Confocal microscope Nikon eclipse	TE2000-E	Leica

Table 2.17. Material and instruments used for tissue processing and imaging.

2.4.4.3 Primary antibodies used for immunohistochemistry and immunocytochemistry

Antibody	Cat. No.	Company	Dilution
1C2	MAB1574	Millipore	1:800
AHNAK	HPA026643	Atlas Antibody	1:500
ApoB	ab20737	Abcam	1:250
ATXN2	611378	BD Transduction	1:50
CALB1	C9848	Sigma	1:1000
CALBq	13176	Cell Signaling	1:1000
GFAP	ZO334	Dako	1:1000
IBA1	019-19741	Wako	1:1000
NeuN	ABN78	Millipore	1:1000

NF-H	18934-1-AP	Proteintech	1:500
P62/SQSTM1	sc25575	Santa Cruz	1:50
PABP1	ab21060	Abcam	1:100
PCBP1	14523-1-AP	Proteintech	1:100
PCBP2	PA5-22350	Thermo Scientific	1:100
PURA	ab79936	Abcam	1:500
RELN	ab78540	Abcam	1:500
TDP43	ab41881	Abcam	1:100
TIA1	sc-1751	Santa Cruz	1:100
VGLUT1	135 011	Synaptic Systems	1:1000
VLDLR	AF2258	R&D Systems	1:500

Table 2.18. Primary antibodies and dilutions used for immunohistochemistry and immunocytochemistry.

2.4.4.4 Secondary antibodies used for immunohistochemistry

Antibody	Cat. No.	Company	Dilution
Alexa Fluor 488 goat anti-mouse IgG	A11029	Invitrogen	1:1000
Alexa Fluor 488 goat anti-rabbit IgG	A11034	Invitrogen	1:1000
Alexa Fluor 565 rabbit anti-goat IgG	A11079	Invitrogen	1:1000
Alexa Fluor 568 donkey anti-sheep IgG	A21099	Invitrogen	1:1000
Alexa Fluor 568 goat anti-rabbit IgG	A11036	Invitrogen	1:1000

Table 2.19. Secondary antibodies used for immunohistochemistry and immunocytochemistry.

2.5 Cell culture

All cell culture work was done in a sterile hood and cells were kept in standard conditions (5% CO_2, 37ºC).

2.5.1 Immortalized cell lines

2.5.1.1 SH-SY5Y and Starvation time-course

The human neuroblastoma derived cell line, SH-SY5Y (Biedler et al 1978), previously transduced with shRNA against ATXN2 mRNA or non-targeted shRNA (Sen et al 2016) were used to evaluate the effect of loss-of-function in an in-vitro model. They were cultured with DMEM, 10% FBS, and Puromycin as a selective antibiotic (1 µg/mL). Starvation time-course was performed in 6-well plates with $5x10^5$ cell per well. The day after seeding, the medium was changed to HBSS or

complete medium in case of the control. At specified time points, cells were collected and RNA was extracted for further analysis.

2.5.1.2 BV2 – NaArs and LPS treatment

Murine microglia cell line BV2 (Blasi et al 1990) was used as an in-vitro model to study the effect of ATXN2 CAG expansions in this cell type. Cells were cultured in DMEM supplemented with 10% FBS, 1x L-glutamine and 1x Pen/Strep. Two different stressors were used. To study the formation of stress granules, BV2 were seeded at $5x10^4$ cells/well on poly-D-lysine (0.1 mg/mL) treated glass slides in a 12-well plate and the next day were stressed with 0.25 mM Sodium Arsenite (NaArs) for 15 min or 30 min. Cells were fixed with 4% PFA at RT for 20 min and washed three times with DPBS before staining them. The second stressor used was Lipopolysaccharide (LPS). $15x10^4$ cells were seeded per well in a poly-D-linsine coated 6-well plate and next day were transfected with either the empty vector myc, myc-Atxn2-Q22, or my-Atxn2-Q79 using lipofectamine 3000 following the manufacture's protocol. The medium was changed right before the transfection. The corresponding plasmid at 1 µg/mL was mixed with the P3000 reagent and Opti-MEM. The mixture was mixed softly, shortly spun down and keept at RT for 5 min. Mean while, Lipofectamine 3000 was mixed with Opti-MEM. After the incubation time, the entire plasmid containing solution was added into the lipofectamine, mixed and incubated at RT for 15 min before adding 250 µL per well. After 36 hours the medium was changed and cells were challenged with different concentrations of LPS to assess their response. The next day, after 24 hours, cells were collected and protein and RNA were extracted from each well.

2.5.2 Primary cultures

2.5.2.1 Mouse Embryonic Fibroblasts – generation and Poly IC treatment

Mouse embryonic skin fibroblasts from *Atxn2*-CAG100-Knock-in mouse line were isolated around embryonic day 17 from heterozygous crosses (Lastres-Becker et al 2016). In order to synchronize the cycle, females were kept in cages with paper chipping from males for few days before the male was moved into the

cage. The pregnancy was followed and at day 17 females were decapitated and the pups were carefully separated from the placenta and surrounding membranes. During the procedure, the embryos were kept in DPBS supplemented with 5x Pen/Strep. One by one, each embryo was decapitated, dissected and a piece of tail was collected to run the genotyping PCR. Then, the tissue was minced; 5 mL of dissection medium (DMEM, 5x Pen/Strep) were added and transferred to a 15 mL falcon tube. 2 mL of 0.05% Trypsin-EDTA were added and incubated at 37ºC for 10 min with occasional shaking. To stop the digestion, 4 mL of medium (DMEM, 15% FBS, 1x L-glutamine, 1x Pen/Strep) were added and tubes were centrifuged at 450 xG for 5 min. Supernatant was removed and cells were re-suspended in 12 mL and seeded in a T-75 flask. Once the genotype was determined and the culture was confluent, MEFs were split 1:3 and frozen.

MEFs were then stressed with poly(IC) following the protocol from (Reineke et al 2018a). They were seeded on top of poly-D-lysine treated slices in a 12 well plate at a confluence of 30.000 cells/well. The next day, they were treated with 100 ng of poly(IC) for 6 hours. After the treatment they were fixed with 4% PFA at RT for 20 min, washed with DPBS three times and further processed.

2.5.2.2 Primary mixed glia culture

P0-P3 pups from heterozygous crosses were used to establish the primary mixed glia cultures (Lian et al 2016). The first part of the protocol was performed in a semi-sterile hood and, once the cells were disaggregated, moved to a sterile hood. The pups were quickly decapitated, the brain was dissected in a sterile 6 cm petri dish, meninges were removed and the cortex and hippocampus were isolated. After moving the tissue to a fresh dish, it was minced using scissors in 5 mL of cold dissection medium (HBSS, 1 M HEPES, 3 gr glucose, 1x Pen/Strep) and moved to a 50 mL falcon. The tissue pieces were then allowed to sediment, the medium was carefully removed and 10 mL of 0.05% Trypsin-EDTA was added. Tubes were then incubated at 37ºC for 15 min and occasionally stirred. To stop the digestion, 10 mL of culture medium (DMEM, 10% FBS, 1x L-Glutamine, 1x Pen/Strep) was added and carefully mixed by inversion. After one minute, 750 µL of 1mg/mL DNase were added to digest the released DNA during

the procedure. Samples were then centrifuged at 400 xG for 5 min, the supernatant was removed and cells were resuspended in 5 mL of warm culture medium. They were seeded on a poly-D-lysine coated T-75 flask in a final volume of 15 mL. The next day, the medium was changed in order to remove debris and then changed every 5 days. After approximately two weeks the culture showed a bottom layer of astrocytes while microglia and some oligodendrocytes were growing on top. To collect microglia, the flasks were tapped vigorously for 10-15 min and the medium with floating cells was moved to another coated T-75 flask, resulting in a purified microglia primary culture.

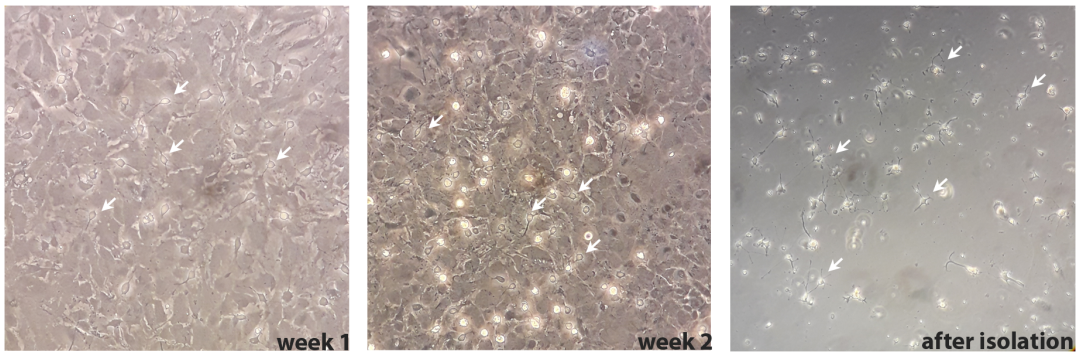

Figure 2.1. Primary mixed glia cultures at different time points and after isolating microglia. Images were acquired with a bright field microscope.

2.5.2.3 Organotypic slice cultures

Organotypic cultures (OTC) from cerebellum were established from P15-17 pups, once the Purkinje neurons had reached their final position. The protocol was carried out in a semi-sterile hood. Pups were decapitated nearby the hood and once the brain was isolated, moved to the semi-sterile hood in a 6 cm petri dish. The cerebellum was dissected from the rest of the brain and fixed on the vibratome-block with a small drop of tissue glue. The block was placed in the vibratome table, filled with dissection medium (MEM, 1x Glutamax, 45% glucose, 1 M HEPES, 1x Pen/Strep, 1 N NaOH, pH 7.3-7.4) and the cerebellum was cut in sagittal sections of 400 µm at 0.14 mm/s. The sections were rescued from the table, moved to a sterile petri dish and transferred to a milli-cell previously equilibrated with 1 mL of dissection medium. The milli-cell containing maximum 3 slides was then moved to a well of a 6-well plate containing 1 mL of culture medium pre-warmed (MEM, BME, heat-inactivated Normal Horse Serum, 1x Glutamax, 1 M HEPES, 1x Pen/Strep, 7.5% Bicarbonat, pH 7.29-7.31). Medium

was changed every 3 days removing only part of the old medium and adding 1 mL of fresh culture medium. After minimum one week of culture, after the slices had flattened, cultures were processed for staining as previously described.

2.5.3 Material used in cell culture

2.5.3.1 Chemicals and reagents

Reagent/Chemical	Cat. No.	Company
0.05% Trypsin-EDTA	25300-054	Gibco
Basal Medium Eagle (BME)	41010026	Gibco
D-(+)-Glucose solution 45%	G8769	Sigma-Aldrich
Deoxyribonuclease I (DNase) 10kU	D4527	Sigma-Aldrich
Dulbecco's Modified Eagle Medium (DMEM)	21969035	Gibco
Dulbecco's Phosphate Buffered Saline (DPBS)	14190094	Gibco
Fetal Bovine Serum Qualified, One shot (FBS)	A3160801	Gibco
GlutaMAX	35050061	Gibco
Hank's Balanced Salt Solution (HBSS)	2402091	Gibco
HEPES 1 M	H0887	Sigma-Aldrich
L-glutamine 200mM	25030-024	Gibco
Lipofectamine 3000	L3000015	Themo Fisher
Lipopolysaccharide from E. Coli (LPS)	tlrl-eblps	InvivoGen
Minimum Essential Medium (MEM)	21575-022	Gibco
Normal Horse Serum (NHS)	26050-088	Invitrogen
Opti-MEM	11058021	Gibco
P3000 (part of Lipofectamine 3000 kit)	L3000015	Themo Fisher
Paraformaldehyde 4% in PBS pH 7.4 (PFA)	11762.01	MORPHISTO
Penicillin Streptomycin (Pen/Strep)	15140122	Gibco
Poly D- Lysine 1 mg/ml in H2O	A-003-E	Millipore
Poly IC	tlrl-picwlv	InvivoGen
Puromycin dihydrochloride	P8833	Sigma-Aldrich
Sodium Arsenite (NaN3)	S-8032	Sigma-Aldrich
Sodium bicarbonat	25080-060	Invitrogen
Sodium hydroxide (NaOH) 1 N	01-830.1000	KMF OptiChem
Ultra pure distilled Water DNase/RNase free	10977-035	Invitrogen

Table 2.20. Chemicals and reagents used in cell culture and primary cell culture

2.5.3.2 Material

Material	Cat. No.	Company
Cell culture bench		Envirco
Cell culture bench Lamin Air	HB2448	Heraeus
Cell culture bench HSC Advantage		Thermo Scientific
CO_2 incubator HERAcell 240i		Thermo Scientific

Vibratome MICROM	HM 650V	Leica

Table 2.21. Material used in cell culture and OTC

2.5.3.3 Constructs used for transfection

Construct	Selection Antibiotic	Source	Cat. No./ Ref.
ATXN2-22Q-Myc (pCMV)	Ampicillin	Custom made	Nonis *et al* 2008
ATXN2-74Q-Myc (pCMV)	Ampicillin	Custom made	Nonis *et al* 2008
Control-Myc (pCMV)	Ampicillin	Clontech	631604

Table 2.22. Constructs used for transfection in cell culture

2.6 Statistical analysis

Statistical tests were performed as unpaired Student's t-test using GraphPad Prism software version 7.02 using the Welch t-test which assumes that both groups of data are sampled from Gaussian populations, but does not assume those two populations have the same standard deviation. Figures displaying mean values and standard error of the mean (SEM). Values $p<0.05$ were considered significant and marked with asterisks: $p<0.05$ *, $p<0.01$ **, $p<0.001$ ***, $p<0.0001$ ****.

One-way or two-way ANOVA tests were also used for behavior or cell culture data analysis when comparing more than one variable.

3 RESULTS

Part 1 – The role of Ataxin 2 in SCA2 and ALS

3.1 Characterization of the novel *Atxn2*-CAG100-Knock-in mouse line

There is a lack of mouse models availability to study the endogenous effect of the CAG expansion in *Atxn2* gene as a cause of SCA2 and risk factor for ALS. Melanie Halbach started the characterization of the *Atxn2*-CAG100-Knock-in mouse line. This mouse model shows a significant reduction in lifespan, dying at the age of 14 months, together with a reduction in weight and substantial motor deficits. ATXN2 aggregates were also found at late stage (14 months) in different areas like the brain stem, pons, cerebellum and spinal cord. Overall, this model recapitulates the symptomatology of SCA2 patients, could help to understand its pathology and design therapies.

In order to better characterize the phenotype of these animals and the molecular changes caused by the introduction of 100 CAGs in the *Atxn2* gene, further behavioral and molecular biology experiments were performed.

3.1.1 The completion of Rotarod and Open field data shows motor deficits

The Rotarod test is widely used to assess motor behavior (Jones & Roberts 1968). The height of the rod is low enough to prevent lesions caused by a fall but high enough to induce avoidance of the fall. Therefore, measuring the time of the animal staying on the accelerating rod provides a measure of their balance, coordination, physical condition and motor planning. The performance of the *Atxn2*-CAG100-KIN animals showed a significant and stable deficit starting around 5 months of age, worsening over time (Figure 3.1).

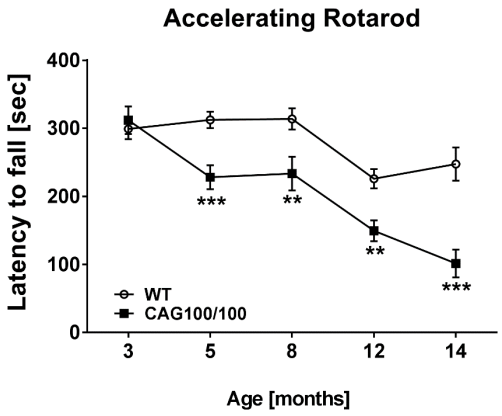

Figure 3.1. Rotarod performance of the CAG100-KIN animals at different ages compared to their WT littermates. A significant decrease in time staying on the accelerating rod for the CAG100/100 (*Atxn2*-CAG100-KIN) animals is evident starting at the age of 5 months and it worsens over time.

Another useful test to evaluate the motor behavior is the Open field test (Drai et al 2001). It allows us to assess general locomotor activity levels, anxiety and willingness to explore. Here, only six parameters are shown to highlight the assessment of spontaneous activity and motor impairment starting at the age of 3 months. Specifically the vertical parameters of movement, activity and time were significantly affected over time indicating problems in balance (Figure 3.2).

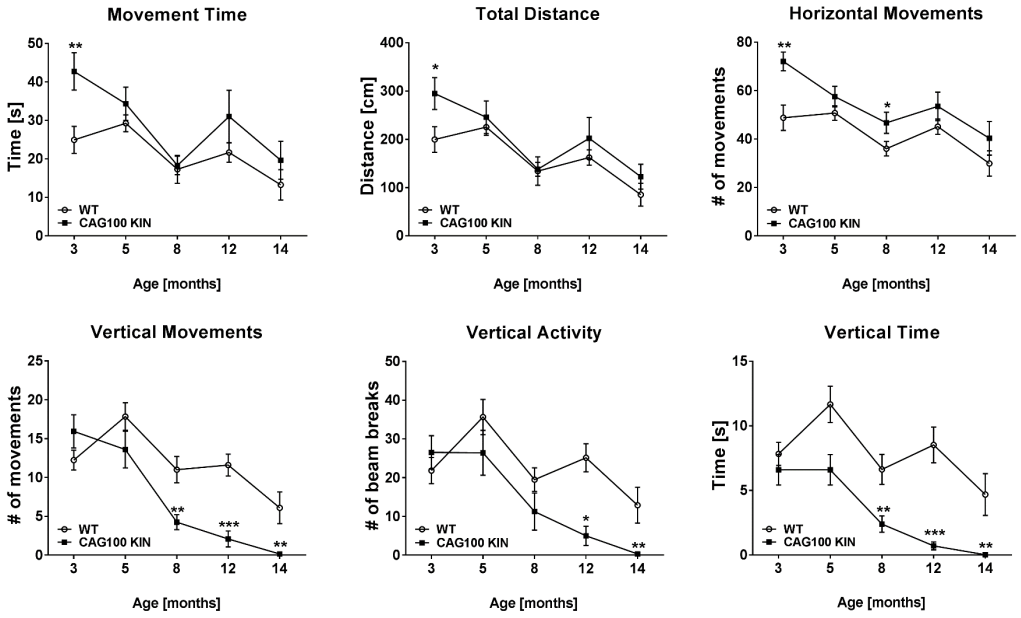

Figure 3.2. Horizontal and vertical activity assessment with Open field test. Overall, horizontal movements are increased in the *Atxn2*-CAG100-KIN animals while the vertical movements are impaired.

3.1.2 Grip strength

The grip strength test is an easy way to evaluate the muscular strength of rodents (mouse or rat) and to assess the effect of neurodegenerative diseases on muscular degeneration (Meyer et al 1979). This is achieved by measuring the maximal peak force generated by a mouse, in this case, when it is gently being pulled by its tail. To do that, age and sex matched pairs from 3 to 13 months of age were assessed; ten measurements were recorded per animal.

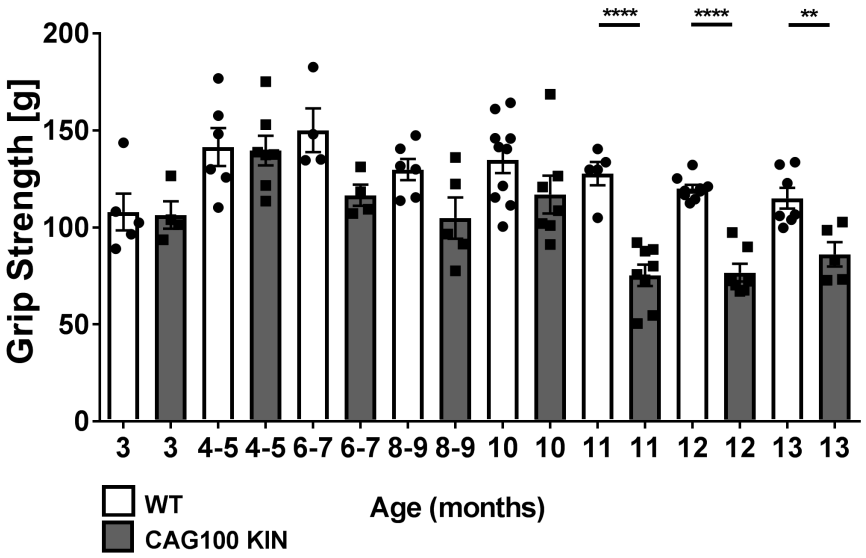

Figure 3.3. Grip strength from 3 to 13 month old CAG-KIN animals compared to their WT littermates. At the age of 11 months there is a significant decrease in the fore limb grip of the CAG100 animals compared to the WT. Un-paired t-test with Welch's correction for 11-months (p-value <0.0001), 12-months (p-value <0.0001) and 13-months (p-value 0.0069) groups.

A significant decrease in the maximal forelimb effort was detected ($p < 0.001$; $F = 10.219$ with 7 degrees of freedom; ANOVA). At the age of 11 months the forelimb strength started to decrease ($p < 0.001$; $F = 9.964$ with 15 degrees of freedom; two-way ANOVA) and was constant until 13 months while the WT remained unaltered.

3.1.3 Paw print

Paw print or foot print test were used to analyze the gait in rodents between the WT and mutant in order to assess potential motor deficits (Carter et al 1999). To perform this test, the paws are coated with non-toxic ink and the animals are allowed to freely walk over a sheet of white paper through a dark tunnel. The

generated pattern is then analyzed.

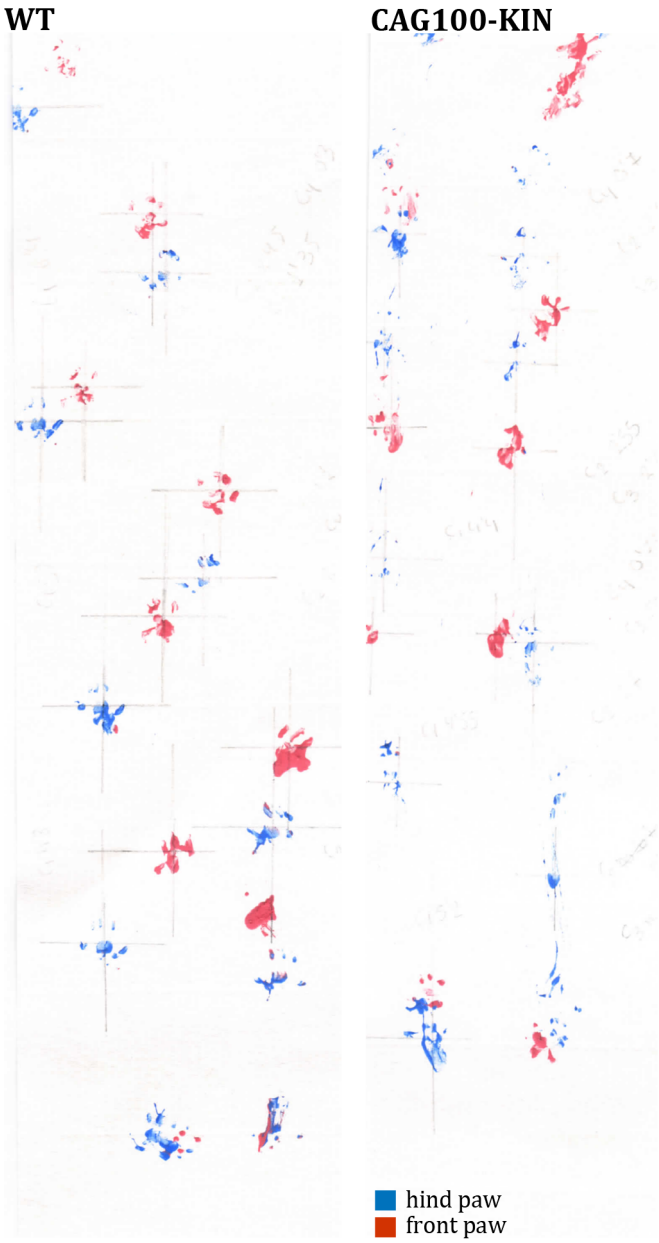

Figure 3.4. Examples of the walking pattern generated during the paw print test. Front paws were colored in red and hind paws in blue. On the left image, the more organized steps from a WT mouse can be appreciated while on the right the altered walking steps from an *Atxn2*-CAG100-KIN animal can be observed.

After several tests with 12 to 14-month old *Atxn2*-CAG100-KIN animals, it was evident that the irregularity of the steps displayed by the mutants made the analysis not possible. In the right panel of the Figure 3.4, the walking difficulties that these animals suffer at the end stage of the disease are easy to appreciate.

3.1.4 Histological analysis of the pathology progression in the cerebellum over time shows increase ATXN2 aggregation and co-localization with PABP1

Although detectable motor symptoms start to be evident around 6 months of age, molecular events can be detected earlier. To better understand the progression of the disease, immunohistochemistry was performed using samples from 3, 6, and 14-month-old animals. A well-known ATXN2 interactor, Poly(A)-binding protein (PABP1) (Mangus et al 1998) was used as a control since it is known to co-aggregate with ATXN2 during cellular stress into stress granules (SG).

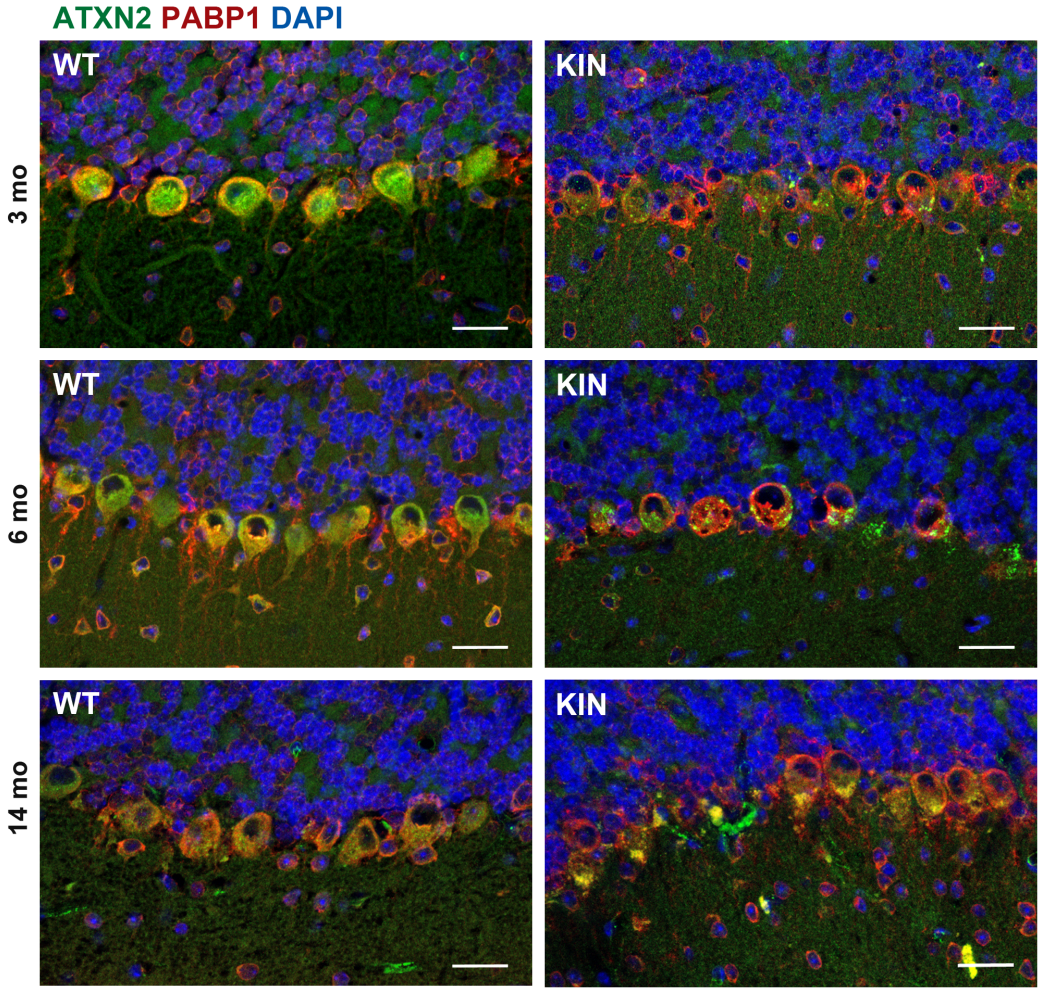

Figure 3.5 ATXN2 (green), PABP1 (red) and DAPI (labeling the nuclei in blue) staining in age- and sex-matched pair show an increasing amount and size of co-aggregates in Purkinje neurons over time. The staining shows the progression of the pathology at the molecular level with discrete aggregates at the early age of three months that increase with age until showing a plug-like structure at the apical base of the Purkinje neurons in 14-month-old animals. Scale bar represents 25 µm.

One of the most impressive results is the early aggregation of ATXN2 (green), already occurring at the age of 3 months, before any behavioral symptoms can be detected. While the cytoplasmic distribution of ATXN2 in the WT animals is constant from 3 to 14 months of age, its aggregates increase in size in the *Atxn2*-CAG100-KIN becoming a plug-like structure at an old age. This could affect the transport of other proteins and mRNA towards the dendrites. Despite the presence of smaller aggregates in the younger samples, the co-localization of PABP1 starts to be detectable around 6 months of age and becomes easily visible at 14 months. These data could suggest that other proteins are sequestered into aggregates over time, thus worsening the pathology due to their loss of function.

3.1.5 Histological analysis of the Purkinje in the cerebellum of *Atxn2*-CAG100-Knock-in over time compared to symptomatic *Atxn2*-Knock-out shows disconnection of the Purkinje at old age

One hallmark of neurodegenerative disorders is the progressive loss of different neuronal types like the predominant degeneration of the dopaminergic nigrostriatal system in Parkinson's disease (PD). The atrophy of the cerebellum is, therefore, a hallmark for spinocerebellar ataxias (Estrada et al 1999, Xia et al 2013). After detecting ATXN2 aggregates at the early age of 3 months and, taking advantage of the well-characterized Purkinje marker calbindin 1 (CALB1) (Barski et al 2003, Whitney et al 2008), we aimed to determine if there was detectable neuronal loss in the cerebellum of the *Atxn2*-CAG100-KIN mouse model. We used the same age points (3, 6, 14 months) as in prior sections to compare the *Atxn2*-CAG100-KIN mouse to the *Atxn2*-Knock-out (*Atxn2*-KO) mouse.

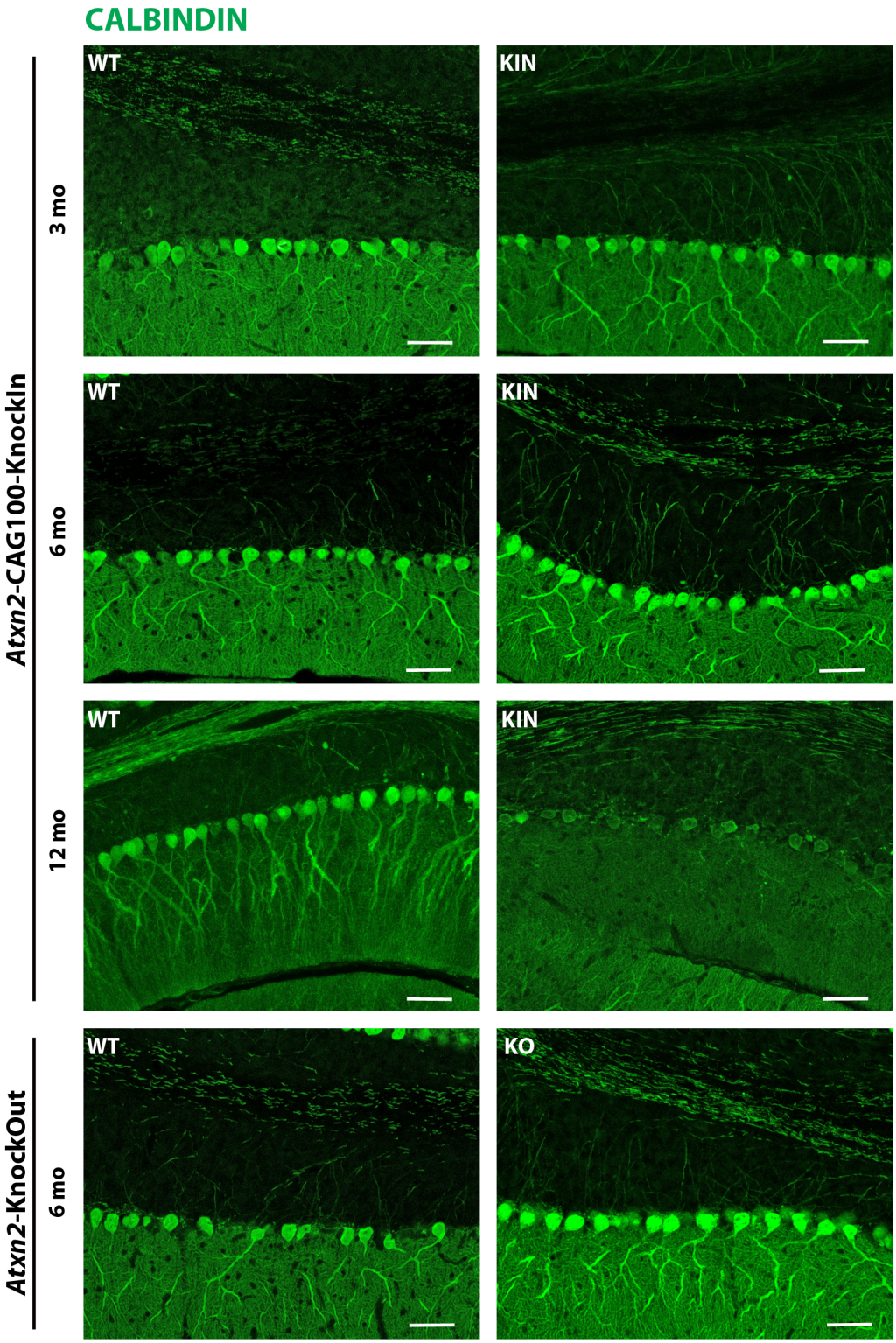

Figure 3.6 Calbindin staining at different ages of the *Atxn2*-CAG-100-Knock-in model compared to the *Atxn2*-Knock-out at 6 months. There was no obvious loss of Purkinje neurons over time since the soma was still evident at 14 months but a neuronal disconnection became evident in old age showing crisscrossing of the axons compared to the WT. Scale bar represents 25 µm.

As mentioned in the introduction, the cerebellar structure is composed of: a molecular layer, where the dendritic tree of the Purkinje neurons (PN) is found together with other neuronal types; the Purkinje layer, where the cell bodies of these neurons are located; and the granular layer, mainly composed by the small granule neurons (GN). Staining with CALB1, the PN bodies can be visualized along with their dendritic tree and the axonal tracks going towards the cerebellar deep nuclei as a sole output. The most striking difference between stainings at different ages was the disconnection observed in the *Atxn2*-CAG100-KIN 14-month-old cerebellar section. The PN bodies were still visible but they appear disconnected and the axonal tracks were not as well organized as in the WT.

3.1.6 Defects in the input to the cerebellum: climbing fiber pathology in *Atxn2*-CAG100-KIN

Neurofilaments (NFs) are the main components of intermediate filaments in neurons and are essential in maintaining neuron structure. There are three different subunits: neurofilament protein L (low molecular weight, NF-L), M (medium molecular weight, NF-M) and H (high molecular weight, NF-H) (Hoffman & Lasek 1975). Moreover, abnormal expression levels, accumulation, or post-transcriptional modifications such as phosphorylation have been linked to neurodegenerative disorders like Alzheimer's disease (AD), PD and Amyotrophic lateral sclerosis (ALS) (Bridel et al 2019, Constantinescu et al 2019, Mattsson et al 2019, Mayeli et al 2019). Although they have been mainly described as crucial for axon structure, NFs can also be translocated to dendrites of specific neurons and seem to be important for proper dendritic arborization (Kong et al 1998, Zhang et al 2002). NF-L has also been associated with schizophrenia-associated behaviour (Yuan et al 2018) evidencing their role in synaptic plasticity. In order to study the neuronal structure in the cerebellum of the *Atxn2*-CAG100-KIN mice, immunohistochemistry for NF-H was performed using cerebellar slices from late stages of the disease (14 months) and compared to age- and sex-matched WT counterparts.

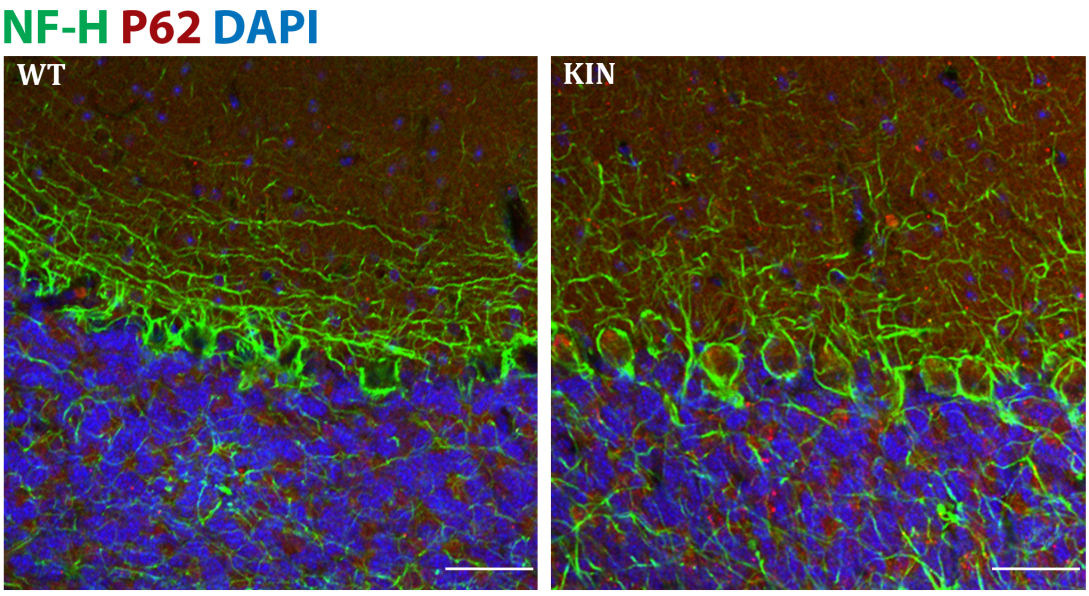

Figure 3.7. Immunohistochemistry for NF-H (green) and P62 (red) shows disorganization this intermediate filament in the *Atxn2*-CAG100-KIN and positive signal for P62 in the Purkinje soma. Scale bar represents 50 µm.

Histological analysis of the cerebellar samples at 14 months showed the disorganization of the NF-H close to the proximal molecular layer. This can suggest defective innervation of the climbing fibers from the inferior olive to the Purkinje neurons. The alteration of the climbing fiber input to the PN has been suggested as a common feature of spinocerebellar ataxias (Smeets & Verbeek 2016).

Climbing fibers are one of two inputs to the cerebellum. They arise from the inferior olive (IO) and innervate the proximal Purkinje dendritic tree with a one-to-one ratio. During development, the climbing fibers arrive at the cerebellum between embryonic day 15.5 and 16.5 and make contact with the PN. At this point, and until approximately postnatal day 7, each Purkinje is innervated by four to five climbing fibers. Only the winning climbing fiber will remain and it will displace the other ones (Kakegawa et al 2015, Watanabe & Kano 2011). A recent study by Uesaka *et al* showed how the expression of *Sema7a* is essential in the retrograde signaling to determine which climbing fiber will be the winner (Uesaka & Kano 2018, Uesaka et al 2014). Therefore, the expression levels of *Sema7a* were assessed in RNA samples from the cerebellum of the *Atxn2*-CAG100-KIN and *Atxn2*-KO models. In all conditions, a significant down-regulation was detected (Figure 3.8) suggesting that the loss of ATXN2 can cause problems in the cerebellar network (*Atxn2*-KO FC 0.8 p-value 0.005; 3 months

Atxn2-CAG100-KIN FC 0.7 p-value 0.013; 14 months *Atxn2*-CAG100-KIN FC 0.7 p-value 0.016).

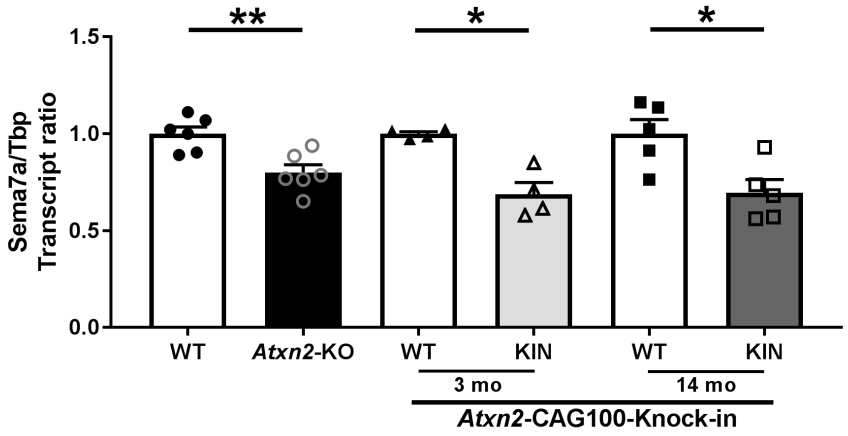

Figure 3.8. Transcript levels of Sema7a in the cerebellum of Atxn2-KO and Atxn2-CAG100-KIN models at different ages. A significant down regulation was detected in all conditions.

Moreover, climbing fiber deficits have been found in mouse models of SCA1, SCA7, SCA14 and SCA23. The deficits range from developmental changes to retraction of climbing fibers in adult mice. Alteration in the glutamatergic signaling has been found in SCA5 and SCA28, also pointing to a climbing fiber deficit and, as a result, in PN dysfunction (Smeets & Verbeek 2016). Climbing fiber pathology was found in the SCA2-58Q transgenic mice (Egorova et al 2018).

3.2 Proteome data set: RNA binding proteins appear up regulated

Prior to this thesis work and in order to gain a deeper insight into SCA2, the proteome data set was generated by free-label mass spectrometry using cerebellar and spinal cord samples of three 14-month-old *Atxn2*-CAG100-KIN mice and three age- and sex-matched WT. The most relevant commonly dysregulated proteins in the spinal cord and cerebellum involved RNA metabolism were further validated and investigated. Table 3.1 is a partial list of two categories related to RNA metabolism that are significantly affected in both tissues of the mouse model at late stage of the disease.

Category	Gene symbol	Protein	Sp. Cord FC	CB FC
Splicing	Dhx15	DEAH-Box Helicase 15	1.3	1.3
	Hcfc1	Host Cell Fctor C1	1.5	1.3

	hnRNPD	AU-Rich Element RNA Binding Protein1	1.5	1.6
	hnRNPE1	Poly(rC)Bining Protein 1	1.3	1.8
	hnRNPE2	Poly(rC)Bining Protein 2	1.3	1.4
	hnRNPF	Heterogeneous Nuclear Ribonucleoprotein F	1.6	1.2
	hnRNPH1	Heterogeneous Nuclear Ribonucleoprotein H1	1.2	1.2
	hnRNPL	Heterogeneous Nuclear Ribonucleoprotein L	1.2	1.2
	hnRNPLL	Heterogeneous Nuclear Ribonucleoprotein L Like	1.3	1.4
	hnRNPR	Heterogeneous Nuclear Ribonucleoprotein R	1.4	1.3
	hnRNPU	Polypyrimidine Tract Binding Protein 1	1.3	1.7
	Nhp2l1	Small Nuclear Ribonucleoprotein 13	0.74	0.71
	Numa1	Nuclear Mitotic Apparatus Protein 1	1.8	1.4
	Prpf19	Pre-mRNA Processing Factor 19	1.2	1.4
	Puf60	Poly(U) Binding Splicing Factor 60	1.3	1.3
	Sarnp	SAP Domain Containing Ribonucleoprotein	1.5	1.7
	Sf3a1	Splicing Factor 3a Subunit 1	1.4	1.4
	Srrm2	Serine/Arginine Repetitive Matrix 2	1.5	1.4
	Srsf1	Serin and Arginine Rich Splicing Factor 1	1.4	1.4
	Thrap3	Thyroid Hormone Receptor Associated Protein 3	1.3	1.5
	U2af2	U2 Small Nuclear RNA Auxiliary Factor 2	1.5	1.6
Stress Granule	Atxn2l	Ataxin 2 Like	1.6	1.3
	Ahnak	AHNAK Nucleoprotein	2	1.6
	Cirbp	Cold Inducible RNA Binding Protein	1.4	1.9
	Ddx1	DEAD-Box Helicase 1	1.2	1.3
	Ddx6	DEAD-Box Helicase 6	1.2	1.5
	Habp4	Hyaluronan Binding Protein 4	0.77	0.74
	Pura	Purine Rich Element Binding Protein A	0.62	0.80
	Syncrip	Synaptotagmin Binding Cytoplasmic RNA Interacting Protein	1.5	1.3
	Ybx1	Y-Box Binding Protein 1	1.7	1.4

Table 3.1 List of several common dysregulated peptides detected by free-label mass spectrometry. Fold change (FC) values for the spinal cord (Sp. Cord) and cerebellum (CB) samples are shown. The samples used to generate this data set were from animals of 14 months of age, WT n=3 and KIN n=3; analysis done with Perseus software.

RNA binding proteins (RBP) are a group of proteins with putative roles involving RNA metabolism that are part of the ribonucleoprotein complexes (RNP), and

are essential for gene expression (Kedersha et al 2013). A large number of them have been involved in neurodegenerative disorders like TDP43 in ALS or ATXN2 in SCA2. Therefore, it is of interest to further investigate the effect of the expanded ATXN2 with respect to RBPs and their functions.

3.3 Several RBPs transcript levels are altered in the *Atxn2*-CAG100-KIN mouse model

Since ATXN2 is an RNA binding protein and it is thought to play a role in translation (Mangus et al 1998, Satterfield & Pallanck 2006), the first hypothesis was that the expanded ATXN2 affected the mRNA levels of other RBPs, thus affecting their protein levels. In order to define this effect, several RBP transcripts were assessed by Q-PCR in the *Atxn2*-CAG100-KIN and *Atxn2*-KO mouse models, using samples from cerebellum and spinal cord at different ages.

3.3.1 AHNAK and AHNAK2 are strongly dysregulated in the proteome data set

AHNAK is a giant protein of 700 kDa also known as desmoyokin (Hashimoto et al 1993) that forms part of multi-protein complexes acting as a structural scaffold. Multiple protein interaction domains are scattered across the protein, especially at the C-terminal (Komuro et al 2004). It has been implicated in a broad range of cellular processes or pathways from the formation of the blood-brain barrier (Ballabh et al 2004, Boveri et al 2006, Gentil et al 2005), cell architecture and migration (Benaud et al 2004, Lee et al 2014, Lim et al 2013), to the regulation of calcium channels (Haase et al 2005, Jin et al 2019, Matza et al 2009, Matza et al 2008) and muscle repair (Huang et al 2007). AHNAK can be found in the nucleus, cytoplasm and plasma membrane (Benaud et al 2004, Masunaga et al 1995, Shtivelman et al 1992, Sussman et al 2001). Moreover, its mRNA has been found to re-localize to SG in stress conditions (Khong et al 2017) and it is one of the highest up-regulated proteins in the proteome data from the cerebellum (FC 1,6) and spinal cord (FC 2).

AHNAK2, or PLD4, is also a giant protein with approximately 600 kDa and shares several features with AHNAK, however its specific function is not known. This protein has been mainly described in cancer (Klett et al 2018, Lu et al 2017) and

also in lupus (Akizuki et al 2019). Most recently, it has been reported to be a genetic cause for Charcot-Marie-Tooth polyneuropathy in a Malaysian family (Tey et al 2019).

3.3.1.1 Ahnak transcript levels are up regulated in the spinal cord and cerebellum of 14-month-old *Atxn2*-CAG100-KIN model and not changed in the hemisphere or cerebellum at the younger ages

The transcript level of *Ahnak* was investigated at different ages in the cerebellum of *Atxn2*-CAG100-KIN animals and compared to their sex- and age-matched controls. A significant up-regulation (FC 1.33; p-value 0.003) was observed at old age, however no differences were detected in the younger (3 and 6 months) samples, nor in the Atxn2-KO (Figure 3.9, A). A significant up-regulation (FC 1.62; p-value 0.038) was detected in the spinal cord of the old *Atxn2*-CAG100-KIN (Figure 3.9, B) correlating with the higher up-regulation observed in the proteome data from the spinal cord (FC 2). Moreover, AHNAK has been reported to be significantly up-regulated after spinal cord injury (Von Boxberg et al 2006).

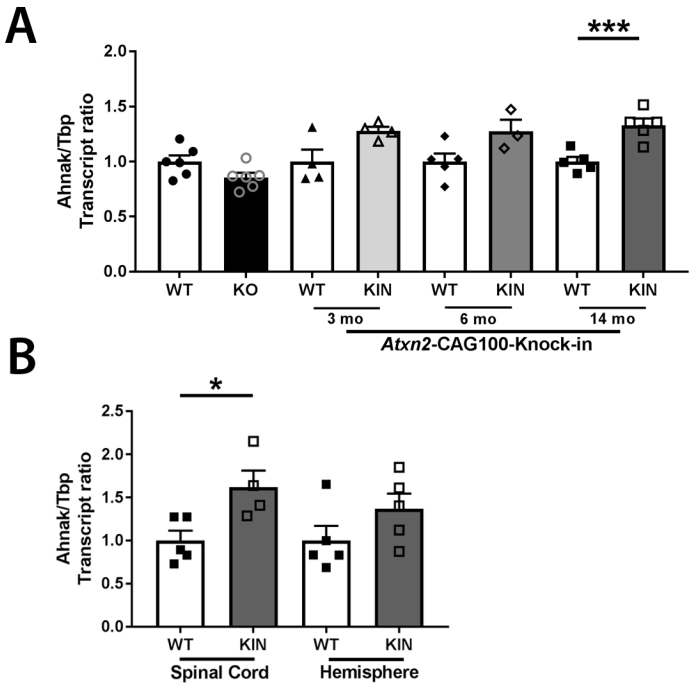

Figure 3.9. Ahnak transcript levels assessed by Q-PCR. (A) The transcript levels are significantly up-regulated in the 14 month old cerebellum of the *Atxn2*-CAG100-KIN mice compared to the age-matched controls. There are no differences in the levels of the *Atxn2*-KO and younger (3 and 6 month old) *Atxn2*-CAG100-KIN cerebellum. (B) A significant up-regulation was detected in the spinal cord samples of the 14-month-old *Atxn2*-CAG100-KIN animals.

3.3.1.2 *Ahnak2* transcript levels are down regulated in the spinal cord of 14 month old Atxn2-CAG-100 animals

The other member of the Ahnak family, Ahnak2, was also checked at the transcript level. Only a down-regulation in the spinal cord of the old *Atxn2*-CAG100-KIN animals was detected (FC 0.62 p-value 0.003) showing again a stronger affection in the spinal cord rather than in other regions of the CNS.

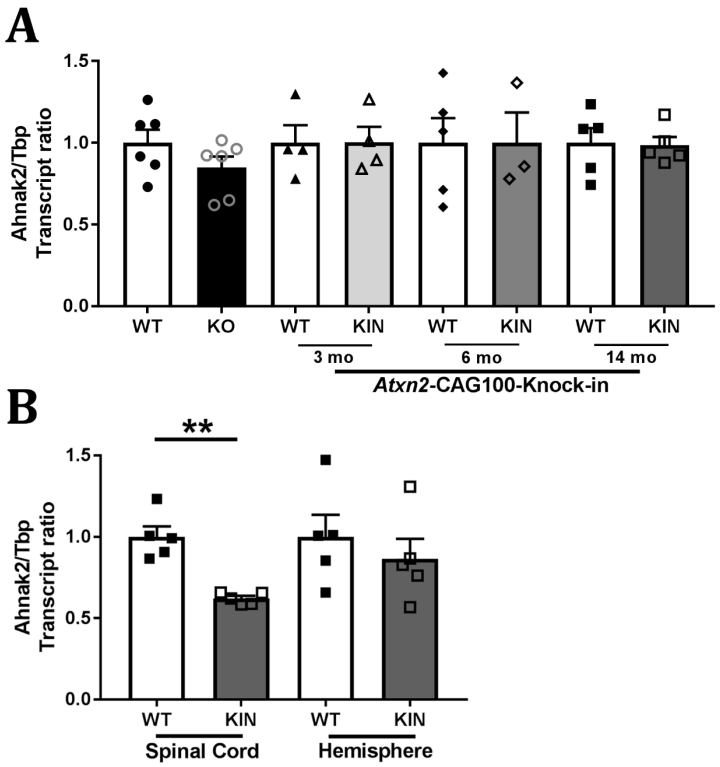

Figure 3.10. Transcript levels of *Ahnak2* assessed by Q-PCR. No differences were detected in the cerebellum of *Atxn2*-KO and *Atxn2*-CAG100-KIN animals (A) nor in the hemisphere of *Atxn2*-CAG100-KIN (B) but a significant down-regulation was observed in the spinal cord of the Atxn2-CAG100-KIN animals at 14 month of age (FC 0.62 p-value 0.003) (B).

3.3.1.3 Co-staining of ATXN2 and AHNAK in the spinal cord of old *Atxn2*-CAG100-KIN animals shows co-aggregation of this two proteins

Because the results from Q-PCR and the proteome data showed a larger effect in the spinal cord at old age rather than in the cerebellum or the hemisphere, immunohistochemistry was performed on 30 µm spinal cord cryosections from 14 month-old *Atxn2*-CAG100-KIN animals (Figure 3.11).

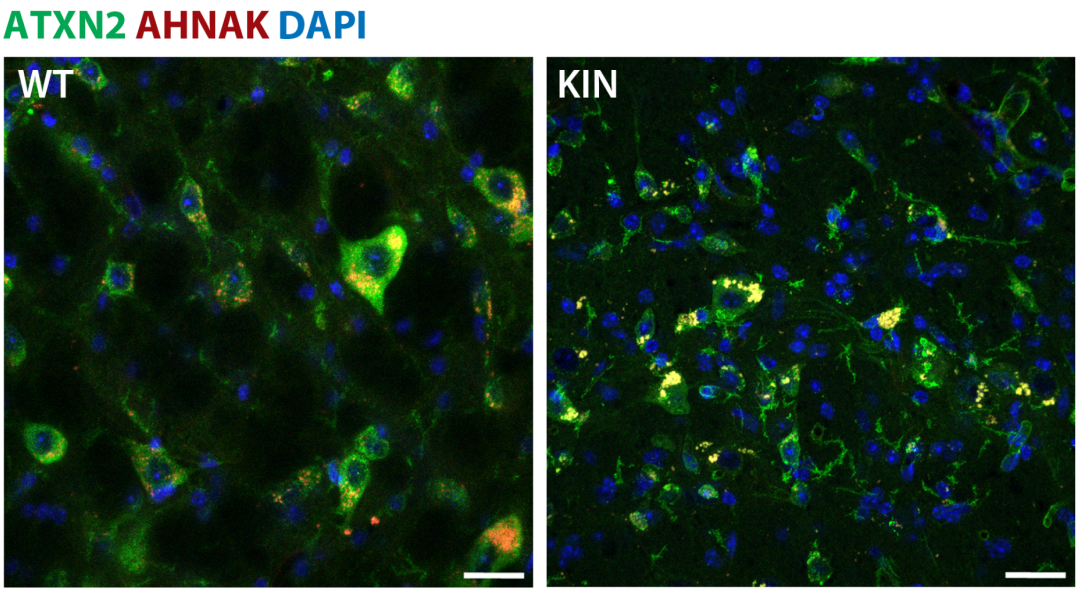

Figure 3.11. Co-staining of ATXN2 and AHNAK in the spinal cord of 14 months old *Atxn2*-CAG100-KIN animal compared to its WT littermate. Co-aggregates (yellow) and ATXN2 aggregates (green) can be observed in the KIN section while ATXN2 has a cytoplasmic distribution in the WT littermate. Scale bar represents 25 µm.

In the left image (Figure 3.11, WT) the normal cytosolic distribution of ATXN2 can be observed (green signal) while AHNAK (red signal) seems to localize around the nuclei probably at the endoplasmic reticulum or close to it of the spinal cord neurons. On the other hand, in the *Atxn2*-CAG100-KIN (right image), a strong yellow signal can be seen corresponding to the co-aggregation of ATXN2 (green) and AHNAK (red) suggesting their interaction in neurons. Another green signal coming from what seem to be glia cells appears in the KIN pointing to an increased expression of ATXN2 in these types of cells.

3.3.1.4 Assessment of *Atxn2*, *Ahnak* and *Ahnak2* in the stress response to sodium arsenite in mouse embryonic fibroblasts

Since AHNAK is a 700 kDa protein, assessing its levels in a WB was difficult to optimize. Therefore, using the mouse embryonic fibroblasts (MEFs) established from the *Atxn2*-CAG100-KIN mouse model, further investigations were carried out regarding *Ahnak* and *Ahnak2* mRNA expression levels. Sodium Arsenite (NaArs) was used at different concentrations (0.5 mM and 1 mM) to induce stress for 30 or 60 min. After the treatment, total RNA was isolated and Q-PCR was used to determine the mRNA level of *Ahnak*, *Ahnka2* and *Atxn2* compared to the non-treated-control for WT and KIN.

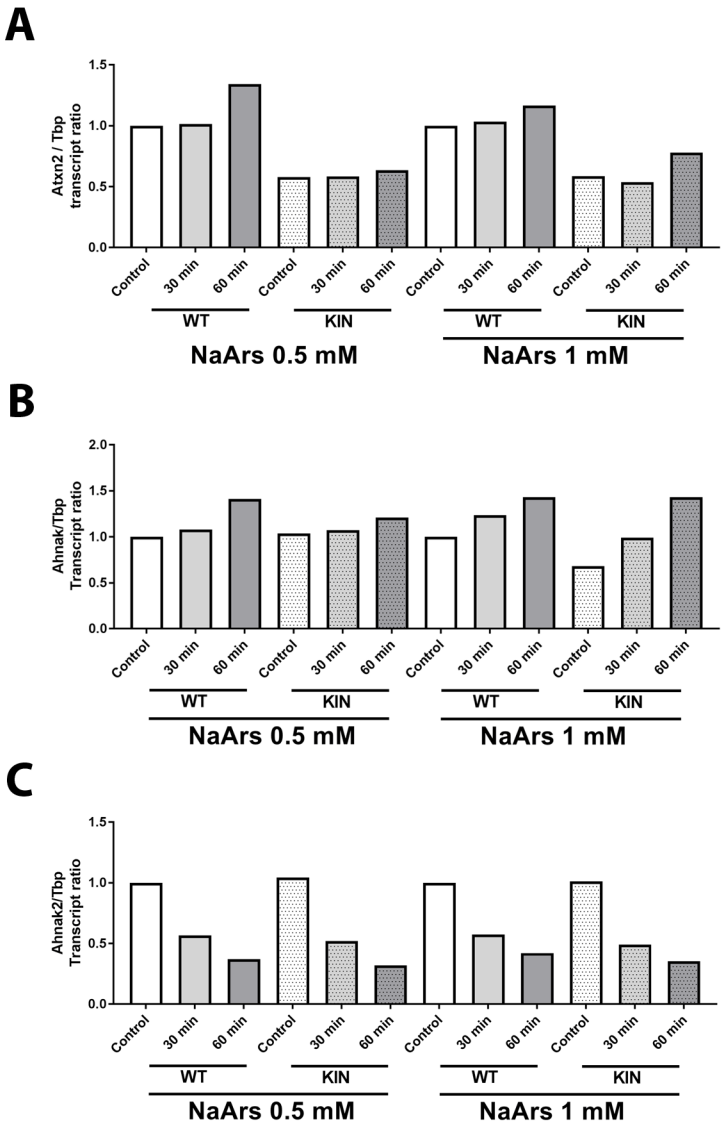

Figure 3.12. Transcript level of *Atxn2* (A), *Ahnak* (B) and *Ahnak2* (C) in mouse embryonic fibroblasts (MEF) from *Atxn2*-CAG100-KIN mice and WT. MEFs (KIN n=1 and WT n=1) were stressed with NaArs at different concentrations (0.5 mM and 1 mM) at two time points (30 min and 60 min) compared to their control.

Only one WT versus one KIN was assessed since KIN MEFs showed half of the *Atxn2* transcript level compared to WT without treatment, mimicking a partial loss-of-function. Consequently, it was not possible to evaluate the effect of the CAG100 expansion and no statistical analysis was performed. However, a constant reduction of *Ahnak2* transcript (Figure 3.12, C) was detected in all cases compared to their controls.

3.3.1.5 Assessment of *AHNAK* transcript levels in SH-SY5Y *ATXN2*-knock-down under starvation stress

After working with MEFs and failing to detect strong changes in the transcript level of *Ahnak* and *Ahnak2*, one hypothesis was that the ATXN2 loss-of-function might strongly affect the transcript levels of *Ahnak* in neuronal cell types since MEFs seem to be quite resistant to stress. To test this hypothesis, the immortalized human neuroblastoma cell line SH-SY5Y was used. The *ATXN2*-Knock-down (ATXN2-KD) and Non-Target-Knock-down (Non-Target-KD) cell lines were generated prior to this work and the response of *ATXN2* transcript level changes in starvation course experiments were reported (Sen et al 2016).

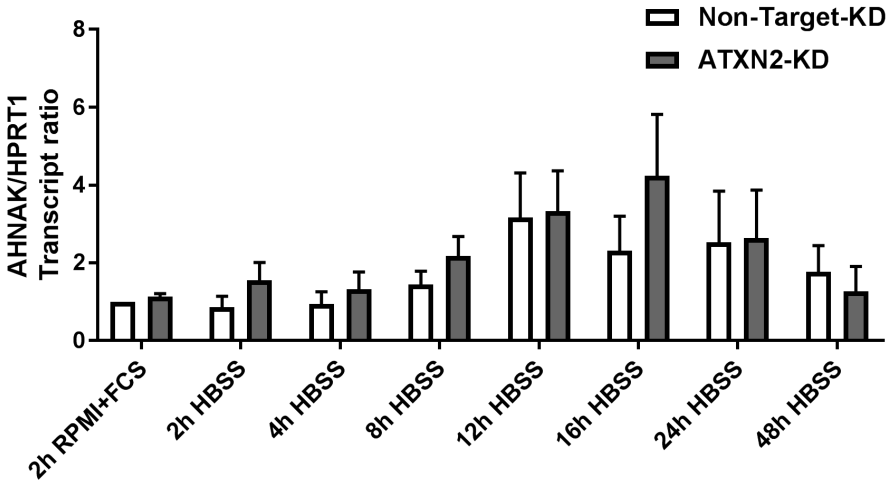

Figure 3.13. Assessment of *AHNAK* transcript levels in SH-SY5Y *ATXN2*-Knock-down and Non-Target-Knock-down under starvation show no significant changes. *HPRT1* was used as housekeeping gene.

Three different sets of Non-Target-KD and ATXN2-KD were assessed to determine the transcript expression level of *AHNAK* under starvation and the effect of the ATXN2 loss for several time points. No significant changes were detected for *AHNAK* even though AHNAK protein levels were up-regulated in the *Atxn2*-CAG100-KIN mouse model, suggesting that either *AHNAK* transcript level was unaffected in SH-SY5Y cultures, or that starvation-induced stress was not affecting AHNAK role/pathways

3.3.2 PCBP1 and PCBP2 are also highlighted by the proteome data

Other altered RBPs found in the cerebellar and spinal cord proteome are PCBP1 and PCBP2. They are part of the heterogeneous nuclear ribonucleoprotein

(hnRNPs) family that can be divided into further categories. The poly(C)-binding protein (PCBP) is one of these categories containing the hnRNP K and hnRNP E1 through 4, also known as α-CPs or PCBP1 through 4. All of these contain three KH domains, first described in hnRNP K (Siomi et al 1993). KH domains consist of 70 amino acids and show high affinity and specificity to polypyrimidine or C-rich regions in RNA, ssDNA or dsDNA (Valverde et al 2008). Their main functions include several RNA and DNA metabolism processes like alternative splicing, mRNA stabilization and transport, translational silencing and enhancement, and iron turnover (Nazarov et al 2019). In 2016, Ghanem *et al.* showed that *Pcbp1* and *Pcbp2* are individually necessary for embryonic development *in vivo* (Ghanem et al 2016), supporting the hypothesis that these two proteins have different roles in the organism even though *Pcbp1* was generated from a retrotransposition event from the most abundant *Pcbp2* mRNA (Makeyev et al 1999). Moreover, they have been shown to affect the translation and gene expression of poliovirus and HIV respectively (Blyn et al 1997, Woolaway et al 2007). PCBP1 has been recently linked to oxidative RNA damage response (Ishii & Sekiguchi 2019).

3.3.2.1 Transcript levels of *Pcbp1* and *Pcbp2* are not changed in the cerebellum, spinal cord, nor hemisphere of the *Atxn2*-CAG-100-KIN mouse model

Similar to the previous section, the transcript levels of *Pcbp1* and *Pcbp2* were evaluated in the cerebellum of *Atxn2*-CAG100-KIN at different ages and *Atxn2*-KO mouse models. No dysregulations were detected, neither in the spinal cord nor hemisphere of the old *Atxn2*-CAG100-KIN animals (Figure 3.14).

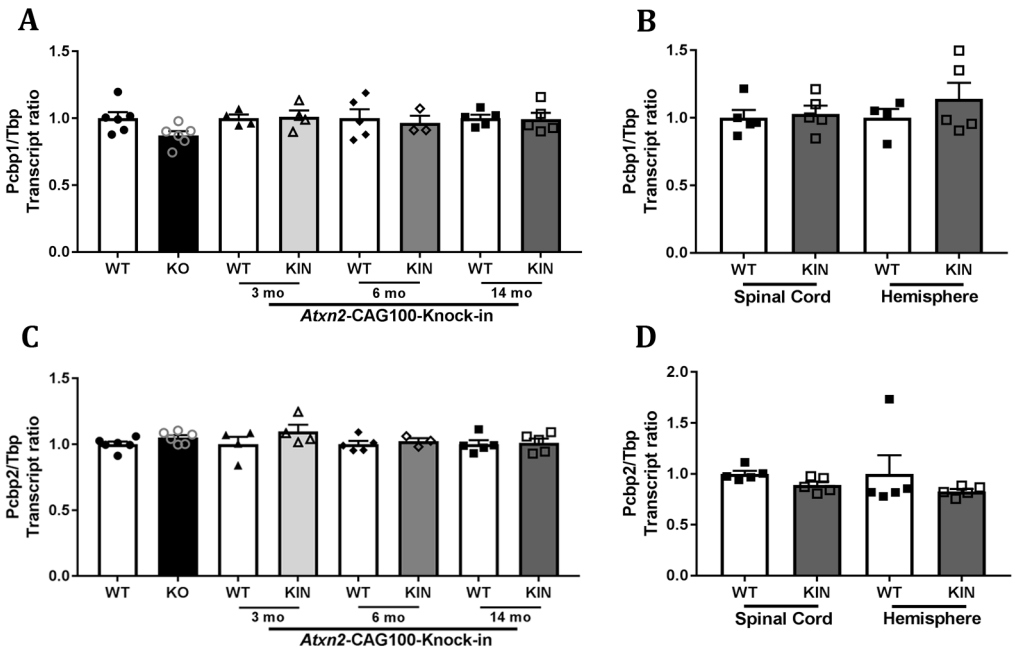

Figure 3.14. Assessment of the transcript levels of Pcbp1 and Pcbp2 shows no alterations. (A, C) Cerebellar samples from *Atxn2*-KO and *Atxn2*-CAG100-KIN at different ages, and (B, D) spinal cord and hemisphere of 14-months-old *Atxn2*-CAG100-KIN samples.

3.3.2.2 Histology PCBP1 and PCBP2 in the cerebellum of old *Atxn2*-CAG100-KIN mice compared to WT shows different pattern

Although the transcript levels of these two proteins did not change under any test conditions, alteration of the protein level or localization could still have occurred. Therefore, immunohistochemistry was used to determine protein localization in 30 µm cerebellar cryosections from 14-month-old *Atxn2*-CAG100-KIN and WT animals.

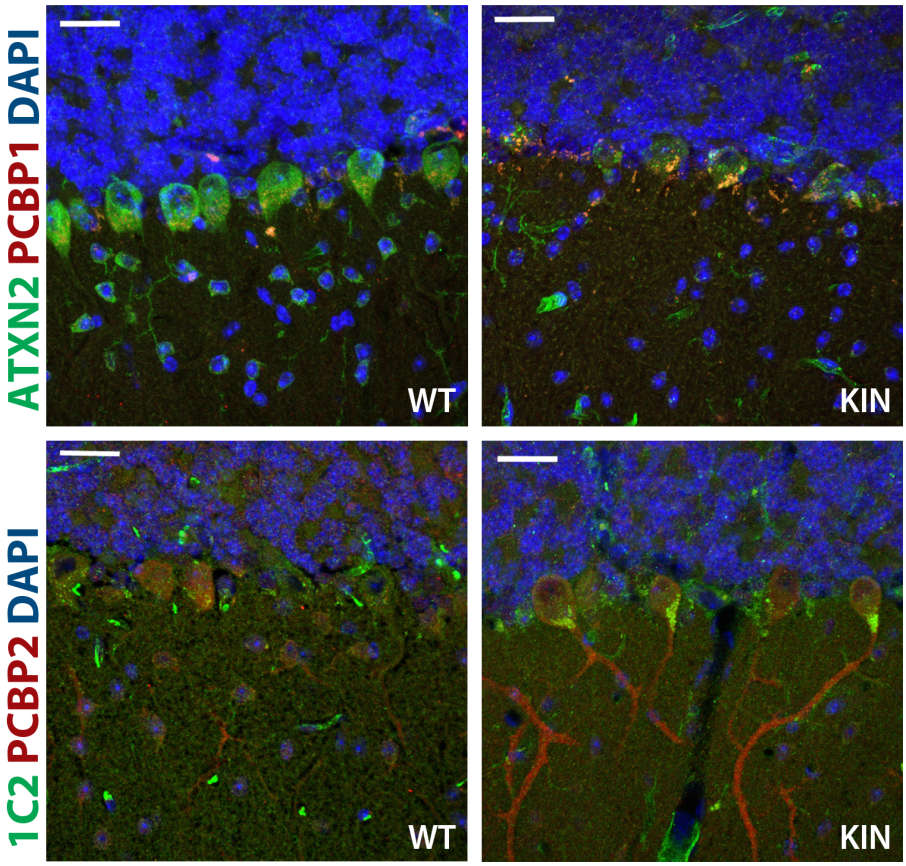

Figure 3.15. Co-immuno staining of PCBP1/PCBP2 (red) with ATXN2/1C2 (green) in the cerebellum of old *Atxn2*-CAG100-KIN mouse compared to its WT shows a different distribution in the KIN. Scale bar represents 25 µm.

In the upper panels of the Figure 3.15, the distribution of PCBP1 can be observed. In the WT, the PCBP1 signal was barely detected; only some discrete punctate can be appreciated in the cytoplasm of the Purkinje neurons (PN). By contrast in the KIN it seems to co-aggregate with ATXN2 towards the apical base of the PN. The lower panels of Figure 3.15 show the co-staining of 1C2 antibody (able to detect the expanded PolyQ section) and PCBP2. Similar to the PCBP1 case, the detected signal for PCBP2 in WT was weak and mainly localized in the cytoplasm of the PN. On the other hand, the KIN shows an increase of PCBP2 signal in PN, especially in the main dendrite. Again, the 1C2 antibody showed aggregates at the apical base of the PN corresponding to the expanded ATXN2.

Overall, the different distribution of PCBP1 and PCBP2 in the KIN cerebellar tissue may reflect their different neuronal roles suggested by prior publications (Ghanem et al 2016) and how they are individually affected by the expanded ATXN2 in the *Atxn2*-CAG100-KIN mouse.

3.3.2.3 The protein level of PCBP1 is up regulated in the cerebellum of 14-month-old *Atxn2*-CAG100-KIN

To further investigate the protein level of PCBP1 in the cerebellum of 14-month-old animals, western blot (WB) were performed using the same antibody as used for the immunohistochemistry. Unfortunately, a clear signal was not detected for PCBP2 so the potential up-regulation observed in the proteome data could not be validated.

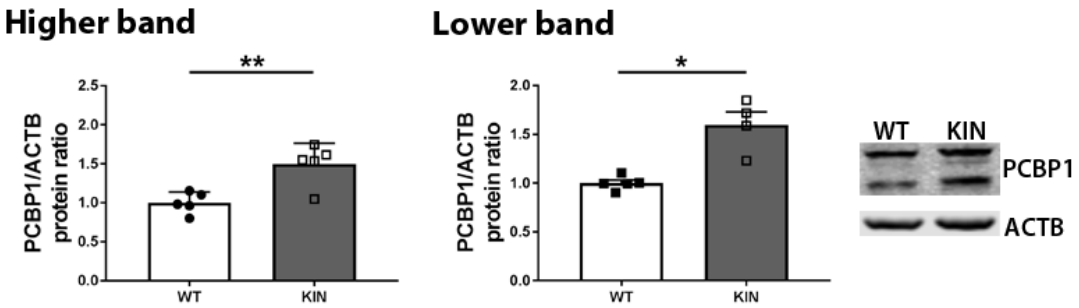

Figure 3.16. WB of PCBP1 shows up-regulation in cerebellar of Atxn2-CAG100-KIN compared to WT. A 5 *versus* 5 sex- and age-matched set of samples were used to determine the protein level of PCBP1 in the old cerebellum of the mouse model.

The antibody against PCBP1 showed two bands around the right size for the protein (37 kDa). Although no isoforms have been described for this protein, both bands were quantified and both showed a significant up-regulation (Higher band FC 1.5 p-value 0.009; Lower band FC 1.6 p-value 0.017). It is possible that the antibody is detecting a similar region from both PCBP1 and PCBP2 proteins, which are exposed after denaturing them when boiled with the loading buffer.

3.3.2.4 Evaluation of PCBP2 in *Atxn2*-CAG100-KIN MEFs in response to poly(IC) treatment

PCBP2 has been involved in different virus infections (Li et al 2019a, Walter et al 2002) and has also been described as a stress granule component (Fujimura et al 2008, Kattuah et al 2019). Therefore, the response to treatment with poly(IC), mimicking a viral infection, was evaluated in the *Atxn2*-CAG100-KIN MEFs with regard to the localization of PCBP2. For that, WT and KIN MEFs were treated with 100 ng of poly(IC) for 6 hours as previously published (Reineke et al 2018b).

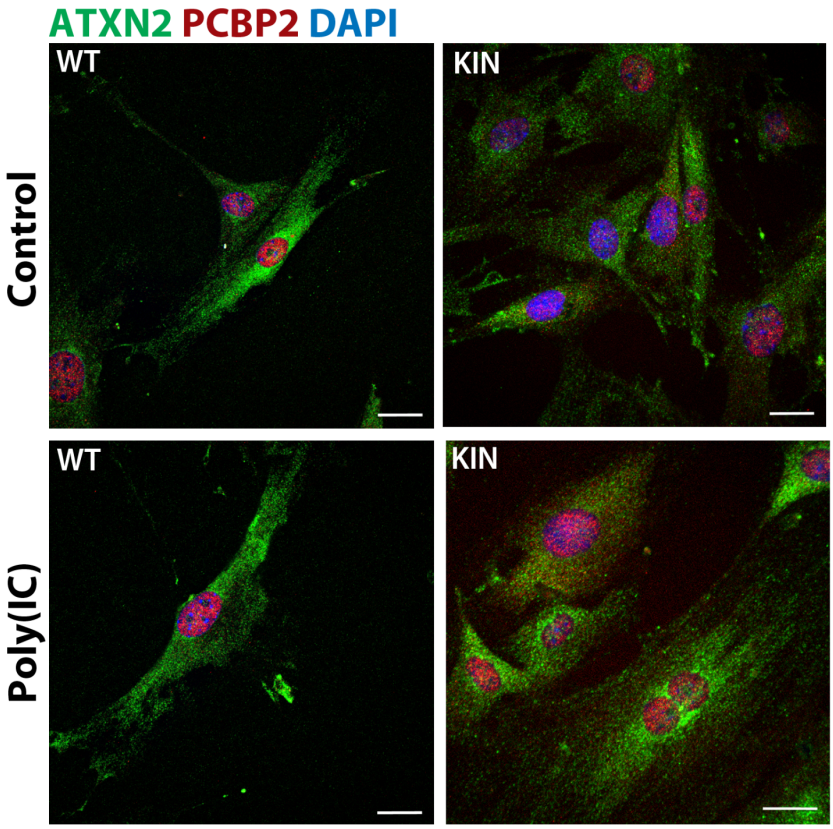

Figure 3.17. Immunocytochemistry for ATXN2 (green) and PCBP2 (red) in MEF control (WT and KIN) compared to MEFs treated with Poly(IC) (WT and KIN). No stress granule formation was detected. Scale bar represents 25 µm.

Although stress granule formation was expected in WT conditions based on the publication of Reineke *et al* 2018, none were detected, nor was any relocalization of the PCBP2 (Figure 3.17).

3.3.3 Several other RBPs appear dysregulated in the proteome data set but only a few are altered at their transcript level

Several other nucleic acid binding proteins were found to be dysregulated in the proteome data set, especially those involved in RNA metabolism. Thus, their transcript levels were investigated by Q-PCR using cerebellar samples from *Atxn2*-KO and *Atxn2*-CAG100-KIN at the late stage of the disease.

The results are shown in tables depending on their properties. Candidate genes have been divided in five categories: RNA metabolism, Heterogeneous Nuclear Ribonucleoprotein (hnRNP), P-body component, Eukaryotic Translation Initiation Factor, and DNA damage response. All categories, excluding the DNA damage response, interact with RNA.

Gene symbol		*Atxn2*-KO FC	*Atxn2*-CAG100-KIN FC
RNA metabolism			
Aar2	AAR2 Splicing Factor	1.022 *n.s.*	**0.765** ***
Celf3	CUGBP Elav-Like Family Member 3	**1.171** *	1.104 *n.s.*
Cirbp	Cold Inducible RNA Binding Protein	0.876 *n.s.*	**1.733** **
Ddx1	DEAD-Box Helicase 1	0.981 *n.s.*	0.931 *n.s.*
Ddx26b	DEAD/H Box Polypeptide 26B	1.01 *n.s.*	**1.121** **
Ddx6	DEAD-Box Helicase 6	0.911 *n.s.*	**0.917** *
Dhx15	DEAH-Box Helicase 15	0.868 *n.s.*	1.013 *n.s.*
Fmr1	Fragile X Mental Retardation 1	0.928 *n.s.*	0.918 *n.s.*
Lsm1	LSM1 Homolog, MRNA Degradation Associated	**0.884** *	0.946 *n.s.*
Pabpc1	Poly(A) Binding Protein Cytoplasmic 1	1.059 *n.s.*	**1.21** *
Prpf19	Pre-MRNA Processing Factor 19	1.038 *n.s.*	**0.896** *
Puf60	Poly(U) Binding Splicing Factor 60	1.089 *n.s.*	**0.869** **
Pura	Purine Rich Element Binding ProteinA	**0.89** *	1.078 *n.s.*
Sf3a1	Splicing factor 3a protein	1.229 *n.s.*	0.991 *n.s.*
Sf3a2	Splicing factor 3a protein	1.098 *n.s.*	**0.853** *
Srrm2	Serine/Arginine Repetitive Matrix 2	0.968 *n.s.*	0.97 *n.s.*
Srsf1	Serine/Arginine Rich Splicing Factor 1	0.963 *n.s.*	1.039 *n.s.*
Srsf2	Serine/Arginine Rich Splicing Factor 2	0.916 *n.s.*	1.039 *n.s.*
Ssb	Small RNA Binding Exonuclease Protection Factor	1.026 *n.s.*	0.938 *n.s.*
Thrap3	Thyroid Hormone Receptor Associated Protein 3	1.042 *n.s.*	0.963 *n.s.*
Tpr	Translocated Promoter Region	1.058 *n.s.*	1.021 *n.s.*
U2af2	U2 Small Nuclear RNA Auxiliary Factor2	0.961 *n.s.*	0.973 *n.s.*
Ybx1	Y-Box Binding Protein 1	**1.257** ***	1.172 *n.s.*

Table 3.2. Evaluation of the transcript level of several RNA Binding Proteins involved in RNA metabolism, especially in RNA splicing, by Q-PCR. Comparing cerebellar samples from *Atxn2*-KO and old *Atxn2*-CAG100-KIN, no common dysregulated genes were found.

A total of 23 RBPs were investigated at the transcript level; many of them have been found in SGs (Nunes et al 2019). Although they appear mainly up-regulated at the proteome data set, only three up-regulations were detected in *Atxn2*-CAG100-KIN (Table 3.2). Five down-regulations affecting splicing factors were also found to be significant in the cerebellar samples of *Atxn2*-CAG100-KIN; all of them quite discrete. No common dysregulations were found in this category for *Atxn2*-KO and *Atxn2*-CAG100-KIN samples. Only the transcript levels of four genes were found dysregulated in the *Atxn2*-KO; two up and two down-regulated.

Gene symbol		*Atxn2*-KO FC	*Atxn2*-CAG100-KIN FC
Heterogeneous Nuclear Ribonucleoprotein			
hnRNP A2B1	Heterogeneous Nuclear Ribonucleoprotein A2/B1	0.927 *n.s.*	**1.327 ****
hnRNP I	Heterogeneous Nuclear Ribonucleoprotein I	1.121 *n.s.*	1.042 *n.s.*
hnRNP D	Heterogeneous Nuclear Ribonucleoprotein D	0.927 *n.s.*	1.03 *n.s.*
hnRNP K	Heterogeneous Nuclear Ribonucleoprotein K	1.019 *n.s.*	1.026 *n.s.*
hnRNP U	Heterogeneous Nuclear Ribonucleoprotein U	1.172 *n.s.*	0.965 *n.s.*
Pcbp 3	Poly(RC) Binding Protein 3	1.056 *n.s.*	0.911 *n.s.*
Pcbp 4	Poly(RC) Binding Protein 4	1.129 *n.s.*	0.865 *n.s.*

Table 3.3. Evaluation of transcript level of several Heterogeneous Nuclear Ribonucleoprotein involved in RNA metabolism, especially in RNA transport. Only the ALS-linked hnRNP A2B1 gene showed a significant but mild up-regulation in the 14-month-old cerebellar Atxn2-CAG100-KIN samples compared to the WT.

Heterogeneous Nuclear Ribonucleoproteins (hnRNPs) are a group of RBP that have been involved in several RNA metabolism functions like splicing, transport and translation (Bryant & Yazdani 2016, Geuens et al 2016, Han et al 2010). Neurons need to closely regulate mRNA homeostasis due to their non-dividing nature. Therefore, it is not surprising that many hnRNPs have been linked to neurodegenerative disorders like Alzheimer's disease (AD), amyotrophic lateral sclerosis (ALS) and fronto-temporal lobe dementia (FTLD) (Appocher et al 2017, Hoek et al 1998, Liu et al 2015, Mohagheghi et al 2016). This group of RBPs has four unique RNA binding domains (RBDs): RNA recognition motif (RRM), quasi-RRM, glycine rich domain RGG box, and KH domain. Under normal conditions, hnRNP are located mainly in the nucleus but they are able to translocate to the cytoplasm after either recruitment or post-translational stimulation. Thus, the transcript levels of 7 hnRNPs were determined by Q-PCR and only one up-regulation for *hnRNP A2/B1* was detected (FC 1.327 p-value 0.003) in the *Atxn2*-CAG100-KIN (Table 3.3). This protein has been linked to ALS and FTLD, and plays an important role in oligodendrocytic and neuronal mRNA trafficking (Shan et al 2003).

Gene symbol		*Atxn2*-KO FC	*Atxn2*-CAG100-KIN FC
P-body components			
Dcp1a	Decapping mRNA 1A	0.844 *n.s.*	0.893 *n.s.*
Dcp1b	Decapping mRNA 1B	0.946 *n.s.*	1.104 *n.s.*
Dcp2	Decapping mRNA 2	**0.655 ***	**0.785 ****
Dcps	Decapping Enzyme Scavenger	0.989 *n.s.*	0.919 *n.s.*

Table 3.4. Evaluation of transcript level of several processing bodies components involved in RNA decay by Q-PCR. These genes are involved in the degradation of RNA and localize in p-bodies. Only one of them was dysregulated and a down-regulation was found in both mouse models, Dcp2 (highlighted in grey).

During periods of stress it might be necessary to stop translation or degrade some mRNAs. Two different cytoplasmic aggregates or sites have been described as responsible for these events; the previously mentioned stress granules (SGs) and the processing bodies (PBs). They are not independent of each other, both are induced by stress and are functionally linked (Kedersha et al 2005). PBs were first described in yeast as a site of mRNA turnover based on deadenylation and decapping (Sheth & Parker 2003) and similar structures were shown in mammalian cells (Cougot et al 2004, Ingelfinger et al 2002). Since ATXN2 has been described to have a role in global mRNA stability and translation (Fittschen et al 2015, Tadauchi et al 2004, Yokoshi et al 2014), several components of PBs were analyzed at their transcript level (Table 3.4). Interestingly, a common down-regulation for *Dcp2* was detected in the cerebellar samples from *Atxn2*-KO and old *Atxn2*-CAG100-KIN animals when compared to their controls.

Gene symbol		*Atxn2*-KO FC	*Atxn2*-CAG100-KIN FC
Eukaryotic Translation Initiation Factor			
Eif2a	Eukaryotic Translation Initiation Factor 2 A	1.042 *n.s.*	1.024 *n.s.*
Eif3a	Eukaryotic Translation Initiation Factor 3 A	0.956 *n.s.*	0.929 *n.s.*
Eif4e	Eukaryotic Translation Initiation Factor 4 E	0.853 *n.s.*	0.975 *n.s.*
Eif5a2	Eukaryotic Translation Initiation Factor 5 A2	**0.589 ***	**0.589 ****
Eif5b	Eukaryotic Translation Initiation Factor 5 B	**0.73 ***	0.92 *n.s.*
Eif6	Eukaryotic Translation Initiation Factor 6	1.174 *n.s.*	0.897 *n.s.*

Table 3.5. Evaluation of the transcript level of several Eukaryotic Translation Initiation Factors that were found dysregulated in the proteome data set. A common down-regulation for Eif5a2 (highlighted in grey) was found for both mouse models.

Translation initiation is a key regulatory step in protein synthesis controlled by several protein factors known as eukaryotic translation initiation factors (Eifs). These factors are responsible for recruiting the ribosomal subunits to the right position to start translation (Obayashi et al 2017). Therefore, they are potential targets for diseases linked to altered protein synthesis like cancer (Chu et al 2016). As previously mentioned, ATXN2 has been linked to mRNA stability (Yokoshi et al 2014) and translation (Tadauchi et al 2004). To explore any potential dysregulation of Eifs caused by the expanded ATXN2 in the *Atxn2*-CAG100-KIN model, several Eifs transcript levels were determined by Q-PCR (Table 3.5). Only one down-regulation was detected in the cerebellum of *Atxn2*-CAG100-KIN mice when compared to their WT, corresponding to *Eif52a* (FC 0.6 p-value <0.0001). A similar down-regulation of *Eif5a2* was detected in the Atxn2-KO samples (FC 0.6 p-value 0.0118) in addition to a more discrete down-regulation of *Eif5b* (FC 0.73 p-value 0.038). Interestingly, Eif5a has been shown to not only participate on the initiation step but also in the elongation step of protein synthesis (Saini et al 2009).

Gene symbol		***Atxn2*-KO FC**	***Atxn2*-CAG100-KIN FC**
DNA damage response			
Atm	Ataxia Telangiectasia Mutated	0.974 *n.s.*	**0.844 ****
Atr	Ataxia Telangiectasia Related	1.039 *n.s.*	1.042 *n.s.*
Blmh	Bleomycin hydrolase	1.147 *n.s.*	0.931 *n.s.*
Pms2	Pms1 Homolog 2, Mismatch Repair	1.127 *n.s.*	0.941 *n.s.*

Table 3.6. Evaluation of the transcript level of several genes related to DNA damage response. No altered transcript levels were found for *Atxn2*-KO mouse model and only *Atm* was found significantly down regulated for *Atxn2*-CAG100-KIN.

The last category, to which their transcript levels were evaluated, corresponds to genes involved in DNA damage response. Several neurodegenerative disorders caused by unstable CAG repeats in the DNA have been linked to defects in DNA damage response (Iyer et al 2015). ATXN2 has also been shown to have a role in

preserving genome integrity by preventing the accumulation of R-loops and maintaining rDNA-repeats stability (Abraham et al 2016, Ostrowski et al 2018).
A total of 4 genes were evaluated at the transcript level and only the recessive ataxia gene *Atm* was down regulated (FC 0.84 p-value 0.0035) in the *Atxn2*-CAG100-KIN samples (Table 3.6).

3.4 Exploring the Spinal Cord pathology in the *Atxn2*-CAG100-KIN mouse model

After analyzing the expression of several RBP in the cerebellum and spinal cord, it was clear that the spinal cord was affected more severely by the CAG expansion. Few publications focusing on SCA2 patient pathology in the spinal cord are available (Estrada et al 1999, Velazquez-Perez et al 2018, Velazquez-Perez et al 2017). Moreover, ATXN2 intermediate expansions have been linked to the pathology of ALS as a risk factor (Elden et al 2010, Gispert et al 2012, Ross et al 2011). Therefore, it is of interest to further investigate the pathology affecting this tissue in the *Atxn2*-CAG100-KIN line at different ages compared to the *Atxn2*-KO, and to understand the effects caused by toxic-gain-of-function compared to those caused by the loss-of-function.

3.4.1 TAR DNA-binding protein 43 is up-regulated in the spinal cord but not in the cerebellum of the *Atxn2*-CAG100-KIN model while Tardbp transcript levels remain unchanged

It has been shown recently that targeting *Atxn2* in a mouse model of ALS overexpressing TDP43 extends the life span of these animals significantly (Becker et al 2017), strongly suggesting a functional interaction between these two proteins. One question that rose from this publication was if the pathology in the spinal cord of the *Atxn2*-CAG100-KIN resembles the pathology observed in TDP43-ALS cases. The first step to answer this question was to determine the protein level of TDP43 in the spinal cord of *Atxn2*-CAG100-KIN animals at 3 months and 14 months compared to cerebellar levels. The *Atxn2*-KO mouse model was also investigated in order to decipherer the differences between the toxic-gain-of-function and loss-of-function. Protein level of the neuronal marker NeuN was also checked since a reduction would point to a decrease in neuronal

count in the spinal cord. NeuN levels were also checked in the cerebellar samples to determine if other neuronal populations aside from PN are affected. A discrete but significant reduction of the Purkinje marker calbindin 1 (CABL1) was already known (Sen et al 2019).

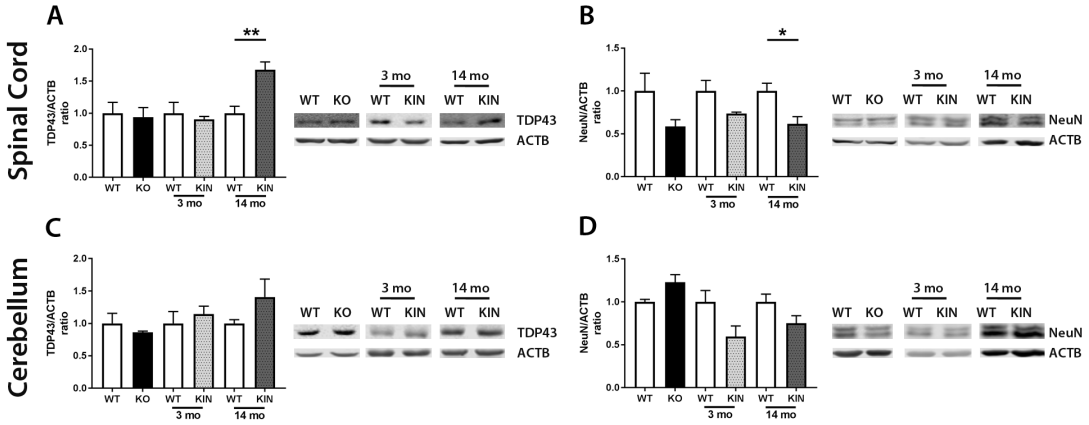

Figure 3.18. Western blots of TDP43 (A, C) and NeuN (B, D), as neuronal marker, in the Spinal Cord and Cerebellum of *Atxn2*-KO and *Atxn2*-CAG100-KIN at 3 and 14 month. An evident increase of TDP43 (FC 1.68 p-value 0.003) in the spinal cord of the old KIN animals can be appreciated together with lower levels of NeuN. No significant dysregulations were detected in the spinal cord nor cerebellum of *Atxn2*-KO and young *Atxn2*-CAG100-KIN animals for these two proteins.

A clear increase of TDP43 protein (FC 1.68 p-value 0.003) was observed in the spinal cord of the old *Atxn2*-CAG100-KIN animals compared to their WT (Figure 3.18,A). No other dysregulation with regards to TDP43 was significant in the spinal cord of the younger and *Atxn2*-KO animals, nor in any cerebellar sample set (Figure 3.18,A and C). These data demonstrates the specific and different affection of the spinal cord compared to the cerebellum. A down-regulation of NeuN level was also detected for the old spinal cord samples (FC 0.61 p-value 0.012) pointing to a loss of neurons in this tissue (Figure 3.18,B).

Next, the transcript levels of *Atxn2* and *Tardbp* were investigated. It is possible that the transcript levels of *Atxn2* were altered due to the addition of 100 CAGs, or that the effects seen in the TDP43 levels were due to an increase of the *Tardpb* transcript levels.

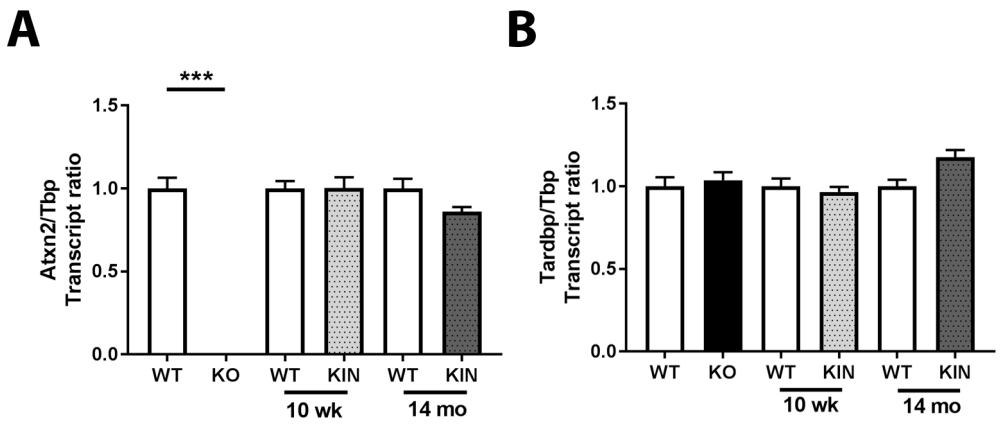

Figure 3.19. Transcript levels of *Atxn2* and *Tardbp* in the spinal cord of *Atxn2*-KO and *Atxn2*-CAG100-KIN at 3 and 14 months compared to their WT. There are no differences except for the case of *Atxn2* levels in the spinal cord of *Atxn2*-KO animals, confirming the Knock out.

No differences in *Atxn2* and *Tardbp* levels were detected in the spinal cord samples (Figure 3.19). Except for the absence of *Atxn2* in *Atxn2*-KO animals. This was as expected, confirming that the CAG expansion is not affecting the transcript levels of *Atxn2* and that the increased levels of TDP43 protein are not caused by an up-regulation of its transcript.

3.4.2 Co-immunofluoresence staining for ATXN2 and TDP43 show co-aggregation in a time dependent manner

TDP43 is known to shuttle from the nuclei to the cytosol in periods of cellular stress and to be part of the stress granules where several mRNAs stall until the non-favorable conditions have passed. ATXN2 also takes part in the formation of stress granules and the expanded ATXN2 forms aggregates in the Purkinje neurons of the *Atxn2*-CAG100-KIN over time (Figure 3.5). After observing an increase of TDP43 levels, it was key to investigate the formation of ATXN2 aggregates in the spinal cord over time and see if TDP43 was also localizing in the same location. To do that, 30 µm cryosections from the thoracic part of the spinal cord of 3, 6 and 14-months-old *Atxn2*-CAG100-KIN and their sex and age-match WT were used. To again confirm that the alterations are caused by a toxic-gain-of-function and not due to the loss-of-function of ATXN2, the *Atxn2*-KO mouse model was used. To verify that the signal detected was the ATXN2 aggregates, PABP1 was again used as a control since it is a known interactor during periods of stress.

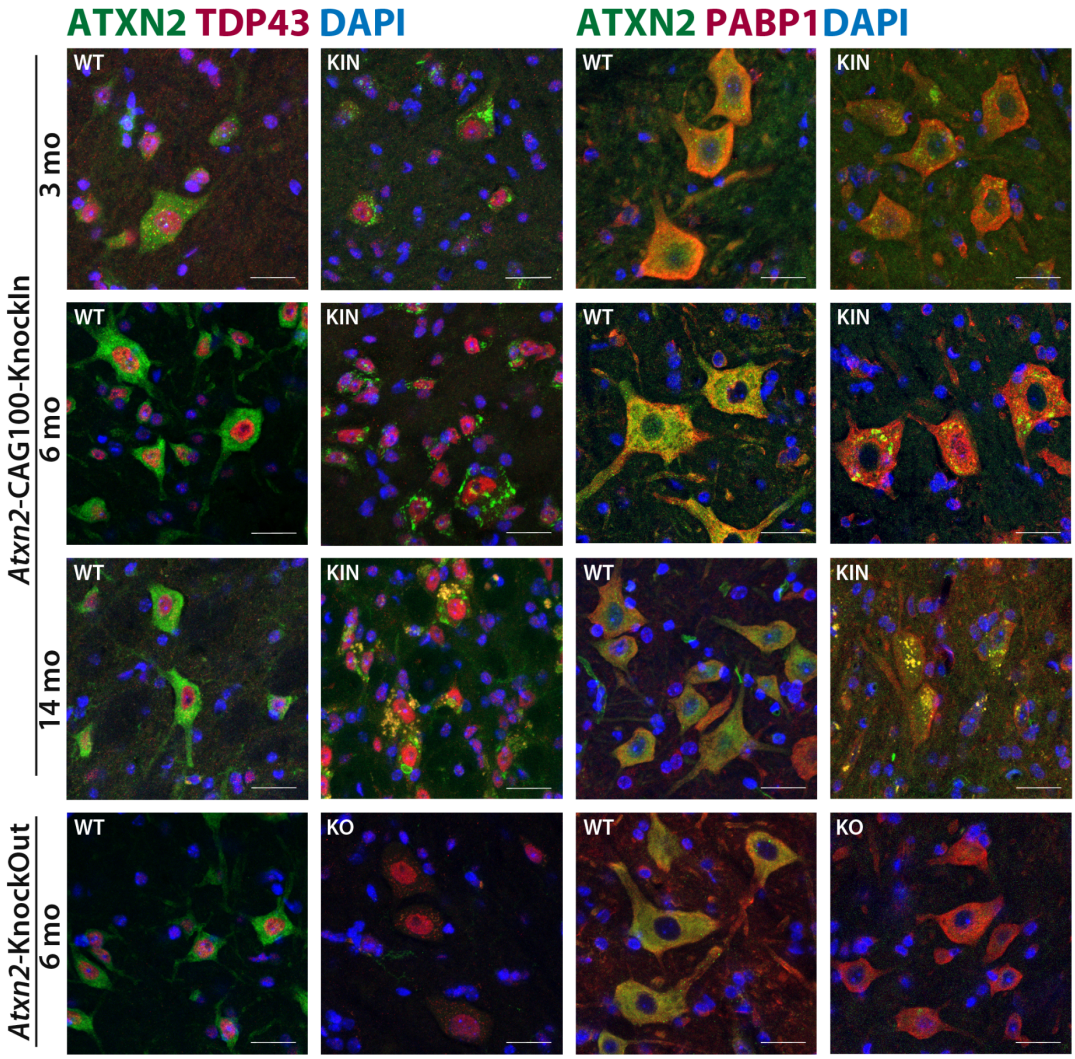

Figure 3.20. Co-immuno staining of ATXN2 (green) with TDP43 or PABP1 (red) in the spinal cord of *Atxn2*-KO or *Atxn2*-CAG-100 animals compared to their WT at different ages shows ATXN2 aggregates and co-localization of TDP43 and PABP1 over time. Nuclei were detected with DAPI (blue). Scale bar represents 25 µm.

In the left-most panels of Figure 3.20 the co-staining of ATXN2 (green) and TDP43 (red) for WT and KIN or KO is displayed. The WT animals show a cytoplasmic distribution for ATXN2 and an exclusive nuclear signal for TDP43 for all ages and genotypes. When comparing the KIN it becomes evident that, like in the cerebellar staining (Figure 3.5), the ATXN2 aggregates start at 3 months of age and increase in number and size over time filling the cytoplasmic space during advanced stage of the disease. TDP43 discretely starts to co-aggregate at 6 months being strongly evident at the age of 14-month-old. To confirm these observations, the right side of the figure shows the co-staining of ATXN2 (green) and PABP1 (red). In the WT pictures, ATXN2 shows a cytoplasmic distribution

like PABP1, while in the KIN pictures the time-dependent co-aggregation can be also observed for PABP1.

3.4.3 Co-immunofluorescence staining of ATXN2 and TIA1 also shows co-aggregation in the spinal cord of old *Atxn2*-CAG100-KIN animals compared to WT

To further characterize the spinal cord pathology, another RBP implicated in ALS was studied: T-Cell-Restricted Intracellular Antigen-1 (TIA-1). TIA-1 is a RBP that mainly localizes in the nuclei but can shuttle to the cytoplasm where it can be part of the stress granules during of environmental stress (Kedersha et al 2000, Kedersha et al 1999). Therefore, immunohistochemistry was performed on the old spinal cord of *Atxn2*-CAG100-KIN and compared to its WT.

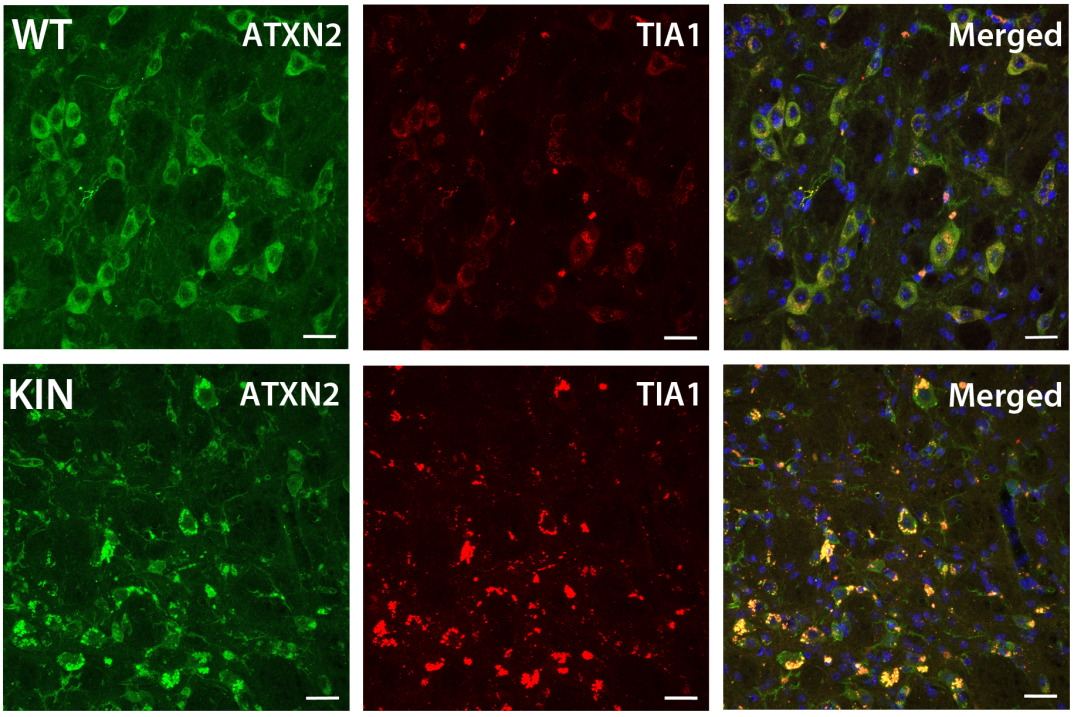

Figure 3.21. Staining of ATXN2 (green) and TIA1 (red) in the spinal cord of old Atxn2-CAG100-KIN animal shows co-aggregation. Nuclei were detected with DAPI (blue). Scale bar 25 µm.

As expected, the TIA 1 (red) signal also co-aggregated with ATXN2 (green) at the late stage of the disease in the *Atxn2*-CAG100-KIN model suggesting an alteration of several ALS-implicated RBP functions (Figure 3.21). Thus, this model would be an excellent option to study the progression and development of spinal cord degeneration without overexpression, nor expression of human genes, allowing a better understanding of the biology of the mouse model.

3.4.4 The protein level of non-cleaved CASP3 is up-regulated specifically in the spinal cord of old *Atxn2*-CAG100-KIN mice while its transcript level is not changed

Several studies showed that TDP43 can be cleaved into C-terminal fragments by caspase 3 (CASP3) (Dormann et al 2009, Nishimoto et al 2010, Zhang et al 2007), accumulating in affected neurons and glia (Igaz et al 2008, Neumann et al 2006). As a follow-up to describing the involvement of ATXN2 as a risk factor in ALS (Elden et al 2010), the same lab investigated the implicated mechanisms (Hart & Gitler 2012). Using three different in vitro models (HEK293T cells, ALS-patient-derived lymphoblast cell lines and differentiated human M17 neuroblastoma cells), they identified the activation of CASP3 in presence of the ATXN2 intermediate-length polyQ expansion responsible for enhancing the production of this C-terminal fragments from TDP43. Caspases are cysteine-aspartic proteases implicated in programmed cell death (apoptosis, pyroptosis and necroptosis) and inflammation. They play an important role in the CNS during neuronal development, axon guidance and ageing (Shalini et al 2015). On the other hand, over-activation of some caspases, like CASP3, has been linked to several neurodegenerative disorders leading to an excess of apoptosis. Moreover, in a mouse model of SCA7 and a drosophila model of SCA3, cleaved fragments of Ataxin 3 and Ataxin 7 were shown to exacerbate the pathology (Jung et al 2009, Young et al 2007). Therefore the levels of CASP3 were determined for its transcript and protein in the *Atxn2*-CAG100-KIN mouse model at different ages comparing to the *Atxn2*-KO mouse model in the spinal cord.

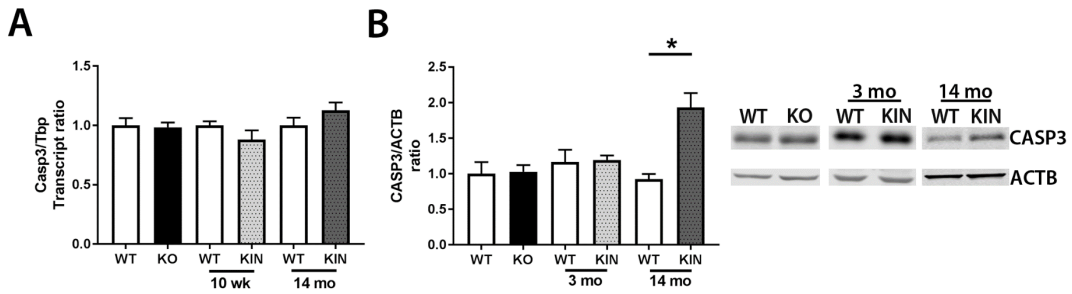

Figure 3.22. Transcript level (A) and protein level (B) of CASP3 in the spinal cord of *Atxn2*-KO and *Atxn2*-CAG100-KIN mice compared to their WT shows an up-regulation at protein level in the old mouse model. While the transcript level stayed unchanged, a significant up-regulation of CASP3 was identified in the spinal cord at old age. No changes were detected for the *Atxn2*-KO model.

No changes were detected in the transcript level (Figure 3.22, A) in either models, although a significant increase of protein was detected in the old samples of the *Atxn2*-CAG100-KIN model (Figure 3.22, B; FC 1.93 p-value 0.011). The antibody used only allows the detection of the non-cleaved CASP3 corresponding to the non-activated form; therefore the activated CASP3 could not be quantified.

The protein levels of CASP3 were also determined for old cerebellar samples of *Atxn2*-CAG100-KIN model and showed no change (Figure 3.23).

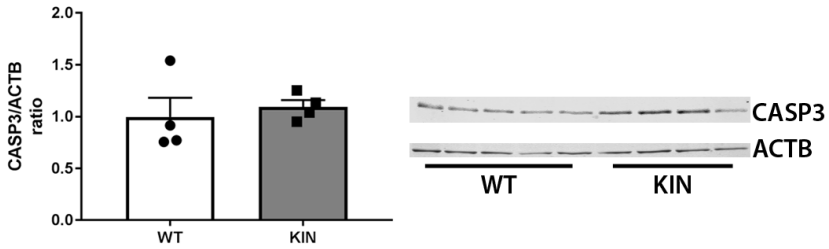

Figure 3.23. Protein levels of CASP3 in the cerebellum of 14-month-old *Atxn2*-CAG100-KIN show no difference compared to their sex- and age-matched WT. Protein homogenates from 5 WT versus 5 KIN were used.

3.5 Transcriptomics from spinal cord of 3 and 14-month-old *Atxn2*-CAG100-KIN mice

After showing all the RBP alterations in the protein level in the spinal cord of the *Atxn2*-CAG100-KIN model, it was of interest to determine which transcripts were altered in the model at the late stage of the disease and which ones were early events. The transcriptomics data sets were generated using the Affymetrix Clariom™ D mouse arrays from ThermoFisher. This type of array allowed us to analyze more than 65000 transcripts. The Transcriptome Analysis Console (TAC) software was used to analyze the data using standard parameters and self-determined filter criteria (fold change < -1.2 or > 1.2; p-value ≤ 0.05).

3.5.1 Experiment design

After reaching the desired age (3 and 14 month) a group of three WT versus three *Atxn2*-CAG100-KIN were sacrificed and dissected. As mentioned before, the tissue was snap frozen in liquid nitrogen to avoid RNA degradation. In both cases, the RNA extraction was performed in parallel for both genotypes in order to reduce technical variation. The entire procedure was performed in an RNase-

free hood to ensure the quality of the resulting RNA. Panel A in the Figure 3.24 shows the workflow followed, and Panel B the genes that passed the filter criteria, highlighted in green for down-regulations or red for up-regulations.

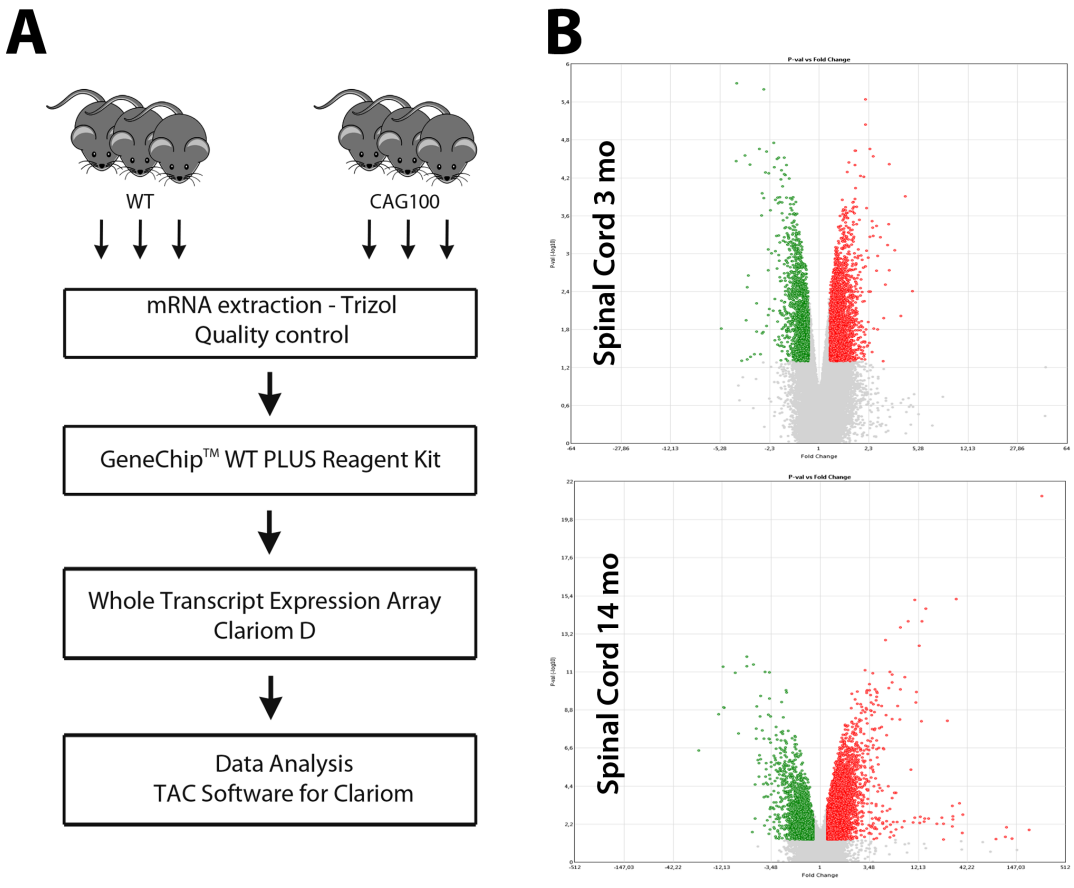

Figure 3.24. (A) Workflow scheme followed to generate the transcriptomics data set. (B) Volcano plots showing the distribution of the generated data. X axis represent fold change and Y axis log(p-value). Up-regulated factors are showed in red and down-regulated in green.

3.5.2 General data from the arrays

As expected for a degenerative disease, a higher number of genes were dysregulated in the old than the young samples. The higher number of up-regulated genes than down-regulated genes was also notable for both young and old cases (Table 3.7).

	Passed filter criteria	Up-regulated	Down-regulated
Spinal cord			
3 months	4642	2952	1690
14 months	11599	7470	4129

Table 3.7. Genes that passed the filter criteria established from a total of 65956 screened transcripts in the spinal cord samples. In both cases, young and old, 3 WT vs. 3 KIN were used to generate the data set.

There are nine different groups in the array: Non-Coding, Multiple Complex (containing more than one of the other groups), Coding, Pseudogene, Precursor microRNA, small RNA, Ribosomal, Unassigned, and tRNA. Since this thesis has been mainly focused on the up-regulations, the representative percentage of each group is only showed only for up-regulations Figure 3.25.

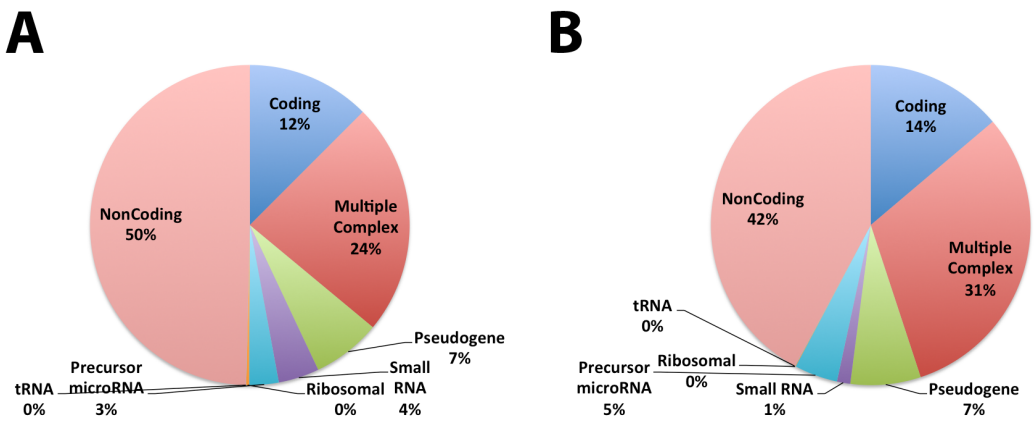

Figure 3.25. Group distribution of the significantly up-regulated transcripts from the array, the non-coding group was prevalent in both conditions. (A) Data from 3-month spinal cord samples, (B) data from 14-month spinal cord samples.

Interestingly, at both ages the Non Coding category shows a higher percentage of up-regulated transcripts (Figure 3.25). Together the Coding and Multiple Complex categories (known protein coding genes) represent 36% of up-regulated transcripts in 3-month-old samples and 45% in 14-month-old samples.

3.5.3 Several Ataxia, ALS and RNA toxicity genes appear to be dysregulated at the transcriptomics level in the old spinal cord of *Atxn2*-CAG100-KIN mouse line

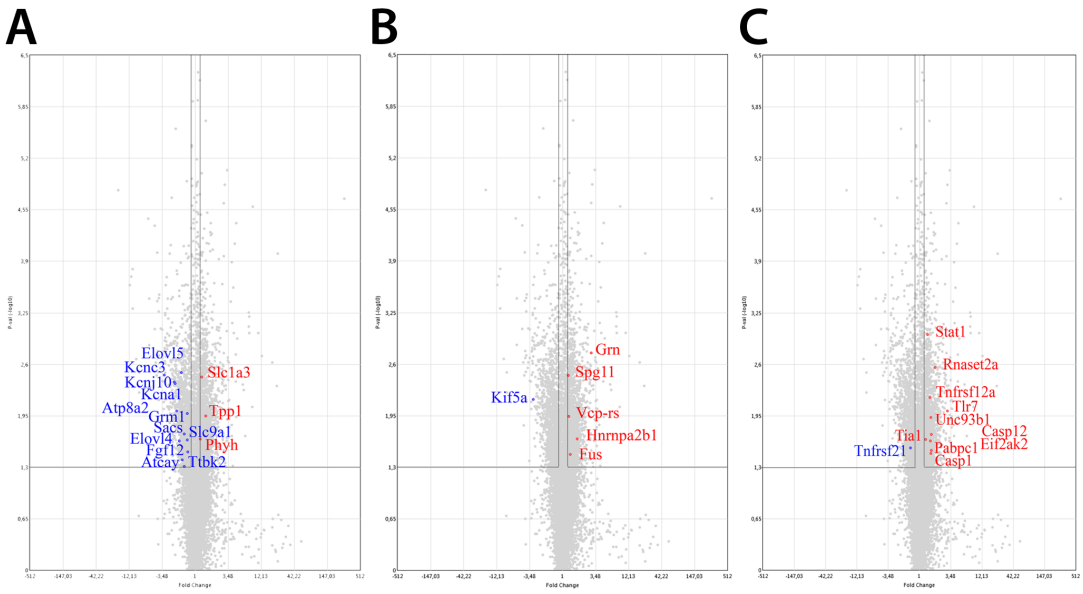

Figure 3.26. Volcano plots showing several affected transcripts related to (A) Ataxia, (B) ALS and (C) RNA toxicity. On the X-axis the p-value is represented and on the Y-axis the Fold Change. The down regulated genes are shown in blue while the up regulated are in red.

Looking closer at the transcriptomics results, several ataxia- and ALS-related genes were dysregulated, strengthening the potential of the mouse model in SCA2 and ALS research (Figure 3.26, A and B). Interestingly, a high number of genes linked to RNA toxicity response (Figure 3.26, C) were also found to be up-regulated pointing to a possible RNA toxic problem caused by the presence of the expanded *Atxn2* mRNA, the transcripts regulated by ATXN2, or both.

3.5.4 Analysis of the 14-months-old spinal cord transcriptomics data with STRING

STRING (Search Tool for the Retrieval of Interacting Genes/Proteins) is a free, constantly updated database and online platform of known and predicted protein-protein interactions (Snel et al 2000, Szklarczyk et al 2015). Therefore, assessing the generated transcriptomics data using this platform allows investigation of affected networks and permits a deeper understanding of cellular processes in the model at different ages.

3.5.4.1 Analysis of the 2-fold down-regulations in the spinal cord of the 14-month-old group shows membrane components to be highly affected

One platform that STRING uses to determine interactions is the Gene Ontology (GO) database. This database takes advantage of the known biological domains and their interactions (geneontology.org) to define functional networks. It takes three different aspects into consideration: Molecular Function (molecular activities performed by the gene-product), Cellular Component (location relative to cellular structures where the gene product performs its function), and Biological Process (larger processes accomplished by multiple molecular activities; e.g., DNA repair).

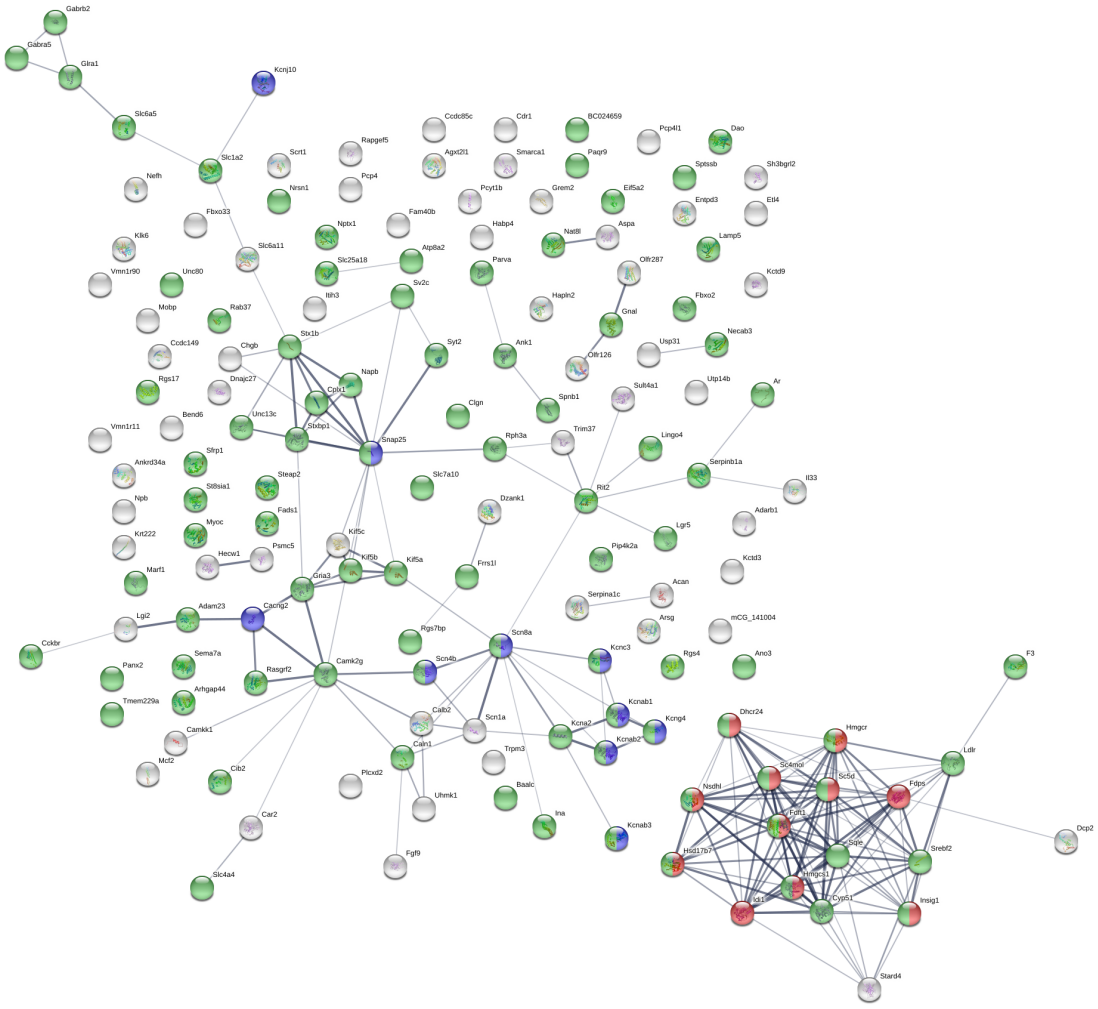

Figure 3.27. Network representation from the 2-fold-down dysregulations found in the 14-month spinal cord transcriptomics. The predominant green bullets correspond to the Cellular Component (GO) *membrane*; red bullets represent the Biological Process (GO) *sterol biosynthetic process*; and blue bullets highlight the *voltage-gated cation channel activity* in the Molecular Function category (GO).

An expected, protein-protein interaction enrichment (p-value <1.0e-16) was detected for the 2-fold down-regulations (Figure 3.27). Among the biological processes defined by GO, the *sterol biosynthetic process* showed enrichment for ten down-regulated factors (*q*= 5.65e-12 red bullets). It is interesting to note the number of affected proteins localizing at the membranes (defined by cellular component *membrane* (GO); *q*= 9.34e-09 green bullets), especially those linked with sterol synthesis (red and green bullets) since cholesterol is an important structural lipid in membranes and myelin sheaths (Dietschy & Turley 2004). The *voltage-gated cation channel activity* (Molecular function in GO) also shows enrichment for ten factors (*q*= 6.51e-05 dark blue bullets), eight of them localizing at the membrane (green and dark blue bullets).

Overall, the 2-fold-down transcripts point to a reduction in sterol biosynthesis and strong alteration of membrane-bound protein transcripts.

3.5.4.2 Analysis of the 2-fold up-regulations in the spinal cord for the 14-month-old group shows a strong network of microglia-enriched genes

Apart from GO, STRING also uses other databases to generate networks like KEGG pathways. This database is based on manually drawn pathway maps showing molecular interaction, reaction, and relation networks for: metabolism, genetic information processing, environmental information processing, cellular processes, organismal systems, human diseases, and drug development (genome.jp/keg/pathway.html).

When the two-fold up-regulations were analyzed with STRING, significant protein-protein interaction enrichment was detected (p-value <1.0e-16) (Figure 3.28). A high number of lysosomal factors described by the KEGG pathways were flagged (*q*= 8.9e-10 purple bullets), together with the biological process *immune system* defined by GO (*q*= 6.2e-13 turquoise bullets). These genes are strongly expressed by microglia in the murine CNS (Zhang et al 2014). Two other GO categories also showed enrichment: *protein binding* in Molecular function (*q*= 2.02e-06 fuchsia bullets) and *extracellular region* in Cellular component (*q*= 3.7e-10 yellow bullets). The *core histone* component, defined by PFAM protein domains, was enriched for seven factors (*q*= 0.0032 dark yellow bullets).

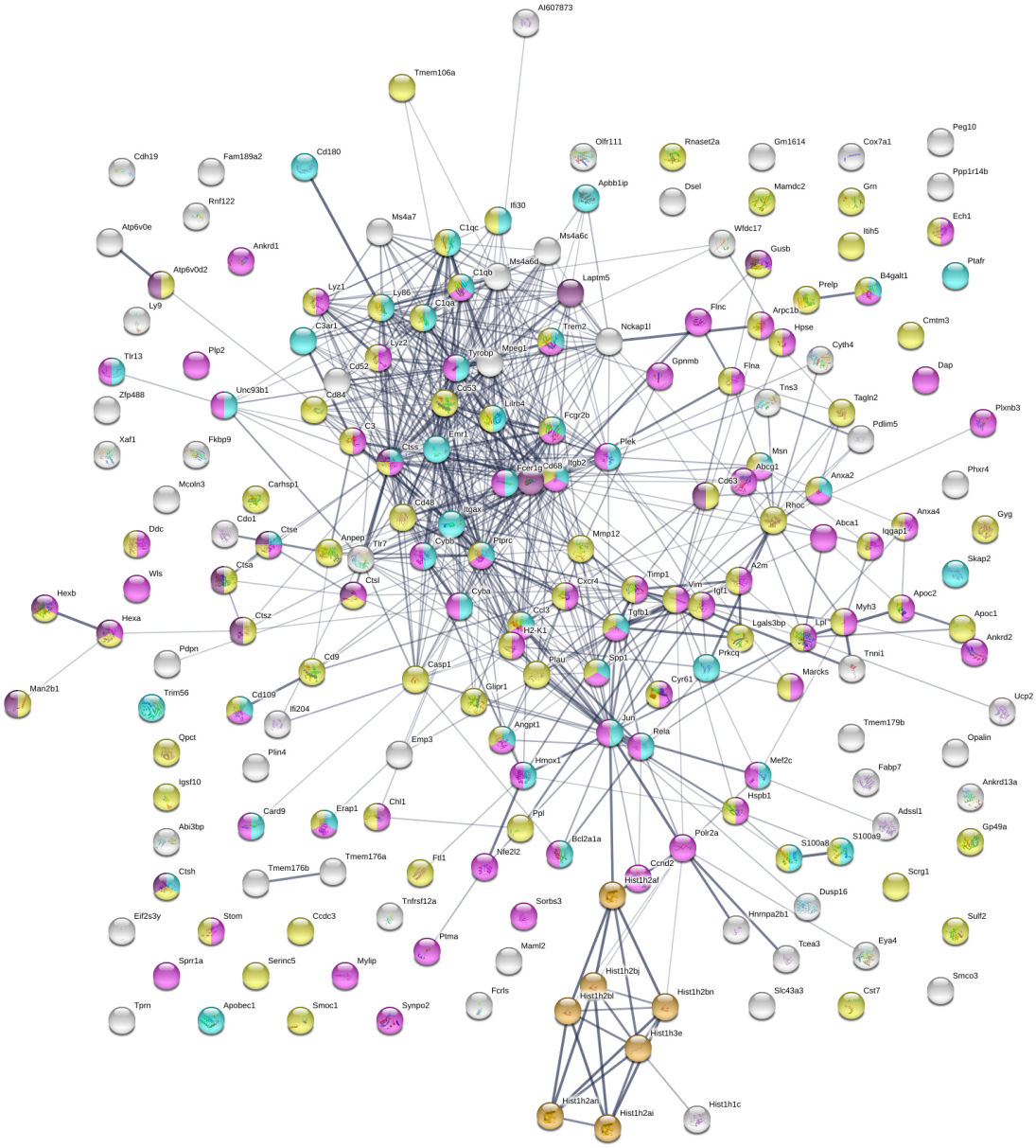

Figure 3.28. Network representation of the 2-fold-up dysregulations found in the 14-month spinal cord transcriptomics. The three categories from Gene Ontology were enriched; bullets in turquoise represent *immune system process* (Biological Process), bullets in fuchsia represent *protein binding* (Molecular Function) and bullets in light yellow represent *extracellular region* (Cellular Component). Bullets in purple represent the Lysosomal pathway based on KEGG Pathways and highlighted in dark yellow the Core Histone defined by PFAM Protein Domains.

Overall, the 2-fold-up dysregulations showed a large quantity of immune and lysosomal factors. A strong microglia response has been long linked to neurodegenerative disorders, especially in AD. It raises the question of whether this non-neuronal cell population is also affected by the CAG expansion in cell-autonomous manner, or if it is an indirect consequence of neuronal affection.

3.5.5 Validation of the transcriptomics data confirms the altered levels of neuroinflammation linked factors *Grn* and *Ripk1*

Receptor-interacting serine/threonine-protein kinase 1 (RIPK1) is a kinase that controls programmed cell death via apoptosis and necroptosis (Meng et al 2018) and was altered in the transcriptomics data set from the old spinal cord samples. Apoptosis is essential for development of the nervous system and is mediated by activation of caspases, a family of protease enzymes (Yuan & Yankner 2000). Caspase-knock-out mice show severe developmental defects (Zheng & Flavell 2000), underscoring the importance of eliminating redundant connections and refining the neuronal network as an evolutionary conserved program (Conradt et al 2016). In contrast, mature neurons become resistant to this intrinsic apoptosis pathway and more independent from trophic factors for survival compared to immature ones (Kole et al 2013, Putcha et al 2000). This resistance can be overcome under pathological conditions like neurodegenerative disorders (ALS, AD, and PD). The extrinsic apoptosis pathway or necroptosis can then be activated, for example due to an increase of the tumor necrosis factor (TNF), inducing cellular death and inflammation (Habbas et al 2015, Kuhle et al 2009, Tarkowski et al 2003, Tarkowski et al 1999, Tateishi et al 2010). Thus, targeting RIPK1, as a mediator of necroptosis, or upstream factors can help and slow-down their progression (Ito et al 2016, Xu et al 2018). Moreover, patients with rare biallelic mutations in Ripk1 have severe immune deficiency, arthritis, intestinal inflammation and developmental delay (Cuchet-Lourenco et al 2018, Li et al 2019b, Uchiyama et al 2019). Therefore, we aimed to assess if RIPK1 was altered in the *Atxn2*-CAG100-KIN spinal cord and cerebellum.

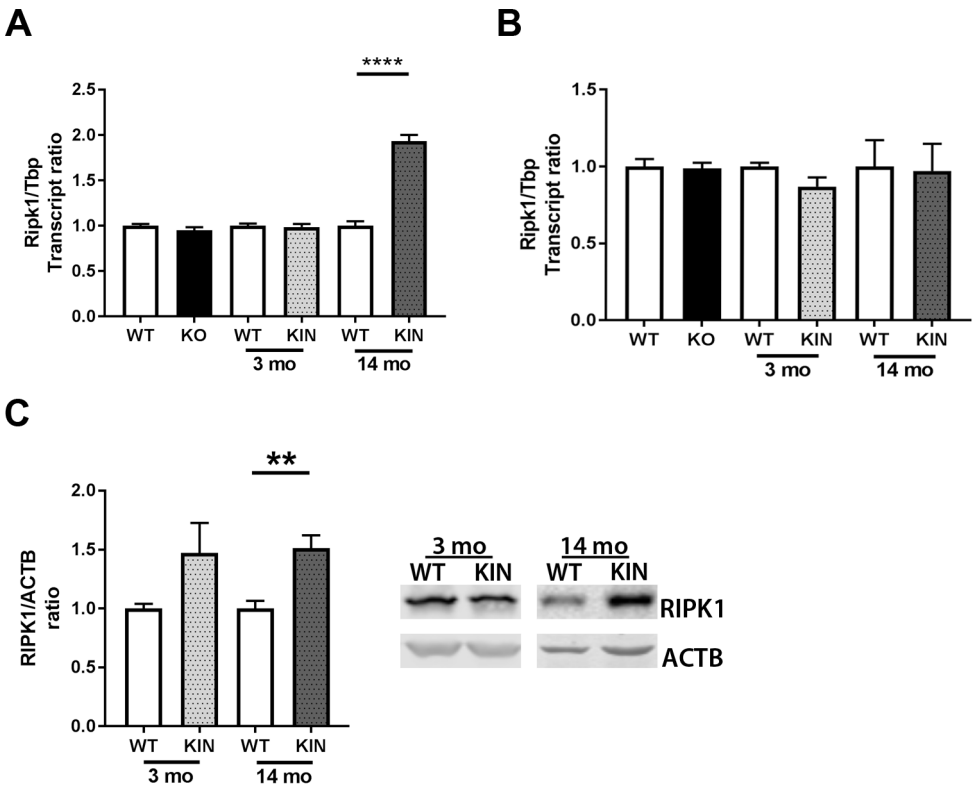

Figure 3.29. Validation of the ALS linked gene *Ripk1* at the transcript and protein level confirms its up-regulation. (A) Transcript evaluation in the spinal cord at 3 and 14 months of *Atxn2*-CAG100-KIN model compared to the *Atxn2*-KO shows a specific effect at the old age of the KIN mice compared to their WT. In contrast, no dysregulation was found in the cerebellar samples of these mouse models (B). The protein level of RIPK1 is also up-regulated in the old spinal cord samples of *Atxn2*-CAG100-KIN animals (C).

An induction of *Ripk1* at transcript (Figure 3.29, A; FC 1.93 p-value <0.0001) and protein level (Figure 3.29, C; FC 1.51 p-value 0.0033) was confirmed in old spinal cord samples of *Atxn2*-CAG100-KIN mice compared to their WT. No dysregulation was detected in young samples or in the *Atxn2*-KO mouse model. Although *Ripk1* was only investigated at the transcript level in the cerebellum, no dysregulation was found there, suggesting a stronger affection of the spinal cord (Figure 3.29,B).

Another factor that was found altered in the transcriptomics data set was progranulin. Progranulin (PGRN) is an evolutionarily conserved glycoprotein with 7.5 conserved granulin domains connected by linker regions (Palfree et al 2015, Tolkatchev et al 2008). Individual granulins can be released when PGRN is proteolytically processed. PGRN and its cleaved products, granulins, were

identified first as growth factors involved in wound healing, vessel growth and cancer (Bateman et al 1990, He et al 2002, He et al 2003). Shortly after, mutations in PGRN gene (GRN) were linked to frontotemporal dementia (FTD), frontotemporal lobar degeneration (FTLD), neuronal ceroid lipofuscinosis (NCL), and Alzheimer's disease (AD) (Almeida et al 2016, Baker et al 2006, Gass et al 2006, Smith et al 2012, Tanaka et al 2014). In FTD-spectrum cases, nonsense mutations and missense mutations in the PGRN gene result in lower protein expression or secretion pointing to haploinsufficiency as predominant mechanism (Shankaran et al 2008, Yu et al 2010). On the other hand, homozygous mutations in *GRN* are the cause of NCL, a lysosomal storage neurodegenerative disease (Smith et al 2012), confirming the dosage effects of PRGN in the disease manifestation and suggesting a role for the regulation of lysosomes (Almeida et al 2016). Additionally, PGRN is a modulator of immune function (Jian et al 2013). In the nervous system, microglia produce and secrete PGRN especially once activated during an insult or trauma (Moisse et al 2009, Naphade et al 2010, Philips et al 2010). Moreover, PGRN has been linked to microglia activation, migration, phagocytosis, and synapse pruning (Lui et al 2016, Martens et al 2012, Pickford et al 2011, Yin et al 2010). Thus, PGRN seems to have a role in microglia-mediated inflammation in neurodegenerative diseases. We further validate and investigate the involvement of PGRN, therefore WB and Q-PCR were performed.

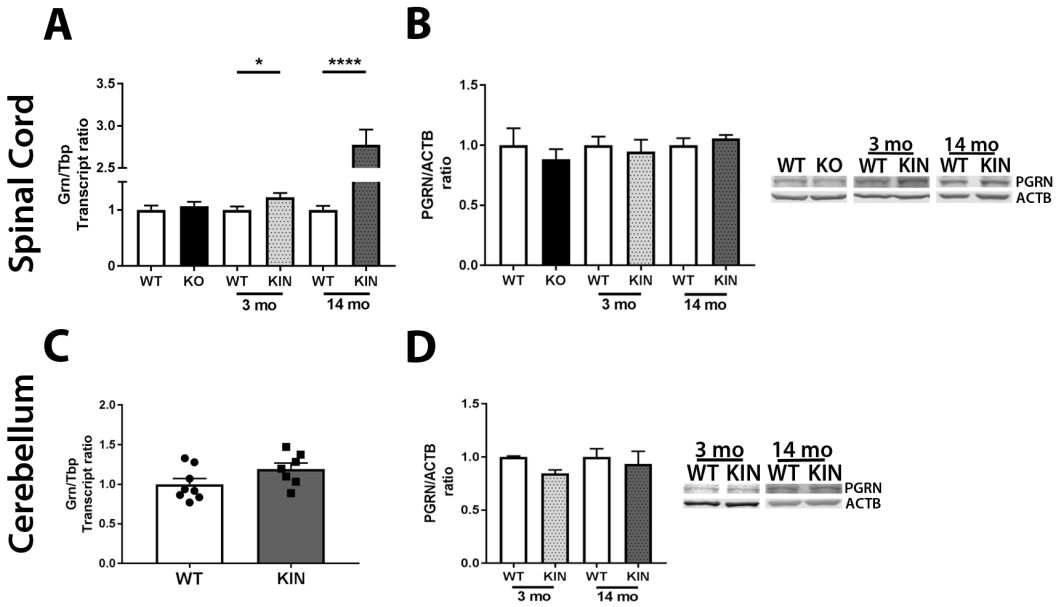

Figure 3.30. Progranulin transcript levels were up-regulated in the spinal cord of *Atxn2*-CAG100-KIN animals starting at the age of 3 month while protein levels were unchanged. (A) *Grn* transcript levels were specifically up-regulated starting at 3 months in the spinal cord of *Atxn2*-CAG100-KIN but not changed in the cerebellum at old age (C). Despite their up-regulation at transcript level, PGRN levels were not changed either in the spinal cord (B) or the cerebellum (D).

The transcript level of *Grn* was found up-regulated in the spinal cord of *Atxn2*-CAG100-KIN animals at ages of 3 (FC 1.22 p-value 0.049) and 14 months (FC 2.775 p-value <0.0001), while no changes were detected in the spinal cord of *Atxn2*-KO (FC 0.94 p-value 0.5912) (Figure 3.30, A) or in the 14-month-old cerebellar samples of *Atxn2*-CAG100-KIN (Figure 3.30, C; FC 1.192 p-value0.093). The protein level of PGRN was not changed in the spinal cord of the *Atxn2*-CAG100-KIN model suggesting either a translational problem or a high degradation rate. The antibody used didn't show the level of granulins (the cleaved product of PGRN), therefore they couldn't be quantified. The PGRN levels were not changed in the cerebellum or *Atxn2*-KO samples either.

Interestingly, two common features of RIPK1 and PGRN are their involvement in neuroinflammation and their high expression in microglia.

3.5.6 Validation of the transcriptomics data confirms the up-regulation of microglia activation and synaptic-pruning related transcripts

Following up with the 2-fold-up STRING analysis we validated and further investigated the involvement of the immune and lysosomal transcript

dysregulations in the spinal cord of *Atxn2*-CAG100-KIN and *Atxn2*-KO mouse models. We specifically focused on those that are highly expressed in microglia, since they are tightly linked to homeostatic maintenance of the nervous system.

The first set of transcripts evaluated were those related to the complement system, TREM2 and DAP12. The classical complement system is the major mediator of inflammation against infections and has been implicated in brain development, homeostasis, and disease (Stevens et al 2007). Complement proteins (C1q, C3 and C4) participate in synapse elimination by tagging weak synaptic connections for removal via phagocytic microglial activity during development (Schafer et al 2012), the so-called synaptic pruning. The complement cascade components C1q and C3 were shown to be crucial for pruning of retino-thalamic axons during development (Stevens et al 2007). Moreover, it has been demonstrated that microglia plays a major role in synaptic pruning during postnatal development in mice actively engulfing synaptic material (Paolicelli et al 2011), and that deficient neuron-microglia signaling impairs functional brain connectivity and alters behaviour (Zhan et al 2014). Altered synaptic pruning caused an excess of dendritic spines and immature synapses leading to an immature brain circuitry and potentially to neurodevelopmental disorders (Matcovitch-Natan et al 2016, Paolicelli et al 2011).

On the other hand, gliosis and neuroinflammation are hallmarks of Alzheimer's disease (AD), PD, ALS and FTD (Salter & Stevens 2017). Recent results point to an inappropriate activation of the complement-dependent pathway and excess of pruning by microglia as mediators of early synapse loss in AD (Hong et al 2016). Furthermore, a high number of loci linked to AD by GWAS (genome wide association studies) are expressed or exclusively expressed by microglia (Efthymiou & Goate 2017). Among these, *TREM2* R47H variant has been also linked to ALS, PD, and FTD (Lill et al 2015). TREM2 (triggering receptor expressed on myeloid cells 2) is an innate immune receptor expressed by microglia and myeloid cells, which mediates inflammatory and phagocytic signaling in immune cells through its co-receptor DAP12. Therefore, mutations impairing TREM2 signaling could affect microglial phagocytosis,

neuroinflammation, and microglia survival in neurodegenerative disorders (Salter & Stevens 2017).

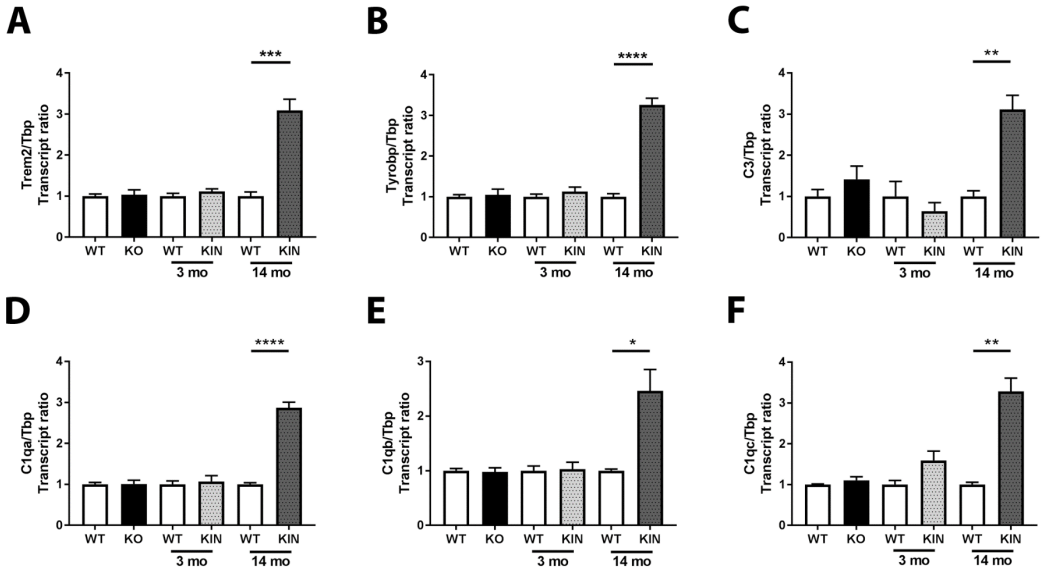

Figure 3.31. Validation of the complement system implicated in synaptic pruning, TREM2 and DAP12 transcripts. Q-PCR data from *Atxn2*-CAG100-KIN and *Atxn2*-KO spinal cord samples show a selective affection for the 14-month-old samples of *Atxn2*-CAG100-KIN mice.

All transcripts evaluated were up-regulated in the spinal cord of the 14-month-old *Atxn2*-CAG100-KIN mice (**Figure 3.31**). The phagocytic-related receptors *Trem2* (FC 3.09 p-value <0.0001) and *Tyrobp* (coding for DAP12; FC 3.26 p-value <0.0001) were found to be significantly up-regulated (**Figure 3.31**, A and B). All complement proteins involved in synaptic pruning analyzed were also up-regulated (*Cq1a* FC 2.87 p-value <0.0001; *C1qb* FC2.46 p-value 0.0138; *C1qc* FC 3.28 p-value 0.0019; *C3* FC 3.11 p-value 0.001) (**Figure 3.31**, C, D, E, and F). These results raised questions related to the activation of microglia and the implications of mutations in RBP, such as TDP43 and ATXN2.

3.5.7 Validation of transcripts involved in RNA/DNA immune response and lysosomal function

Several toll-like receptors (TLR) that recognize intracellular nucleic acids at the endosome were found to be up-regulated at the transcriptome data set from the 14-month-old spinal cord samples (Kawai & Akira 2010). Specifically, *Tlr3* (recognizing double stranded RNA), *Tlr7* (recognizing single stranded RNA), and

Tlr9 (recognizing DNA) were found to be strongly up-regulated. These receptors are part of the innate immune system, the first line of defense against viral, bacterial, fungal, and protozoa infections. Different types of receptors, called pattern recognition receptors (PRRs), are able to recognize pathogen associated molecular patterns (PAMPs) and are part of this system. PRRs are also able to activate a series of defense mechanisms to eliminate the infection (Chen et al 2017).

Aside from the TLR family, there are five more families classified based on their protein domains: RIG-I like receptors (RLRs), NOD-like receptors (NLRs), C-type lectin receptors (CLRs), AIM2-like receptors (ALRs), and the cytosol DNA sensing PRR cyclic GMP-AMP synthases (cGAS) (Chen et al 2017). PRRs also recognize endogenous damage associated molecular patterns (DAMPs) from the host, therefore they are also important to maintain homeostasis. However, PRR dysregulation can lead to autoimmune diseases (Chen et al 2017). Interestingly, TLR3 is up stream of RIPK1, which also localizes in the membrane of astrocytes and microglia (Verma & Bharti 2017), while granulins (PGRN cleaved products) are cofactors for TLR9 signaling (Park et al 2011). Further down-stream from the TLR activation, interleukin receptor-associated kinase 1 and 4 (IRAK1 and IRAK4) (Flannery & Bowie 2010) were also up-regulated. As a result of the TLR activation, proinflammatory cytokines, and anti-viral type I interferon (IFN) inducing factors are activated (Kawai & Akira 2010). Other factors involved in pathogen/immune response that were found dysregulated in the transcriptome data are the Signal transducer and activator of transcription 1 (STAT1), LYN Proto-Oncogene Src Family Tyrosine Kinase (LYN), and cerebellar degeneration-related autoantigen 1 (CDR1) (Sthoeger et al 2013). The Ribonuclease T2 (RNASET2), implicated in the innate immune system, has been shown to participate in the lysosomal degradation of ribosomal RNA in zebrafish (Haud et al 2011). RNASET2 transcript was also up-regulated in the transcriptome data set. Moreover, both Cytochrome B-245 Beta chain and Alpha chain (CYBB and CYBA) transcripts, as critical components of the membrane-bound oxidase of phagocytes responsible for generating microbicidal superoxide, were up-regulated as well. Based on the implication of all of these factors in RNA/DNA immune response, proinflammatory response, degradation of RNA, and

phagocytosis, we validated the transcriptome results by Q-PCR in the spinal cord of 3-month-old and 14-month-old *Atxn2*-CAG100-KIN and 6-month-old *Atxn2*-KO animals.

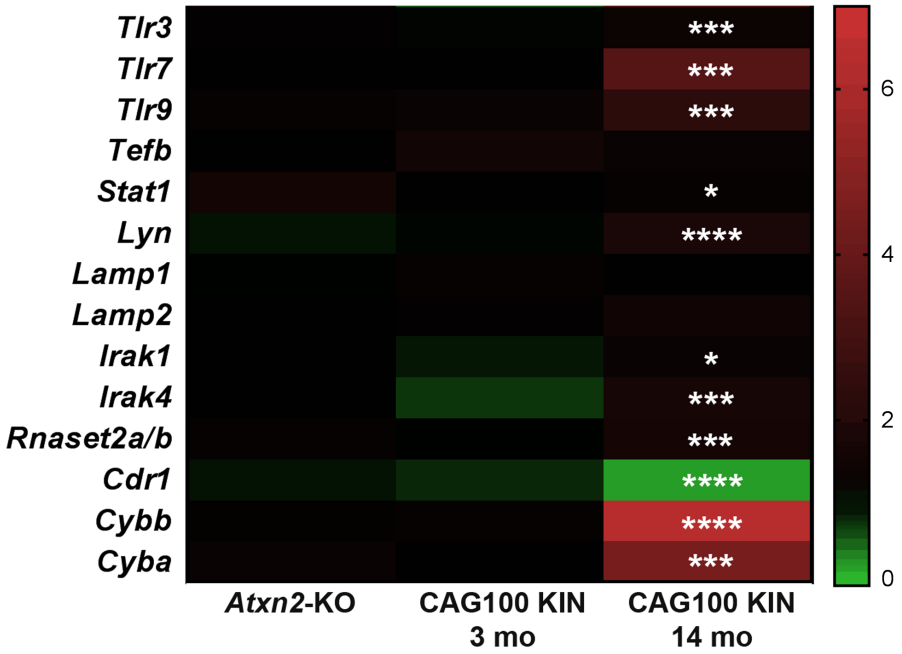

Figure 3.32. Heatmap validation by Q-PCR of genes involved in RNA/DNA immune response and lysosomal function. Validation of the selected factors by Q-PCR in 3-month-old (3 mo) *Atxn2*-CAG100-KIN, 14-month-old (14 mo) *Atxn2*-CAG100-KIN and *Atxn2*-KO spinal cord samples.

All of the transcripts that were found dysregulated in the trasncriptome data set of Atxn2-CAG100-KIN 14-month-old spinal cord samples were validated by Q-PCR (*Tlr3* FC 1.33 p-value 0.0002; *Tlr7* FC 3.47 p-value 0.0001; *Tlr9* FC 2.26 p-value 0.0002; *Stat1* FC 1.2 p-value 0.0434; *Lyn* FC 1.76 p-value <0.0001; *Irak1* FC 1.27 p-value 0.0195; *Irak4* FC 1.62 p-value 0.0004; *Rnaset2a/b* FC 1.59 p-value 0.0001; *Cdr1* FC 0.23 p-value <0.0001; *Cybb* FC 6.36 p-value <0.0001; *Cyba* FC 4.478 p-value 0.0003). Moreover, the transcript levels of the transcription factor EB (*Tfeb*), the master gene for lysosomal biogenesis (Sardiello et al 2009), and the two lysosomal markers lysosomal-associated membrane protein 1 and 2 (*Lamp1* and *Lamp2*), were evaluated in order to determine the lysosomal response. All three (*Tfeb*, *Lamp1*, *Lamp2*) were not dysregulated in the 14-month-old spinal cord samples, suggesting that overall lysosomal mass was unchanged. No dysregulation was detected for the 3-month old *Atxn2*-CAG100-

KIN or *Atxn2*-KO spinal cord samples regarding these transcripts pointing to a time-dependent response in the tissue.

3.5.8 Glia markers are affected in the spinal cord and cerebellum of the *Atxn2*-CAG100-KIN mouse model

After validation of the spinal cord transcriptome data regarding factors related to immune response and lysosomal function implicated in RNA toxicity, we wanted to define the response from glia in the mouse model. Over time, more important roles in the CNS have been attributed to glia cells; therefore the classic view of exclusive neuronal dysfunction in neurological diseases has been challenged. Two different glia cell types were investigated by Q-PCR and WB: microglia (Figure 3.33) and astroglia (Figure 3.34).

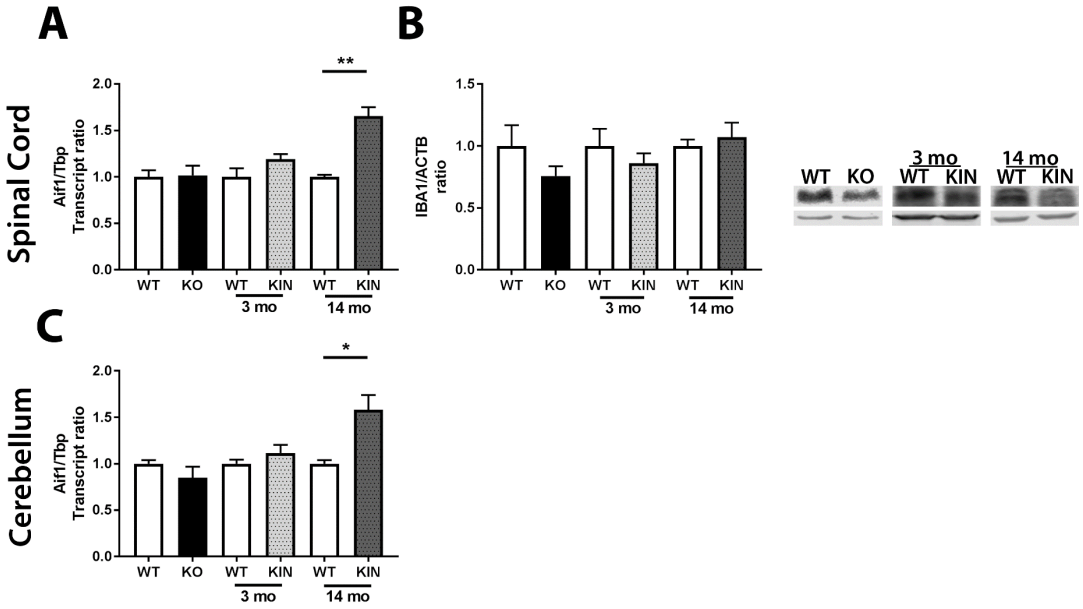

Figure 3.33. Evaluation of the transcript level of *Aif1* and protein level of IBA1 as microglia marker in the *Atxn2*-CAG100-KIN and *Atxn2*-KO mouse models. The well-established microglia marker IBA1, product of the *Aif1* gene, was used to analyze the microglia response in the spinal cord and cerebellum. A higher significant up-regulation was observed for the transcript level of *Aif1* in the 14-month-old samples of *Atxn2*-CAG100-KIN mice (A; FC 1.65 p-value 0.0002) compared to the up-regulation in the cerebellum in the same animals (C; FC 1.45 p-value 0.0296). No differences were observed in the 3-month-old samples (cerebellar and spinal cord) of *Atxn2*-CAG100-KIN nor for *Atxn2*-KO samples regarding *Aif1* levels (A and C). No dysregulation was detected at the protein level for IBA1 (B) in any condition.

As expected, the microglia/macrophage gene marker *Aif1* (Allograft inflammatory factor 1) was also up-regulated in the 14-month-old spinal cord samples (Figure 3.33, A; FC 1.65 p-value 0.0002). *Aif1* is strongly and specifically

expressed in microglia in the CNS and its product, IBA1 (ionized calcium-binding adapter molecule 1), is a widely used marker to detect microglia. Despite all the up-regulations seen in transcripts related to microglia activation and synaptic pruning in the 14-month-old spinal cord samples, the protein level of IBA1 was not changed in WB experiments (Figure 3.33,B). The transcript level of *Aif1* was also investigated in the cerebellum of 3-month-old and 14-month-old *Atxn2*-CAG100-KIN and *Atxn2*-KO animals by Q-PCR. An up-regulation of *Aif1* was again detected for the 14-month-old samples (Figure 3.33, C; FC 1.45 p-value 0.0296). The protein level of IBA1 in the cerebellum wasn't determined, since recent publications point to higher rates of basal turnover and increased expression of proinflammatory genes in this tissue (Stowell et al 2018).

Astrocytes are the largest cell population in the CNS with increasing presence with phylogeny and brain complexity (Nedergaard et al 2003). In the human cortex there are 1.4 astrocytes for every neuron (Bass et al 1971, Nedergaard et al 2003). They are also the most heterogeneous group of glia cells and are distributed in a non-overlapping manner throughout the entire CNS (Sofroniew & Vinters 2010). The classical view of the astrocytes as only providing structural support has been discarded after their implication in a wide variety of essential functions in the CNS such as synapse development, neurotransmitter homeostasis, glycogen storage, and blood brain barrier maintenance (Palmer & Ousman 2018, Sofroniew & Vinters 2010). Moreover, astrocyte dysfunction has been implicated in neurodegenerative diseases such as AD, PD and ALS (Palmer & Ousman 2018). Therefore, we aimed to characterize the astrocyte activation by quantifying the levels of GFAP (glial fibrillary acidic protein), since it is highly specific to the astroglial lineage (Reeves et al 1989) and since it has been shown to be up-regulated in reactive astrocytes (Nedergaard et al 2003, Palmer & Ousman 2018).

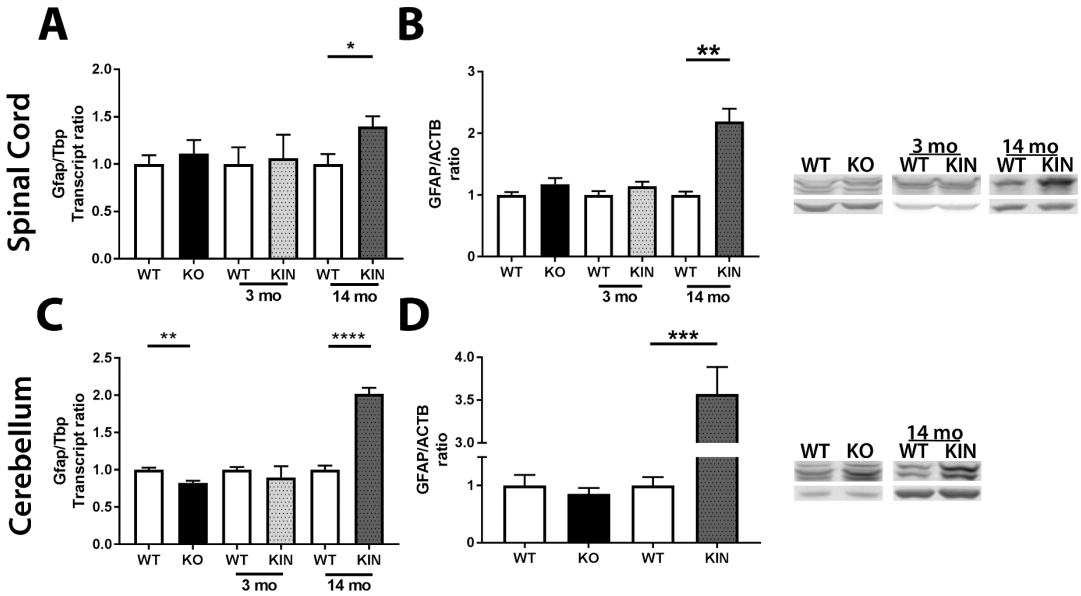

Figure 3.34. Evaluation of the transcript level of *Gfap* and protein level of GFAP as an astroglia marker in *Atxn2*-CAG100-KIN and *Atxn2*-KO mouse models. An up-regulation for *Gfap* was detected in spinal cord (FC 1.4 p-value 0.021) and cerebellar (FC 2.02 p-value <0.0001) samples from the 14-month-old *Atxn2*-CAG100-KIN mice. A significant increase of GFAP levels were also detected in spinal cord (FC 2.19 p-value 0.0017) and cerebellar (FC 3.57 p-value 0.0004) samples from the 14-month-old *Atxn2*-CAG100-KIN mice. A slight but significant down-regulation of *Gfap* was detected in the cerebellar samples (FC 0.83 p-value 0.0012) of *Atxn2*-KO mice but without changes at the protein level.

Similar to the transcript levels of *Aif1*, *Gfap* showed an up-regulation at 14-month-old in both tissues (cerebellum and spinal cord) at the age of 14 months from the *Atxn2*-CAG100-KIN mouse model. An up-regulation of GFAP level was also detected by WB in both tissues pointing to an activation of astrocytes over time. Interestingly, a discrete but significant down-regulation of *Gfap* was detected in the cerebellar samples of *Atxn2*-KO.

These data point to a pathologic ageing in this mouse model affecting glia cells, which could aggravate the underlying pathology.

3.5.9 Stress granule formation in BV2 murine microglia cell line under NaArs stress

As mentioned in the introduction, stress granules (SG) are cytoplasmic regions with a high density of RNA and RBP where translation has been stalled. SG form during cellular stress, such as oxidative stress, starvation, or Sodium Arsenite (NaArs) treatment. Using the murine microglia cell line BV2, we decided to determine if stress granules were formed during NaArs stress by

immunocytochemistry. PABP1 was used as a marker since its presence in SG has been established (Kedersha et al 2000, Kedersha et al 2005) together with ATXN2 (Figure 3.35, A). Moreover, TDP43 has been recently implicated in microglia function (Paolicelli et al 2017), thus it was also of interest to determine its localization during NaArs treatment, and specifically if it was co-localizing with ATXN2 in SG.

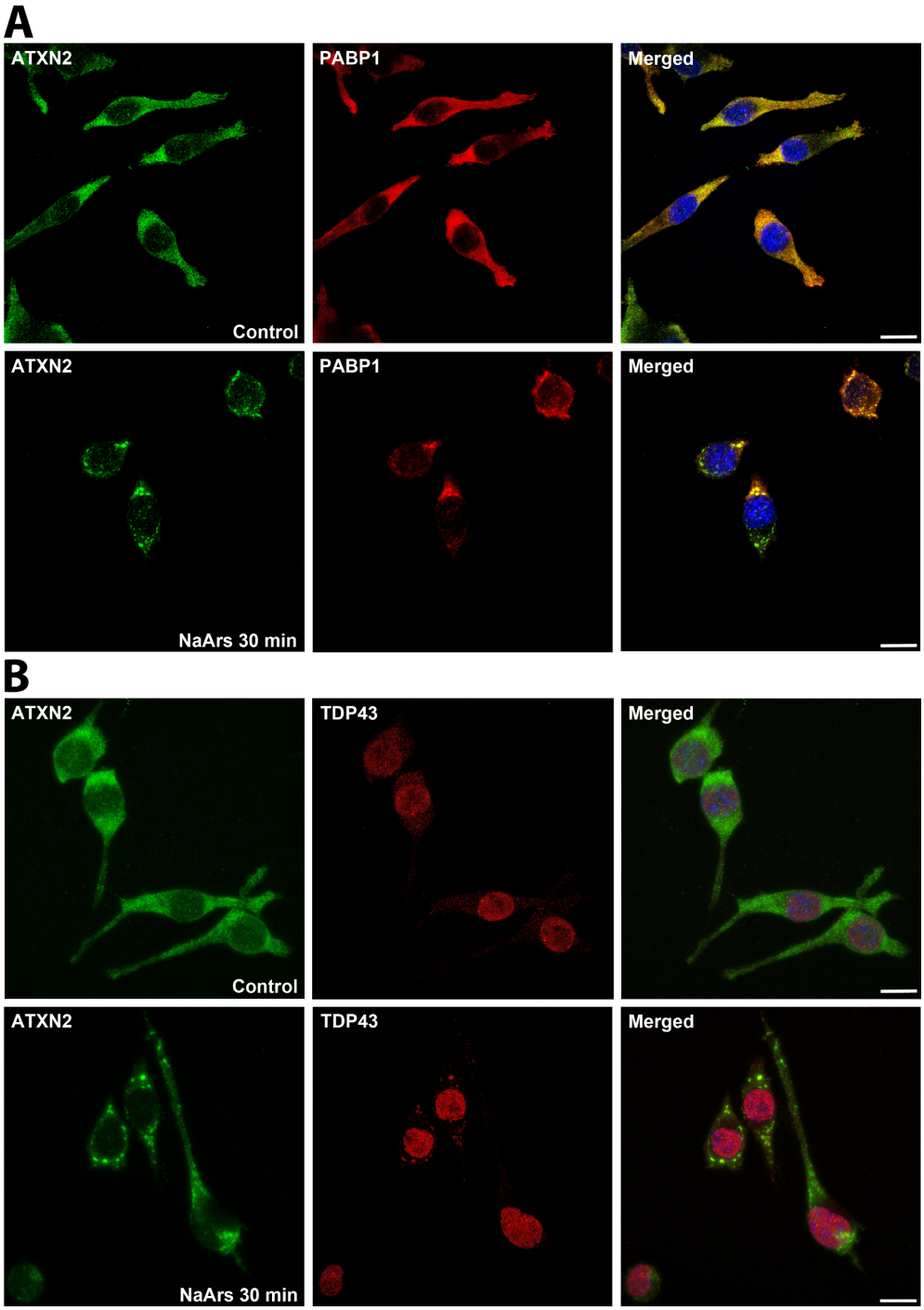

Figure 3.35. Immunocytochemistry of non-stressed (control) and NaArs-stressed BV2 cells. ATXN2 is stained in green and PABP2 (A) or TDP43 (B) in red. In all of the merged panels, DAPI was used to stain the nuclei in blue. Scale bar 50 μm.

As expected, ATXN2 and PABP1 localize in the cytosol and TDP43 in the nuclei under control conditions (Figure 3.35, A and B). However, when BV2 cells were stressed with NaAs for 30 min, ATXN2 and PABP1 co-localized in granule-like structures suggesting SG formation in the BV2 microglia cell line (Figure 3.35, A). TDP43 discretely shuttled out of the nuclei after NaAs treatment and seemed to co-localize with ATXN2 in SG (Figure 3.35, B).

Stress granule formation seems to be a widely evolutionary conserved mechanism among different types of cells in mammalian organisms necessary to deal with translation during periods of stress. These data show the formation of SG and the participation of disease associated RBP, such as ATXN2 and TDP43 in the microglia cell line BV2.

3.5.10 Microglia shows ATXN2 positive aggregates in the spinal cord of 14-month-old *Atxn2*-CAG100-KIN mice

After confirming that ATXN2 is present in the murine microglia cell line BV2 and localizes in SG during cell stress periods, the next step was to examine the presence of aggregates in microglia in the spinal cord by immunohistochemistry. The microglia marker IBA1 was used to first detect these small cells and then look for ATXN2 presence within IBA1-positive cells. Spinal cord sections from 6-month-old *Atxn2*-CAG100-KIN and *Atxn2*-KO animals were used together with sex- and age-matched WT sections to confirm that the signal detected by the monoclonal antibody against ATXN2 was indeed detecting the signal in microglia (IBA1-positive) cells.

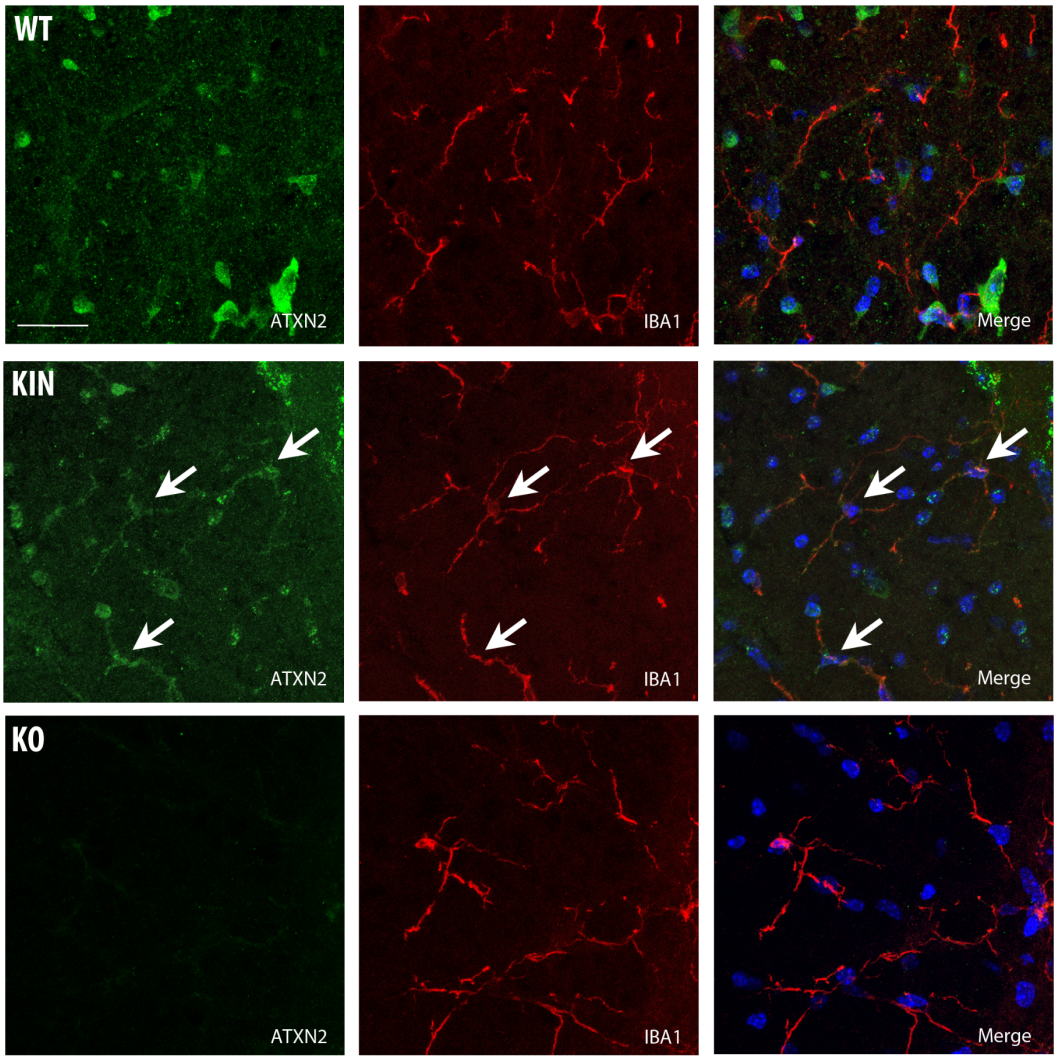

Figure 3.36. Co-immunohistochemical staining of ATXN2 (green) and IBA1 (red) in spinal cord sections of 6-month-old *Atxn2*-CAG100-KIN and *Atxn2*-KO animals compared to sex- and age-matched WT shows increase of ATXN2 signal in the IBA1-positive cells in the *Atxn2*-CAG100-KIN section. Nuclei were detected with DAPI (blue). Scale bar represents 25 µm.

Immunohistochemistry of ATXN2 (green) in WT sections of 6-month-old animals did not show a highly positive signal in the microglia cells detected with IBA1 (red) (Figure 3.36, first row). Microglia are small cells, therefore the cytoplasm area where ATXN2 localizes under normal conditions is rather limited. On the other hand, microglia detected in the spinal cord of *Atxn2*-CAG100-KIN sections showed a stronger signal for ATXN2 (Figure 3.36, second row) suggesting a time-dependent accumulation of this protein in microglia. In the spinal cord sections of *Atxn2*-KO animals, no signal for ATXN2 was detected but IBA1-positive cells

were also observed, corresponding to microglia in this mouse model (Figure 3.36, third row).

To follow up, immunohistochemistry in the 14-month-old spinal cord sections of *Atxn2*-CAG100-KIN mice was performed. We aimed to elucidate the presence of ATXN2 aggregates in microglia at the old stage of the disease for this model.

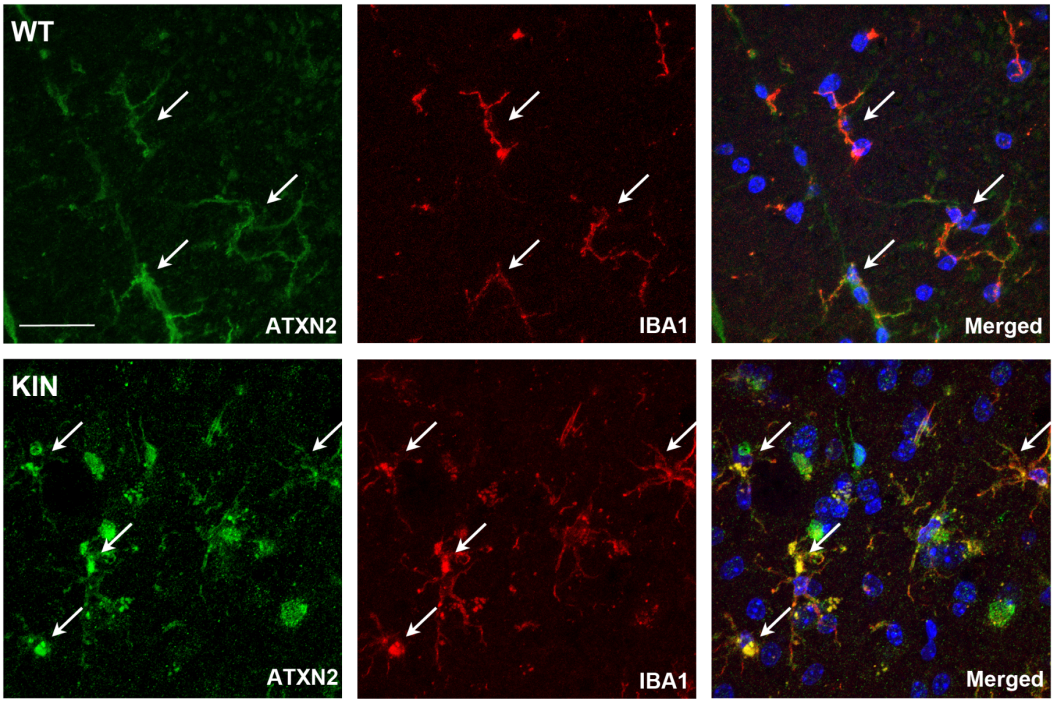

Figure 3.37. Co-immunohistochemical staining of ATXN2 (green) and IBA1 (red) in the spinal cord sections of 14-month-old *Atxn2*-CAG100-KIN mice compared to sex- and age-matched WT shows ATXN2 aggregates in IBA1-positive cells. Nuclei were detected with DAPI (blue). Scale bar represents 25 µm.

By comparing the WT samples from 6-month-old (Figure 3.36, first row) and 14-month old (Figure 3.37, first row) animals, an increase of positive ATXN2 signal can be seen. Over time, microglia turnover slows down and their transcript profile also changes (Fuger et al 2017), thus ATXN2 could be accumulating under normal conditions. In case of the *Atxn2*-CAG100-KIN samples, ATXN2 aggregates were detected in microglia (IBA1-positive) cytoplasm, pointing to a potential accumulation of endogenous ATXN2 and/or phagocytosis of debris from dying neurons.

3.5.11 Establishing new tools to study the effect of ATXN2 in microglia function

One of the big limitation points of working with tissue homogenates is the inability to determine the response from a specific cell type. For example, one cannot define if a transcript is being up-regulated exclusively in microglia or if neurons also play a role. In order to overcome this problem, primary microglia cultures were established from postnatal day 0 (P0) pups. Heterozygous crosses were used to have both genotypes, WT and KIN (*Atxn2*-CAG100-KIN), as offspring from the same animals, to reduce variation.

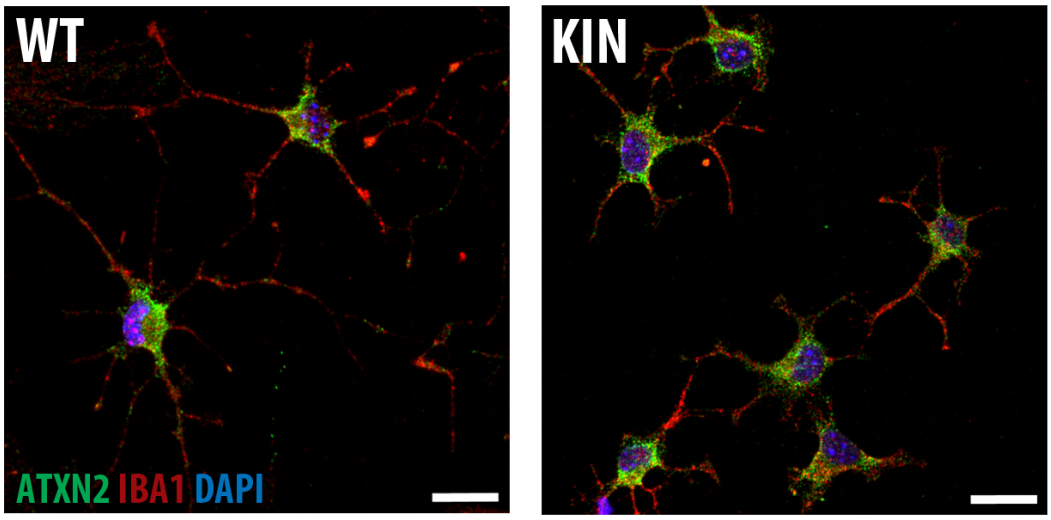

Figure 3.38. Immunocytochemistry of primary microglia cell cultures from P0 pups. The cultures were established in parallel from the same litter. ATXN2 (green) was detected in all microglia cells, which are IBA1-positive (red). Nuclei were detected with DAPI (blue). Scale bar represents 15 µm.

Following the protocol specified in Material and Methods, and once the cultures were confluent and the microglia cells were growing on top of the astrocyte layer, microglia were isolated. To check the purity of microglia after isolating them, IBA1 was used as a marker (Figure 3.38). To further demonstrate the expression of ATXN2 by microglia, it was co-immunohistochemically stained with IBA1 (Figure 3.38). The positive signal of ATXN2 antibody in the purified microglia primary cultures verified once more its presence in this cell type.

Despite the clear advantages of working with primary cultures, there are several points to consider such as the number of pups used and the challenges in continuously generating such cultures. Therefore, a second tool was proposed in

order to evaluate the effect of different size expansions in ATXN2 in microglia. The murine microglia cell line BV2 was previously employed to demonstrate the presence of ATXN2 and its response to NaArs-stress (Figure 3.35). In addition, BV2 cells are easy to culture and manipulate making them a perfect model for further experiments. In order to understand the effect of ATXN2 expansion in microglia function, we stressed them with LPS, mimicking a bacterial infection instead of stressing them with NaArs. The BV2 cells were transfected with the empty vector myc, myc-Atxn2-Q22 (ATXN2 with an expansion of 22 glutamines), myc-Atxn2-Q79 (ATXN2 with 79Q), or only treated with the transfection agent lipofectamine 3000 (control). Independent triplicates were generated for each condition and the non-LPS treated control (Lipo) was used as reference point in the analysis.

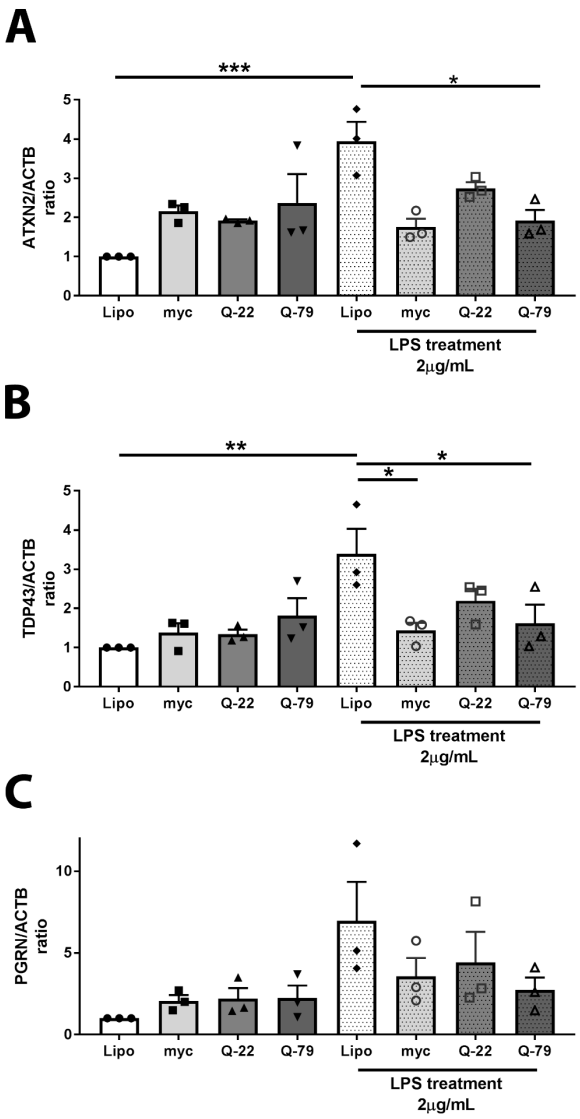

Figure 3.39. Two-way ANOVA from WB quantification data of ATXN2, TDP43 and PGRN in control and LPS-treated BV2 RIPA fraction. Evaluation of the LPS effect on transfected BV2 cells compared to non-LPS-treatment and lipofectamine control by WB.

Although lipofectamine is widely used to transfect BV2 cells and the reagent itself does not induce microglia activation (Smolders et al 2018), we cannot rule out unspecific effects via introducing foreign DNA into this cell type. A significant up-regulation of ATXN2 levels were detected between the Lipo-control and the Lipo-treated with LPS (FC 2.95 p-value 0.0003), while ATXN2 levels did not increase significantly in the myc-Atxn2-Q79 LPS treated when compared to the Lipo-treated group (p-value 0.0123). Similarly, TDP43 levels were up-regulated in the control group when treated with LPS (FC 2.4 p-value 0.0044), however the other groups did not up-regulate TDP43 levels (Lipo-treated vs myc-treated: p-value 0.023; Lipo-treated vs Q-79 treated: p-value 0.047). PRGN levels did not

reach any significance in the statistical analysis due to high variance in the LPS-treated groups.

3.6 Transcriptomics from 3- and 14-month-old cerebellum of *Atxn2*-CAG100-KIN mice

To complete the description at the mRNA level of the *Atxn2*-CAG100-KIN mouse model, two more transcriptomics data sets were generated using the Affymetrix Clariom™ D mouse arrays from ThermoFisher. The experimental design was the same as previously described (Figure 3.24, A) and the analysis was carried out with the TAC software following the same standard parameters and self-determined filter criteria as for the spinal cord samples (fold change <-1.2 or > 1.2; p-value ≤ 0.05).

3.6.1 General data from the arrays shows a higher number of up-regulated genes at both ages

Similar to the data obtained from the spinal cord transcriptomics, the cerebellar data shows a higher number of up-regulations that passed the filter criteria compared to down-regulations (Table 3.8). In the volcano plots (Figure 3.40) the distribution of dysregulated genes can be appreciated.

	Passed filter criteria	Up regulated	Down regulated
Cerebellum			
3 months	2041	1378	663
14 months	3857	2222	1635

Table 3.8. Genes that passed the filter criteria established from a total of 65,956 screened transcripts. Three WT and three KIN were used in each condition; 3 and 14 months.

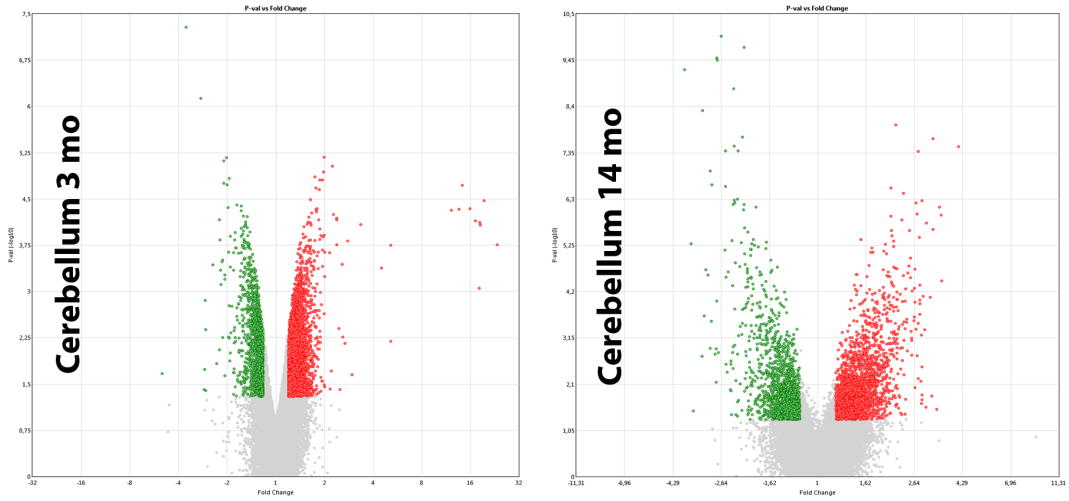

Figure 3.40. Volcano plot showing the distribution of the genes that passed the filter criteria. Significantly up-regulated transcripts are highlighted in red and significantly down-regulated in green. Fold-change values are plotted.

When comparing the different groups in the array with the percentages corresponding to the significantly dysregulated transcripts, the Non-Coding group shows the highest percentage of all; 59% in the 3-month-old and 68% in the 14-month-old cerebellar samples. This effect was also observed in both spinal cord transcriptomic data sets (50% of Non-Coding in the significantly up-regulated transcripts in the 3-month-old data set and 42% in the 14-month-old spinal cord data set).

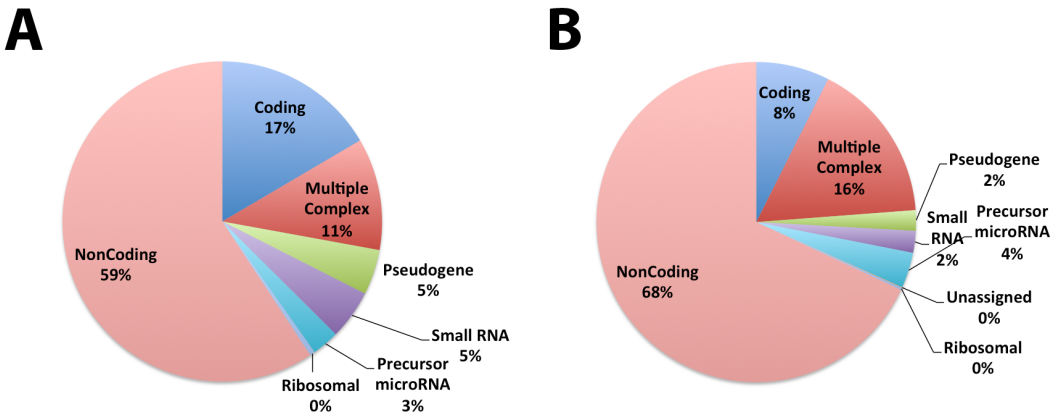

Figure 3.41. Percentage distribution of the significantly up-regulated transcripts in the different categories from the array corresponding to (A) 3 mo and (B) 14 mo. The highest percentage of significantly up-regulated transcripts corresponds in both cases to the Non-Coding category followed by the Multiple Complex and Coding categories.

3.6.2 A common significant dysregulated pathway in all transcriptomics data sets is the Cholesterol metabolism

The Transcriptome Analysis Console (TAC) software generates lists of differentially expressed genes and determines pathways of interest from publicly available databases such as *Wikipathways*. A commonly affected pathway that was identified in all data sets was the Cholesterol metabolism. When the data sets were screened for transcripts involved in biosynthesis, degradation, and transports of cholesterol, a high number of them were dysregulated in all conditions. Therefore, we wanted to visualize the distribution of the raw data corresponding to these transcripts to further identify candidates in the *Atxn2*-CAG100-KIN mouse model that could be useful to follow the progression of the disease. The expression values were first normalized to define background values in the microarray and then plotted in a heatmap with Spotfire Decision site 9.1.2 software to better compare the different ages and tissues used (Figure 3.42). The normalized expression values were only visualized in the heatmap, therefore no statistical analysis was performed at this point.

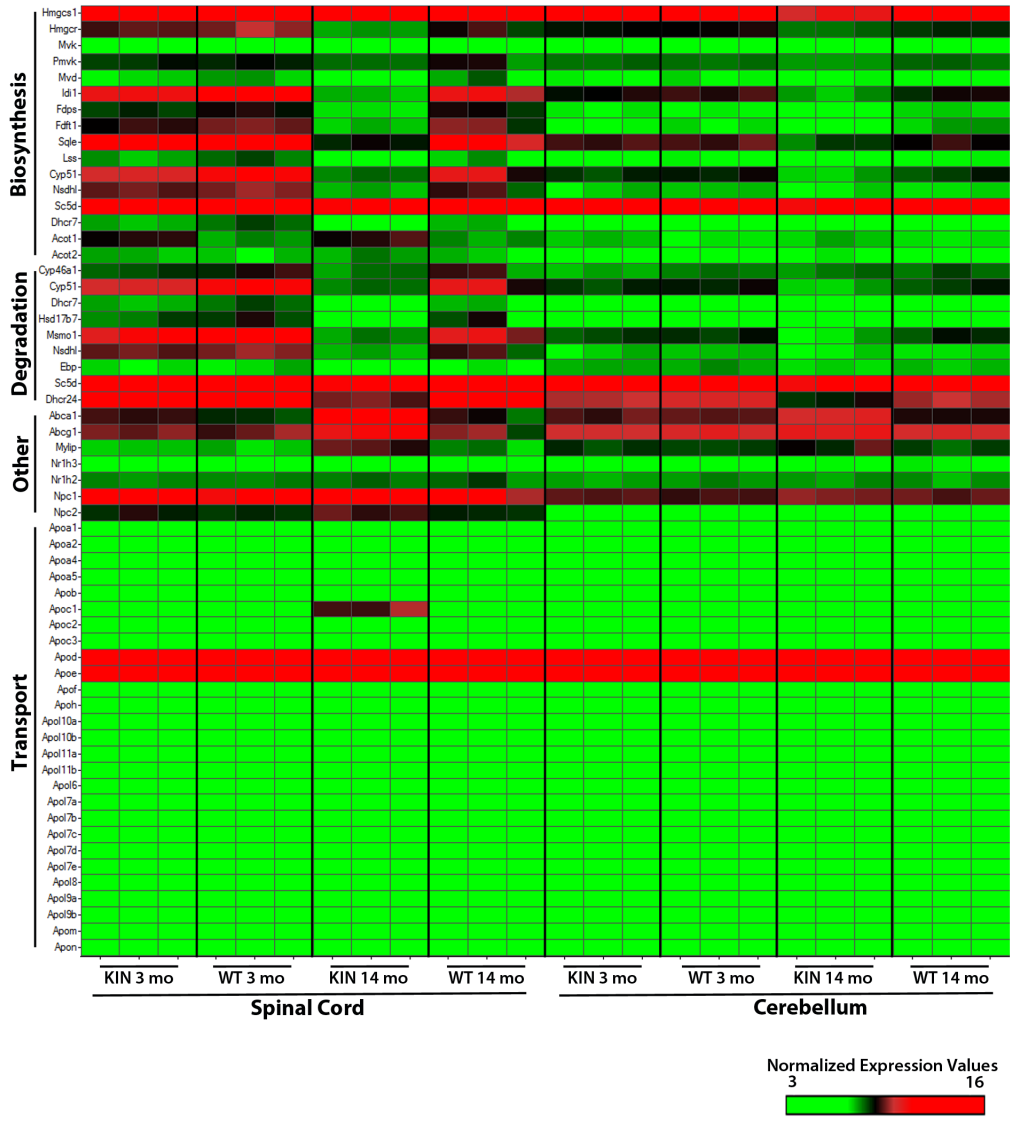

Figure 3.42. Heatmap generated with the Spotfire Decision site 9.1.2 software showing the normalized expression values from the array corresponding to the Cholesterol metabolism pathway. The heatmap allows us to visualize the differences in the raw expression values and compare them between the different age and tissue conditions used to generate the transcriptomics data sets.

Overall, the cholesterol biosynthesis related transcripts were highly expressed in the 3-month-old spinal cord samples, showing a similar pattern between the mutant and WT. Regarding the 3-month-old cerebellar samples, overall fewer transcripts seem to be highly expressed compared to the spinal cord. Therefore, a more discrete affection of the biosynthesis of cholesterol was expected especially in the cerebellum of 3-month-old *Atxn2*-CAG100-KIN animals compared to the sex- and age-matched WT. On the other hand, when comparing the cholesterol biosynthesis in the spinal cord of 14-month-old *Atxn2*-CAG100-

KIN animals to the WT there was a clear reduction in expression values for an important number of implicated factors. A similar effect was also observed for the cerebellar samples where the *Atxn2*-CAG100-KIN showed lower expression values than the WT. Next, factors implicated in degradation of cholesterol were also visualized (Figure 3.42); the cholesterol is known to have a slow turnover in the CNS. Interestingly, in both spinal cord and cerebellar samples from 14-month-old *Atxn2*-CAG100-KIN a different pattern for the transcripts plotted could be observed, suggesting that not only biosynthesis, but also degradation of cholesterol was affected.

3.6.3 Validation of dysregulated transcripts identified via transcriptomics regarding cholesterol metabolism in cerebellar samples of *Atxn2*-CAG100-KIN and *Atxn2*-KO mouse models

Ataxin2 has been implicated in lipid metabolism and *Atxn2*-KO mice show an increase of weight and insulin resistance (Kiehl et al 2006, Lastres-Becker et al 2008a). Moreover, these animals present an increase of cholesterol levels in serum, lipid and glycogen accumulation in the liver, and alteration of lipids and lipid metabolism-related molecules in the cerebellum pointing to a general dysregulation of lipid metabolism in absence of *Atxn2* (Lastres-Becker et al 2008a, Meierhofer et al 2016).

Cholesterol is an essential structural component for cellular membranes. The brain is the most cholesterol-rich organ containing around 20% of the body's cholesterol (Björkhem & Meaney 2004), thus it is an essential component for neuronal physiology. The cholesterol metabolism in the brain is independent from the peripheral tissues due to the presence of the blood brain barrier (BBB) (Jeske & Dietschy 1980). An important percentage of cholesterol in the adult brain forms the myelin sheaths to insulate axons with the rest present in plasma membranes to maintain the morphology and synaptic transmission in neurons and other cell types, such as astrocytes (Dietschy & Turley 2004). Moreover, cholesterol depletion in neurons impairs synaptic vesicle exocytosis, neuronal activity, and neurotransmission, leading to dendritic spine and synapse degeneration (Zhang & Liu 2015). Defects in brain cholesterol have been linked to neurodegenerative disorders such as AD, PD, and Huntington's disease (HD).

Therefore, validation efforts were made to further investigate the cholesterol metabolism in the cerebellum of the *Atxn2*-CAG100-KIN model. Several transcripts that were identified via transcriptomics in both spinal cord and cerebellar tissue were analyzed in 3-month-old and 14-month-old *Atxn2*-CAG100-KIN cerebellar samples together with *Atxn2*-KO samples.

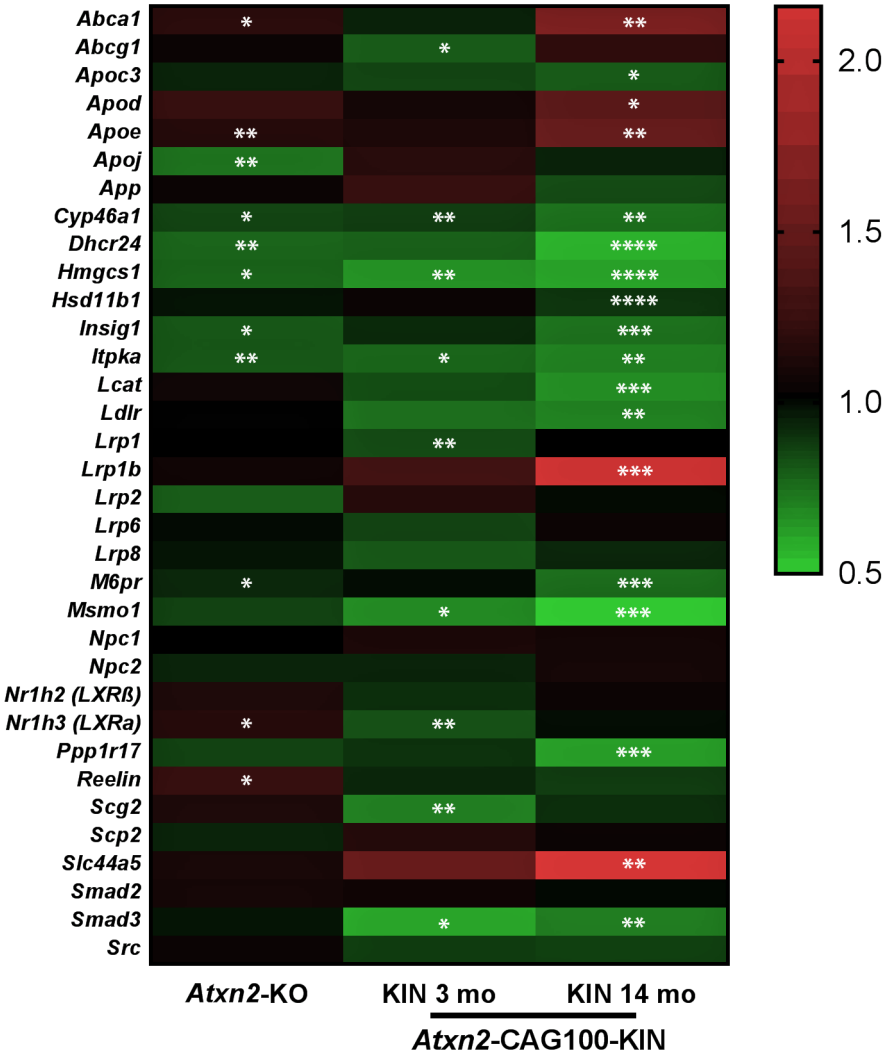

Figure 3.43. Heatmap generated with GraphPad plotting the Fold-Change values from Q-PCR experiments. Validation of several dysregulated genes in the cerebellum of Atxn2-KO and Atxn2-CAG100-KIN mice at different ages compared to their WT. Stars correspond to significances obtained from GraphPad analysis.

Three important enzymes implicated in the biosynthesis and degradation of cholesterol were found to be down-regulated in almost all conditions tested: *Cyp46a1* (Cytochrome P450 family 46 subfamily A member 1, implicated in degradation), *Dhcr24* (24-Dehydrocholesterol reductase, implicated in degradation), and *Hmgcs1* (3-Hydroxy-3-methylglutaryl-CoA synthase 1,

implicated in biosynthesis). The upstream factor of *Hmgcs1*, *Insig1* (Insulin induced gene 1), was also found to be down-regulated in *Atxn2*-KO and 14-month-old *Atxn2*-CAG100-KIN samples thereby suggesting a loss of feedback control in cholesterol synthesis. On the contrary, the astrocyte membrane cholesterol transporter *Abca1* (ATP binding cassette subfamily A member 1) was found up-regulated in both *Atxn2*-KO and 14-month-old *Atxn2*-CAG100-KIN samples sets. The Apolipoprotein E transcript (*Apoe*), which has been long implicated in AD, was found significantly up-regulated in *Atxn2*-KO and 14-month-old *Atxn2*-CAG100-KIN samples. Overall, these data suggest that the loss-of-function of ATXN2 either via knocking out or via aggregation due to poly(Q) expansions affects the synthesis and degradation of key factors in cholesterol metabolism, likely leading to an imbalance of this essential component in membranes and myelin sheaths.

Part 2 – Ataxia Telangiectasia Mutated

Ataxia Telangiectasia (A-T) is a recessive form of ataxia caused by loss-of-function mutations in the ataxia telangiectasia mutated (ATM) gene. Affected patients suffer from a progressive cerebellar ataxia that develops into general motor dysfunction, immunodeficiency, and radiosensitivity, predisposing them to cancer (Chun & Gatti 2004, Shiloh & Lederman 2017). The evaluation of alpha-fetoprotein in blood serum is used as a biomarker since it is usually detectable early in disease progression (Schieving et al 2014). We aimed to characterize new molecular biomarkers using cerebrospinal fluid (CSF) samples from patients and controls, and to obtain novel insights into the progression of the ataxia. This work was done in collaboration with the laboratory of Professor Ralf Schubert in the department for children and adolescents at Goethe University; they kindly provided all the murine samples and patients' data used in this part.

3.7 A-T patient cerebrospinal fluid shows progressive elevation of protein albumin

In order to identify novel molecular biomarkers of risk and progression in A-T, the CSF from 12 patients and 12 sex- and age-matched control individuals was analyzed. In addition to diagnostic tests such as neuroimaging (Figure 3.44, A), clinical ataxia scores and determination of alpha-fetoprotein levels were documented (Table 3.9).

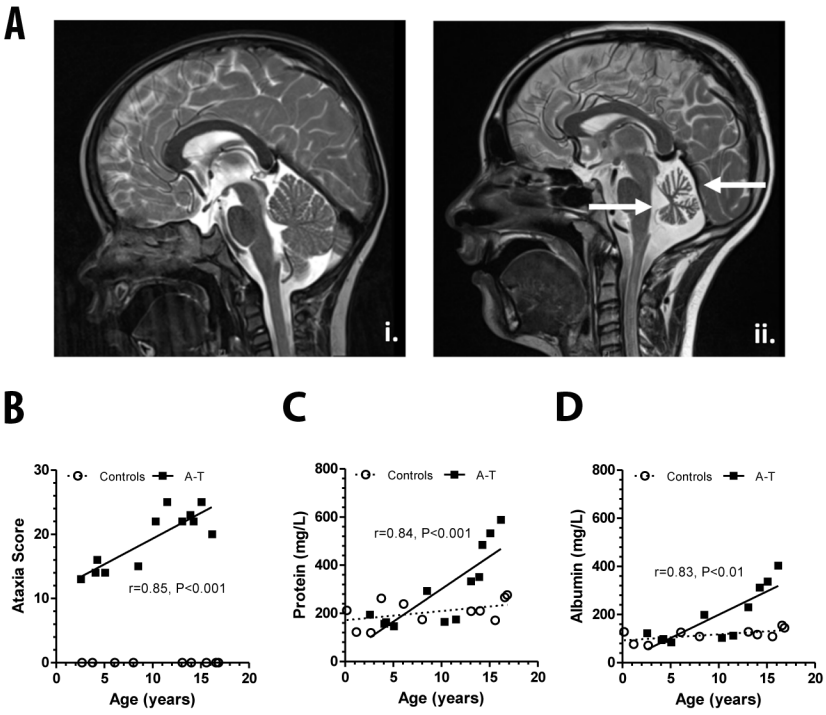

Figure 3.44. Progressive neurodegeneration in A-T: (A) MRI images from (i) a 3-year-old and (ii) a 16-year-old patient with A-T. The shrinking cerebellum of the older A-T patient is surrounded by an excess amount of CSF (highlighted by white arrows). This extracellular fluid generates high intensity values (shown as light gray or white) in the T2-weighted magnetic resonance image. (B) Age-associated progression of ataxia scores is documented for 12 patients. Controls showed no signs of ataxia (score = 0). (C) Total protein and (D) albumin concentrations analyzed in CSF of the 12 A-T patients and control individuals. Correlation between these parameters and age in A-T was assessed by calculating Pearson's correlation coefficient.

Parameters	Controls (*n*=12)	A-T patients (*n*=12)
Age [years]	8.5±6.4	10.0±4.8
Sex [female/male]	4/8	5/7
Height [cm]	128±40.4	128±26.3
Weight [kg]	32.0±23.7	31.1±19.4
Ataxia score	0±0.0	20.2±4.2
α-Fetoprotein [ng/mL]	<10.0	334±215
Number of identified CSF proteins in MS[a, b]	678±95	685±56[b]

Table 3.9. Patient's characteristics. [a] With at least two unique peptides. [b] Derived from 11 A-T patients and 9 controls.

The CSF data from A-T patients showed an increase in total protein and albumin levels compared to the controls (Figure 3.44 C and D), in good correlation with the ataxia score (Figure 3.44, B) and the determination of alpha-fetoprotein levels (Table 3.9). Among patients aged 10 to 16 years, total protein and albumin levels showed better correlation to age than ataxia scores.

3.7.1 Global proteomics reveals several dysregulations in the reelin signaling pathway

The three oldest patients (14-16 years) with the strongest increase in total protein and albumin were selected to study the most advanced pathology in comparison to their matched controls. The analysis of the proteome data from the CSF identified a similar number of proteins in the two groups (Table X); 678 proteins were detected in A-T patients and 685 in controls. A total of 68 proteins were found with significant differences in expression: 47 were down-regulated and 21 up-regulated (Canet-Pons et al 2018). Our data confirm all 13 priority proteins reported previously in the CSF of A-T patients (Dzieciatkowska et al 2011), however only secretogranin (CHGB; Log_2FC -1.58; MinusLog(p-value) 2.71), SPARC (Log_2FC -1.28; MinusLog(p-value) 1.79) and cathepsin D (CTSD; Log_2FC -0.97; MinusLog(p-value) 1.34) dysregulations were significant.

Visualization of the data in a volcano plot (Figure 3.45, A), showed a prominent PN vulnerability with a marked reduction of CALB1 (Log_2FC -2.49, decreased to 18%) (Figure 3.45, C). CALB1 is an abundant calcium-homeostasis factor, specific for GABA-ergic PN, which usually shows reduced content in cerebellar ataxias (Barski et al 2003, Koeppen 2005, Xia et al 2013). This deficiency contrasted with the up-regulation of the PN-generated apolipoprotein J, or clusterin (CLU, increase to 287%) (Figure 3.45, G). Moreover, several factors expressed and secreted by the glutamatergic granular neurons (GN) were also abnormal: reelin (RELN) down to 21%; cerebellin-1 (CBLN1) down to 8%; and cerebellin-3 (CBLN3) down to 6% (Figure 3.45, B, D and E). A strong up-regulation to 1085% was also detected for apolipoprotein B100 (APOB).

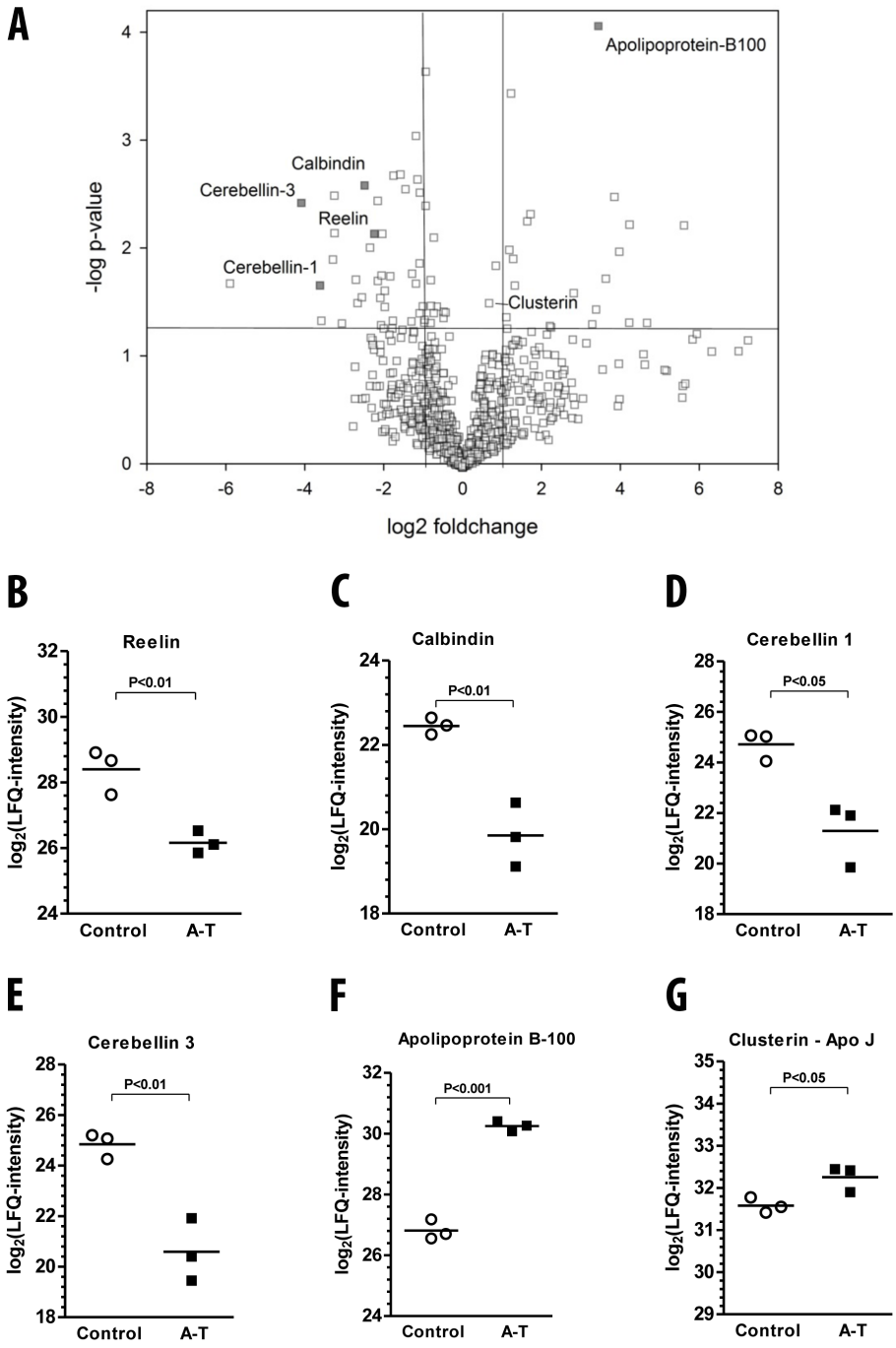

Figure 3.45. Proteomic analysis of the CSF collected from the three oldest patients and three controls (age 14-17 years), performed by a label-free protein quantification approach using nano-ultra-high performance liquid chromatography/ nano-electrospray mass spectrometry (nano-UPLC/ nano-ESI-MS). (A) Analysis of the data was performed with the MaxQuant and Perseus quantitative proteomic software and is illustrated by a volcano plot. Label-free quantification is shown for (B) reelin, (C) calbindin (D) cerebellin-3, (E) cerebellin-1, (F) apolipoprotein B-100, and (G) clusterin in the three oldest A-T patoents compared to their controls.

Among all 68 dysregulations previously mentioned (Canet-Pons et al 2018), 10 factors had previously been implicated in the pathogenesis of ataxia: APOB (up to 1085%) (Bereczki et al 2008, Hentati et al 2012), RELN (down to 21%) (Hirotsune et al 1995), CALB1 (down to 18%) (Airaksinen et al 1997), CBLN1 (down to 8%) (Hirai et al 2005), MANBA (beta-manosidase, down to 60%) (Labauge et al 2009), CTSD (down to 51%) (Ehling et al 2013, Hersheson et al 2014), FAT2 (FAT atypical cadherin 2, to 11%) (Nakayama et al 2002, Nibbeling et al 2017), CNTN6 (contactin 6, to 44%) (Takeda et al 2003), LAMA4 (laminin subunit alpha 4, to 29%) (Wallquist et al 2005), and NEU1 (neuraminidase 1, to 24%) (Seyrantepe et al 2003).

Age correlation plots (**Figure 3.46**) and linear regression models (data not shown) were employed in the CSF proteome of 11 patients versus 9 controls to assess which of these factors seem most useful as potential molecular biomarker in view of its correlation with age and genotype. As expected, CALB1 levels in patients progressively declined with age (data not shown). Interestingly, RELN appeared to decrease earlier and correlate with age more strongly (**Figure 3.46**, B). Reelin levels also showed a strong correlation with ataxia scores (**Figure 3.46**, A), and a normalization of its depletion versus the progressive increase of CSF protein content enhanced the steepness of the regression.

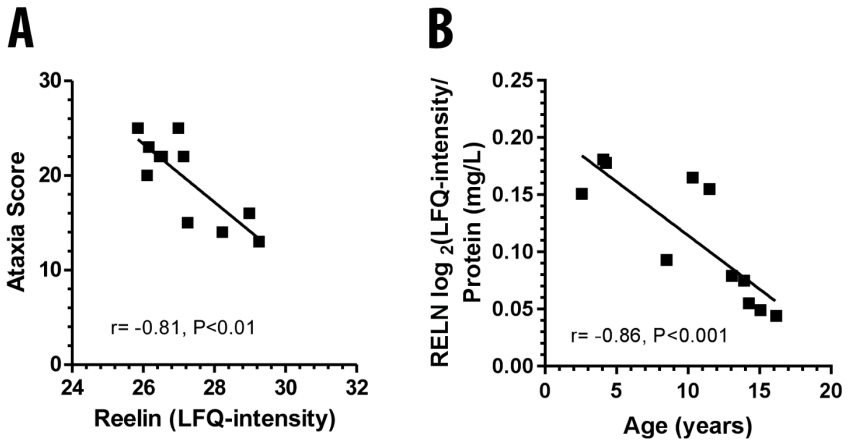

Figure 3.46. Reelin levels showed strong correlation with ataxia scores. A normalization of its depletion versus the progressive increase of CSF protein content enhanced the steepness of the regression line.

3.7.2 Protein interaction bioinformatics suggest glutamatergic axon input to Purkinje neurons as site of pathology, while identifying molecular biomarkers of neuroinflammation

Additional unbiased bioinformatics analysis with STRING of all significantly dysregulated proteins was performed. The analysis was performed to look for enrichment of specific GO terms (*cellular components*, *biological processes*, and *molecular function*), of KEGG pathways, and of protein domains.

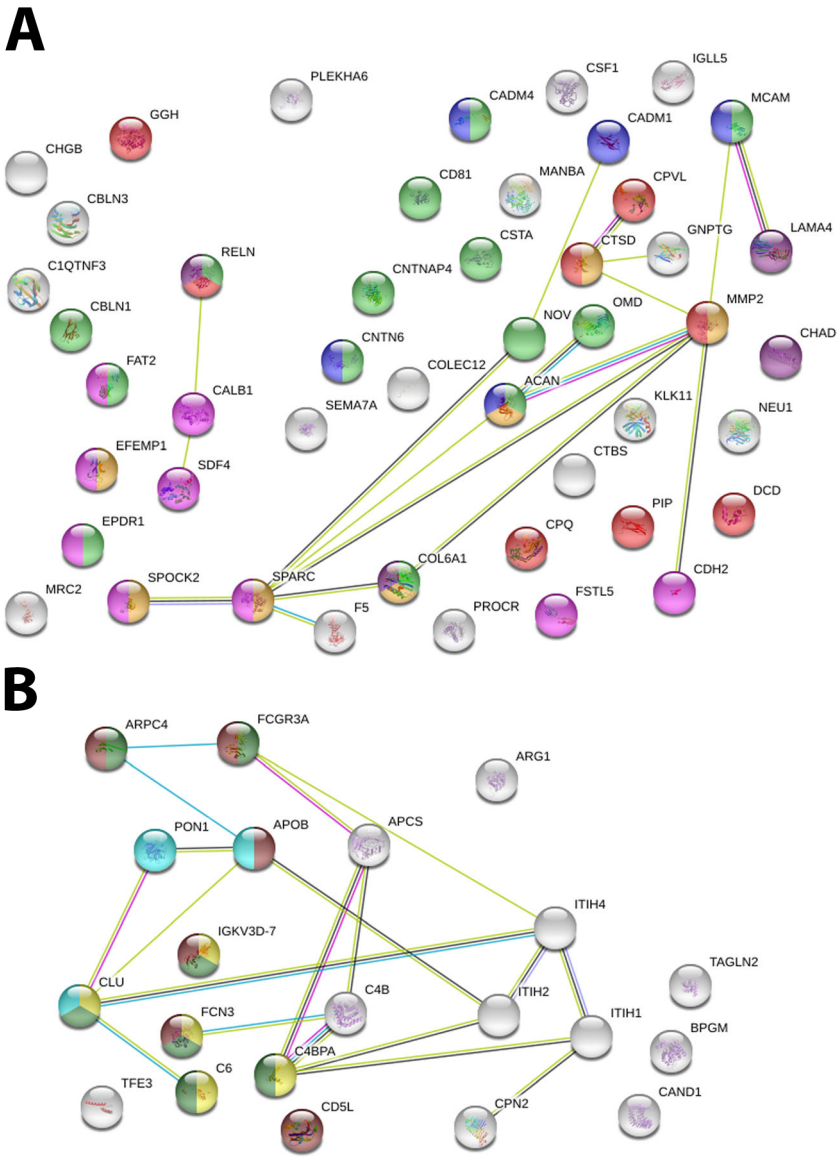

Figure 3.47. STRING diagram of protein-protein interactions and pathway enrichments among all 68 dysregulated factors in the CSF from the three oldest A-T patients, separately for down- and up-regulations. (A) Among the significant down-regulated factors, there were pathways enrichments for *extracellular matrix-receptor interaction* (purple bullets), *biological adhesion* (green bullets), *extracellular matrix organization* (dark yellow bullets) *calcium ion binding* (fuchsia bullets), *peptidase activity* (red bullets), and *immunoglobulin subtypes* (dark blue bullets). (B) Among the

significant up-regulations, there was pathway enrichment for *complement activation* (yellow bullets), *immune effector process* (dark green bullets), *endocytosis* (brown bullets), and *plasma lipoprotein particles* (blue bullets).

As expected, significant protein-protein interaction enrichment was observed for both down-regulations (pvalue 0.00948) and up-regulations (pvalue 1.11e-15). Among the *cellular components*, enrichment for the extracellular region was detected for 36 down-regulated (false discovery rate *q*= 9.36e-14) and 18 up-regulated proteins (*q*=3.96e-08), typical for a CSF study.

Focusing on the 47 down-regulations (Figure 3.47, A), for the GO *biological processes*, "biological adhesion" showed a significant enrichment of 14 factors (*q*=0.0001, green bullets), including CNTN6 (contactin6, down to 44%), CBLN1, and CBLN3. "Extracellular matrix organization" was enriched too (*q*=0.03, dark yellow bullets), also in the *biological processes* category. A total of seven factors were down-regulated including SPARC (secreted protein acidic and cysteine rich, to 41%), which is involved in the response to irradiation (Chetty et al 2012). Among the GO *molecular functions*, the category "calcium ion binding" showed an enrichment of 9 factors (*q*= 0.04, fuchsia bullets). One of these factors was FAT2, previously implicated in ataxia pathology (Nakayama et al 2002, Nibbeling et al 2017). In *molecular functions*, "peptidase activity" showed enrichment for 8 factors (*q*= 0.04, red bullets). A significant enrichment for the KEGG pathway "extracellular matrix-receptor interaction" of 4 factors was also detected (*q*=0.01, purple bullets). InterPro is another resource integrated in the STRING platform that provides functional analysis of protein sequences, classifies them into families, and predicts the presence of domains and important sites (https: ebi.ac.uk/interpro/). Among its defined domains, the "immunoglobulin subtype" showed an enrichment of 5 factors (*q*= 0.002, dark blue bullets). Overall, key factors of PN connectivity with their glutamatergic input axons are prominent among the down-regulations.

Regarding the 21 up-regulations (Figure 3.47, B), the GO *biological process* categories of "complement activation" (5 factors, *q*=8.83e-06, yellow bullets) and "immune effector process" (7 factors, *q*=0.0002, dark green bullets) were enriched. One up-regulated factor in these categories was C4BPA (complement component-4 binding protein A, to 4884%) that binds abnormal DNA to inhibit DNA-mediated complement activation and inflammatory responses against

necrotic cells (Trouw et al 2005). Three other factors involved in immune response weren't identified by automated bioinformatics: IGHM (immunoglobulin heavy constant mu chain, to 1567%), CPN2 (carboxypeptidase-N subunit-2, to 1238%), and CD5L (CD5 like, to 1876%) (Matthews et al 2004, Sanjurjo et al 2015). Overall, neuroinflammatory responses are prominent among the up-regulations, but the dysregulation of lipoprotein particles and endocytosis pathways may be a direct effect of ApoB/RELN and ATM membrane functions.

3.8 Validation in Atm-KO cerebellar mRNA confirms the excess of Apoe/Apoh and deficit of reelin receptor transcripts

To assess whether these pathways have a prominent role in cerebellar tissue of an A-T mouse model, we used 1.5 to 3 month cerebellar samples from *Atm -/-* animals (Barlow et al 1996). These animals die at an age of 4 to 6 months due to thymic lymphomas without showing signs of cerebellar degeneration. A hallmark of these mice is the high level of oxidative stress by reactive oxygen species (ROS) that affects several tissues, including the cerebellum (Barlow et al 1999). We aimed to identify which of the candidates detected in the CSF of A-T patients are early events ocurring in the cerebellum. Instead of quantifying secreted factors or studying their extracellular turnover, we analyzed transcript levels of key components of cholesterol-apolipoprotein trafficking, reelin signaling, glutamatergic input to PN, glutamate receptors, calcium homeostasis, oxidative stress, neuroinflammation, and cell adhesion pathways (Figure 3.48).

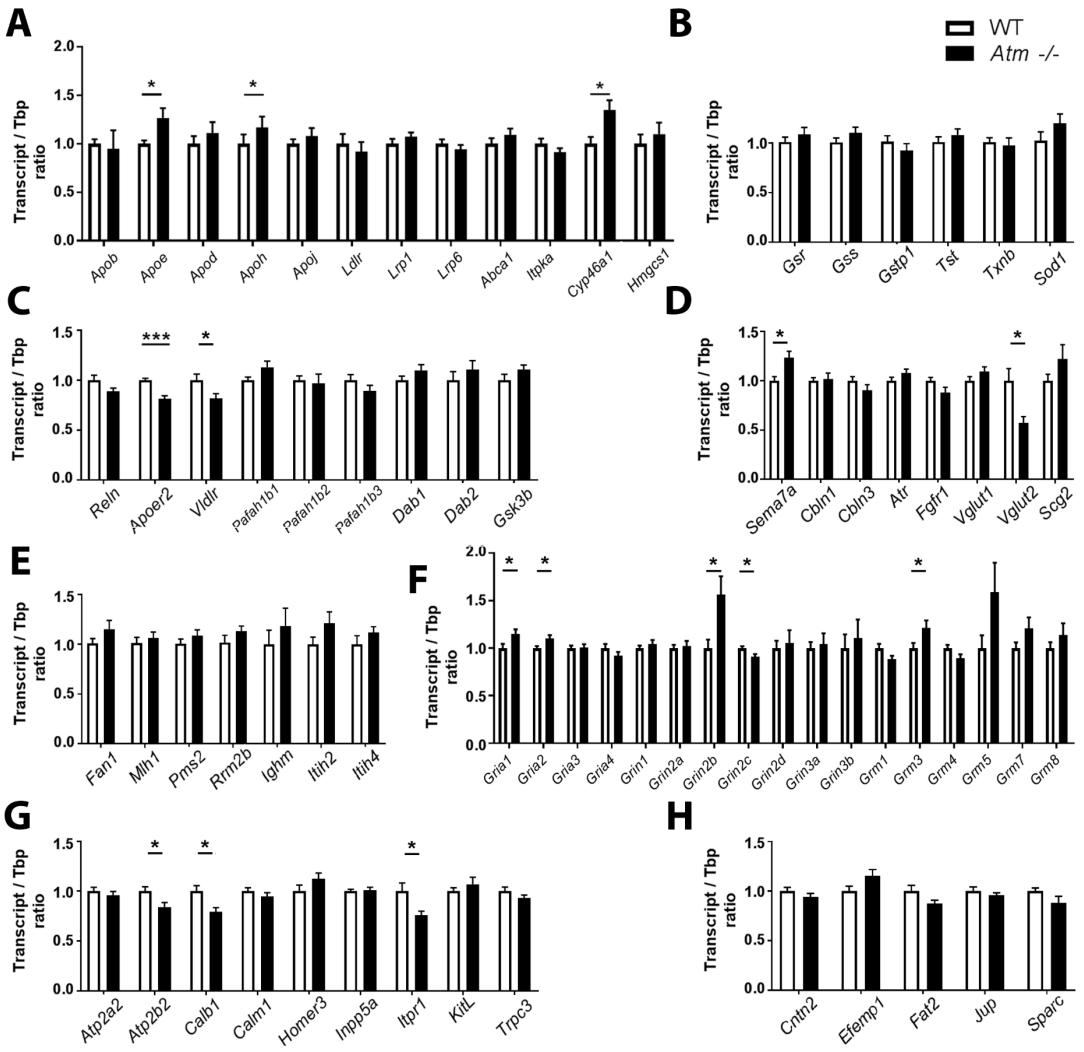

Figure 3.48. In cerebellar tissue from 2-month-old *Atm-/-* (n=8, black bars) versus WT mice (n=8, white bars), the mRNA levels were assessed by Q-PCR for crucial factors in several relevant pathways. (A) Key factors of apolipoprotein and cholesterol trafficking, significant up-regulations were detected for *Apoe*, *Apoh* and *Cyp46a1*. (B) No changes were detected at this age for any factor in the oxidative stress response. (C) In the reelin signaling pathway, both receptors (*Apoer2* and *Vldlr*) showed significantly reduced transcript levels. (D) Among modulators between PN and afferent excitatory presynapses, an elevation of *Sema7a* and reduction of *Vglut2* were detected, both of them linked to climbing fiber pathology. (E) No DNA damage repair or neuroinflammation markers were found altered. (F) Glutamate receptor exhibited elevation of the NMDA subunit *Grin2b* transcript level, decrease of *Grin2c* and increase for the AMPA subunit *Gria1* and *Gria2*, as well as the metabotropic subunit *Grm3*. (G) The essential factors of calcium-dependent excitability *Atp2b2*, *Calb1* and *Itpr1* were found significantly down-regulated, reflecting the incipient dysfunction of PN. (H) Despite various changes in PN postsynapses and glutamatergic synapses, no alterations of the specific cell adhesion factors between cerebellar circuits were detected at this stage. The Y-axis shows the ratio of a transcript of interest versus Tbp as housekeeping gene, normalized versus WT, reflecting the fold change in mutants.

Significant increases were observed for the cholesterol-transporting apolipoproteins *Apoe* (FC1.27 p-value 0.033), *Apoh* (FC 1.59 p-value 0.032) and the cholesterol efflux regulator *Cyp46a1* (FC 1.35 p-value 0.02), while markers

for oxidative stress showed no dysregulation at this stage (Figure 3.48, B). These changes serve as evidence that altered cholesterol trafficking and increased synthesis of ligands may substitute for reelin (Figure 3.48, A). A crucial confirmation of the reelin reduction in patients' CSF was that the *Atm-/-* cerebella showed significant mRNA reduction for reelin receptors, *Vldlr* (FC 0.82 p-value 0.037) and *Apoer2* (FC 0.82 p-value 0.0003), even at a young age (Figure 3.48, C). The transcript levels of *Reln* and its intracellular transducers *Pafah1b1*, *Pafah1b2*, *Pafah1b3*, *Dab1*, *Dab2*, and *Gsk3b* were not changed (Figure 3.48, C).

3.9 Validation in Atm-KO cerebellar tissue confirms the excess of ApoB protein and deficit of the VLDL receptor

In order to gain deeper insight at the protein level and determine whether the dysregulation of apolipoprotein signaling pathways precedes the neurodegeneration, quantitative immunoblots were used. Three different apolipoproteins were checked (ApoB, ApoE and ApoJ), together with the levels of RELN and its receptor VLDLR. CALB1 and NeuN were used as neuronal markers, for PN and GN respectively, to confirm that at the age of ~2 months there is no degeneration in the cerebellum of *Atm-/-* mice.

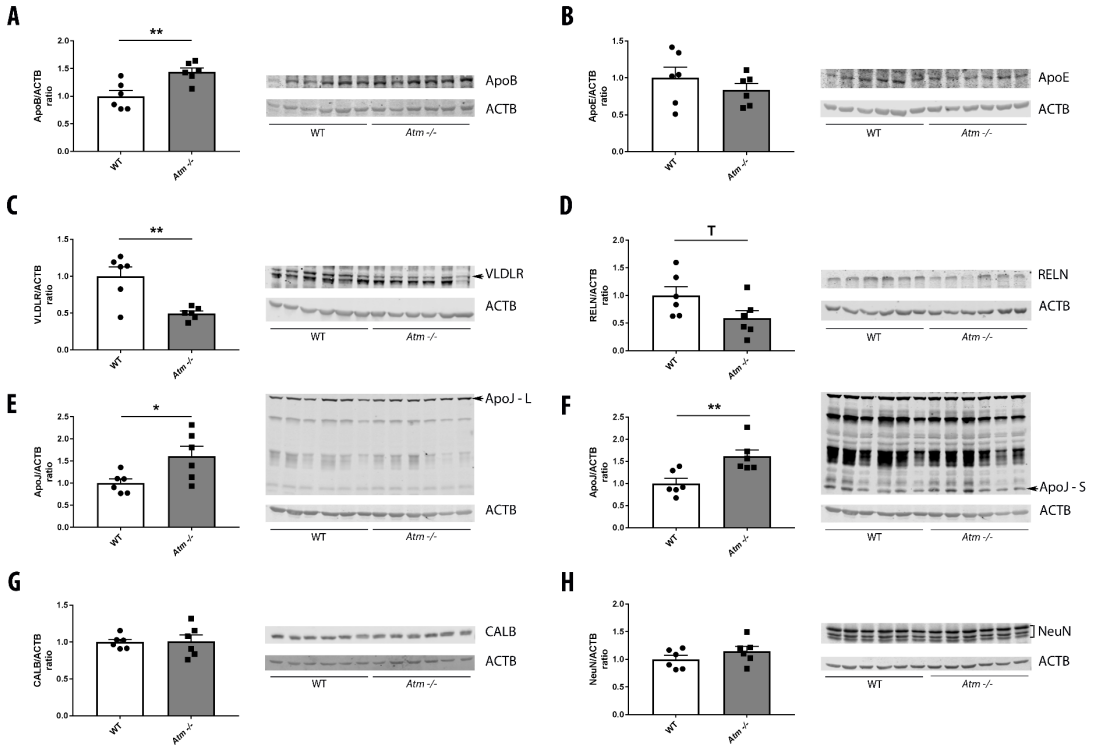

Figure 3.49. In cerebellar tissue from 2-month-old *Atm-/-* (n=6, gray bars) versus WT mice (n=6, white bars), the protein levels were assessed by quantitative

immunoblots for crucial factors in several relevant pathways. (A) ApoB (FC 1.43 p-value 0.0007); (B) ApoE (FC 0.84 p-value 0.36); (C) VLDLR (FC 0.49 p-value 0.0095); (D) RELN (to 60% p-value 0.08, illustrated by T for statistical Trend); (E) ApoJ full-length and glycosylated isoform as uppermost band (FC 1.61 p-value 0.04); (F) ApoJ cleaved and deglycosylated isoform as lowest band (FC 1.61 p-value 0.008); (G) CALB1 (FC 1, p-value 0.92); (H) NeuN (FC 1, p-value 0.24). The Y-axis of each plot shows the ratio of a protein of interest versus ACTB as loading control, normalized versus WT, reflecting the fold change in mutants.

These experiments confirmed that ApoB showed an increase to 143% (FC 1.43 p-value 0.0007; in RIPA fraction) and VLDLR showed a decrease to 50% (FC 0.49 p-value 0.0095; SDS fraction). Among ApoJ isoforms, the large full-length glycosylated band exhibited an increase to 160% (FC 1.61 p-value 0.04; RIPA fraction) and the smallest cleaved and deglycosylated band an elevation to 161% (FC 1.61 p-value 0.008; RIPA fraction). No evidence of PN or GN loss was apparent at this stage (CALB1: FC 1 p-value 0.92; NeuN: FC 1 p-value 0.24).

These results are in agreement with previous literature showing that ApoB and VLDLR levels are inversely correlated (Kobayashi et al 1996) and that ATM depletion modulates specific isoforms of ApoJ (Luo et al 2014). Interestingly, an up-regulation of ApoB protein levels occurred before RELN steady-state levels changed significantly.

3.10 Co-immunofluorescence staining confirms the absence of neuronal death

Co-immunofluorescence studies with the same antibodies used for WB confirmed the absence of neuronal death as well as the preferential PN localization of VLDLR (Figure 3.50, C). As receptor ligands, both the GN-secreted reelin (Figure 3.50, A) and GN/PN secreted ApoB (Figure 3.50, B) were found to accumulate in PN.

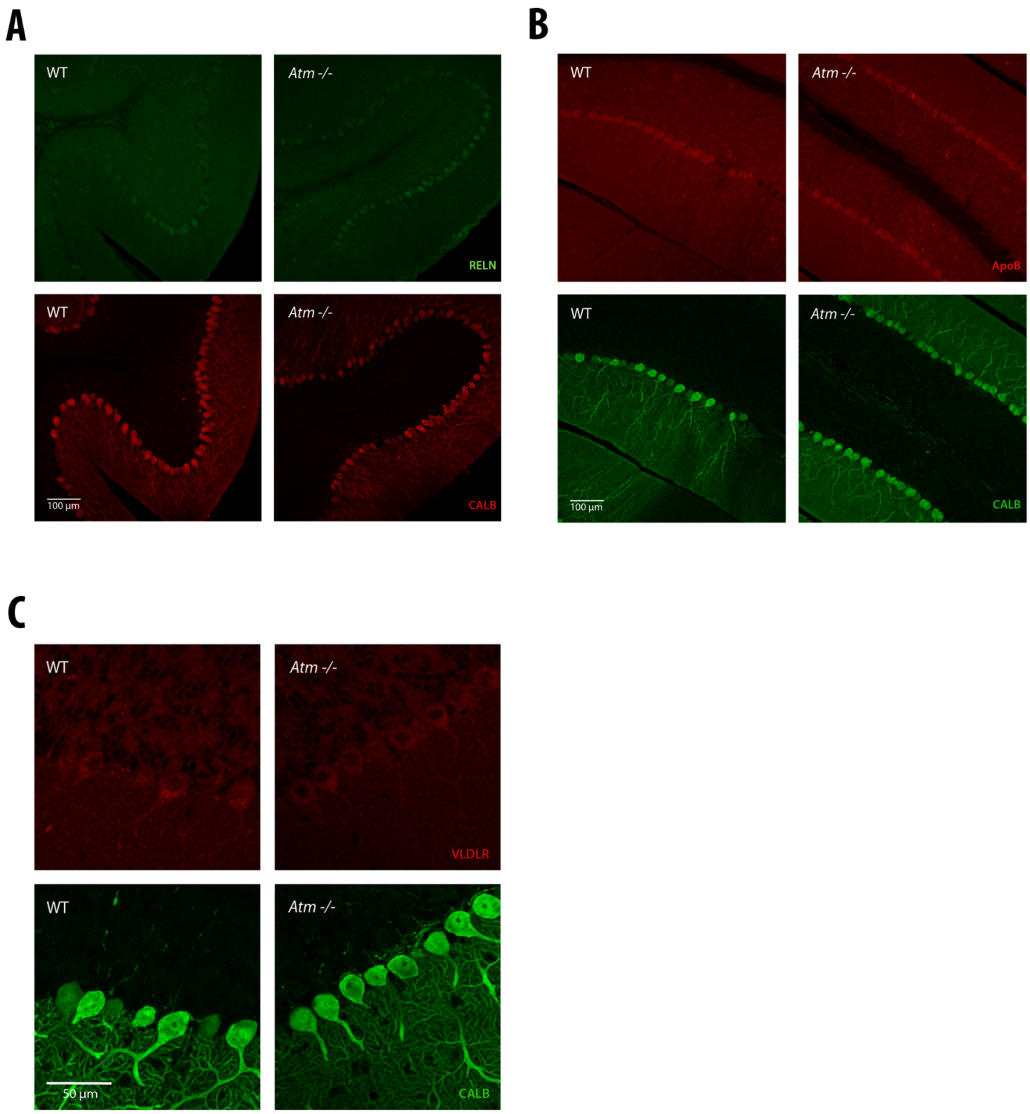

Figure 3.50. Coimmunofluorescence stainings confirming the absence of neuronal death and the preferential PN localization of VLDLR. (A) Labeled in green RELN and in red CALB1, no obvious differences were found between the WT and *Atm-/-*. (B) Labeled in green CALB1 and in red ApoB, showing a preferential localization to the PN. (C) Labeled in green CALB1 and in red VLDLR, showing again preferential localization at the PN layer.

3.11 Schematic representation of the altered pathways identified in patients and validated in the *Atm-/-* mouse model

As an attempt to summarize and integrate all the data presented until now, a schematic representation of the potential events happening in the mouse model at early ages was generated (Figure 3.51). Red letters were used to highlight up-regulated factors and blue letters for down-regulations.

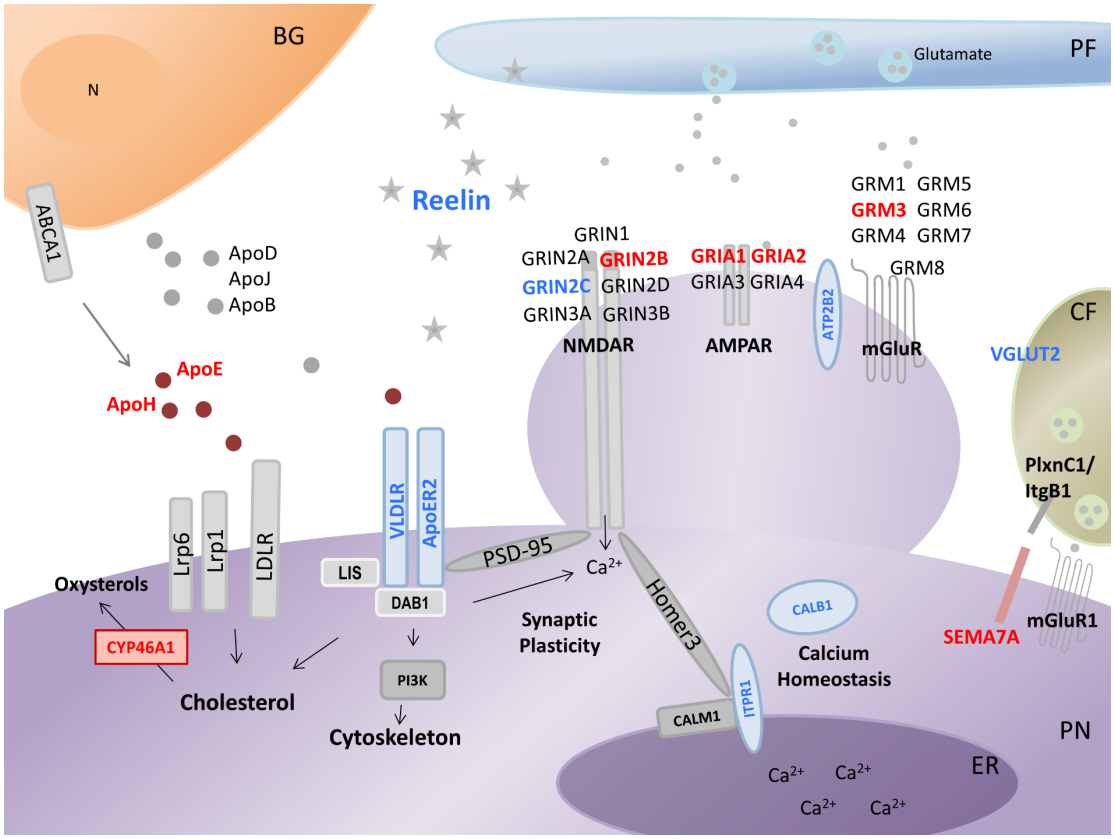

Figure 3.51. Schematic overview of apolipoprotein and glutamate signaling modulated via reelin within neural circuits of the cerebellum (PN for Purkinje neuron, CF for climbing fiber, PF for parallel fiber, BG for Bergmann glia, ER for endoplasmic reticulum, N for nucleus). Relevant Q-PCR and immunoblot findings in the 2-month-old *Atm−/−* cerebellum were highlighted (red for up-regulations, blue for down-regulations).

3.12 The generation of a transcriptomics data set from 12-month-old *Atm-/-* cerebellum versus WT mice shows a higher number of down-regulations

As previously mentioned, the lifespan of the Atm-/- mice is decreased by a number of lymphomas that cause animal death around 6 months, making it impossible to study the degeneration of the cerebellum in this model (Barlow et al 1999, Xu et al 1996). A way to overcome this time limitation is through bone marrow transplantation. After the intervention, these animals can live up to 12 months of age and show loss of PN (Pietzner et al 2013). After investigating the pathology in the cerebellum of younger animals, a novel transcriptomics data set was generated using cerebellar samples from four 12-month-old *Atm-/-* animals versus their sex and age-matched WT. Affymetrix Clariom™ D mouse arrays from Thermo Fisher were used and the analysis was carried out with the

Transcriptome Analysis Console (TAC) software using standard parameters and self-determined filter criteria (fold change <-1.2 or >1.2; p-value ≤ 0.05).

3.12.1 Experiment design

The bone marrow transplantation of *Atm-/-* mice was crucial to generate this data set from older cerebellar samples (Figure 3.52, A). To perform the transplant, an Atm-/- recipient was conditioned administrating 0.125 mg/mL of anti-CD4 antibody and 0.125 mg/mL of anti-CD8 antibody seven days before the intervention. One day before the surgery, a second dose of each antibody was administrated together with 200 mg/kg of cyclophosphamide for non-myeloblative conditioning. Bone marrow cells were harvested in sterile manner from CD-90.2 depleted donors on the same day of the intervention, and $5x10^6$ cells were injected intravenously into the conditioned recipients (Bagley et al 2004, Pietzner et al 2013).

Once the animals reached the desired age, four mutants and four WT were sacrificed and the cerebellum was dissected. RNA extraction was performed in parallel for both genotypes in order to reduce technical variation. All procedures were performed in an RNase-free hood to ensure the quality and integrity of the resulting RNA. Panel B in Figure 3.52 shows the genes that passed the filter criteria plotted in a volcano plot. Down-regulations are highlighted in green and up-regulations are highlighted in red.

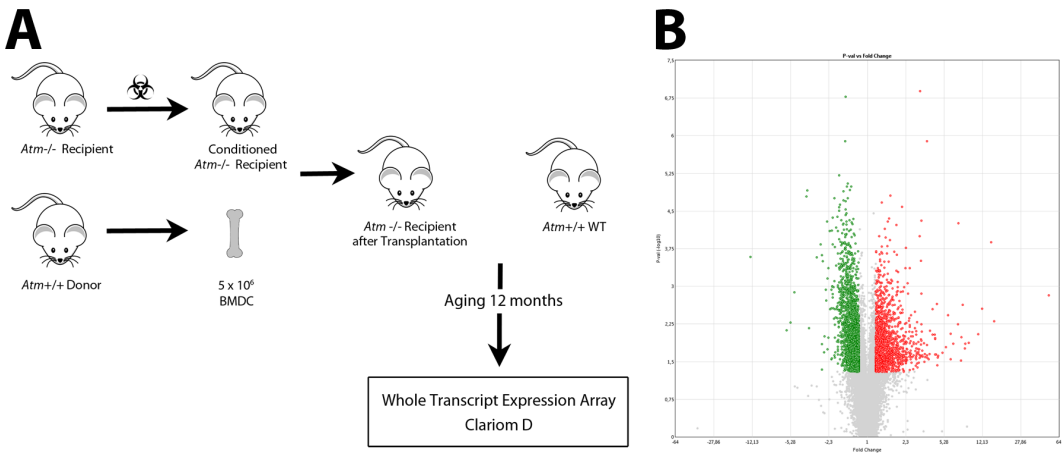

Figure 3.52. Work flow scheme followed to generate the transcriptome data set. (A) Scheme of the generation of the transplanted bone marrow *Atm-/-*. (B) Volcano plot showing the distribution of the significant down-regulations (green) and up-regulations

(red) after the analysis of the data set with the TAC software. The Y-axis shows p-value and the X-axis Fold Change.

3.12.2 General data from the array

A closer look at the genes that passed the filter criteria previously established showed that only 3.43% were found dysregulated (representing 2260 out of more than 65000 genes detected by the array). Of these, 58.32% were down- and 41.68% were up-regulated as shown in the Table 3.10.

	Passed filter criteria	Up-regulated	Down-regulated
Cerebellum			
12 months	2260 (3.43%)	942 (41.68%)	1318 (58.32%)

Table 3.10. General distribution of the genes that passed the filter criteria. Among the 3.43% total genes that passed the filter criteria the majority of them were found down-regulated.

There are nine defined groups in the array: Non-Coding, Multiple Complex (containing more than one of the other groups), Coding, Pseudogene, Precursor microRNA, small RNA, Ribosomal, Unassigned, and tRNA. In Figure 3.53 the percentages corresponding to each category are plotted in pie charts for up-regulations (Figure 3.53, A) and down-regulations (Figure 3.53, B). Interestingly, a high number of non-coding RNAs (ncRNA) were detected among the significant down-regulations. A number of ncRNA have been implicated in neuronal development, homeostasis, and neurodegenerative and psychiatric disorders (Salta & De Strooper 2012).

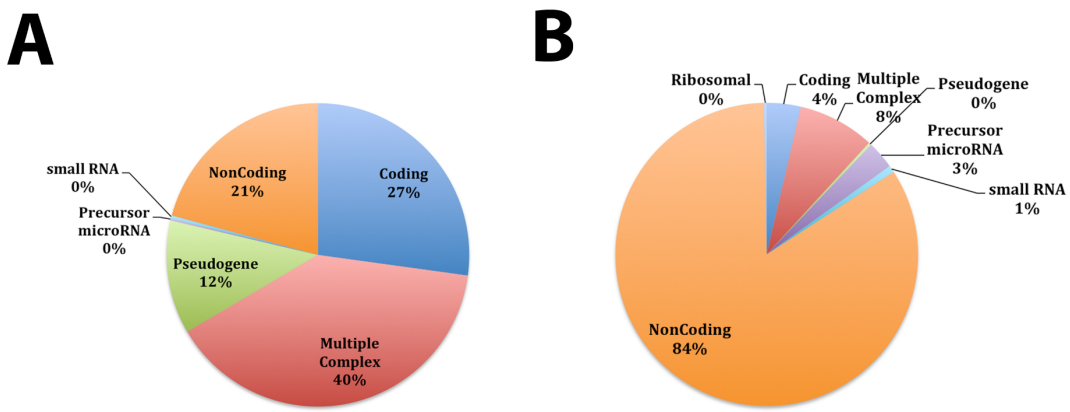

Figure 3.53. Percentages of the different dysregulated categories from the transcriptomics data set. (A) Up-regulated genes corresponding to each category are

shown in a pie chart. (B) The same representation for down-regulated genes shows a strong Non Coding category taking up to 84% of all down-regulations.

For further analysis only the categories “coding” and “multi complex”, gene categories coding for proteins, will be used.

3.12.3 STRING analysis of the 2-fold-up-regulated genes shows affected neuronal compartments

The STRING webserver was used to determine protein-protein interactions from the 2-fold-up-regulations detected in the transcriptome data set.

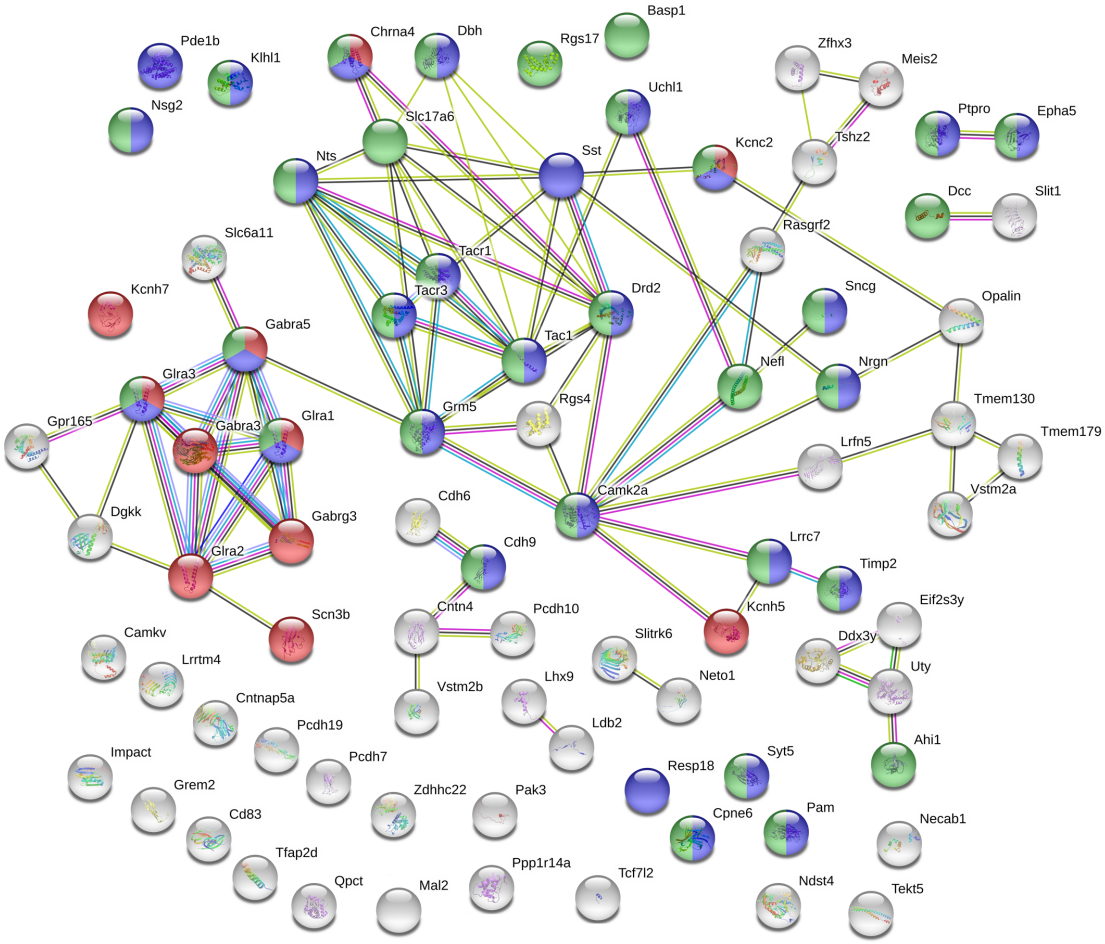

Figure 3.54. STRING analysis of the 2-fold-up-regulations shows dysregulation of neuronal components. Significant pathway enrichment was detected for *ion gated channel activity* (red bullets), *somatodendritic compartment* (blue bullets), and *neuron projection* (green bullets).

As expected, significant protein-protein interaction enrichment was observed for the up-regulations (p-value <1.0e-16). Among the molecular functions defined by GO, enrichment for *ion gated channel activity* was detected (*q*= 7.29e-06, red bullets), especially showing glutamatergic channels. For GO cellular components,

enrichments for *somatodendritic compartment* (*q*=1.08e-14, blue bullets) and *neuron projection* (*q*=9.95e-14, green bullets) were observed. The *somatodendritic compartment* corresponds to the cell body (soma) and dendrites from neurons but excludes axons, while the *neuron projection* shows all genes and gene products annotated to neuron projections (axon or dendrite). Based on the GO cellular compartments, a total of 24 up-regulations out of the 99 analyzed with STRING are part of the dendritic compartment (blue/green bullets). Six are located at the axons (solid green bullets) and 3 at the soma (solid blue bullets). These data could point to an impaired input to PN as an explanation for the PN degeneration observed in A-T patients.

3.12.4 STRING analysis of the 1.5-fold-down-regulated genes show altered secreted factors

Of the significant down-regulations detected in the array, only few of them were part of the coding or multi complex categories. Therefore, the 1.5-fold-down-regulations were analyzed by STRING.

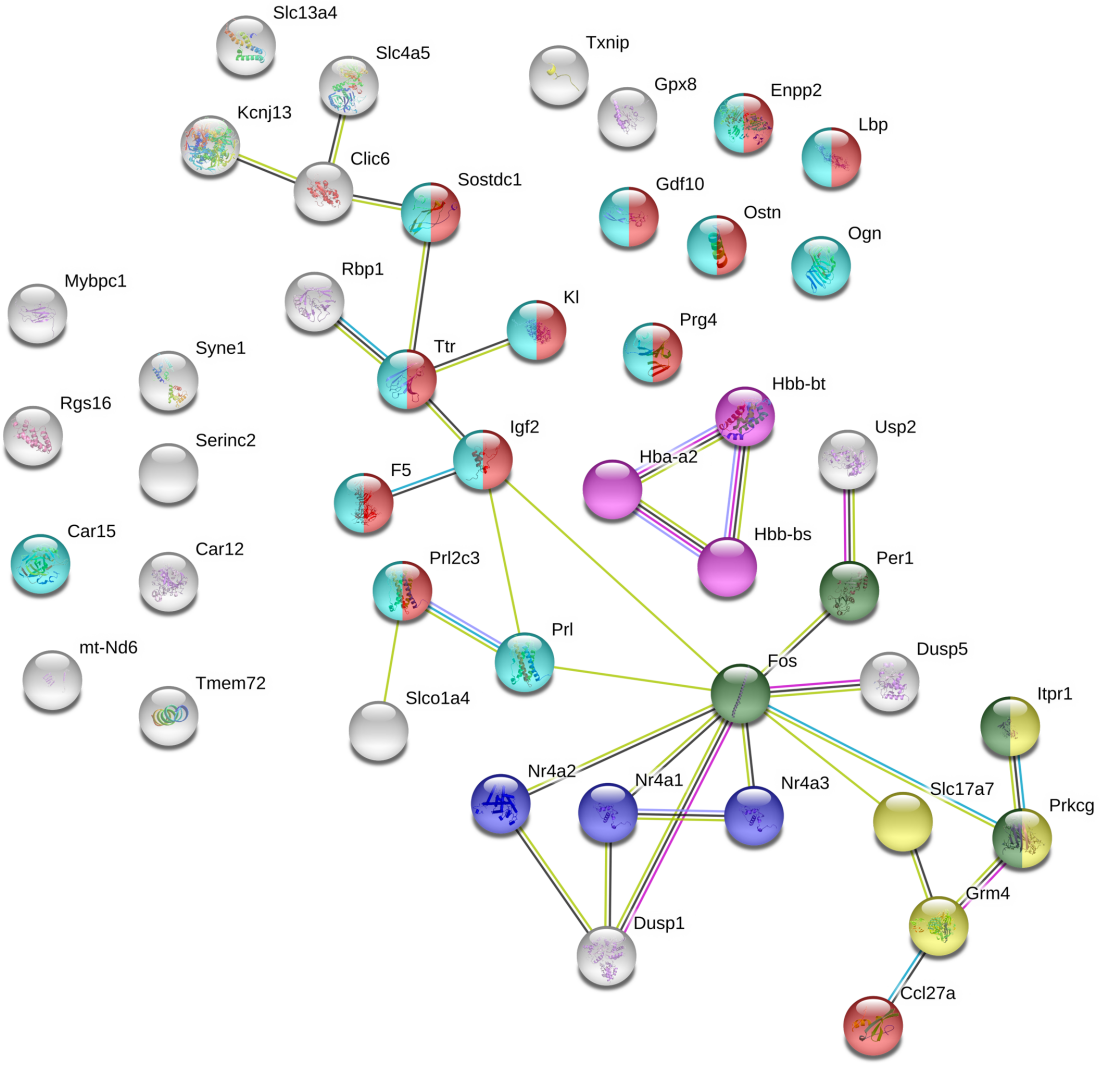

Figure 3.55. STRING analyses of the 1.5-fold-down-regulations show a high number of secreted factors altered. Significant KEGG pathway enrichment was detected for "glutamatergic synapse" (yellow bullets) and "circadian entrainment" (green bullets)

Significant protein-protein interaction enrichment was detected for the 1.5-down-fold-regulations (p-value 2.81e-12). Among the GO *cellular compartment* category the GO-term "extracellular space" showed an enrichment of 12 factors (q= 0.0016, red bullets). Two KEGG Pathways were enriched as well: "Glutamatergic synapse" (q=0.0036, yellow bullets) and "Circadian entrainment" (q= 0.0036, green bullets). Based on another database integrated in STRING called Reactome (reactome.org) that provides interpretation and analysis of known pathways, the "nuclear receptor transcription pathway" showed enrichment of three factors (q= 0.0376, dark blue bullets). These three factors pertain to the orphan nuclear receptors 4A subfamily and have been proposed as potential targets to modulate response to chronic inflammation (Rodriguez-

Calvo et al 2017). Based on the UniProt Keywords, "secreted" showed an enrichment of 14 factors (q= 0.0082, turquoise bullets). The alpha (Hba) and beta (Hbb-bt, Hbb-bs) hemoglobins, part of the "globin" PFAM protein domain (q=0.00046, fuchsia bullets), were also highlighted by the STRING analyses.
Overall, the glutamatergic synapses have been consistently altered together with the extracellular space factors/secreted factors.

3.13 Validation of several ataxia related genes dysregulated in the transcriptome data set by Q-PCR

Among all dysregulated transcripts that appeared in the transcriptomics set, several of them had been previously linked to neurodegenerative disorders. A total of 32 factors of interest were identified based on literature knowledge. Some of them together with other related factors were further investigated by Q-PCR to validate their alteration in the 12-month-old cerebellar *Atm-/-* samples (Table 3.11).

Gene symbol	Gene	Fold change	P-value
Als2	Amyotrophic Lateral Sclerosis 2 protein	0.94	0.704 n.s.
Atm	Ataxia Telangiectasia Mutated	0.58	**0.0008** ***
Atr	Ataxia Telangiectasia Related	0.91	0.176 n.s.
Cacna1a	Calcium voltage-gated channel subunit alpha1 A	0.99	0.836 n.s.
Cadps2	Calcium dependent secretion activator 2	0.83	**0.016** *
Car8	Carbonic anhydrase 8	0.81	**0.048** *
Car15	Carbonic anhydrase 15	0.91	0.320 n.s.
Cbln1	Cerebellin 1	0.77	0.169 n.s.
Cbln2	Cerebellin 2	48.8	**0.039** *
Cbln3	Cerebellin 3	0.79	0.129 n.s.
Cbln4	Cerebellin 4	13.8	**0.029** *
Fat2	FAT atypical cadherin 2	1.11	0.460 n.s.
Fgf14	Fibroblast growth factor 14	0.75	**0.011** *
Fos	AP-1 Transcription factor subunit	0.68	0.321 n.s.
Grid2	Glutamate ionotropic receptor delta subunit 2	0.84	**0.001** **
Grik2	Glutamate ionotropic receptor kainate subunit 2	0.79	**<0.0001** ****

Grm4	Glutamate metabotropic receptor 4	0.77	**0.015** *
Itpr1	Inositol 1,4,5-Trisphosphate receptor 1	0.82	0.215 n.s.
Kcna1	Potassium voltage-gated channel subfamily A member 1	0.88	0.445 n.s.
Mtcl1	Microtubule crosslinking factor 1	0.84	**0.005** **
Nr4a1	Nuclear receptor subfamily 4 group A member 1	0.45	**0.014** *
Nr4a2	Nuclear receptor subfamily 4 group A member 2	0.39	**0.012** *
Nr4a3	Nuclear receptor subfamily 4 group A member 3	0.26	**0.003** **
Prkcg	Protein Kinase C Gamma	1.09	0.460 n.s.
Pten	Phosphatase and tensin homolog	0.80	0.156 n.s.
Rora	RAR related Orphan Receptor A	0.92	0.191 n.s.
Sgk1	Serum/Glucocorticoid Regulated Kinase1	0.63	0.104 n.s.
Slc1a6	Solute carrier family 1 member 6	0.81	**0.005** **
Slc17a6	Solute carrier family 17 member 6	0.80	**0.047** *
Slc17a7	Solute carrier family 17 member 7	0.82	**0.007** **
Stxbp5l	Syntaxin binding protein 5 like	0.76	**0.007** **
Syne1	Spectrin repeat containing nuclear envelope protein 1	0.82	**0.027** *
Zic4	Zic family member 4	0.99	0.933 n.s.

Table 3.11. Q-PCR validation of dysregulated transcripts detected in the cerebellum by the Clariom D Array comparing *Atm-/-* (n=4) versus WT (n=4).

A total of 18 factors among the 32 investigated were found to be significantly dysregulated. Only two of them were found up-regulated and the rest, 16 factors, were down-regulated. Table 3.12 summarizes the validated dysregulated genes in the *Atm-/-* mouse model and which human-diseases each gene has been shown to be implicated with.

Gene	Disease in humans	Reference
Cadps2	Autism and ataxia	Bovio *et al* 2018; Sadakata *et al* 2007
Car8	Cerebellar ataxia; implicated in SCA14 and SCA29	Lamont *et al* 2015; Ando *et al* 2018; Shimobayashi *et al* 2018
Cbln2/4		Seigneur *et al* 2018a Seigneur *et al* 2018b
Fgf14	SCA 27	Van Swieten *et al* 2003; Schesny *et al* 2019
Grid2	SCAR18	Veerapandiyan *et al* 2017; Hills *et al* 2013

Grik2	SCA11	Nieding *et al* 2016; Guzmán *et al* 2017
Grm4		Pekhletski *et al* 1996; Abitbol *et al* 2008; Antflick *et al* 2012; Power and Empson 2014
Mtcl1	Early-onset ataxia	Krygier *et al* 2019
Nr4a1-3		Rodríguez-Calvo *et al* 2017
Slc1a6	SCA5/SPARCA1	Ikeda *et al* 2006; Stankewich *et al* 2010; Perkins *et al* 2016
Slc17a6		Leo *et al* 2009; Cheng *et al* 2017
Slc17a7	SCA27	Tempia *et al* 2015; Cheng *et al* 2017; Lin *et al* 2017
Stxbp5l	Recessive neurodegeneration	Geerts *et* al 2015; Kumar *et al* 2015
Syne1	SCAR8	Gros-Louis *et al* 2007; Synofzik *et al* 2016

Table 3.12. Murine genes found dysregulated in the transcriptome data set and validated by Q-PCR, diseases they are implicated with in humans, and associated references.

3.14 Three novel factors appear dysregulated as early events in the ~2-month-old cerebellar samples of *Atm-/-*

Using the ~2-month-old samples, we aimed to investigate if any of these new dysregulated candidates were altered before neurodegeneration is detected in the mouse model. This would help to understand which are the early events happening and to define new potential targets to stop or slow down the pathology. Using Q-PCR we checked the transcript levels of 11 new factors (Table 3.13).

Gene symbol	Gene	Fold Change	P-value
Als2	Amyotrophic Lateral Sclerosis 2 protein	0.99	0.938 n.s.
Cadps2	Calcium dependent secretion activator 2	0.97	0.683 n.s.
Car15	Carbonic anhydrase 15	0.77	**0.002 ****
Fgf14	Fibroblast growth factor 14	1.02	0.738 n.s.
Grik2	Glutamate ionotropic receptor kainate subunit 2	1.04	0.529 n.s.
Grm4	Glutamate metabotropic receptor 4	0.89	0.072 n.s.
Mtcl1	Microtubule crosslinking factor 1	0.88	**0.008 ****
Slc17a7	Solute carrier family 17 member 7	1.48	**0.013 ***
Slc1a6	Solute carrier family 1 member 6	0.82	**0.015 ***

Stxbp5l	Syntaxin binding protein 5 like	1.05	0.409 n.s.
Syne1	Spectrin repeat containing nuclear envelope protein 1	0.97	0.423 n.s.

Table 3.13. Transcript levels of several factors in the cerebellum of *Atm-/-* (n=8) versus WT (n=8) from 1.5 to 3-month-old mice. Highlighted in gray are three factors that could be early events and were also dysregulated in the 12-month-old samples.

Four dysregulated factors were significantly dysregulated among the 11 we checked but only three were dysregulated in the 12-month-old samples. *Mtcl1* (microtubule crosslinking factor 1; FC 0.88 p-value 0.008) is a microtubule associated factor essential for axonal polarity in PN and its knockdown causes ataxia in mice (Satake et al 2017). Moreover, MTCL1 has been recently proposed as a genetic cause for autosomal recessive ataxia after a NGS (next-generation sequencing) analysis of a Polish ataxia cohort (Krygier et al 2019). Another commonly down-regulated gene was *Slc1a6*, which encodes the protein EAAT4 (excitatory amino acid transporter 4). The EAATs are an ion-gradient-dependent glutamate transporter family composed of 5 members or subtypes (EAAT1-5) (Machtens et al 2015). Each member of the family has a specific location in the nervous system; for example EAAT1 and EAAT2 are found in glia (Lehre et al 1995). EAAT4 is expressed in neurons and has been shown that its loss affects the spontaneous firing pattern and survival of PN (Perkins et al 2018). The last dysregulated factor was *Slc17a7*, which codes for VGLUT1 (vesicular glutamate transporter 1). Unlike EAATs, VGLUTs fill up the synaptic vesicles with glutamate so it can be released into the synapse when necessary and they do not depend on ion-gradients. VGLUT1 and VGLUT2 are widely expressed in the nervous system with almost no overlap (Liguz-Lecznar & Skangiel-Kramska 2007). In the cerebellum VGLUT1 is expressed in the parallel fibers while VGLUT2 is present in climbing fibers and PN dendrites (Fremeau et al 2001, Hisano et al 2002). Most interestingly, it has been shown that ATM and ATR associate with excitatory (VGLUT1 positive) and inhibitory (VGAT positive) vesicles respectively (Cheng et al 2018, Li et al 2009). Thus, *Slc17a7* could be an interesting biomarker and potential target for future therapies.

3.15 VGLUT1 as a potential marker for A-T, shows no protein level changes in the cerebellum of 1.5-3-months old Atm-/- mouse model

After validating the down-regulation of *Slc17a7* by Q-PCR analysis, we aimed to determine if the protein level of this factor coding for VGLUT1 was also altered in the cerebellum of young *Atm-/-* mice compared to their sex and age-matched WT.

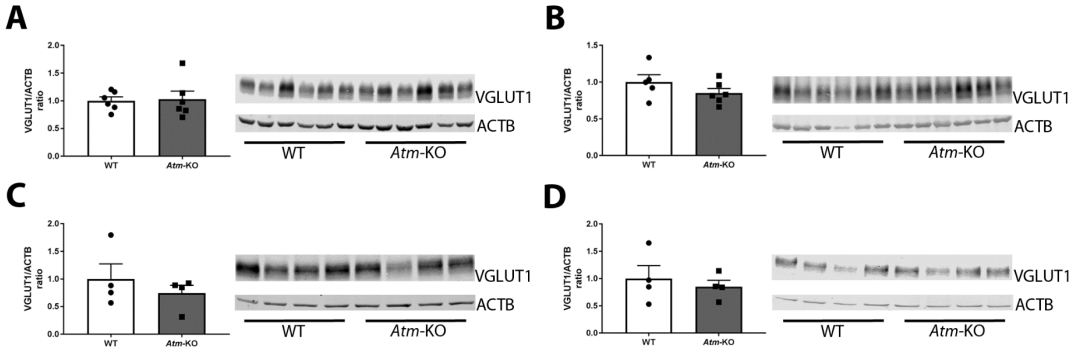

Figure 3.56. Western bolt results for VGLUT1 protein levels. (A) RIPA and (B) SDS fraction of 2-month-old cerebellar samples from Atm-KO (n=6) and WT (n=6) mice. (C) RIPA and (D) SDS fraction of 3 to 4-month-old cerebellar samples from Atm-KO (n=4) and WT (n=4) mice.

Two different age groups' samples were used (~2-months-old and ~4-months – old) to determine if there were differences between the cerebellar samples of *Atm-/-* and WT mice. In both groups there were not significant differences between the mutants and WT, neither with RIPA nor SDS fraction, although the transcript level was found down-regulated. This could be due to the sensitivity of the method or a later effect on the protein level compared to the transcript level.

3.16 No altered localization of VGLUT1 could be detected upon immunohistochemistry using 6-month-old cerebellar samples from Atm-/- compared to its WT

Although the protein level was not affected, we checked the distribution of the VGLUT1 in sagittal free-floating sections of *Atm-/-* cerebella compared to its WT. We hypothesized that due to the absence of ATM, VGLUT1 might show a different localization pattern in the mutant compared to the WT.

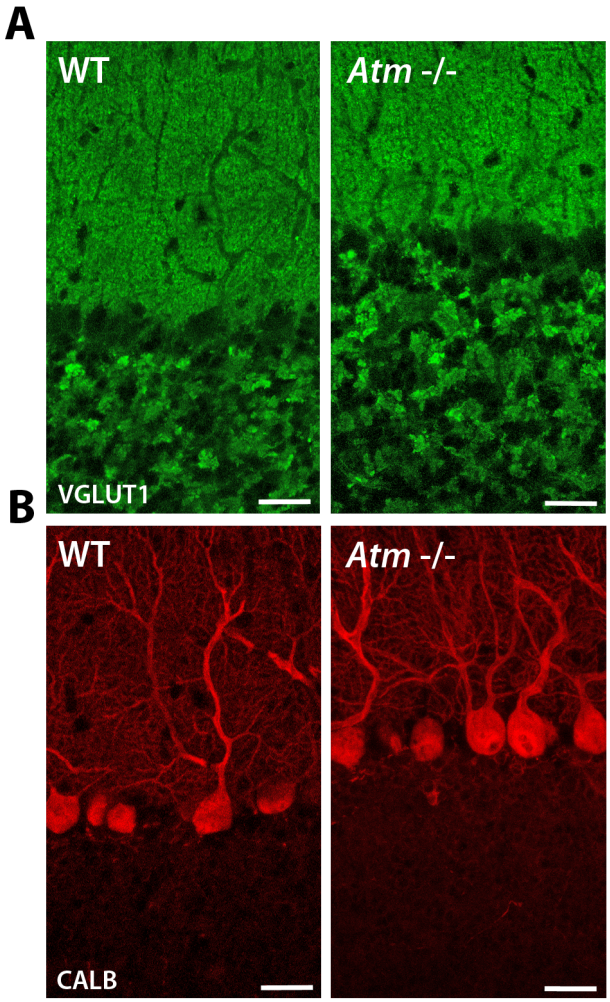

Figure 3.57. Staining for VLGUT1 and CALB in the cerebellum of 6-month-old WT and *Atm-/-* mice (n=1 for each genotype) shows no difference. Scale bar 25 um.

In the cerebellum, VGLUT1 is expressed by parallel fibers rising from the GN that innervate the distal part of the PN dendritic tree. Due to the cut in sagittal orientation, the parallel fibers can't be properly appreciated although the GN layer is visible together with the PN dendritic arborization. No obvious differences were detected between the mutant (**Figure 3.57**, panels on the right) and WT (**Figure 3.57**, panels on the left).

3.17 Future perspectives: applications for Organotypic cell culture in A-T research

A limitating aspect of the *Atm-/-* mouse model is that they die at the age of 6 months due to lymphomas before showing no gross ataxic symptoms or loss of PN (Barlow et al 1999, Barlow et al 1996, Barlow et al 2000) although deficient calcium spike bursts and calcium currents have been detected (Chiesa et al

2000). This is not entirely unexpected since neurodegenerative disorders are mainly characterized by their progression over time. Thus, the ataxic phenotype and loss of PN appears once the lifespan of this mouse model is extended by bone marrow transplantation (BMT) (Pietzner et al 2013). The BMT intervention opens a new possibility to study the degeneration of the cerebellum but is an expensive intervention and time is still a limiting factor since the animals have to be aged. Therefore, it would be interesting to establish another method that would allow identifying potential candidates and accelerating the research with the lifespan-extended *Atm-/-* animals.

Organotypic cell cultures (OTC) were established in 1947 (Hogue 1947) and quickly became an important technique in the field of neuroscience. OTC allows the culture of different neuronal and cellular types while conserving the neuronal network. These advantages over dissociated neuronal cell cultures are of high importance for the cerebellum since PN are difficult to culture. OTCs also offer the possibility to test drugs or challenge the system using fewer animals than *in vivo* experiments. Therefore, we aimed to establish this culture from *Atm-/-* mice to accelerate the research in the A-T field.

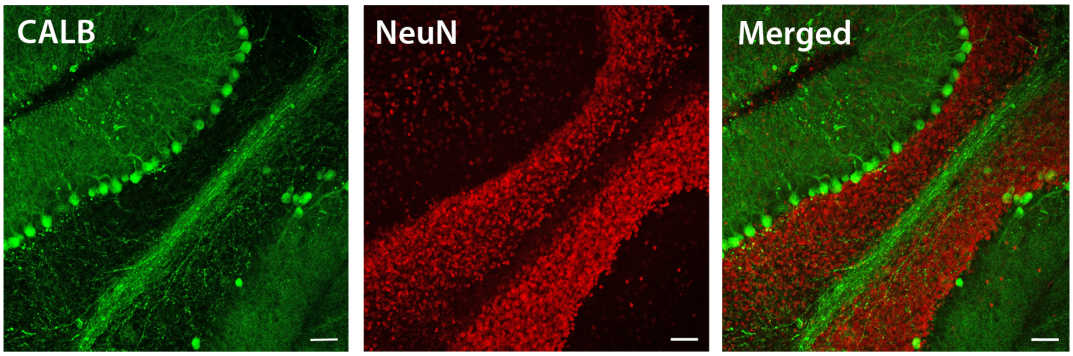

Figure 3.58. Organotypic cerebellar cultures from P17 WT mouse after one week *in vitro* shows PN axonal track and good neuronal viability. In the green channel, CALB1 was detected as PN marker. Labeled in red, NeuN, as a neuronal marker except PN. Scale bar represents 50µm.

The cerebellum reaches maturity around post-natal day 15 (P15), thus the first attempt of cultured cerebellar slices was done with P15 pups. Unfortunately, the results were not as good as expected since few PN showed proper localization and/or dendritic arborization (data not shown), therefore we decided to use older animals. The best results obtained were with P17 pups (Figure 3.58). The slices were cultured for a week, as specified in the materials and methods

section, to ensure their attachment to the membrane and recovery from the slicing process, which causes a strong gliosis. One important observation to determine the viability of the slice is if it starts to flatten and slightly spread on the membrane. In the left panel of the Figure 3.58, corresponding to the CALB staining, the axonal track, PN bodies and dendritic tree can be appreciated as crucial structures in the cerebellar architecture. The NeuN staining (Figure 3.58, middle panel) shows the viability of GN and the other neuronal types present in the different layers of cerebellum. The right panel of Figure 3.58 is the merged previous images showing the typical cerebellar architecture.

Overall, OCT is a promising technique that can be used to treat cerebellar slices with different drugs or recombinant RELN to evaluate the viability of PN in the *Atm-/-* mice (Hellwig et al 2011) or other mouse models without depending on a prolonged period of ageing or using an excessive amount of animals to screen potential therapeutic approaches.

4 DISCUSSION

Ataxias are neurodegenerative disorders affecting mainly the cerebellum and its connections. There is currently no cure for ataxias, but specific mutations in several genes have been identified as underlying causes. Deciphering the pathomechanisms underlying these disorders can lead to a better understanding of neurodegeneration *per se* and enable the development of therapies to cure or delay the symptoms.

Part 1 – The role of Ataxin 2 in SCA2 and ALS

Spinocerebellar ataxia type 2 (SCA2) is an autosomal dominant neurodegenerative disorder caused by CAG expansions in the *ATXN2* gene. The most prominently affected neuron populations are the Purkinje neurons in the cerebellum and motor neurons in the spinal cord. CAG expansions larger than 33 repeats lead to SCA2 while intermediate expansions contribute to the risk to suffer from Parkinson's Disease (PD) and Amyotrophic Lateral Sclerosis (ALS).

4.1 Characterization of *Atxn2*-CAG100-KIN mouse model

Humans and mice share many common genetic features. Therefore, mouse models are extremely useful tools to gain deeper insight into human genetic disorders and to speed up the process towards developing new drugs and therapies.

A mouse model harboring a 42 CAG expansion in the mouse locus of *Atxn2* was previously generated (Damrath et al 2012). Unfortunately the first symptoms appeared at the late age of 18 months limiting the usefulness of the model. Since longer CAG repeats have been associated with earlier and stronger disease phenotype in SCA2 patients (Almaguer-Mederos et al 2013), a novel mouse model was generated introducing an expansion of 100 CAGs in the first exon of

Atxn2; the *Atxn2*-CAG100-KIN mouse model. Thus, the first part of this thesis was focused on the characterization of this new mouse model to define whether its phenotype mimics the pathology of SCA2 and if it permits us to elucidate the molecular and cellular underpinning.

4.1.1 *Atxn2*-CAG100-KIN shows loss of weight over time, genetic instability, and increased rate of death

One of our initial observations regarding the phenotype of this mouse model was the significant loss of weight over time. When the weight was recorded during the life span of these animals, an initial significant gain of weight in homozygous *Atxn2*-CAG100-KIN females was noticed. This pre-symptomatic stage was followed by a progressive loss of weight accompanied with locomotor problems and tremors in both genders (Sen et al 2019). Based on the prominent accumulation of lipids and obesity seen in the *Atxn2*-KO mouse model (Lastres-Becker et al 2008a), we suspect that the initial gain of weight corresponds to a loss-of-function of ATXN2 which is followed by deleterious gain-of-function. Moreover, other SCA2 mouse models also show reduced weight over time (Damrath et al 2012, Dansithong et al 2015) and longitudinal studies in SCA2 families also reported an initial gain of weight followed by a progressive loss (Abdel-Aleem & Zaki 2008). Differences in the brain size and weight were also detected in the homozygous pointing to a loss of lipid content and myelin in the CNS. Myelination defects have been shown in SCA2 patients with massive expansions (Paciorkowski et al 2011). In addition, instability of the expansion and somatic mosaicism were detected in the *Atxn2*-CAG100-KIN colony. Over generations, the repeat expansions can increase in SCA2 patients and mosaicism has been detected in somatic cells (Cancel et al 1997). Interestingly, the instability of the expansion leads to larger sizes, which correlates with the higher instability of pure CAG-repeat regions at the DNA level observed in patients, thereby leading to larger expansion in the following generations. Since larger repeat expansions lead to an earlier and stronger progression of the pathology with earlier death (Almaguer-Mederos et al 2013) in SCA2 patients, the lifetime of the *Atxn2*-CAG100-KIN mice (homozygous and heterozygous compared to WT

littermates) was followed over time. Decreased life span with higher number of sudden deaths was detected for the homozygous *Atxn2*-CAG100-KIN animals.

4.1.2 Behavioural tests demonstrate progressive motor deficits compatible with spinocerebellar ataxia

A rotarod was used to test the motor coordination of *Atxn2*-CAG100-KIN compared to sex- and age-matched WT. As expected, they showed significantly reduced performance starting at the age of 5 months when compared to WT. Over time, the deficit observed for the mutants worsened, correlating with the progression of the pathology (Figure 3.1). The open field test detected a significant decrease of vertical movements from the age of 8 months, which also worsened over time. However, the total distance and horizontal movements were significantly higher in the *Atxn2*-CAG100-KIN at 3 months (Figure 3.2). This initial hyperactivity correlates with the initial loss-of-function hypothesis, similar to the initial gain of weight observed in the homozygous mutant females. Motor hyperactivity was also reported for the *Atxn2*-KO animals (Lastres-Becker et al 2008a). The reduced vertical movements in the *Atxn2*-CAG100-KIN mice are due to balance problems, mirroring the ataxic gait in SCA2 patients. These data and further behavioural experiments, such as grip strength (Figure 3.3) and paw print (Figure 3.4), point to an early vulnerability of the cerebellar circuits and motor neurons.

4.1.3 Progressive brain atrophy and neuronal aggregates are detected upon immunohistochemical analysis

The previously mentioned loss of brain weight and size shrinkage in the *Atxn2*-CAG100-KIN animals compared to WT could reflect neuronal loss together with myelin and lipid loss. Although in SCA2 patients the cerebellum is the prominently affected area with an early and massive loss of PN, also degeneration in other brain regions has been detected. This affection in different brain areas varies between patients but it generally includes the pons, inferior olive, substantia nigra, cerebral cortex, and the anterior horn of the spinal cord (Auburger 2012, Estrada et al 1999, Rub et al 2013, Rub et al 2007). Therefore,

the general reduction of brain size in the mouse mutant correlates with the neuronal atrophy observed in SCA2 patients.

Another important hallmark of poly(Q) diseases is the neuronal accumulation of nuclear/cytoplasmic aggregates. While several spinocerebellar ataxias and HD show nuclear inclusions, SCA2 patients primarily present cytoplasmic aggregates (Rub et al 2013). Immunohistochemistry experiments at the terminal stage of the pathology of the *Atnx2*-CAG100-KIN showed positive ATXN2 aggregates in the typical SCA2-affected regions such as inferior olive, pons, cerebellum, cerebral cortex and hippocampus (Sen et al 2019). Aggregates were also detected in hippocampal neurons and in the spinal cord.

We next aimed to characterize the progression of the aggregation pathology in the cerebellum of this mouse model by comparing with sex- and age-matched WT. Immunohistochemical analyses were performed in *Atxn2*-CAG100-KIN cerebellar slices at different stages (Figure 3.5): at the presymptomatic stage of 3 months, symptomatic stage of 6 months, and final stage of 14 months. The time course aggregation of the expanded ATXN2 was compared with its known interactor PABP1, which was sequestered into insolubility in the *Atxn2*-CAG42-KIN mouse model (Damrath et al 2012, Mangus et al 1998). While ATXN2 signal in WT cerebellar sections showed a homogeneous distribution in the cytoplasm, in the mutant tissue the ATXN2 positive aggregates were detected as early as 3 months of age (Figure 3.5, first row). Interestingly, PABP1 was still showing a homogenous cytoplasmic signal at this age in almost all neurons, but as the aggregates became more obvious at the age of 6 months, the PABP1 signal started to colocalize in the ATXN2 aggregates (Figure 3.5, second row). This progression correlates with the first behavioural alterations observed in the mouse model, which worsened over time (Figure 3.1, Figure 3.2, Figure 3.3).
At the terminal stage of the disease for the *Atxn2*-CAG100-KIN mouse model, 14 months, the number of aggregates was reduced but the size notably increased. Moreover, these larger aggregates seem to localize towards the axon hillock of the PN and might be blocking the axonal transport, therefore impairing the output from the PN to the deep cerebella nuclei (Figure 3.5, bottom row). This

progressive accumulation of ATXN2 aggregates in the *Atxn2*-CAG100-KIN PN seems to correlate with the altered axonal organization observed in CALB1 immunostainings of cerebellar sections. These data suggest PN disconnection around the old age of 14 months in the mutants while there is no obvious loss of PN soma number (Figure 3.6). The PN disconnection could be caused directly by the toxic effect of the expanded ATXN2 in cell-autonomous manner, or by the combination with altered climbing fiber input to the PN. Climbing fiber alterations have been implicated in several spinocerebellar ataxias, including another SCA2 mouse model, and could lead to loss of motor control (Egorova et al 2018, Matilla-Duenas et al 2014, Smeets & Verbeek 2016).

Further immunohistochemical characterization with antibodies against the high molecular weight subunit of neurofilaments showed disorganization of these neuronal intermediate filaments towards the proximal molecular layer (Figure 3.7). Climbing fibers make synaptic contacts in this area and the disorganization of neurofilaments could reflect the altered input to the PN. In addition, significantly altered transcript levels of the gene *Sema7a* were identified starting at 3 months of age and were constantly down-regulated in 14-month-old cerebellar samples (Figure 3.8). *Sema7a* has been implicated in the retrograde signaling to target weak glutamate synapses, an important process to select the "winning" climbing fiber, which would innervate the proximal dendritic area of one PN (Uesaka & Kano 2018). Interestingly, a significant down-regulation of *Sema7a* was also detected in cerebellar samples of *Atxn2*-KO animals suggesting an ATXN2 loss-of-function being responsible for the alteration of this transcript levels even though no neurological symptoms have been reported for the *Atxn2*-KO mouse model (Lastres-Becker et al 2008a).

Overall this mouse model reproduces the characteristic olivo-ponto-cerebellar atrophy observed in SCA2 patients (Auburger 2012, Estrada et al 1999, Rub et al 2013). No electrophysiological analyses have been reported so far, but similar to other spinocerebellar ataxias and mouse models, climbing fiber pathology seems plausible based on the data discussed.

4.2 Proteome data shows a high number of dysregulated RNA binding proteins pointing to RNA metabolism alterations

Neurons, as post-mitotic cells with a complex architecture, need to tightly control all aspects of RNA metabolism, therefore RBP and other implicated factors are essential for proper neuronal function and survival (Bryant & Yazdani 2016, Hutten & Dormann 2016, Lenzken et al 2014, Sephton & Yu 2015). Ataxin 2 is an RNA binding protein that preferentially binds to the 3' UTR of transcripts to stabilize them (Yokoshi et al 2014). ATXN2 was found to up-regulate proteins involved in RNA splicing, polyadenylation, and 3' end processing, among others (Yokoshi et al 2014). A high number of dysregulated nucleic-acid-binding proteins were detected in the proteome data sets generated from 14-month-old *Atxn2*-CAG100-KIN cerebellum and spinal cord pointing to RNA metabolism dysregulations. However in contrast to the proteome profiles, validation efforts at the transcript level of 44 factors implicated in RNA metabolism (Table 3.2, Table 3.3, Table 3.4, Table 3.5) and DNA damage response (Table 3.6) in cerebella of 14-month-old *Atxn2*-CAG100-KIN and *Atxn2*-KO showed few significant dysregulations. Interestingly, the heterogeneous nuclear ribonucleoprotein A2/B1 (hnRNPa2/B1) was significantly up-regulated in the cerebellar samples from the *Atxn2*-CAG100-KIN animals (Table 3.3). Since no alterations were detected in the cerebellar samples of *Atxn2*-KO, this effect could be caused by the toxic gain-of-function of the expanded ATXN2. The factor hnRNPA2/B1 has been implicated in ALS and familial-inherited degeneration affecting muscle, brain, motor neuron, and bone (Kim et al 2013). ATXN2 has been already shown to interact with at least three more ALS-linked factors that serve as RNA-binding-proteins: FUS, C9ORF72 and TDP43 (Vucic et al 2014). Therefore, the up-regulation seen for *Hrnp2ab1* could further implicate ATXN2 in the pathology of ALS. A commonly dysregulated factor significantly reduced to 60% in both *Atxn2*-KO and *Atxn2*-CAG100-KIN was *Eif5a2* (Table 3.5). This eukaryotic translation initiation factor has been implicated in the elongation step of protein synthesis (Saini et al 2009). ATXN2 has been found to associate with the translation apparatus (Tadauchi et al 2004) based on yeast experiments, but it is not essential for translation and its modulatory functions have not been elucidated. It is also interesting to note that Eif5a protein influences the

translation of viral RNA (Caceres et al 2016) and that ATXN2 has been implicated in the cell response to poliovirus (Jagdeo et al 2018). It would be highly interesting to further investigate the potential ATXN2 loss-of-function effect on this translation initiation and elongation factor during viral infections.

Four other dysregulated factors in cerebellum and spinal cord proteome data sets were investigated further. The first, AHNAK, acts as a structural scaffold having multiple protein interaction domains across its sequence (Komuro et al 2004). The interest for this factor arose from its implication in spinal cord injury (Von Boxberg et al 2006) and the localization of its mRNA in SG under stress conditions (Khong et al 2017). Moreover, AHNAK has been implicated in other cellular processes such as regulation of calcium channels (Haase et al 2005, Jin et al 2019, Komuro et al 2004, Matza et al 2009). Calcium signaling is essential in neuronal function (Kitamura & Kano 2013) and mutations in several calcium factors are causative of SCA, such as CACNA1A (SCA6) and ITPR1 (SCA15/29) (Huang et al 2012, van de Leemput et al 2007, Zhuchenko et al 1997).
The second factor was AHNAK2, the other member of the AHNAK family. The exact function of this protein is unknown but it recently it has been implicated in Charcot-Marie-Tooth disease (Tey et al 2019). The characterization at transcript level by Q-PCR showed up-regulation of *Ahnak* and down-regulation of *Ahnak2* in the 14-month-old *Atxn2*-CAG100-KIN spinal cord (Figure 3.9, Figure 3.10). Moreover, AHNAK was found to co-aggregate with ATXN2 in the spinal cord of these animals upon immunohistochemical analysis (Figure 3.11). Based on these results, it seems that pathological expansions in ATXN2 alter both AHNAK family members transcript and protein levels, and sequesters AHNAK into aggregates in the spinal cord. These events could alter the physiological functions of AHNAK and AHNAK2. Unfortunately, all other efforts to characterize the relationship between the AHNAK family and ATXN2 did not lead to any further conclusions (Figure 3.12, Figure 3.13).

The other two factors investigated were the Poly(C) binding proteins 1 and 2, PCBP1 and PCBP2. They are part of the heterogeneous nuclear ribonucleoprotein (hnRNP) family with RNA and DNA metabolism functions.

They are individually necessary for embryonic development (Ghanem et al 2016) and have been shown to have distinct roles affecting translation and gene expression in different types of viruses (Blyn et al 1997, Woolaway et al 2007). Stress granule formation has been implicated in viral infection as an important component of the host cell antiviral defense (Zhang et al 2019). Moreover, SG composition seems to vary according to the inducing stimulus, and different virus families have been reported to interact with different RBP (Zhang et al 2019). ATXN2 has been identified as a host cell substrate of poliovirus together with other RBP, pointing to a viral infection response role potentially through the formation of SG. The effect of ATXN2 regarding PCBP1 and PCBP2 seems to be exclusively at protein level since no dysregulations were detected at the transcript level of these two factors (Figure 3.14, Figure 3.16). Upon immunohistochemical analysis, PCBP1 seems to co-aggregate with ATXN2 in PN of 14-month-old *Atxn2*-CAG100-KIN cerebellar slices, while PCBP2 accumulates at the dendrites of this cell type (Figure 3.15). Further experiments employing mouse embryonic fibroblasts (MEF) established from *Atxn2*-CAG100-KIN animals and their WT littermates failed to show any altered localization of PCBP2 upon Poly(IC) treatment. This could be explained based on several reports showing that different viruses affect different SG components, and that host cell response might differ depending on origin.

Overall, comparing the results obtained via proteome analysis and transcript analysis by Q-PCR, ATXN2 seems to affect a higher number of RBP at their protein level rather than at the transcript level. Only a few dysregulations were detected upon Q-PCR analysis.

4.3 TDP43 pathology in the spinal cord of *Atxn2*-CAG100-KIN mouse model overlaps with ALS

The spinal cord controls the voluntary muscles of the trunk and extremities, while also receiving sensory input from these areas of the body. The spinal cord primarily transmits the nerve signals from the motor cortex to the body, and from the afferent fibers of the sensory neurons to the sensory cortex (Bican et al 2013). Recently, evidence of corticospinal tract dysfunction in pre-ataxic SCA2

patients has been published (Velazquez-Perez et al 2018) and motor neuron degeneration has been detected in SCA2 mutation carriers before the onset of cerebellar ataxia (Velazquez-Perez et al 2014, Velazquez-Perez et al 2011, Velazquez-Perez et al 2017). In addition, intermediate expansions of the poly(Q) domain in ATXN2 have been implicated in ALS, a neurodegenerative disorder also showing degeneration of corticospinal motor neurons (Elden et al 2010, Gispert et al 2012, Ross et al 2011, Taylor et al 2016). Further experiments with the TDP43 overexpressing mouse model strengthened the role of ATXN2 in ALS pathology after showing significantly longer lifespan when crossed with the mouse mutant *Atxn2*-KO (Becker et al 2017). Therefore, the *Atxn2*-CAG100-KIN mice, with conserved spatial and temporal expression of ATXN2, is an ideal model to study the spinal cord pathology observed in SCA2 patients, and gain deeper insight into the relationship between TDP43 and the expanded ATXN2.

Based on the accumulating evidence of ATXN2 and TDP43 interaction, questions regarding the similarities of ALS and SCA2 spinal cord pathology arose. To investigate these similarities, the transcript and protein levels of TDP43 in the spinal cord of the *Atxn2*-CAG100-KIN at 3 and 14 months were determined. To differentiate between a toxic gain-of-function or loss-of-function caused by the expansion in ATXN2, samples from the mouse mutant *Atxn2*-KO were also used. A significant up-regulation of TDP43 protein level was detected in the spinal cord at the age of 14 months, however no differences at the transcript level were detected, neither in the 3-month-old *Atxn2*-CAG100-KIN and 6-month-old *Atxn2*-KO samples (Figure 3.18, A and Figure 3.19,B). In addition, the transcript levels of *Atxn2* were determined in the spinal cord and no significant differences were detected in the *Atxn2*-CAG100-KIN mouse model. The depletion of *Atxn2* mRNA in the spinal cord of *Atxn2*-KO mice mutants was confirmed (Figure 3.19, A).

Alterations in the transcription and translation of *Atxn2* have been shown in the cerebellum of this mouse model (Sen et al 2019), the fact that no dysregulations were detected at the transcript level in the spinal cord may be due to tissue differences, however the protein level of ATXN2 was not determined in the spinal cord samples. Moreover, the protein levels of NeuN (as a neuronal

marker) were also investigated in the same sample sets, showing a significant reduction in the 14-month-old *Atxn2*-CAG100-KIN (Figure 3.18, B). This result points to a reduction in number of neurons in the spinal cord at the terminal stage of *Atxn2*-CAG100-KIN pathology. Previous differences in the level of CALB1 (as PN marker in the cerebellum) were identified in WB showing reduced levels of this marker, however the soma of PN was still visible in cerebellar immunohistochemistry experiments (Sen et al 2019).

To further characterize the differences between the cerebellum and the spinal cord, NeuN and TDP43 protein levels were investigated in the cerebellum of 3- and 14-month-old *Atxn2*-CAG100-KIN animals and *Atxn2*-KO mice (Figure 3.18, C and D). No differences were detected for either of these two proteins, meaning that no further neuronal loss aside from the PN could be detected, and that TDP43 protein levels were not altered in the cerebellum.

Characterization at the histological level of the spinal cord in this mouse model was performed using cryo-sections from 3-, 6-, and 14-month-old animals compared to WT and *Atxn2*-KO mutants. The aggregation pattern over time was similar to that in the cerebellum. ATXN2 positive aggregates were detected at 3 months and increased in size over time, sequestrating PABP1 and TDP43 (Figure 3.20). Another SG marker, TIA1, was used to further confirm the presence of SG-related proteins into the ATXN2 positive aggregates (Figure 3.21). A hallmark of ALS is the presence of cytoplasmic TDP43-positive inclusions found in neurons and glia (Neumann et al 2006). Therefore, this mouse model reproduces, at least in part, the pathology observed in ALS.

TDP43 can be cleaved at its C-terminal domain by CASP3 (Dormann et al 2009, Nishimoto et al 2010, Zhang et al 2007), accumulating in neurons and glia (Igaz et al 2008, Neumann et al 2006). Reports implicating ATXN2 intermediate expansions in ALS, influencing TDP43 aggregation via enhanced CASP3 activation and production of pathological C-terminal fragments from TDP43, have been published (Elden et al 2010, Hart & Gitler 2012). In addition, cleaved fragments of Ataxin3 and Ataxin7 exacerbating the pathology have been detected

in mouse and *Drosophila* models (Jung et al 2009, Young et al 2007). CASP3 protein levels were found significantly up-regulated in the spinal cord of 14-month-old *Atxn2*-CAG100-KIN animals (Figure 3.22, B). No dysregulation was found at the transcript level in any condition tested, nor were the protein levels in the 3-month-old *Atxn2*-CAG100-KIN and *Atxn2*-KO spinal cord samples (Figure 3.22). In addition, CASP3 levels were investigated at 14 months in the cerebellum of *Atxn2*-CAG100-KIN and no alterations were detected. Thus, the pathology of TDP43 and accumulation of CASP3 seems to be spinal cord specific.

Overall, the alteration of TDP43 protein levels and the reduced amount of NeuN were specific events in the spinal cord while the cerebellum showed reduced levels of CALB1 and down-regulation of the expanded *Atxn2* transcript. The immunohistochemistry analyses revealed a similar time pattern of ATXN2 aggregation in the spinal cord as previously defined in the cerebellum of *Atxn2*-CAG100-KIN at 3, 6, and 14 months of the pathology. Moreover, increased CASP3 levels were only detected in the old spinal cord samples of *Atxn2*-CAG100-KIN, which could be linked to the TDP43 aggregation observed.

4.4 Transcriptomics of the spinal cord reveals RNA toxicity and microglia activation

The spinal cord pathology observed in the *Atxn2*-CAG100-KIN mice showed the implication of ATXN2 and other ALS-related RBP that co-localized into aggregates. Thus, to gain deeper insight in the RNA metabolism pathology pointed by the proteome data, we generated transcriptome data sets from 3- and 14-month-old spinal cord *Atxn2*-CAG100-KIN samples (Figure 3.24, A). The Clariom™ D mouse array from ThermoFisher was used to generate both transcriptomics data sets and the data were analyzed with TAC (Transcriptome Analysis Console) software. Standard parameters and self-determined criteria were used to determine the significant up- and down-regulations (Figure 3.24, B). At both ages, a high number of non-coding RNAs were found significantly up-regulated (Figure 3.25) that could reflect dysregulation of RNA-based regulatory mechanisms (Wei et al 2018). Due to a lack of tools to study these types of regulatory mechanisms, we did not further pursue this hypothesis.

Several ataxia- and ALS-related genes were found dysregulated in the 14-month-old transcriptome data set. In addition, a high number of genes linked to RNA toxicity response, such as several toll-like receptors, and TNF (tumor necrosis factor) receptors, were also found to be up-regulated (Figure 3.26). Further analysis of the significant two-fold up-regulations with the STRING platform showed a high number of lysosomal factors, described by KEGG pathway, and factors implicated in "immune system", defined by GO biological process (Figure 3.28). Importantly, all of these factors are highly expressed in microglia (Zhang et al 2014).

Microglia are cells of myeloid lineage that populate the CNS during early development. These cells make up between 5 and 20% of the CNS cells depending on the brain structure, and constitute the main resident immune cell population (Grabert et al 2016, Lawson et al 1990, Stowell et al 2018). Microglia are actively involved in the refinement of neuronal connections during development (Verney et al 2010), eliminating redundant synapses through the chemokine signaling system (Paolicelli et al 2011), also referred to as synaptic pruning. Deficient neuron-microglia signaling during development leads to the impairment of functional brain connectivity and alters social behaviour (Kim et al 2017, Zhan et al 2014). More recently, a report identifying a stepwise developmental program of microglia in synchrony with the developing brain has been published (Matcovitch-Natan et al 2016), further associating microglia with neurodevelopmental disorders. Additionally, microglia have been implicated in the maintenance of the brain homeostasis during adulthood and ageing (Tremblay et al 2011). Surveying microglia, in their basal and ramified status, can phagocyte neuronal material without becoming activated (Sierra et al 2010). On the contrary, reactive microglia have been implicated in increasing severity of several neurodegenerative disorders (Block et al 2007). Recent evidence suggests that microglial reaction to CNS pathology is not uniform, and depends on the timing and diversity of microglial subtypes involved (Spiller et al 2018).

The transcriptome data set generated from the 14-month-old *Atxn2*-CAG100-KIN spinal cord samples showed significant up-regulations of factors implicated in

microglia activation, such as TREM2 and DAP12, and factors linked to synaptic pruning reactivation, like the complement system. Part of these factors was further validated via Q-PCR confirming the up-regulation observed in the microarray (**Figure 3.31**). Reactive gliosis and neuroinflammation are hallmarks of neurodegenerative diseases, such as AD, PD, ALS, and FTD (Salter & Stevens 2017). Reports based on transcriptomic studies have identified microglia-related pathways as central to AD risk and pathogenesis (Lambert et al 2013, Zhang et al 2013a). Additionally, genome wide association studies (GWAS) have identified more than 20 loci linked to AD that are expressed or exclusively expressed in microglia or myeloid cells (Efthymiou & Goate 2017, Villegas-Llerena et al 2016). Moreover, microglia accumulate in active sites of demyelination and neurodegeneration in multiple sclerosis (MS), and once activated they can damage other CNS cells, in particular oligodendrocytes and neurons (Zrzavy et al 2017).

Moreover, two neuroinflammation-linked factors that have been implicated in ALS, *Ripk1* and *Grn*, were also found up-regulated (Figure 3.29, Figure 3.30). RIPK1, a kinase controlling programmed cell death via apoptosis and necroptosis (Meng et al 2018), was up-regulated at the transcript and protein level in the 14-month-old *Atxn2*-CAG100-KIN spinal cord samples (Figure 3.29). No further dysregulations were detected at the transcript level in the 3-month-old *Atxn2*-CAG100-KIN and *Atxn2*-KO spinal cord samples, nor in cerebellar samples of any group. This kinase plays a central role in mediating neuroinflammation by promoting activation of microglia in ALS, AD, and MS (Caccamo et al 2017, Ito et al 2016). Indeed, RIPK1 has been implicated in regulating disease-associated microglia factors leading to impairment in the lysosomal pathway in an AD mouse model (Ofengeim et al 2017). RIPK1 can be suppressed by inhibitory phosphorylation mediated by TAK1 (Transforming growth factor-beta-activated kinase 1) whose expression is modulated by TBK1 (TANK-binding kinase 1) (Xu et al 2018). Both kinases, TAK1 and TBK1, are highly expressed by microglia (Xu et al 2018, Zhang et al 2014), and mutant *TBK1* alleles have been implicated in ALS and FTD (Freischmidt et al 2017). Haploinsufficiency of *Tbk1* in mice together with heterozygosity of myeloid TAK1 expression caused microgliosis

with activated amoeboid-like microglia and expression of 40 genes involved in innate immunity (Xu et al 2018). Therefore, the lack of RPIK1 suppression leads to neuroinflammation and microgliosis.

Progranulin is an evolutionary conserved glycoprotein that can be cleaved into individual granulins. PGRN is a key regulator of inflammation, and its deficiency causes an aberrant increase in phagocytosis and pro-inflammatory cytokine production in microglia and macrophages (Kao et al 2011, Martens et al 2012, Yin et al 2010). Rare homozygous *GRN* mutations in humans cause neuronal ceroid lipofuscinosis (NCL) sharing similar neuropathological characteristics with FTLD patients with *GRN* mutations (Smith et al 2012). In addition, a study comparing FTLD patients with *GRN* mutations (FTLD-GRN) and FTLD cases with C9ORF72 mutations (FTLD-C9ORF72) showed different microglia responses (Sakae et al 2019). FTLD-GRN patients showed more IBA1-positive ameboid microglia and also had more microglia with nuclear condensation, possibly indicating apoptosis (Sakae et al 2019). PGRN has also been shown to mediate caspase-dependent cleavage of TDP43 (Zhang et al 2007) and has recently been implicated in the lysosomal homeostasis and lipid metabolism (Evers et al 2017). Moreover, progranulin deficiency has been shown to promote synaptic pruning by microglia via excessive complement production and to cause lysosomal defects (Lui et al 2016). As previously mentioned, STRING analysis of up-regulated factors in the 14-month-old spinal cord transcriptome data set pointed to an increase of lysosomal and immune related factors (Figure 3.28, **Figure 3.31**, Figure 3.32). Despite the up-regulation of *Grn* transcript levels detected at 3- and 14-month-old *Atxn2*-CAG100-KIN spinal cord samples, PGRN protein levels were not found dysregulated based on WB experiments (Figure 3.30). Additionally, PGRN seems to be under the control of the transcript factor EB (TFEB), which plays an important role in the regulation of lysosomal biogenesis and autophagy (Belcastro et al 2011, Sardiello et al 2009), and has been shown to up-regulate lysosomal biogenesis in microglia (Bao et al 2016). The subcellular localization and activity of TFEB is regulated by mTOR-mediated phosphorylation. Phosphorylated TFEB is retained in the cytoplasm while dephosphorylated TFEB can translocate to the nucleus and induce the transcription of target genes

(Napolitano & Ballabio 2016). Although the transcript level of TFEB was not dysregulated in the spinal cord of *Atxn2*-CAG100-KIN mice (Figure 3.32), posttranscriptional changes cannot be ruled out based on the inhibitory effect of ATXN2 on mTOR signaling (Bar et al 2016, DeMille et al 2015, DeMille et al 2014, Lastres-Becker et al 2016, Takahara & Maeda 2012).

Therefore, RIPK1 and PGRN further implicate microglia to the pathology observed in the *Atxn2*-CAG100-KIN mouse model, and raise questions regarding lysosomal function and autophagy in glia cells (Strohm & Behrends 2019).

In addition, *Aif1* and *Gfap* transcripts, as microglia and astroglia markers respectively, were found up-regulated in the 14-month-old *Atxn2*-CAG100-KIN spinal cord and cerebellar samples. Despite the up-regulation observed in *Aif1*, quantification of IBA1 did not show any dysregulations in WB. These data could point to an affection of microglia either caused by the neuronal dysfunction, by its endogenous CAG100-ATXN2 expression, or by a combination of both events, leading to an impaired proliferation of this self-renewal cell type. Additionally, microglia have been described as long-lived tissue-resident macrophages with low turnover (Fuger et al 2017) showing age-related changes that may contribute to age-related cognitive decline and neurodegenerative diseases (Hefendehl et al 2014).

4.5 Microglia express Ataxin 2 and show aggregates in the spinal cord

A functional screening of neurodegeneration-linked factors on microglia phagocytosis identified TDP43 as a regulator (Paolicelli et al 2017). No previous evidence was found regarding ATXN2 expression in microglia even though *Atxn2* transcript has been detected in this cell type (Zhang et al 2014). Therefore, we investigated the ATXN2 levels first in BV2 murine microglia cell line showing its presence through immunocytochemistry (Figure 3.35). Treatment with an oxidative stressor, NaArs, showed formation of SG detected by antibodies against ATXN2, PABP1, and TDP43 (Figure 3.35). Therefore, ATXN2 is expressed at the transcript and protein level, and it is functionally implicated in SG formation under oxidative stress in this microglia cell line.

Characterization of the microglia in the spinal cord of 6-month-old *Atxn2*-CAG100-KIN and *Atxn2*-KO via immunohistochemistry showed the presence of ATXN2 in microglia (IBA1-positive cells) from *Atxn2*-CAG100-KIN samples (Figure 3.36, second row). Interestingly, no signal was detected in the microglia from WT spinal cord at 6 months of age, probably due to the small size and cytoplasm area of these cells (Figure 3.36, first row). Indeed, primary cell cultures established from WT and *Atxn2*-CAG100-KIN littermates at postnatal day 0 showed ATXN2 signal upon immunocytochemistry (Figure 3.38) demonstrating ATXN2 protein expression in this cell type. No signal of ATXN2 was detected in the spinal cord sections of *Atxn2*-KO while IBA1 antibody was able to detect microglia cells (Figure 3.36, last row).

Further immunohistochemical analysis from 14-month-old spinal cord sections of *Atxn2*-CAG100-KIN and WT animals showed an increase of ATXN2 expression in WT (Figure 3.37, first row) and ATXN2 aggregates in *Atxn2*-CAG100-KIN (Figure 3.37, second row) microglia. The detection of ATXN2 in microglia from older spinal cord sections rather than 6-month-old sections from WT implicates this factor in the process of ageing, agreeing with prior reports showing that microglia expression profile changes during ageing (Grabert et al 2016, Sierra et al 2007, Streit et al 2009). While the levels of ATXN2 seem to increase in WT microglia and show homogeneous distribution in the cytoplasm of this cell type, *Atxn2*-CAG100-KIN microglia already shows increased expression of ATXN2 at 6 months of age and ATXN2-positive cytoplasmic aggregates at 14 months (Figure 3.36, Figure 3.37). Therefore, expanded ATXN2 seems to accumulate and aggregate over time in microglia either due to the endogenous ATXN2 protein, following phagocytosis of neuronal debris, or a combination of both events.

4.6 Evaluation of the spinal cord and cerebellar transcriptomics reveals common dysregulation of cholesterol degradation and biosynthesis

To complete the description at the transcript level, transcriptomics data was generated from 3- and 14-month-old *Atxn2*-CAG100-KIN cerebellar samples (Table 3.8). The same microarray kit was used, therefore the cerebellar and

spinal cord transcriptomics data sets of both age groups were directly comparable (Figure 3.40).

In looking for commonly dysregulated pathways among the data sets generated, we identified a consistent down-regulation of the cholesterol metabolism pathway (Figure 3.42). Cholesterol is an essential component of cell membranes influencing cellular structure and function (Levitan et al 2014, Lippincott-Schwartz & Phair 2010, Manes & Martinez 2004). This lipid also serves as a precursor to steroid hormone and bile acid synthesis, thus it has a critical role in body metabolism (Martin et al 2014). The brain is the organ richest in cholesterol (Björkhem & Meaney 2004), and within the brain, an important fraction of cholesterol forms part of the myelin sheath. Neurons and glia also contain large amounts of cholesterol to maintain their morphology and synaptic transmission (Bjorkhem 2006). Moreover, there is an increasing amount of evidence demonstrating that defects in brain cholesterol metabolism contribute to neurodegenerative disorders, such as AD, HD, PD, and Niemann-Pick disease Type C (Martin et al 2014).

Due to the blood brain barrier (BBB), all cholesterol in the CNS has to be locally synthesized (Björkhem & Meaney 2004). Cellular cholesterol is synthesized primarily at the endoplasmic reticulum (ER) from acetyl-CoA (acetyl coenzyme A) in a process that involves more than 30 enzymatic steps (Arenas et al 2017). The enzyme HMGCS, implicated in the second reaction to condense acetyl-CoA with acetoacetyl-CoA to form HMG-CoA (3-hydroxy-3-methylglutaryl-CoA), was consistently down-regulated in the transcriptome data sets and further validated in 3- and 14-month-old *Atxn2*-CAG100-KIN and *Atxn2*-KO cerebellar samples by Q-PCR (Figure 3.43). It is possible that the loss-of-function of ATXN2 in both mutants affects the production of cholesterol. This effect could be due to low levels of acetyl-CoA linking ATXN2 and metabolism control.

Acetyl-CoA participates in many biochemical reactions as an intermediate in various pathways, such as the citric acid cycle, fatty acid metabolism, steroid synthesis, acetylcholine synthesis, and melatonin synthesis. Moreover, proteomic

and metabolomics studies in *Atxn2*-KO have reported down-regulation of ACADS (Acyl-CoA dehydrogenases), which are involved in fatty acid β-oxidation (Meierhofer et al 2016). Moreover, *Atxn2*-KO liver also showed down-regulation of the BCAA (brain-chain amino acid) pathway, fatty acid metabolism, and the citric acid cycle (Meierhofer et al 2016). Therefore, alteration of cholesterol synthesis in absence or loss-of-function of ATXN2 seems plausible.

Transcript levels of *Dhcr24*, another enzyme implicated in the Bloch cholesterol biosynthesis pathway, were also found down-regulated in transcriptome data sets. Validation by Q-PCR showed consistency in the 14-month-old *Atxn2*-CAG100-KIN and *Atxn2*-KO cerebellum (Figure 3.43). The Bloch pathway is the predominant astrocyte pathway for cholesterol biosynthesis in this cell type. Missense mutations in its gene have been linked to desmosterolosis (Schaaf et al 2011). Therefore, it could be possible that astrocyte cholesterol syntheses, which have higher capability than neurons to produce cholesterol *de novo*, shows time-dependent impairment and further contributes in the cholesterol metabolism dysregulation.

Regarding the degradation of cholesterol, CYP46A1 (Cholesterol 24-hydroxylase) constitutes the major excretion pathway transforming cholesterol into the BBB permeable 24-OHC (24-Hydroxycholesterol) (Russell et al 2009). CYP46A1 is a brain-specific enzyme highly expressed in neurons, particularly in PN and cerebellar interneurons (Ramirez et al 2008). Moreover, CYP46A1 activates the mevalonate pathway of cholesterol synthesis, which intermediate compounds implicated in cellular pathways, such as endocytosis, autophagy, and synaptic transmission (Moutinho et al 2016). Additionally, loss of cholesterol during glutamate-mediated excitotoxicity has been reported, which was prevented by knocking-down CYP46A1 (Sodero et al 2012).

The transcript level of CYP46A1 was down-regulated in the transcriptomics data sets and further validated in the 3- and 14-month-old *Atxn2*-CAG100 and *Atxn2*-KO cerebellar samples (Figure 3.43). Moreover, down-regulation of CYP46A1 has been detected in mouse models of AD and SCA3, and affected brain regions of HD

patients (Boussicault et al 2016, Burlot et al 2015, Nobrega et al 2019). Recently, the administration of AAV-CYP46A1 (Adeno-associated virus) to the cerebellum of a transgenic SCA3 mouse model showed that it could significantly ameliorate their motor impairment (Nobrega et al 2019). Therefore, modulating the levels of *Cyp46a1* to compensate for the consistent down-regulation observed in the *Atxn2*-CAG100-KIN could improve their motor deficits and lead to therapeutic strategies for SCA2 patients.

4.7 Conclusions and perspectives

Overall, the characterization of the *Atxn2*-CAG100-KIN mice demonstrated that this mouse model reproduces the symptomatology observed in SCA2 patients. The significant loss of weight detected over time together with the brain atrophy could be based on the increased toxicity of the expanded ATXN2 forming aggregates. Moreover, this model allows us to study the effect of the ATXN2 poly(Q) expansions in non-neuronal cells and peripheral tissues since the expansion was inserted in the *Atxn2* mouse locus.

The characterization of the spinal cord pathology in the *Atxn2*-CAG100-KIN mouse model further evidences the pathology in the spinal cord suffered by the SCA2 patients and its spatio-temporal progressive affection by the disease. Despite the similar pattern observed in the formation of ATXN2-positive aggregates, the RBP-pathology seemed to be more pronounced in the spinal cord rather than the cerebellum evidencing differences between CNS areas. Therefore, this mouse model can help develop new therapies and evaluate their effect in differently affected areas.

Analyzing and validating the 14-month-old *Atxn2*-CAG100-KIN spinal cord transcriptomic data set helps to further understand the pathology observed in this tissue. The implication of a high number of up-regulated factors linked to immune response and lysosomes pointed to an implication of microglia in the pathology of this mouse model.

The time-dependent co-aggregation or protein-level alteration of several RBP caused by the 100 CAG expansion in ATXN2 could lead to a cytoplasmic accumulation of unprotected RNA. These increased levels of RNA could then trigger the innate immune system mimicking a viral infection. Moreover, *Atxn2* mRNA could also be toxic due to the presence of the expansion (Fiszer & Krzyzosiak 2013) and further exacerbate the response to RNA. Although we cannot rule out the neuronal contribution to the alteration of many of these factors, the characterization of microglial response and the potentially deleterious effects of the expanded ATXN2 in this cell type could lead to therapies to improve patients' living standards or delay the symptoms' onset. For instance, peripheral administration of a detoxified TLR4 ligand (monophosphoryl lipid A) was shown to stimulate microglia phagocytosis without excessive inflammatory response, improving cognitive deficits in a mouse model of AD (Michaud et al 2013).

Establishing primary microglia cultures was the first step in further pursuing the research of this cell type involvement in the SCA2 pathology. The contribution of microglia to other neurodegenerative diseases, such as AD, PD, and ALS has already been proven and seems to be region- and time-dependent. Therefore, continuing the investigation of other non-neuronal cell type contribution to the pathology might lead to defining new therapeutic strategies that could slow down and ameliorate the progression of the disease in patients.

The last part of this work was the identification and validation of common altered pathways in all four transcriptome data sets generated. The cholesterol metabolism pathway was consistently dysregulated in both tissues, therefore modulating this pathway could be helpful for SCA2 and other neurodegenerative diseases, such as ALS. The characterization of *Cyp46a1* down-regulation seems to be of importance since it has been shown to be down-regulated in AD, HD and SCA3. Moreover, it opens a potential therapeutic approach since AAV-CYP46A1 administration to a SCA3 mouse model significantly improved their motor deficits. Additionally, CYP46A1 silencing caused accumulation of lysosomes and

endosomes in the mouse brain linking this enzyme to autophagolysosome accumulation and dysfunction (Menzies et al 2015).

Part 2 – Ataxia Telangiectasia Mutated

Autosomal recessive ataxia telangiectasia (A-T) is characterized by radiosensitivity, immunodeficiency, and cerebellar neurodegeneration. A-T is caused by inactivating mutations in the ataxia telangiectasia mutated (ATM) gene; a serine-threonine protein kinase involved in DNA damage response, oxidative stress, mitochondrial functions, mitophagy regulation, and excitatory neurotransmission.

4.8 Ataxia telangiectasia alters the ApoB and reelin pathway

OMICS technologies have become useful tools to understand and evaluate altered pathways in disorders such as cancer and neurodegenerative diseases. The application of these technologies in medicine would help to counsel families regarding disease risk, progression, and benefits of therapy (Hasin et al 2017).
For A-T diagnostics, the level of alpha-fetoprotein in blood is a well-established biomarker that allows monitoring of the progression diseases (Rothblum-Oviatt et al 2016, Stray-Pedersen et al 2007). During the course of this thesis, A-T cerebrospinal fluid (CSF) was evaluated through quantitative global screening and compared to healthy controls (Canet-Pons et al 2018).

4.8.1 Global proteomics reveals several dysregulations in the reelin signaling pathway

To identify further molecular biomarkers to follow the progression of A-T in extracellular fluids, we studied CSF from 12 patients and 12 sex- and age-matched control individuals. Studies were conducted using global proteome profiling with label-free mass spectrometry (MS). In addition, clinical ataxia scores and determination of alpha-fetoprotein levels were documented (Table 3.9). The ataxia scores showed a progressive increase during ageing. The CSF total protein and albumin levels also increased significantly in patients over time, but not in controls (Figure 3.44). Among patients aged 10 to 16 years, total

protein and albumin levels showed better correlation to age than the ataxia scores.

Global proteome bioinformatics analysis identified similar numbers of CSF proteins in patients and controls (Table 3.9). It also revealed prominent PN vulnerability in patients showing a strong reduction of calbindin (CALB1). Decreases of CALB1 levels have been reported in other cerebellar ataxias (Koeppen 2005) and CALB1 has been used as a PN marker (Whitney et al 2008), therefore its levels could be correlated with degeneration of the cerebellum (Barski et al 2003). Moreover, among the dysregulations detected in the A-T patients' CSF, ten factors have been previously implicated in the pathogenesis of ataxia. These findings may improve our mechanistic understanding of how ATM deficiency preferentially affects the cerebellum.

Looking for novel potential biomarkers using linear regression models we identified RELN. RELN appeared to decrease earlier and correlate with age better than CALB1 (**Figure 3.46**). Its protein levels also showed a strong correlation with ataxia scores, and a normalization of its insidious depletion versus the progressive increase of CSF protein content enhanced the steepness of the regression line (**Figure 3.46**). The strong RELN deficit in A-T patients around the age of 15 years is a novel finding.

The absence of reelin triggers programmed cell death in the cerebellum via apoptosis and autophagy mainly for GN after parallel fiber morphology changes (Castagna et al 2016). Therefore, the deficiency of GN-expressed reelin (Pesold et al 1998) could be upstream from PN degeneration in A-T. Deficiency in reelin has been implicated in a rare autosomal recessive ataxia with cerebellar hypoplasia and lissencephalopathy (Hong et al 2000). In addition, a spontaneous reelin deletion in mice (reeler mouse mutant) causes ataxia over time due to brain cortex foliation defects, which prominently affect cerebellar PN (D'Arcangelo et al 1995, Miyata et al 2010).

Reelin is a large secreted extracellular glycoprotein that activates the apolipoprotein receptors APOER2 and VLDLR. Their interaction controls neuronal positioning during brain development and synaptic plasticity during adulthood (Herz & Chen 2006, Nakamura et al 2016). Reelin also influences postsynapses in their glutamatergic NMDA receptor composition, modulating postnatal neurogenesis, and enhancing spine hypertrophy and long-term potentiation (Sinagra et al 2005).

The strong up-regulation observed for APOB further supports the central role of reelin signaling in this proteome profile. This lipid transporter shows preferential expression in GN and PN of the cerebellum, based on Allen mouse brain atlas data. The levels of APOB and VLDLR are known to inversely correlate (Kobayashi et al 1996). A significant up-regulation was also detected for the apolipoprotein J (ApoJ, also known as clusterin, CLU) in A-T patients' CSF. A secreted isoform of ApoJ acts as a ligand for VLDLR and APOER2 to signal via the reelin pathway (Leeb et al 2014). Additionally, ApoJ is a PN pathology marker and its plasma concentration is associated with brain atrophy (Thambisetty et al 2012). Thus, there is a clear enrichment of ataxia pathogenesis factors, reelin/ApoB signaling and apolipoprotein homeostasis factors among the A-T CSF dysregulations.

Additional unbiased bioinformatics analyses of the CSF data were done with the STRING server looking for enrichment of GO terms such as cellular components, biological processes, molecular functions, KEGG pathways, and protein domains. Among cellular components, enrichments for extracellular region were detected in the down-regulated factors. Further significant enrichment for down-regulations was found for the KEGG pathway "extracellular matrix-receptor interaction", the GO biological processes "biological adhesion" and "extracellular organization", the GO molecular functions "calcium ion binding" and "peptidase activity", and the INTERPRO domain "immunoglobulin subtype" (Figure 3.47, A). In summary, markers for the glutamatergic parallel fiber afferents to PN, which originate in cerebellar GN, appeared to be at least as diminished as PN markers.

Overall, key factors of PN connectivity with their glutamatergic input axons are prominent among the down-regulations. Regarding the analysis of up-regulated factors, novel insights included enrichments for the KEGG pathway “complement and coagulation cascades”; the GO biological processes “complement activation”, “immune effector process”, and “endocytosis”; and the GO cellular component “plasma lipoprotein particles” (Figure 3.47, B). Overall, neuroinflammatory responses are prominent among up-regulations, but the dysregulation of lipoprotein particles and endocytosis pathways may be a direct effect of ApoB/RELN and ATM membrane functions.

The CSF findings identified prominent and consistent changes of reelin/apolipoprotein signaling and possibly endocytosis/adhesion at sites of glutamatergic input to PN, accompanied by neuroinflammation activation. The deficiency of reelin may have specificity for A-T, since increased reelin levels were observed in the CSF of AD, FTD patients, and in the cerebellum of SCA37 patients (Corral-Juan et al 2018, Saez-Valero et al 2003). The molecular dysregulations observed may be part of the irradiation and DNA damage repair pathways but the pathogenesis may also relate to altered glutamatergic excitation of PN dendrites. The endosome-associated fraction of ATM in cerebellar GN (Kuljis et al 1999) was shown to be a crucial facilitator of synaptic excitatory vesicle release, in balance with ATR being responsible for inhibitory neurotransmission (Cheng et al 2018). ATM levels rise in response to blockade of NMDA receptors (Cheng et al 2018), so the influence of reelin on NMDA receptor composition and synaptic plasticity may play a key role in ATM deficiency. Dysfunction of the glutamatergic parallel fiber input is known to result in PN death (Slemmer et al 2005). Conversely, changed abundance of reelin was previously observed in mouse intestines to trigger transcript dysregulation of key factors in lipid metabolism, modulators of lipogenesis and gluconeogenesis, intracellular cholesterol flux gatekeepers, and glutamate receptors subunits (Garcia-Miranda et al 2012).

4.8.2 Validation in *Atm*-/- cerebellar mRNA and tissue homogenates confirms Reelin pathway and ApoB alterations

Although patient data are extremely valuable, these types of samples are not always available. The use of mouse models has sped-up the research in many genetic based diseases and has allowed researchers to find new biomarkers or develop new therapies. Therefore, after analyzing the CSF proteome data from A-T patients and controls, we aimed to reproduce these findings in the *Atm*-/- mouse model and gain deeper insights (Barlow et al 1996). A hallmark of these mice is the high level of oxidative stress by ROS, affecting several tissues including the cerebellum (Barlow et al 1999).

We analyzed transcript levels in ~2-month-old cerebellar tissue for key components of cholesterol-apolipoprotein trafficking, reelin signaling, glutamatergic input to PN, glutamate receptors, calcium homeostasis, oxidative stress, neuroinflammation, and cell adhesion suggested by the A-T patient CSF proteomic profiles (Figure 3.48). Our results showed up-regulation of transcripts implicated in cholesterol transport (Apolipoproteins *Apoe* and *Apoh*) and the cholesterol efflux regulator *Cyp46a1*. Significant mRNA reduction of both reelin receptors, *Vldlr* and *Apoer2*, were detected as a confirmation of the reelin pathway alteration in the patients' CSF (Figure 3.48, A and C). However, the transcript levels of reelin and intracellular transducers were not changed in the 2-month-old cerebellar *Atm-/-* samples. The transcript level of *Sema7a*, a recently described factor implicated in the elimination of weak climbing fibers (Uesaka & Kano 2018, Uesaka et al 2014), was up-regulated while *Vglut2*, a marker for climbing fibers that is affected in the early pathology of SCA1 (Barnes et al 2011), was down-regulated pointing to an early climbing fiber affection in the *Atm-/-* cerebellum (Figure 3.48, D). Consistent with the concept of altered lipid signaling and glutamatergic afferents, the glutamate NMDA receptor (N-methyl-D-aspartate receptor) subunit *Grin2b* transcript showed strong up-regulation. Reelin levels are known to modulate GRIN2B levels in a reverse correlation (Groc et al 2007, Sinagra et al 2005), the elevation of *Grin2b* levels supports the notion of deficient reelin signaling in *Atm-/-* cerebellar samples as early as ~2 months of age. Regarding calcium homeostasis factors, a significant

decrease of the PN marker CALB1 was detected together with a more discrete reduction of *Atp2b2* (plasma membrane calcium ATPase) and *Itpr1* (ER-associated inositol-1,4,5-triphosphate-receptor1) transcripts. The reduction of these calcium homeostasis factors reflects the deficient excitability of PN downstream of reelin and glutamate signals. Interestingly oxidative stress, DDR, neuroinflammation, and adhesion markers analyzed showed no dysregulation (Figure 3.48, B, E, H).

The transcriptional analyses confirmed reelin signaling deficits before altered locomotor behaviour or PN death were detected. These data also point to alterations of the lipid and glutamate pathways with downstream calcium dependent excitability affected before DDR, oxidative stress response, neuroinflammation, and cellular adhesion show significant changes.

To determine if dysregulation of lipid transport and reelin signaling precedes the neurodegeneration in the ~2-month-old *Atm-/-* cerebella, we used quantitative immunoblots. The apolipoproteins ApoB and two isoforms of ApoJ were found up-regulated while the reelin receptor VLDLR showed a decreased to 50% (Figure 3.49, A, C, E, and F). No evidence of cerebellar PN/GN loss was apparent at this stage; neither CALB1 nor NeuN protein levels were dysregulated (Figure 3.49, G and H), and coimmunofluorescence stainings confirmed the absence of neuronal death (Figure 3.50). No changes were detected for ApoE protein levels and only a statistical trend for reelin pointing to down-regulation was identified (Figure 3.49, B and D). Interestingly, an up-regulation of ApoB protein was detected before reelin protein levels changed significantly. These findings correlated with previous literature, which stated that ApoB and VLDLR levels show inverse correlation (Kobayashi et al 1996) and that ATM depletion modulates specific isoforms of ApoJ (Luo et al 2014).

Q-PCR and WB results in *Atm-/-* cerebella from ~2-month-old mice are consistent and support a concept where ApoB and reelin signaling affection constitute a novel, early, and important feature in the pathogenesis of A-T neurodegeneration. Furthermore, our data suggested that the alterations in

signaling and excitability occurred before responses to DNA damage, oxidative stress, neuroinflammation, or cell adhesion deficits become notable. Our protein studies suggested that the ApoB excess and VLDLR decrease may even precede the reelin deficit, and that they certainly precede the cerebellar neuronal death. Deficiency of ApoB is a known cause of cerebellar ataxia and acanthocytosis in autosomal recessive disorders known as hypo- or a-betalipoproteinemia (Hentati et al 2012, Homer et al 2005). In addition, overexpression of ApoB-100 causes severe cerebellar degeneration (Bereczki et al 2008). Moreover, ATM is known to modulate the endocytosis of ApoB-48 influencing the up-take of cholesterol and vitamin E (Averna et al 1993, Homer et al 2005, Wu et al 2005, Wu et al 2014). Deficiency in cholesterol and vitamin E has been implicated in ataxia (Hentati et al 2012). This could explain the significantly reduced levels of vitamin E (alpha-tocopherol) detected in blood plasma of A-T patients (Reichenbach et al 1999).

4.8.3 Conclusions and perspectives

Overall, our findings support a scenario where the deficit of vesicle-associated ATM in cerebellar GN parallel fibers alters the secretion of ApoB, reelin, and glutamate (Figure 3.51). These defects would lead to postsynaptic adaptations in PN and synaptic plasticity via transcriptional changes. While a complete loss of reelin would result in neuron migration and connection problems at embryonal stages, it is possible that milder reelin deficiency permits the prenatal establishment of neural circuits while being insufficient to sustain differentiation and maintenance of synaptic contacts at older ages. This notion is consistent with analogous observations that the total loss-of-function in homozygous mutants in “staggerer” and “pcd” ataxia models have embryonal and postnatal difficulties to establish cerebellar circuitry, while the corresponding heterozygous mutants show adult age-associated neurodegenerative phenotypes (Hadj-Sahraoui et al 2001, Hadj-Sahraoui et al 1997).

To establish new approaches of neuroprotective value, it is interesting to note that the addition of recombinant reelin to hippocampal organotypic slice cultures via conditioned medium rescued the pathology of synaptic vesicles and paired-pulse facilitation in reeler mutant mice (Hellwig et al 2011). In addition,

the expression of reelin and VLDLR can be up-regulated by the administration of the psychotropic drug olanzapine (Fatemi et al 2009). Finally, the supplementation of A-T patients' diet with vitamin E could be beneficial for their cerebellar ataxia.

4.9 Evaluation of the 12-month-old cerebellar transcriptome data set from *Atm*-/- animals reveals alteration of Ataxia-related gene network

Ataxia telangiectasia patients present progressive cerebellar ataxia starting in early childhood. Later on they develop conjunctival telangiectasia, other progressive neurologic degeneration, sinopulmonary infection, and malignancies (Gatti et al 1991). Prognosis for A-T patients has not changed since 1954 and the life expectancy is lower among patients with mutations in ATM causing total loss of function. Cancer and respiratory tract infections are the major risk factor for mortality among patients and treatment of malignancies with radiation can be fatal to AT patients (Micol et al 2011).

Bone marrow transplantation (BMT) with reduced-intensity conditioning regimen has been proposed as a therapy after being proved to restore immune system function and prevent lymphoma in *Atm-/-* mice (Bagley et al 2004). Further studies using this mouse model showed bone marrow-derived cells (BMDCs) migrated to the thymus, spleen, and lung tissues but not to the CNS due to the blood-brain barrier (BBB) (Pietzner et al 2013). The life span of *Atm-/-* animals is between 4 and 6 months due to malignant thymic lymphomas before ataxic and other neurologic symptoms appear (Barlow et al 1996).

Thanks to the BMT, the life expectancy of these animals was extended up to 12 months and ataxic behaviour together with loss of PN in the cerebellum was detected (Pietzner et al 2013). Using cerebellar samples of life-extended *Atm-/-* animals via BMT can help to decipher the pathomechanisms implicated in the ataxia and other neurologic symptoms of A-T patients. Therefore, we generated a novel transcriptomics data set from 12-month-old cerebellar *Atm-/-* samples.

4.9.1 Transcriptomics data set of 12-month-old *Atm-/-* cerebella points to a non-coding RNA pathology and glutamatergic input deficiency

The transcriptomics data was analyzed with the TAC software using standard parameters and self-determined filter criteria. A higher number of down-regulations (58%) were detected compared to up-regulations (42%) regarding all transcripts that passed the filter criteria. Interestingly, 84% of the significant down-regulated transcripts were part of the Non-Coding category (Figure 3.53).

Thanks to improvements in sequencing technologies, an increasing number of non-coding RNA (ncRNA) have been implicated in neuronal development, homeostasis, and neurodegenerative and psychiatric disorders (Salta & De Strooper 2012). Moreover, recent evidence suggests the implication of ncRNA and interference RNA (RNAi) in efficient recognition and repair of DSBs (Burger et al 2019a). This effect could be mediated by c-Abl (Abelson kinase) that can be activated by ionizing radiation (IR) in a DNA-PK- and ATM-dependent manner (Burger et al 2019b). Therefore, the absence of ATM kinase activity might be affecting the response to DNA damage through c-Abl or other factors controlling the expression of key ncRNAs.

Further bioinformatics analyses with the altered transcripts part of the coding and multiplex categories were performed using the online platform STRING. Significant protein-protein interaction enrichment was detected for the significantly up-regulated and down-regulated transcripts analyzed. Among the up-regulations, enrichment for GO molecular functions “ion gated channel activity”, for GO cellular components “somatodendritic compartment” and “neuron projection” were identified. The highest number of up-regulated factors was identified to localize at the dendritic compartment (Figure 3.54), this effect could be as a result of compensatory effect to an impaired input from afferent projections. Among the down-regulations, enrichment for the GO cellular compartment “extracellular space”, for the KEGG pathway “glutamatergic synapse” and “circadian entrainment”, and the Reactome pathway “nuclear receptor transcription pathway” was detected. Overall, the affection of glutamatergic synapses has been consistent through all the data analyzed so far

together with extracellular space factors and secreted factors. The lack of glutamatergic input to the PN could be responsible for the compensatory effect observed for the up-regulation of dendritic compartment transcripts (Hoxha et al 2018).

4.9.2 Validation efforts confirm the down-regulation of several ataxia and neurodegeneration implicated factors

The 12-month-old *Atm-/-* cerebellar transcriptome data set and Q-PCR validation efforts revealed the down-regulation to ~80% of six factors that have been previously implicated in the pathogenesis of ataxias: *Cadps2*, *Car8*, *Fgf14*, *Stxbp5l*, *Syne1*, and *Mtcl1*.

The calcium-dependent activator protein for secretion 2, *Cadps2*, was one of them and it is known to show the highest expression in the cerebellum (Nagase et al 2000). *Cadps2*-KO mice show autistic-like behaviour and BDNF (brain-derived neurotrophic factor) secretion impairment from neocortical and cerebellar neurons, leading to defects in the neocortical and hippocampal neurons differentiation and survival of cerebellar PN (Sadakata et al 2007).

Car8 (Carbonic anhydrase 8) transcript levels were also down-regulated in the microarray data, and CAR8 has been previously implicated in SCA14 (Shimobayashi & Kapfhammer 2018) and SCA29 (Ando et al 2018). “Waddles” mice show an ataxic phenotype due to homozygous mutation in *Car8* causing non-functional CAR8 protein (Lamont & Weber 2015). Moreover, abnormal extension of climbing fibers to distal PN dendrites in combination with abnormalities of parallel fibers and dendritic spines were detected in this mouse mutant, suggesting a role of CAR8 in maintenance of proper synaptic morphology and function in the cerebellum (Hirasawa et al 2007).

Stxbp5l, also known as Tomosyn-2, implicated in neurotransmitter release inhibition was also down-regulated in the transcriptome data set and validated via Q-PCR. Homozygous variants in *STXBP5L* have been identified in two patients with recessive neurodegeneration (Kumar et al 2015) and *Stxbp5l*-KO mice

showed impaired motor performance accompanied by synaptic changes at the neuromuscular junction (Geerts et al 2015).

Syne1 (Spectrin repeat-containing nuclear envelope protein 1) and *Fgf14* (Fibroblast growth factor 14) have already been implicated in SCAR8 (spinocerebellar ataxia recessive 8) and SCA27 (spinocerebellar ataxia type 27) previously (Synofzik et al 2016, van Swieten et al 2003). *Syne1* has been implicated in linking the nuclear plasma membrane to the actin cytoskeleton. The mouse model with C-terminal deletion of SYNE1 showed hindlimb weakness and abnormal gait (Puckelwartz et al 2009). On the contrary, *Fgf14* is important for neuron excitability and it has been shown to regulate the intrinsic excitability of cerebellar PN (Shakkottai et al 2009).

Therefore, these data points to alterations in maintenance of cerebellar morphology, survival of PN, and neuronal excitability. This could eventually help define the events taking place during the cerebellar degeneration in A-T patients and explain the stronger affection of the Purkinje neurons.

4.9.3 Three novel factors appear dysregulated in ~2-month-old *Atm-/-* cerebella as early events in the degeneration of the cerebellum

Further efforts were made to identify novel early events that could help understand the cerebellar degeneration in A-T. Therefore, samples from ~2-month-old *Atm-/-* cerebella were used to quantify the transcript levels of 11 factors dysregulated in the transcriptome data set (Table 3.13). Only three transcripts were found to be dysregulated in both ~2 months and 12 months *Atm-/-* cerebellar samples sets: *Mtcl1*, *Slc17a7*, and *Slc1a6*.

The microtubule crosslinking factor 1, *Mtcl1*, showed a constant down-regulation to ~80% of its transcripts levels in *Atm-/-* cerebella compared to WT. *Mtcl1* is a microtubule-associated factor necessary to maintain axonal polarity highly expressed in PN. *Mtcl* gene disruption in mice has been shown to cause abnormal coordination and PN degeneration (Satake et al 2017). In addition, *MTCL1* homozygous loss-of-function variants have been implicated in recessive

cerebellar ataxia (Krygier et al 2019). Therefore, its constant down-regulation at transcript level could result in a lower protein level that over time could impair the maintenance of microtubule bundles at the proximal axon of PN leading to impaired output from the cerebellum.

The two other commonly down-regulated factors, *Slc1a6* and *Slc17a7*, are glutamate transporters. *Slc1a6* encodes the ion-gradient-dependent glutamate transporter EAAT4 expressed in neurons. The loss of EAAT4 affects the spontaneous firing pattern and survival of PN (Perkins et al 2018). *Slc17a7* encodes the vesicular glutamate transporter 1, VGLUT1, which is expressed by parallel fibers in the cerebellum. This glutamate transporter caught our attention since ATM has been recently associated to excitatory neuronal vesicles, VGLUT1 positive vesicles (Cheng et al 2018). Therefore, the absence of ATM could affect the excitatory/inhibitory balance and could lead to neural network dysfunction (Bateup et al 2013). Additionally, A-T patients can also show degeneration in other brain regions in addition to suffering from cerebellar and non-cerebellar cognitive deficits (Hoche et al 2014, Hoche et al 2012, Sahama et al 2015).

4.9.4 Evaluation of VLGUT1 at protein level in ~2-month-old and ~4-month-old *Atm-/-* cerebellar samples does not show significant dysregulation and no altered localization upon immunohistochemistry

Despite our efforts to detect changes at the protein level of VLGUT1 at ~2 and ~4 months of age in the *Atm-/-* mouse model cerebella, none were detected via quantitative immunoblots (Figure 3.56). This method is less sensitive than transcript analysis via Q-PCR, therefore it could be possible that small changes are not being quantified and older tissue is necessary to confirm VGLUT1 levels alterations.

It can also be argued that before the protein level of VGLUT1 changes, its localization might be altered due to the absence of ATM (Cheng et al 2018, Li et al 2009). Thus, we decided to characterize the VGLUT1 location via immunohistochemistry experiments using slices from ~6-month-old *Atm-/-* cerebellum compared to age- and sex-matched WT (**Figure 3.57**). Although the

staining was not repeated in a higher number of animals and no quantification was possible, no obvious alteration in the VGLUT1 signal was identified comparing the two genotypes.

4.9.5 Conclusions and perspectives

Overall, our data consistently shows alteration of the glutamatergic signal and the implication of ataxia/neurodegeneration factors that can explain the preferential affection in the cerebellum. The strong up-regulation of the adhesion factors *Cbln2* and *Cbln4* could be a consequence of compensatory efforts from the system due to the important number of down-regulations involved in neuron excitability and glutamate receptors (Rong et al 2018). The consistent down-regulation of *Slc17a7* in the different aged cerebellar samples tested from the *Atm-/-* mouse model confirms the previous observations implicating ATM in excitatory (VGLUT1+) vesicle–associated functions (Cheng et al 2018) and could explain NMDA receptor alterations observed. Despite not being able to detect changes at protein level via WB or affected VGLUT1 localization via immunohistochemistry, further efforts to quantify VGLUT1/*Slca17a7* in blood of the *Atm-/-* mouse model and A-T patients should be pursued since public RNAseq data shows expression (gtexportal.org). If VGLUT1/*Slc17a7* dysregulated levels can be detected in patients' blood, it could become an important biomarker for the degeneration of the cerebellum and complement the information obtained from alpha-fetoprotein levels coming from the liver (Ishiguro et al 1986, Rothblum-Oviatt et al 2016).

4.10 Cerebellar organotypic cultures as a tool to speed up A-T research

The limited life expectancy of the *Atm-/-* mouse model due to lymphomas (Barlow et al 1996) has been overcome thanks to BMT (Bagley et al 2004, Pietzner et al 2013), opening new possibilities to study the cerebellar degeneration in this A-T mouse model. Unfortunately, BMT is an expensive intervention and, together with ageing the animals, time consuming. Therefore, we successfully established organotypic cell cultures (OTC) (Figure 3.58) as a

complementary method that will allow the identification of potential candidates and test drugs in a conserved neuronal network (Hellwig et al 2011).

5 SUMMARY

Cerebellar ataxias are a group of neurodegenerative disorders primarily affecting the cerebellum. Imbalance and coordination problems are broader symptoms exhibited by patients (Akbar & Ashizawa 2015). There is currently no cure for ataxias and although mutations in several genes have been identified as causative, there is a lack of understanding of why some neurons are more sensitive than others.

Cerebellar ataxias can be acquired, inherited or sporadic (without defined genetic cause or acquired etiology). Inherited ataxias, those with a defined genetic cause, can be classified in four different categories: dominant ataxias, recessive ataxias, mitochondrial ataxias, and X-linked ataxias.

Spinocerebellar ataxia type 2 (SCA2) is a dominant ataxia caused by repeat expansion mutations in the *ATXN2* gene, which encodes the protein Ataxin2 (ATXN2). A polyglutamine (polyQ) tract consisting of CAG repeats interrupted by CAA was identified at exon 1 of *ATXN2* (Imbert et al 1996, Pulst et al 1996, Sanpei et al 1996). Healthy individuals have between 22 and 23 glutamines (Qs), with a sequence of $(CAG)_8CAA(CAG)_4CAA(CAG)_8$, while expansions longer than 33 CAG repeats cause SCA2 (Fernandez et al 2000). The most noticeable symptom that SCA2 patients show is ataxic gait; however they also show cerebellar dysarthria, dysdiadochokinesia, and ocular dysmetria caused by the progressive cerebellar degeneration. Slow or absent saccade velocity is one predominant ocular symptom from SCA2 patients due to degeneration of the oculomotor brainstem(Auburger 2012, Lastres-Becker et al 2008b, Velazquez-Perez et al 2011). Histological analysis of *post-mortem* samples from SCA2 patients showed a general reduction of the brain size with significant atrophy of the cerebellum, brainstem, and frontal lobe. A reduction of the cerebral and cerebellar white matter was also detected (Estrada et al 1999). Further studies

of spinal cord samples showed severe and widespread neurodegeneration of the central somatosensory system (Rub et al 2007).

Ataxin 2 (ATXN2) is an evolutionary conserved RNA binding protein (RBP) (Jiménez-López & Guzmán 2014) that has been linked to several RNA processing roles. ATXN2 interacts with PABP1 through its PAM2 domain. PABP1 is an RBP important for poly-A tailing, translation, and mRNA decay (Xie et al 2014). Moreover, ATXN2 can bind to uridine-rich elements (AU-rich element, ARE) at the 3'UTRs of its mRNA targets through the LSm domain, thereby stabilizing the mRNA targets (Yokoshi et al 2014). ATXN2 also has a proline-rich domain towards the C-terminal that has been described to mediate the association of ATXN2 with the receptor endocytosis apparatus and influence the trophic state of the cells (Drost et al 2013, Nonis et al 2008).

To model the SCA2 disease, we generated a new mouse model where 100 CAG repeats were introduced in the mouse *Atxn2* gene via homologous recombination. The characterization of this mouse model, *Atxn2*-CAG100-KIN, demonstrated that it reproduces the symptomatology observed in SCA2 patients. These animals showed significant loss of weight over time, brain atrophy, and motor deficits (Sen et al 2019). Moreover, this model allowed us to study the effect of the ATXN2 poly(Q) expansions outside of the cerebellum since the expansion was inserted in the *Atxn2* mouse locus.

In addition, ATXN2 intermediate expansions have been linked to the pathology of Amyotrophic lateral sclerosis (ALS) as a risk factor (Elden et al 2010). ALS is a fatal neurodegenerative disease where the motor neurons in the brain and spinal cord degenerate. A hallmark of ALS is the presence of TDP43-positive inclusions in neurons and glia (Neumann et al 2006). Few publications focusing on SCA2 patient pathology in the spinal cord are available (Estrada et al 1999, Rub et al 2007, Velazquez-Perez et al 2018, Velazquez-Perez et al 2017). Therefore, it was of interest to further investigate the pathology affection this tissue in the *Atxn2*-CAG100-KIN line and the relationship between ATXN2 and TDP43 (Becker et al 2017).

The characterization of the spinal cord pathology via protein quantification, transcript quantification, and immunohistochemistry showed a preferential affection of RNA binding proteins (RBP) in the spinal cord rather than the cerebellum. The ALS-linked factors TDP43 and TIA1 showed time-dependent co-aggregation with ATXN2 in spinal cord sections together with an increase of CASP3 levels. Reports implicating ATXN2 intermediate expansions in ALS, influencing TDP43 aggregation via enhanced CASP3 activation and production of pathological C-terminal fragments from TDP43, have been published (Elden et al 2010, Hart & Gitler 2012). Therefore, this mouse model can help develop new therapies and evaluate their effect in differently affected areas.

The generation of a transcriptome data set from *Atxn2*-CAG100-KIN spinal cord samples at the final disease stage of this mouse model showed a strong up-regulation of RNA toxicity-, immune- and lysosome-implicated factors. These data pointed to a pathological reactivation of the synaptic pruning and phagocytosis in microglia. Moreover, two inflammation factors implicated in ALS that are highly expressed by microglia were also found up-regulated: *Ripk1* and Grn. Therefore, microglia seems to be implicated in the spinal cord pathology observed in the *Atxn2*-CAG100-KIN mouse model.

TDP43 levels have been shown to modulate microglia phagocytic activity (Paolicelli et al 2017). Thus, we aimed to determine the expression of ATXN2 in this cell type and further investigate their affection. Through immunocytochemistry we demonstrated the presence of ATXN2 in the murine microglia cell line BV2 and in microglia primary cell cultures derived from *Atxn2*-CAG100-KIN and WT animals. Based on immunohistochemical analysis we also demonstrated an increase of ATXN2 expression in microglia from *Atxn2*-CAG100-KIN spinal cord sections at the age of 6 months compared to sex- and age-matched WT. Moreover, a time-dependent ATXN2 aggregation was observed in 14-month-old spinal cord microglia from *Atxn2*-CAG100-KIN animals. This could be caused by an increase debris phagocytosis by microglia, an accumulation of endogenous ATXN2 protein, or both leading to an altered function of this cell type.

The characterization of microglial response and the potentially deleterious effects of the expanded ATXN2 in this cell type could lead to therapies to improve patients' living standards or delay the symptoms' onset. For instance, peripheral administration of a detoxified TLR4 ligand was shown to stimulate microglia phagocytosis without excessive inflammatory response, improving cognitive deficits in a mouse model of Alzheimer's disease (Michaud et al 2013).

The second part of this thesis was focused on an autosomal recessive form of cerebellar ataxia, Ataxia Telangiectasia (A-T), with childhood onset. A-T patients show severe cerebellar atrophy manifesting as ataxia when the child starts to walk (Chun & Gatti 2004). Other movement symptoms are hypotonia, dystonia, tremor, and Parkinsonism (Nissenkorn & Ben-Zeev 2015). Moreover, A-T patients show predisposition to malignancies, immune defects, hypersensitivity to radiotherapy, and endocrine abnormalities (Nissenkorn et al 2016). Alpha-fetoprotein (AFP) blood level is used to follow the progression of the disease (Rothblum-Oviatt et al 2016).

The genetic cause of A-T is loss-of-function-mutations in the Ataxia Telangiectasia Mutated gene (*ATM*). ATM is a Serine/Threonine kinase involved in DNA damage response (DDR) and oxidative stress. Moreover, ATM has been implicated in insulin resistance and autophagy through the mTOR (mammalian target of rapamycin) pathway (Alexander et al 2010, Zhang et al 2015). More recently, ATM has been implicated in synaptic function specifically associated with excitatory vesicles (Cheng et al 2018).

Working with proteome data from cerebrospinal fluid of 12 A-T patients and 12 healthy controls, we aimed to define novel biomarkers that would allow following the neurodegeneration in extracellular fluid. Among the dysregulated factors detected in the A-T patient's CSF, ten factors have been previously implicated in the pathogenesis of ataxia. Searching for novel potential biomarkers we identified Reelin (RELN), a secreted extracellular glycoprotein that activates the apolipoprotein receptors APOER2 and VLDLR. The down-regulation of RELN protein levels showed a strong correlation with ataxia scores.

Moreover, the apolipoprotein B and J were found up-regulated further supporting the implication of RELN signaling in this proteome profile.

Validation efforts using ~2-month-old *Atm*-knock-down (*Atm*-/-) mouse cerebellar samples confirmed Reelin pathway and ApoB alterations before loss of Purkinje neurons (PN) or behaviour alteration can be detected in this mouse model (Barlow et al 1999, Barlow et al 2000, Chiesa et al 2000). No changes at the transcript level were detected for DNA damage response, oxidative stress, neuroinflammation, or cell adhesion suggesting that alterations in signaling and excitability are early events in the pathology. Overall, our findings support a scenario where the deficit of vesicle-associated ATM alters the secretion of ApoC, reelin, and glutamate. As extracellular factors, apolipoproteins and their cargo such as vitamin E may be useful for neuroprotective interventions (Canet-Pons et al 2018).

The life span of *Atm*-/- animals is between 4 and 6 months due to malignant thymic lymphomas before ataxic and other neurologic symptoms appear (Barlow et al 1996). Thanks to bone marrow transplantation (BMT), the life expectancy of these animals was extended up to 12 months when ataxic behaviour and PN loss can be detected (Pietzner et al 2013). To gain deeper insight into pathomechanisms implicated in ataxia and other neurologic symptoms of A-T patients, we generated a novel transcriptomics data set from 12-month-old cerebellar *Atm*-/- samples.

The data obtained from the transcriptome and further validation experiments via quantitative PCR (Q-PCR) showed the down-regulation of six factors that have been previously implicated in the pathogenesis of ataxias: *Cadps2*, *Car8*, *Fgf14*, *Stxbp5l*, *Syne1*, and *Mtcl1*. Among them, only *Mtcl1* (Microtubule crosslinking factor 1) was found to be an early event being down-regulated in both ~2-month-old and 12-month-old cerebellar samples. *Mtcl* gene disruption in mice has been shown to cause abnormal coordination and PN degeneration (Satake et al 2017). Moreover, *Slc1a6* and *Slc17a7* were commonly down-regulated in both age sample sets pointing to glutamate deficits. *Slc17a7* encodes the vesicular glutamate transporter 1, VGLUT1, which is expressed by parallel

fibers in the cerebellum. ATM has been associated to excitatory neuronal vesicles, VGLUT1 positive vesicles (Cheng et al 2018). The absence of ATM could affect the excitatory/inhibitory balance and could lead to neural network dysfunction (Bateup et al 2013). If VGLUT1/*Slc17a7* dysregulated levels can be detected in patient's blood, it could become an important biomarker for the degeneration of the cerebellum and complement the information obtained from alpha-fetoprotein levels (Rothblum-Oviatt et al 2016).

6 ZUSAMMENFASSUNG

Kleinhirnataxien sind eine Gruppe von neurodegenerativen Erkrankungen, die hauptsächlich das Kleinhirn betreffen. Ungleichgewichts- und Koordinationsprobleme sind umfassendere Symptome, die Patienten aufweisen (Akbar & Ashizawa 2015). Es gibt derzeit keine Heilung für Ataxien, und obwohl Mutationen in mehreren Genen als ursächlich identifiziert wurden, fehlt das Verständnis, warum einige Neuronen empfindlicher sind als andere.

Kleinhirnataxien können erworben, vererbt oder sporadisch (ohne definierte genetische Ursache oder erworbene Ätiologie) sein. Vererbte Ataxien, die eine definierte genetische Ursache haben, können in vier verschiedene Kategorien eingeteilt werden: dominante Ataxien, rezessive Ataxien, mitochondriale Ataxien und X-chromosomale Ataxien.

Spinocerebellare Ataxie Typ 2 (SCA2) ist eine dominante Ataxie, die durch wiederholte Expansionsmutationen im ATXN2-Gen verursacht wird, welches Protein Ataxin2 (ATXN2) kodiert. Ein Polyglutamin (polyQ) -Trakt, der aus durch CAA unterbrochenen CAG-Wiederholungen bestand, wurde im Exon 1 von ATXN2 identifiziert (Imbert et al 1996, Pulst et al 1996, Sanpei et al 1996). Gesunde Personen haben zwischen 22 und 23 Glutamine (Qs) mit einer Sequenz von $(CAG)_8CAA(CAG)_4CAA(CAG)_8$, während Expansionen, die länger als 33 CAG-Wiederholungen sind, SCA2 verursachen (Fernandez et al 2000). Das auffälligste Symptom bei SCA2-Patienten ist der ataxische Gang. Sie zeigen jedoch auch Kleinhirn-Dysarthrie, Dysdiadochokinese und Augendysmetrie, die durch die fortschreitende Kleinhirn-Degeneration verursacht werden. Langsame oder fehlende Sakkadengeschwindigkeit ist ein vorherrschendes Augensymptom bei SCA2-Patienten aufgrund einer Degeneration des okulomotorischen Hirnstamms (Auburger 2012, Lastres-Becker et al 2008b, Velazquez-Perez et al 2011). Die histologische Analyse von Obduktionsproben von SCA2-Patienten zeigte eine allgemeine Verringerung der Gehirngröße mit einer signifikanten Atrophie des

Kleinhirns, des Hirnstamms und des Frontallappens. Eine Reduktion der zerebralen und zerebellären weißen Substanz wurde ebenfalls festgestellt (Estrada et al 1999). Weitere Untersuchungen an Rückenmarksproben ergaben eine schwere und weit verbreitete Neurodegeneration des zentralen somatosensorischen Systems (Rub et al 2007).

Ataxin 2 (ATXN2) ist ein evolutionär konserviertes RNA-Bindungsprotein (RBP) (Jiménez-López & Guzmán 2014), das mit mehreren RNA-Verarbeitungsrollen verknüpft ist. ATXN2 interagiert mit PABP1 über seine PAM2-Domäne. PABP1 ist ein RBP, das für das Poly-A-Tailing, die Translation und den mRNA-Zerfall wichtig ist (Xie et al 2014). Darüber hinaus kann ATXN2 an den 3'UTRs seiner mRNA-Ziele über die LSm-Domäne an uridinreiche Elemente (AU-rich element, ARE) binden, wodurch die mRNA-Ziele stabilisiert werden(Yokoshi et al 2014). ATXN2 hat auch eine prolinreiche Domäne gegenüber dem C-Terminus, von der beschrieben wurde, dass sie die Assoziation von ATXN2 mit dem Rezeptorendozytoseapparat vermittelt und den trophischen Zustand der Zellen beeinflusst (Drost et al 2013, Nonis et al 2008).

Um die SCA2-Krankheit zu modellieren, haben wir ein neues Mausmodell erstellt, bei dem 100 CAG-Wiederholungen über homologe Rekombination in das Maus-Atxn2-Gen eingeführt wurden. Die Charakterisierung dieses Mausmodells, Atxn2-CAG100-KIN, zeigte, dass es die bei SCA2-Patienten beobachtete Symptomatik reproduziert. Diese Tiere zeigten im Laufe der Zeit einen signifikanten Gewichtsverlust, eine Hirnatrophie und motorische Defizite (Sen et al 2019). Darüber hinaus konnten wir mit diesem Modell den Effekt der ATXN2-Poly (Q) -Expansionen außerhalb des Kleinhirns untersuchen, da die Expansion in den *Atxn2*-Mauslocus eingefügt wurde.

Darüber hinaus wurden ATXN2-Zwischenexpansionen mit der Pathologie der Amyotrophen Lateralsklerose (ALS) als Risikofaktor in Verbindung gebracht (Elden et al 2010). ALS ist eine tödliche neurodegenerative Erkrankung, bei der die Motoneuronen im Gehirn und Rückenmark entartet sind. Ein Kennzeichen von ALS ist das Vorhandensein von TDP43-positiven Einschlüssen in Neuronen

und Glia (Neumann et al 2006). Es sind nur wenige Veröffentlichungen verfügbar, die sich mit der Pathologie von SCA2-Patienten im Rückenmark befassen (Estrada et al 1999, Rub et al 2007, Velazquez-Perez et al 2018, Velazquez-Perez et al 2017). Daher ist es von Interesse, die Pathologie dieses Gewebes in der Atxn2-CAG100-KIN-Linie und die Beziehung zwischen ATXN2 und TDP43 weiter zu untersuchen (Becker et al 2017).

Die Charakterisierung der Pathologie des Rückenmarks mittels Proteinquantifizierung, Transkriptquantifizierung und Immunhistochemie zeigte eine bevorzugte Beeinflussung von RNA-bindenden Proteinen (RBP) im Rückenmark anstelle nicht aber im Kleinhirn. Die ALS-verknüpften Faktoren TDP43 und TIA1 zeigten eine zeitabhängige Co-Aggregation mit ATXN2 in Rückenmarksschnitten zusammen mit einem Anstieg der CASP3-Spiegel. Es wurden Berichte veröffentlicht, die ATXN2-Zwischenexpansionen bei ALS implizieren und die Aggregation von TDP43 über eine verstärkte CASP3-Aktivierung und die Produktion pathologischer C-terminaler Fragmente aus TDP43 beeinflussen (Elden et al 2010, Hart & Gitler 2012). Daher kann dieses Mausmodell dazu beitragen, neue Therapien zu entwickeln und deren Wirkung in unterschiedlich betroffenen Bereichen zu bewerten.

Die Erzeugung eines Transkriptomdatensatzes aus Atxn2-CAG100-KIN-Rückenmarksproben im Endstadium der Erkrankung dieses Mausmodells zeigte eine starke Hochregulation der RNA-Toxizitäts-, Immun- und Lysosomen-implizierten Faktoren. Diese Daten wiesen auf eine pathologische Reaktivierung des synaptischen Schnitts und der Phagozytose in Mikroglia hin. Darüber hinaus wurden zwei Entzündungsfaktoren, die an ALS beteiligt sind und in hohem Maße durch Mikroglia exprimiert werden, als hochreguliert befunden: Ripk1 und Grn. Daher scheint Mikroglia mit der im Atxn2-CAG100-KIN-Mausmodell beobachteten Pathologie des Rückenmarks in Zusammenhang zu stehen.

Es wurde gezeigt, dass TDP43-Spiegel die phagozytische Aktivität von Mikroglia modulieren (Paolicelli et al 2017). Daher wollten wir die Expression von ATXN2 in diesem Zelltyp bestimmen und deren Affektion weiter untersuchen. Nach

Immunzytochemie zeigen wir das Vorhandensein von ATXN2 in der Maus-Mikroglia-Zelllinie BV2 und in Mikroglia-Primärzellkulturen, die von Atxn2-CAG100-KIN- und WT-Tieren stammen. Basierend auf einer immunhistochemischen Analyse zeigen wir auch einen Anstieg der ATXN2-Expression in Mikroglia aus Atxn2-CAG100-KIN-Rückenmarksschnitten im Alter von 6 Monaten im Vergleich zu geschlechts- und altersangepassten WT. Darüber hinaus wurde eine zeitabhängige ATXN2-Aggregation in 14 Monate alten Rückenmarksmikroglia von Atxn2-CAG100-KIN-Tieren beobachtet. Dies könnte durch eine erhöhte Trümmerphagozytose durch Mikroglia, eine Akkumulation von endogenem ATXN2-Protein oder beides verursacht werden, was zu einer veränderten Funktion dieses Zelltyps führt.

Die Charakterisierung der Mikroglia-Reaktion und die potenziell schädlichen Wirkungen des expandierten ATXN2 in diesem Zelltyp könnten zu Therapien führen, mit denen der Lebensstandard der Patienten verbessert oder der Beginn der Symptome verzögert werden kann. Beispielsweise wurde gezeigt, dass die periphere Verabreichung eines entgifteten TLR4-Liganden die Mikroglia-Phagozytose ohne übermäßige Entzündungsreaktion stimuliert und kognitive Defizite in einem Mausmodell der Alzheimer-Krankheit verbessert (Michaud et al 2013).

Der zweite Teil dieser Arbeit befasste sich mit einer autosomal rezessiven Form der Kleinhirnataxie, Ataxia Telangiectasia (A-T), mit Beginn während der Kindheit. A-T-Patienten zeigen eine schwere Atrophie des Kleinhirns, die sich als Ataxie manifestiert, wenn das Kind zu laufen beginnt (Chun & Gatti 2004). Andere Bewegungssymptome sind Hypotonie, Dystonie, Zittern und Parkinson (Nissenkorn & Ben-Zeev 2015). Darüber hinaus sind A-T-Patienten anfällig für Malignome, Immundefekte, Überempfindlichkeit gegen Strahlentherapie und endokrine Anomalien (Nissenkorn et al 2016). Der Blutspiegel von Alpha-Fetoprotein (AFP) wird verwendet, um das Fortschreiten der Krankheit zu verfolgen (Rothblum-Oviatt et al 2016).

Die genetische Ursache von A-T sind Funktionsverlustmutationen im Ataxia Telangiectasia Mutated Gen (ATM). ATM ist eine Serin / Threonin-Kinase, die an der DNA-Schadensantwort und dem oxidativen Stress beteiligt ist. Darüber hinaus wurde ATM über den mTOR-Signalweg (mammalian target of rapamycin) in die Insulinresistenz und Autophagie einbezogen (Alexander et al 2010, Zhang et al 2015). In jüngerer Zeit wurde ATM in die synaptische Funktion einbezogen, die spezifisch mit erregenden Vesikeln assoziiert ist (Cheng et al 2018).

In Zusammenarbeit mit Proteomdaten aus der Liquor cerebrospinalis von 12 A-T-Patienten und 12 gesunden Kontrollpersonen sollten neue Biomarker definiert werden, mit denen die Neurodegeneration in der extrazellulären Flüssigkeit verfolgt werden kann. Unter den dysregulierten Faktoren, die im Liquor des A-T-Patienten nachgewiesen wurden, waren zuvor zehn Faktoren an der Pathogenese der Ataxie beteiligt. Auf der Suche nach neuen potenziellen Biomarkern haben wir Reelin (RELN) identifiziert, ein sekretiertes extrazelluläres Glykoprotein, das die Apolipoproteinrezeptoren APOER2 und VLDLR aktiviert. Die Herunterregulierung der RELN-Proteinspiegel zeigte eine starke Korrelation mit den Ataxie-Scores. Darüber hinaus wurde festgestellt, dass das Apolipoprotein B und J hochreguliert sind, was die Implikation der RELN-Signalübertragung in diesem Proteomprofil unterstützt.

Validierungsversuche unter Verwendung von *Atm*-Knock-down (*Atm*-/-) -Maus-Kleinhirnproben bestätigten Reelin-Signalweg- und ApoB-Veränderungen, bevor in diesem Mausmodell ein Verlust von Purkinje-Neuronen (PN) oder eine Verhaltensänderung festgestellt werden kann (Barlow et al 1999, Barlow et al 2000, Chiesa et al 2000). Es wurden keine Veränderungen auf der Transkriptebene für die DNA-Schadensantwort, den oxidativen Stress, die Neuroinflammation oder die Zelladhäsion festgestellt, was darauf hindeutet, dass Veränderungen in der Signalgebung und der Erregbarkeit frühe Ereignisse in der Pathologie sind. Insgesamt stützen unsere Ergebnisse ein Szenario, in dem das Defizit an vesikelassoziiertem ATM die Sekretion von ApoC, Reelin und Glutamat verändert. Als extrazelluläre Faktoren können Apolipoproteine und ihre Ladung

wie Vitamin E für neuroprotektive Interventionen nützlich sein (Canet-Pons et al 2018).

Die Lebensdauer von *Atm*-/- Tieren beträgt aufgrund von malignen Thymuslymphomen zwischen 4 und 6 Monaten, bevor ataxische und andere neurologische Symptome auftreten (Barlow et al 1996). Dank einer Knochenmarktransplantation (BMT) konnte die Lebenserwartung dieser Tiere auf bis zu 12 Monate verlängert werden, wenn ataktisches Verhalten und PN-Verlust festgestellt werden konnten (Pietzner et al 2013). Um einen tieferen Einblick in Pathomechanismen zu erhalten, die mit Ataxie und anderen neurologischen Symptomen von A-T-Patienten zusammenhängen, haben wir einen neuen Transkriptomik-Datensatz aus 12 Monate alten *Atm*-/- Proben des Kleinhirns erstellt.

Die aus dem Transkriptom und weiteren Validierungsexperimenten mittels quantitativer PCR (Q-PCR) erhaltenen Daten zeigten die Herunterregulierung von sechs Faktoren, die zuvor an der Pathogenese von Ataxien beteiligt waren: *Cadps2*, *Car8*, *Fgf14*, *Stxbp5l*, *Syne1* und *Mtcl1*. Unter diesen wurde festgestellt, dass nur *Mtcl1* (Microtubule Crosslinking Factor 1) ein frühes Ereignis ist, das sowohl in ~2 Monate alten als auch in 12 Monate alten Kleinhirnproben herunterreguliert wird. Es wurde gezeigt, dass eine Unterbrechung des *Mtcl*-Gens bei Mäusen eine abnormale Koordination und PN-Degeneration verursacht (Satake et al 2017). Darüber hinaus wurden *Slc1a6* und *Slc17a7* in beiden Altersgruppen häufig herunterreguliert, was auf Glutamatdefizite hindeutet. *Slc17a7* codiert den vesikulären Glutamattransporter 1, VGLUT1, der durch parallele Fasern im Kleinhirn exprimiert wird. ATM wurde mit exzitatorischen neuronalen Vesikeln, VGLUT1-positiven Vesikeln, in Verbindung gebracht (Cheng et al 2018). Das Fehlen von ATM kann das Gleichgewicht zwischen Erregung und Hemmung beeinträchtigen und zu einer Funktionsstörung des neuronalen Netzes führen (Bateup et al 2013). Wenn dysregulierte VGLUT1/*Slc17a7*-Spiegel im Blut des Patienten nachgewiesen werden können, könnte dies zu einem wichtigen Biomarker für die Degeneration des Kleinhirns

werden und die Informationen aus den Alpha-Fetoprotein-Spiegeln ergänzen (Rothblum-Oviatt et al 2016).

7 REFERENCES

Abdel-Aleem A, Zaki MS. 2008. Spinocerebellar ataxia type 2 (SCA2) in an Egyptian family presenting with polyphagia and marked CAG expansion in infancy. *Journal of neurology* 255: 413-9

Abraham KJ, Chan JN, Salvi JS, Ho B, Hall A, et al. 2016. Intersection of calorie restriction and magnesium in the suppression of genome-destabilizing RNA-DNA hybrids. *Nucleic acids research* 44: 8870-84

Abraham RT. 2004. PI 3-kinase related kinases: 'big' players in stress-induced signaling pathways. *DNA repair* 3: 883-7

Adamowicz M, Vermezovic J, d'Adda di Fagagna F. 2016. NOTCH1 Inhibits Activation of ATM by Impairing the Formation of an ATM-FOXO3a-KAT5/Tip60 Complex. *Cell reports* 16: 2068-76

Aguiar J, Fernandez J, Aguilar A, Mendoza Y, Vazquez M, et al. 2006. Ubiquitous expression of human SCA2 gene under the regulation of the SCA2 self promoter cause specific Purkinje cell degeneration in transgenic mice. *Neuroscience letters* 392: 202-6

Airaksinen MS, Eilers J, Garaschuk O, Thoenen H, Konnerth A, Meyer M. 1997. Ataxia and altered dendritic calcium signaling in mice carrying a targeted null mutation of the calbindin D28k gene. *Proceedings of the National Academy of Sciences of the United States of America* 94: 1488-93

Aizer A, Kalo A, Kafri P, Shraga A, Ben-Yishay R, et al. 2014. Quantifying mRNA targeting to P-bodies in living human cells reveals their dual role in mRNA decay and storage. *Journal of cell science* 127: 4443-56

Akbar U, Ashizawa T. 2015. Ataxia. *Neurologic clinics* 33: 225-48

Akizuki S, Ishigaki K, Kochi Y, Law SM, Matsuo K, et al. 2019. PLD4 is a genetic determinant to systemic lupus erythematosus and involved in murine autoimmune phenotypes. *Annals of the rheumatic diseases* 78: 509-18

Al-Ramahi I, Perez AM, Lim J, Zhang M, Sorensen R, et al. 2007. dAtaxin-2 mediates expanded Ataxin-1-induced neurodegeneration in a Drosophila model of SCA1. *PLoS genetics* 3: e234

Alexander A, Cai SL, Kim J, Nanez A, Sahin M, et al. 2010. ATM signals to TSC2 in the cytoplasm to regulate mTORC1 in response to ROS. *Proceedings of the National Academy of Sciences of the United States of America* 107: 4153-8

Almaguer-Mederos LE, Aguilera Rodriguez R, Gonzalez Zaldivar Y, Almaguer Gotay D, Cuello Almarales D, et al. 2013. Estimation of survival in spinocerebellar ataxia type 2 Cuban patients. *Clinical genetics* 83: 293-4

Almeida MR, Macario MC, Ramos L, Baldeiras I, Ribeiro MH, Santana I. 2016. Portuguese family with the co-occurrence of frontotemporal lobar degeneration and neuronal ceroid lipofuscinosis phenotypes due to progranulin gene mutation. *Neurobiology of aging* 41: 200 e1-00 e5

Alves-Cruzeiro JM, Mendonca L, Pereira de Almeida L, Nobrega C. 2016. Motor Dysfunctions and Neuropathology in Mouse Models of Spinocerebellar Ataxia Type 2: A Comprehensive Review. *Frontiers in neuroscience* 10: 572

Ambrose M, Goldstine JV, Gatti RA. 2007. Intrinsic mitochondrial dysfunction in ATM-deficient lymphoblastoid cells. *Human molecular genetics* 16: 2154-64

Anderson P, Kedersha N. 2009. RNA granules: post-transcriptional and epigenetic modulators of gene expression. *Nature reviews. Molecular cell biology* 10: 430-6

Anding AL, Baehrecke EH. 2017. Cleaning House: Selective Autophagy of Organelles. *Developmental cell* 41: 10-22

Ando H, Hirose M, Mikoshiba K. 2018. Aberrant IP3 receptor activities revealed by comprehensive analysis of pathological mutations causing spinocerebellar ataxia 29. *Proceedings of the National Academy of Sciences of the United States of America* 115: 12259-64

Appocher C, Mohagheghi F, Cappelli S, Stuani C, Romano M, et al. 2017. Major hnRNP proteins act as general TDP-43 functional modifiers both in Drosophila and human neuronal cells. *Nucleic acids research* 45: 8026-45

Arai T, Hasegawa M, Akiyama H, Ikeda K, Nonaka T, et al. 2006. TDP-43 is a component of ubiquitin-positive tau-negative inclusions in frontotemporal lobar degeneration and amyotrophic lateral sclerosis. *Biochemical and biophysical research communications* 351: 602-11

Arenas F, Garcia-Ruiz C, Fernandez-Checa JC. 2017. Intracellular Cholesterol Trafficking and Impact in Neurodegeneration. *Frontiers in molecular neuroscience* 10

Auburger G, Gispert S, Lahut S, Omur O, Damrath E, et al. 2014. 12q24 locus association with type 1 diabetes: SH2B3 or ATXN2? *World journal of diabetes* 5: 316-27

Auburger GW. 2012. Spinocerebellar ataxia type 2. *Handbook of clinical neurology* 103: 423-36

Averna M, Seip RL, Mankowitz K, Schonfeld G. 1993. Postprandial lipemia in subjects with hypobetalipoproteinemia and a single intestinal allele for apoB-48. *J Lipid Res* 34: 1957-67

Awasthi P, Foiani M, Kumar A. 2015. ATM and ATR signaling at a glance. *Journal of cell science* 128: 4255-62

Bagley J, Cortes ML, Breakefield XO, Iacomini J. 2004. Bone marrow transplantation restores immune system function and prevents lymphoma in Atm-deficient mice. *Blood* 104: 572-8

Baker M, Mackenzie IR, Pickering-Brown SM, Gass J, Rademakers R, et al. 2006. Mutations in progranulin cause tau-negative frontotemporal dementia linked to chromosome 17. *Nature* 442: 916-9

Bakkenist CJ, Kastan MB. 2003. DNA damage activates ATM through intermolecular autophosphorylation and dimer dissociation. *Nature* 421: 499-506

Ballabh P, Braun A, Nedergaard M. 2004. The blood-brain barrier: an overview: structure, regulation, and clinical implications. *Neurobiology of disease* 16: 1-13

Bao J, Zheng L, Zhang Q, Li X, Zhang X, et al. 2016. Deacetylation of TFEB promotes fibrillar Abeta degradation by upregulating lysosomal biogenesis in microglia. *Protein Cell* 7: 417-33

Bar DZ, Charar C, Dorfman J, Yadid T, Tafforeau L, et al. 2016. Cell size and fat content of dietary-restricted Caenorhabditis elegans are regulated by ATX-2, an mTOR repressor. *Proceedings of the National Academy of Sciences of the United States of America* 113: E4620-9

Baretic D, Maia de Oliveira T, Niess M, Wan P, Pollard H, et al. 2019. Structural insights into the critical DNA damage sensors DNA-PKcs, ATM and ATR. *Progress in biophysics and molecular biology*

Barlow C, Dennery PA, Shigenaga MK, Smith MA, Morrow JD, et al. 1999. Loss of the Ataxia-Telangiectasia Gene Product Causes Oxidative Damage in Target Organs. *PNAS* 96: 9915 - 19

Barlow C, Hirotsune S, Paylor R, Liyanage M, Eckhaus M, et al. 1996. Atm-Deficient Mice: A Paradigm of Ataxia Telangiectasia. *Cell* 86: 159–71

Barlow C, Ribaut-Barassin C, Zwingman TA, Pope AJ, Brown KD, et al. 2000. ATM is a cytoplasmic protein in mouse brain required to prevent lysosomal accumulation. *Proceedings of the National Academy of Sciences of the United States of America* 97: 871-6

Barnes JA, Ebner BA, Duvick LA, Gao W, Chen G, et al. 2011. Abnormalities in the climbing fiber-Purkinje cell circuitry contribute to neuronal dysfunction in

ATXN1[82Q] mice. *The Journal of neuroscience : the official journal of the Society for Neuroscience* 31: 12778-89

Barski JJ, Hartmann J, Rose CR, Hoebeek F, Morl K, et al. 2003. Calbindin in cerebellar Purkinje cells is a critical determinant of the precision of motor coordination. *The Journal of neuroscience : the official journal of the Society for Neuroscience* 23: 3469-77

Bass NH, Hess HH, Pope A, Thalheimer C. 1971. Quantitative cytoarchitectonic distribution of neurons, glia, and DNa in rat cerebral cortex. *The Journal of comparative neurology* 143: 481-90

Bateman A, Belcourt D, Bennett H, Lazure C, Solomon S. 1990. Granulins, a novel class of peptide from leukocytes. *Biochemical and biophysical research communications* 173: 1161-8

Bateup HS, Johnson CA, Denefrio CL, Saulnier JL, Kornacker K, Sabatini BL. 2013. Excitatory/inhibitory synaptic imbalance leads to hippocampal hyperexcitability in mouse models of tuberous sclerosis. *Neuron* 78: 510-22

Becker LA, Huang B, Bieri G, Ma R, Knowles DA, et al. 2017. Therapeutic reduction of ataxin-2 extends lifespan and reduces pathology in TDP-43 mice. *Nature* 544: 367-71

Belcastro V, Siciliano V, Gregoretti F, Mithbaokar P, Dharmalingam G, et al. 2011. Transcriptional gene network inference from a massive dataset elucidates transcriptome organization and gene function. *Nucleic acids research* 39: 8677-88

Benaud C, Gentil BJ, Assard N, Court M, Garin J, et al. 2004. AHNAK interaction with the annexin 2/S100A10 complex regulates cell membrane cytoarchitecture. *J Cell Biol* 164: 133-44

Bencokova Z, Kaufmann MR, Pires IM, Lecane PS, Giaccia AJ, Hammond EM. 2009. ATM activation and signaling under hypoxic conditions. *Mol Cell Biol* 29: 526-37

Bensimon A, Schmidt A, Ziv Y, Elkon R, Wang SY, et al. 2010. ATM-dependent and -independent dynamics of the nuclear phosphoproteome after DNA damage. *Sci Signal* 3: rs3

Bereczki E, Bernat G, Csont T, Ferdinandy P, Scheich H, Santha M. 2008. Overexpression of human apolipoprotein B-100 induces severe neurodegeneration in transgenic mice. *Journal of proteome research* 7: 2246-52

Bican O, Minagar A, Pruitt AA. 2013. The spinal cord: a review of functional neuroanatomy. *Neurologic clinics* 31: 1-18

Biedler JL, Roffler-Tarlov S, Schachner M, Freedman LS. 1978. Multiple neurotransmitter synthesis by human neuroblastoma cell lines and clones. *Cancer research* 38: 3751-7

Bigbee WL, Langlois RG, Swift M, Jensen RH. 1989. Evidence for an elevated frequency of in vivo somatic cell mutations in ataxia telangiectasia. *American journal of human genetics* 44: 402-8

Birsa N, Bentham MP, Fratta P. 2019. Cytoplasmic functions of TDP-43 and FUS and their role in ALS. *Seminars in cell & developmental biology*

Bjorkhem I. 2006. Crossing the barrier: oxysterols as cholesterol transporters and metabolic modulators in the brain. *Journal of internal medicine* 260: 493-508

Björkhem I, Meaney S. 2004. Brain Cholesterol: Long Secret Life Behind a Barrier. *Arterioscler Thromb Vasc Biol* 24: 806-15

Blackford AN, Jackson SP. 2017. ATM, ATR, and DNA-PK: The Trinity at the Heart of the DNA Damage Response. *Molecular cell* 66: 801-17

Blasi E, Barluzzi R, Bocchini V, Mazzolla R, Bistoni F. 1990. Immortalization of murine microglial cells by a v-raf/v-myc carrying retrovirus. *J Neuroimmunol* 27: 229-37

Blignaut M, Loos B, Botchway SW, Parker AW, Huisamen B. 2019. Ataxia-Telangiectasia Mutated is located in cardiac mitochondria and impacts oxidative phosphorylation. *Sci Rep* 9: 4782

Block ML, Zecca L, Hong JS. 2007. Microglia-mediated neurotoxicity: uncovering the molecular mechanisms. *Nature reviews. Neuroscience* 8: 57-69

Blyn LB, Towner JS, Semler BL, Ehrenfeld E. 1997. Requirement of poly(rC) binding protein 2 for translation of poliovirus RNA. *Journal of virology* 71: 6243-6

Boder E, Sedgwick RP. 1958. Ataxia-telangiectasia; a familial syndrome of progressive cerebellar ataxia, oculocutaneous telangiectasia and frequent pulmonary infection. *Pediatrics* 21: 526-54

Boehrs JK, He J, Halaby MJ, Yang DQ. 2007. Constitutive expression and cytoplasmic compartmentalization of ATM protein in differentiated human neuron-like SH-SY5Y cells. *J Neurochem* 100: 337-45

Boussicault L, Alves S, Lamaziere A, Planques A, Heck N, et al. 2016. CYP46A1, the rate-limiting enzyme for cholesterol degradation, is neuroprotective in Huntington's disease. *Brain : a journal of neurology* 139: 953-70

Boveri M, Kinsner A, Berezowski V, Lenfant AM, Draing C, et al. 2006. Highly purified lipoteichoic acid from gram-positive bacteria induces in vitro blood-brain barrier disruption through glia activation: role of pro-inflammatory cytokines and nitric oxide. *Neuroscience* 137: 1193-209

Bridel C, van Wieringen WN, Zetterberg H, Tijms BM, Teunissen CE, et al. 2019. Diagnostic Value of Cerebrospinal Fluid Neurofilament Light Protein in Neurology: A Systematic Review and Meta-analysis. *JAMA neurology*

Bryant CD, Yazdani N. 2016. RNA-binding proteins, neural development and the addictions. *Genes, brain, and behavior* 15: 169-86

Buchan JR, Parker R. 2009. Eukaryotic stress granules: the ins and outs of translation. *Molecular cell* 36: 932-41

Buratti E, Baralle FE. 2010. The multiple roles of TDP-43 in pre-mRNA processing and gene expression regulation. *RNA biology* 7: 420-9

Burger K, Ketley RF, Gullerova M. 2019a. Beyond the Trinity of ATM, ATR, and DNA-PK: Multiple Kinases Shape the DNA Damage Response in Concert With RNA Metabolism. *Frontiers in molecular biosciences* 6: 61

Burger K, Schlackow M, Gullerova M. 2019b. Tyrosine kinase c-Abl couples RNA polymerase II transcription to DNA double-strand breaks. *Nucleic acids research* 47: 3467-84

Burlot MA, Braudeau J, Michaelsen-Preusse K, Potier B, Ayciriex S, et al. 2015. Cholesterol 24-hydroxylase defect is implicated in memory impairments associated with Alzheimer-like Tau pathology. *Human molecular genetics* 24: 5965-76

Caccamo A, Branca C, Piras IS, Ferreira E, Huentelman MJ, et al. 2017. Necroptosis activation in Alzheimer's disease. *Nature neuroscience* 20: 1236-46

Caceres CJ, Angulo J, Contreras N, Pino K, Vera-Otarola J, Lopez-Lastra M. 2016. Targeting deoxyhypusine hydroxylase activity impairs cap-independent translation initiation driven by the 5'untranslated region of the HIV-1, HTLV-1, and MMTV mRNAs. *Antiviral research* 134: 192-206

Cali JJ, Hsieh CL, Francke U, Russell DW. 1991. Mutations in the bile acid biosynthetic enzyme sterol 27-hydroxylase underlie cerebrotendinous xanthomatosis. *The Journal of biological chemistry* 266: 7779-83

Cam H, Easton JB, High A, Houghton PJ. 2010. mTORC1 signaling under hypoxic conditions is controlled by ATM-dependent phosphorylation of HIF-1alpha. *Molecular cell* 40: 509-20

Cancel G, Durr A, Didierjean O, Imbert G, Burk K, et al. 1997. Molecular and clinical correlations in spinocerebellar ataxia 2: a study of 32 families. *Human molecular genetics* 6: 709-15

Canet-Pons J, Schubert R, Duecker RP, Schrewe R, Wolke S, et al. 2018. Ataxia telangiectasia alters the ApoB and reelin pathway. *Neurogenetics* 19: 237-55

Carbonari M, Cherchi M, Paganelli R, Giannini G, Galli E, et al. 1990. Relative increase of T cells expressing the gamma/delta rather than the alpha/beta receptor in ataxia-telangiectasia. *The New England journal of medicine* 322: 73-6

Carmo-Silva S, Nobrega C, Pereira de Almeida L, Cavadas C. 2017. Unraveling the Role of Ataxin-2 in Metabolism. *Trends in endocrinology and metabolism: TEM* 28: 309-18

Carstea ED, Morris JA, Coleman KG, Loftus SK, Zhang D, et al. 1997. Niemann-Pick C1 disease gene: homology to mediators of cholesterol homeostasis. *Science* 277: 228-31

Carter RJ, Lione LA, Humby T, Mangiarini L, Mahal A, et al. 1999. Characterization of progressive motor deficits in mice transgenic for the human Huntington's disease mutation. *The Journal of neuroscience : the official journal of the Society for Neuroscience* 19: 3248-57

Castagna C, Merighi A, Lossi L. 2016. Cell death and neurodegeneration in the postnatal development of cerebellar vermis in normal and Reeler mice. *Annals of anatomy = Anatomischer Anzeiger : official organ of the Anatomische Gesellschaft* 207: 76-90

Chamberlain S, Shaw J, Rowland A, Wallis J, South S, et al. 1988. Mapping of mutation causing Friedreich's ataxia to human chromosome 9. *Nature* 334: 248-50

Chen N, Xia P, Li S, Zhang T, Wang TT, Zhu J. 2017. RNA sensors of the innate immune system and their detection of pathogens. *IUBMB life* 69: 297-304

Cheng A, Zhao T, Tse KH, Chow HM, Cui Y, et al. 2018. ATM and ATR play complementary roles in the behavior of excitatory and inhibitory vesicle populations. *Proceedings of the National Academy of Sciences of the United States of America* 115: E292-E301

Chetty C, Dontula R, Gujrati M, Dinh DH, Lakka SS. 2012. Blockade of SOX4 mediated DNA repair by SPARC enhances radioresponse in medulloblastoma. *Cancer letters* 323: 188-98

Chiesa N, Barlow C, Wynshaw-Boris A, Strata P, Tempia F. 2000. Atm-DEFICIENT MICE PURKINJE CELLS SHOW AGE DEPENDENT DEFECTS IN CALCIUM SPIKE BURSTS AND CALCIUM CURRENTS. *Neuroscience* 96: 575–83

Choi H, Merceron C, Mangiavini L, Seifert EL, Schipani E, et al. 2016. Hypoxia promotes noncanonical autophagy in nucleus pulposus cells independent of MTOR and HIF1A signaling. *Autophagy* 12: 1631-46

Chu J, Cargnello M, Topisirovic I, Pelletier J. 2016. Translation Initiation Factors: Reprogramming Protein Synthesis in Cancer. *Trends in cell biology* 26: 918-33

Chun HH, Gatti RA. 2004. Ataxia-telangiectasia, an evolving phenotype. *DNA repair* 3: 1187-96

Ciosk R, DePalma M, Priess JR. 2004. ATX-2, the C. elegans ortholog of ataxin 2, functions in translational regulation in the germline. *Development* 131: 4831-41

Ciura S, Sellier C, Campanari ML, Charlet-Berguerand N, Kabashi E. 2016. The most prevalent genetic cause of ALS-FTD, C9orf72 synergizes the toxicity of ATXN2 intermediate polyglutamine repeats through the autophagy pathway. *Autophagy* 12: 1406-8

Coller JM, Tucker M, Sheth U, Valencia-Sanchez MA, Parker R. 2001. The DEAD box helicase, Dhh1p, functions in mRNA decapping and interacts with both the decapping and deadenylase complexes. *RNA* 7: 1717-27

Conradt B, Wu YC, Xue D. 2016. Programmed Cell Death During Caenorhabditis elegans Development. *Genetics* 203: 1533-62

Constantinescu R, Rosengren L, Eriksson B, Blennow K, Axelsson M. 2019. Cerebrospinal fluid neurofilament light and tau protein as mortality biomarkers in parkinsonism. *Acta neurologica Scandinavica* 140: 147-56

Corrado L, Del Bo R, Castellotti B, Ratti A, Cereda C, et al. 2010. Mutations of FUS gene in sporadic amyotrophic lateral sclerosis. *Journal of medical genetics* 47: 190-4

Corral-Juan M, Serrano-Munuera C, Rabano A, Cota-Gonzalez D, Segarra-Roca A, et al. 2018. Clinical, genetic and neuropathological characterization of spinocerebellar ataxia type 37. *Brain : a journal of neurology* 141: 1981-97

Cougot N, Babajko S, Seraphin B. 2004. Cytoplasmic foci are sites of mRNA decay in human cells. *J Cell Biol* 165: 31-40

Cuchet-Lourenco D, Eletto D, Wu C, Plagnol V, Papapietro O, et al. 2018. Biallelic RIPK1 mutations in humans cause severe immunodeficiency, arthritis, and intestinal inflammation. *Science* 361: 810-13

D'Arcangelo G, Miao GG, Chen SC, Soares HD, Morgan JI, Curran T. 1995. A protein related to extracellular matrix proteins deleted in the mouse mutant reeler. *Nature* 374: 719-23

Damrath E, Heck MV, Gispert S, Azizov M, Nowock J, et al. 2012. ATXN2-CAG42 sequesters PABPC1 into insolubility and induces FBXW8 in cerebellum of old ataxic knock-in mice. *PLoS genetics* 8: e1002920

Dansithong W, Paul S, Figueroa KP, Rinehart MD, Wiest S, et al. 2015. Ataxin-2 regulates RGS8 translation in a new BAC-SCA2 transgenic mouse model. *PLoS genetics* 11: e1005182

Date H, Onodera O, Tanaka H, Iwabuchi K, Uekawa K, et al. 2001. Early-onset ataxia with ocular motor apraxia and hypoalbuminemia is caused by mutations in a new HIT superfamily gene. *Nature genetics* 29: 184-8

David G, Abbas N, Stevanin G, Durr A, Yvert G, et al. 1997. Cloning of the SCA7 gene reveals a highly unstable CAG repeat expansion. *Nature genetics* 17: 65-70

de Moura MB, dos Santos LS, Van Houten B. 2010. Mitochondrial dysfunction in neurodegenerative diseases and cancer. *Environmental and molecular mutagenesis* 51: 391-405

DeJesus-Hernandez M, Mackenzie IR, Boeve BF, Boxer AL, Baker M, et al. 2011. Expanded GGGGCC hexanucleotide repeat in noncoding region of C9ORF72 causes chromosome 9p-linked FTD and ALS. *Neuron* 72: 245-56

Delatycki MB, Knight M, Koenig M, Cossee M, Williamson R, Forrest SM. 1999. G130V, a common FRDA point mutation, appears to have arisen from a common founder. *Human genetics* 105: 343-6

Delatycki MB, Williamson R, Forrest SM. 2000. Friedreich ataxia: an overview. *Journal of medical genetics* 37: 1-8

DeMille D, Badal BD, Evans JB, Mathis AD, Anderson JF, Grose JH. 2015. PAS kinase is activated by direct SNF1-dependent phosphorylation and mediates inhibition of TORC1 through the phosphorylation and activation of Pbp1. *Molecular biology of the cell* 26: 569-82

DeMille D, Bikman BT, Mathis AD, Prince JT, Mackay JT, et al. 2014. A comprehensive protein-protein interactome for yeast PAS kinase 1 reveals direct inhibition of respiration through the phosphorylation of Cbf1. *Molecular biology of the cell* 25: 2199-215

Dietschy JM, Turley SD. 2004. Thematic review series: brain Lipids. Cholesterol metabolism in the central nervous system during early development and in the mature animal. *J Lipid Res* 45: 1375-97

Ding D, Li K, Wang C, Chen Z, Long Z, et al. 2016. ATXN2 polymorphism modulates age at onset in Machado-Joseph disease. *Brain : a journal of neurology* 139: e59

Dominiczak MH, Caslake MJ. 2011. Apolipoproteins: metabolic role and clinical biochemistry applications. *Annals of clinical biochemistry* 48: 498-515

Dormann D, Capell A, Carlson AM, Shankaran SS, Rodde R, et al. 2009. Proteolytic processing of TAR DNA binding protein-43 by caspases produces C-terminal fragments with disease defining properties independent of progranulin. *J Neurochem* 110: 1082-94

Drai D, Kafkafi N, Benjamini Y, Elmer G, Golani I. 2001. Rats and mice share common ethologically relevant parameters of exploratory behavior. *Behavioural brain research* 125: 133-40

Drost J, Nonis D, Eich F, Leske O, Damrath E, et al. 2013. Ataxin-2 modulates the levels of Grb2 and SRC but not ras signaling. *Journal of molecular neuroscience : MN* 51: 68-81

Duenas AM, Goold R, Giunti P. 2006. Molecular pathogenesis of spinocerebellar ataxias. *Brain : a journal of neurology* 129: 1357-70

Dzieciatkowska M, Qi G, You J, Bemis KG, Sahm H, et al. 2011. Proteomic Characterization of Cerebrospinal Fluid from Ataxia-Telangiectasia (A-T) Patients Using a LC/MS-Based Label-Free Protein Quantification Technology. *International journal of proteomics* 2011: 578903

Efthymiou AG, Goate AM. 2017. Late onset Alzheimer's disease genetics implicates microglial pathways in disease risk. *Molecular neurodegeneration* 12: 43

Egorova PA, Gavrilova AV, Bezprozvanny IB. 2018. In Vivo Analysis of the Climbing Fiber-Purkinje Cell Circuit in SCA2-58Q Transgenic Mouse Model. *Cerebellum* 17: 590-600

Ehling R, Noskova L, Stranecky V, Hartmannova H, Pristoupilova A, et al. 2013. Cerebellar dysfunction in a family harboring the PSEN1 mutation co-segregating with a cathepsin D variant p.A58V. *Journal of the neurological sciences* 326: 75-82

Elden AC, Kim HJ, Hart MP, Chen-Plotkin AS, Johnson BS, et al. 2010. Ataxin-2 intermediate-length polyglutamine expansions are associated with increased risk for ALS. *Nature* 466: 1069-75

Elson A, Wang Y, Daugherty CJ, Morton CC, Zhou F, et al. 1996. Pleiotropic defects in ataxia-telangiectasia protein-deficient mice. *Proceedings of the National Academy of Sciences of the United States of America* 93: 13084-9

Estrada R, Galarraga J, Orozco G, Nodarse A, Auburger G. 1999. Spinocerebellar ataxia 2 (SCA2): morphometric analyses in 11 autopsies. *Acta neuropathologica* 97: 306-10

Evers BM, Rodriguez-Navas C, Tesla RJ, Prange-Kiel J, Wasser CR, et al. 2017. Lipidomic and Transcriptomic Basis of Lysosomal Dysfunction in Progranulin Deficiency. *Cell reports* 20: 2565-74

Farg MA, Soo KY, Warraich ST, Sundaramoorthy V, Blair IP, Atkin JD. 2013. Ataxin-2 interacts with FUS and intermediate-length polyglutamine expansions enhance FUS-related pathology in amyotrophic lateral sclerosis. *Human molecular genetics* 22: 717-28

Fatemi SH, Reutiman TJ, Folsom TD. 2009. Chronic psychotropic drug treatment causes differential expression of Reelin signaling system in frontal cortex of rats. *Schizophrenia research* 111: 138-52

Fernandez M, McClain ME, Martinez RA, Snow K, Lipe H, et al. 2000. Late-onset SCA2: 33 CAG repeats are sufficient to cause disease. *Neurology* 55: 569-72

Fischer N, Weis K. 2002. The DEAD box protein Dhh1 stimulates the decapping enzyme Dcp1. *EMBO J* 21: 2788-97

Fiszer A, Krzyzosiak WJ. 2013. RNA toxicity in polyglutamine disorders: concepts, models, and progress of research. *Journal of molecular medicine* 91: 683-91

Fittschen M, Lastres-Becker I, Halbach MV, Damrath E, Gispert S, et al. 2015. Genetic ablation of ataxin-2 increases several global translation factors in their transcript abundance but decreases translation rate. *Neurogenetics* 16: 181-92

Flannery S, Bowie AG. 2010. The interleukin-1 receptor-associated kinases: critical regulators of innate immune signalling. *Biochemical pharmacology* 80: 1981-91

Foerster BR, Pomper MG, Callaghan BC, Petrou M, Edden RA, et al. 2013. An imbalance between excitatory and inhibitory neurotransmitters in amyotrophic lateral

sclerosis revealed by use of 3-T proton magnetic resonance spectroscopy. *JAMA neurology* 70: 1009-16

Freischmidt A, Muller K, Ludolph AC, Weishaupt JH, Andersen PM. 2017. Association of Mutations in TBK1 With Sporadic and Familial Amyotrophic Lateral Sclerosis and Frontotemporal Dementia. *JAMA neurology* 74: 110-13

Fremeau RT, Jr., Troyer MD, Pahner I, Nygaard GO, Tran CH, et al. 2001. The expression of vesicular glutamate transporters defines two classes of excitatory synapse. *Neuron* 31: 247-60

Fuger P, Hefendehl JK, Veeraraghavalu K, Wendeln AC, Schlosser C, et al. 2017. Microglia turnover with aging and in an Alzheimer's model via long-term in vivo single-cell imaging. *Nature neuroscience* 20: 1371-76

Fujimura K, Kano F, Murata M. 2008. Identification of PCBP2, a facilitator of IRES-mediated translation, as a novel constituent of stress granules and processing bodies. *RNA* 14: 425-31

Garcia-Miranda P, Vazquez-Carretero MD, Gutierrez G, Peral MJ, Ilundain AA. 2012. Lack of reelin modifies the gene expression in the small intestine of mice. *Journal of physiology and biochemistry* 68: 205-18

Gass J, Cannon A, Mackenzie IR, Boeve B, Baker M, et al. 2006. Mutations in progranulin are a major cause of ubiquitin-positive frontotemporal lobar degeneration. *Human molecular genetics* 15: 2988-3001

Gatti RA, Berkel I, Boder E, Braedt G, Charmley P, et al. 1988. Localization of an ataxia-telangiectasia gene to chromosome 11q22-23. *Nature* 336: 577-80

Gatti RA, Boder E, Vinters HV, Sparkes RS, Norman A, Lange K. 1991. Ataxia-telangiectasia: an interdisciplinary approach to pathogenesis. *Medicine* 70: 99-117

Geerts CJ, Plomp JJ, Koopmans B, Loos M, van der Pijl EM, et al. 2015. Tomosyn-2 is required for normal motor performance in mice and sustains neurotransmission at motor endplates. *Brain structure & function* 220: 1971-82

Gentil BJ, Benaud C, Delphin C, Remy C, Berezowski V, et al. 2005. Specific AHNAK expression in brain endothelial cells with barrier properties. *Journal of cellular physiology* 203: 362-71

Geuens T, Bouhy D, Timmerman V. 2016. The hnRNP family: insights into their role in health and disease. *Human genetics* 135: 851-67

Ghanem LR, Kromer A, Silverman IM, Chatterji P, Traxler E, et al. 2016. The Poly(C) Binding Protein Pcbp2 and Its Retrotransposed Derivative Pcbp1 Are Independently Essential to Mouse Development. *Mol Cell Biol* 36: 304-19

Gispert S, Kurz A, Waibel S, Bauer P, Liepelt I, et al. 2012. The modulation of Amyotrophic Lateral Sclerosis risk by ataxin-2 intermediate polyglutamine expansions is a specific effect. *Neurobiology of disease* 45: 356-61

Grabert K, Michoel T, Karavolos MH, Clohisey S, Baillie JK, et al. 2016. Microglial brain region-dependent diversity and selective regional sensitivities to aging. *Nature neuroscience* 19: 504-16

Graham ME, Lavin MF, Kozlov SV. 2017. Identification of ATM Protein Kinase Phosphorylation Sites by Mass Spectrometry. *Methods in molecular biology* 1599: 127-44

Grewal RP, Tayag E, Figueroa KP, Zu L, Durazo A, et al. 1998. Clinical and genetic analysis of a distinct autosomal dominant spinocerebellar ataxia. *Neurology* 51: 1423-6

Groc L, Choquet D, Stephenson FA, Verrier D, Manzoni OJ, Chavis P. 2007. NMDA receptor surface trafficking and synaptic subunit composition are developmentally regulated by the extracellular matrix protein Reelin. *The Journal of neuroscience : the official journal of the Society for Neuroscience* 27: 10165-75

Gros-Louis F, Dupre N, Dion P, Fox MA, Laurent S, et al. 2007. Mutations in SYNE1 lead to a newly discovered form of autosomal recessive cerebellar ataxia. *Nature genetics* 39: 80-5

Gu X, Qi Y, Feng Z, Ma L, Gao K, Zhang Y. 2018. Lead (Pb) induced ATM-dependent mitophagy via PINK1/Parkin pathway. *Toxicology letters* 291: 92-100

Guo Z, Kozlov S, Lavin MF, Person MD, Paull TT. 2010. ATM activation by oxidative stress. *Science* 330: 517-21

Gwinn-Hardy K, Chen JY, Liu HC, Liu TY, Boss M, et al. 2000. Spinocerebellar ataxia type 2 with parkinsonism in ethnic Chinese. *Neurology* 55: 800-5

Haase H, Alvarez J, Petzhold D, Doller A, Behlke J, et al. 2005. Ahnak is critical for cardiac Ca(V)1.2 calcium channel function and its beta-adrenergic regulation. *FASEB journal : official publication of the Federation of American Societies for Experimental Biology* 19: 1969-77

Habbas S, Santello M, Becker D, Stubbe H, Zappia G, et al. 2015. Neuroinflammatory TNFalpha Impairs Memory via Astrocyte Signaling. *Cell* 163: 1730-41

Hadj-Sahraoui N, Frederic F, Zanjani H, Delhaye-Bouchaud N, Herrup K, Mariani J. 2001. Progressive atrophy of cerebellar Purkinje cell dendrites during aging of the heterozygous staggerer mouse (Rora(+/sg)). *Brain research. Developmental brain research* 126: 201-9

Hadj-Sahraoui N, Frederic F, Zanjani H, Herrup K, Delhaye-Bouchaud N, Mariani J. 1997. Purkinje cell loss in heterozygous staggerer mutant mice during aging. *Brain research. Developmental brain research* 98: 1-8

Halaby MJ, Hibma JC, He J, Yang DQ. 2008. ATM protein kinase mediates full activation of Akt and regulates glucose transporter 4 translocation by insulin in muscle cells. *Cellular signalling* 20: 1555-63

Han SP, Tang YH, Smith R. 2010. Functional diversity of the hnRNPs: past, present and perspectives. *The Biochemical journal* 430: 379-92

Hansen ST, Meera P, Otis TS, Pulst SM. 2013. Changes in Purkinje cell firing and gene expression precede behavioral pathology in a mouse model of SCA2. *Human molecular genetics* 22: 271-83

Hart MP, Gitler AD. 2012. ALS-associated ataxin 2 polyQ expansions enhance stress-induced caspase 3 activation and increase TDP-43 pathological modifications. *The Journal of neuroscience : the official journal of the Society for Neuroscience* 32: 9133-42

Hashimoto T, Amagai M, Parry DA, Dixon TW, Tsukita S, et al. 1993. Desmoyokin, a 680 kDa keratinocyte plasma membrane-associated protein, is homologous to the protein encoded by human gene AHNAK. *Journal of cell science* 105 (Pt 2): 275-86

Hasin Y, Seldin M, Lusis A. 2017. Multi-omics approaches to disease. *Genome biology* 18: 83

Haud N, Kara F, Diekmann S, Henneke M, Willer JR, et al. 2011. rnaset2 mutant zebrafish model familial cystic leukoencephalopathy and reveal a role for RNase T2 in degrading ribosomal RNA. *Proceedings of the National Academy of Sciences of the United States of America* 108: 1099-103

He Z, Ismail A, Kriazhev L, Sadvakassova G, Bateman A. 2002. Progranulin (PC-cell-derived growth factor/acrogranin) regulates invasion and cell survival. *Cancer research* 62: 5590-6

He Z, Ong CH, Halper J, Bateman A. 2003. Progranulin is a mediator of the wound response. *Nature medicine* 9: 225-9

Hefendehl JK, Neher JJ, Suhs RB, Kohsaka S, Skodras A, Jucker M. 2014. Homeostatic and injury-induced microglia behavior in the aging brain. *Aging Cell* 13: 60-9

Hellwig S, Hack I, Kowalski J, Brunne B, Jarowyj J, et al. 2011. Role for Reelin in neurotransmitter release. *The Journal of neuroscience : the official journal of the Society for Neuroscience* 31: 2352-60

Hentati F, El-Euch G, Bouhlal Y, Amouri R. 2012. Ataxia with vitamin E deficiency and abetalipoproteinemia. *Handbook of clinical neurology* 103: 295-305

Henze K, Martin W. 2003. Evolutionary biology: essence of mitochondria. *Nature* 426: 127-8

Her J, Bunting SF. 2018. How cells ensure correct repair of DNA double-strand breaks. *The Journal of biological chemistry* 293: 10502-11

Hersheson J, Burke D, Clayton R, Anderson G, Jacques TS, et al. 2014. Cathepsin D deficiency causes juvenile-onset ataxia and distinctive muscle pathology. *Neurology* 83: 1873-5

Herz J, Chen Y. 2006. Reelin, lipoprotein receptors and synaptic plasticity. *Nature reviews. Neuroscience* 7: 850-9

Hirai H, Pang Z, Bao D, Miyazaki T, Li L, et al. 2005. Cbln1 is essential for synaptic integrity and plasticity in the cerebellum. *Nature neuroscience* 8: 1534-41

Hirasawa M, Xu X, Trask RB, Maddatu TP, Johnson BA, et al. 2007. Carbonic anhydrase related protein 8 mutation results in aberrant synaptic morphology and excitatory synaptic function in the cerebellum. *Molecular and cellular neurosciences* 35: 161-70

Hirotsune S, Takahara T, Sasaki N, Hirose K, Yoshiki A, et al. 1995. The reeler gene encodes a protein with an EGF-like motif expressed by pioneer neurons. *Nature genetics* 10: 77-83

Hisano S, Sawada K, Kawano M, Kanemoto M, Xiong G, et al. 2002. Expression of inorganic phosphate/vesicular glutamate transporters (BNPI/VGLUT1 and DNPI/VGLUT2) in the cerebellum and precerebellar nuclei of the rat. *Brain research. Molecular brain research* 107: 23-31

Hnizda A, Blundell TL. 2019. Multicomponent assemblies in DNA-double-strand break repair by NHEJ. *Current opinion in structural biology* 55: 154-60

Hoche F, Frankenberg E, Rambow J, Theis M, Harding JA, et al. 2014. Cognitive phenotype in ataxia-telangiectasia. *Pediatric neurology* 51: 297-310

Hoche F, Seidel K, Theis M, Vlaho S, Schubert R, et al. 2012. Neurodegeneration in ataxia telangiectasia: what is new? What is evident? *Neuropediatrics* 43: 119-29

Hoek KS, Kidd GJ, Carson JH, Smith R. 1998. hnRNP A2 selectively binds the cytoplasmic transport sequence of myelin basic protein mRNA. *Biochemistry* 37: 7021-9

Hoffman PN, Lasek RJ. 1975. The slow component of axonal transport. Identification of major structural polypeptides of the axon and their generality among mammalian neurons. *J Cell Biol* 66: 351-66

Hogue MJ. 1947. Human fetal ependymal cells in tissue cultures. *The Anatomical record* 99: 523-9

Homer VM, George PM, du Toit S, Davidson JS, Wilson CJ. 2005. Mental retardation and ataxia due to normotriglyceridemic hypobetalipoproteinemia. *Annals of neurology* 58: 160-3

Hong S, Beja-Glasser VF, Nfonoyim BM, Frouin A, Li S, et al. 2016. Complement and microglia mediate early synapse loss in Alzheimer mouse models. *Science* 352: 712-16

Hong SE, Shugart YY, Huang DT, Shahwan SA, Grant PE, et al. 2000. Autosomal recessive lissencephaly with cerebellar hypoplasia is associated with human RELN mutations. *Nature genetics* 26: 93-6

Hoxha E, Balbo I, Miniaci MC, Tempia F. 2018. Purkinje Cell Signaling Deficits in Animal Models of Ataxia. *Frontiers in synaptic neuroscience* 10: 6

Huang L, Chardon JW, Carter MT, Friend KL, Dudding TE, et al. 2012. Missense mutations in ITPR1 cause autosomal dominant congenital nonprogressive spinocerebellar ataxia. *Orphanet journal of rare diseases* 7: 67

Huang Y, Laval SH, van Remoortere A, Baudier J, Benaud C, et al. 2007. AHNAK, a novel component of the dysferlin protein complex, redistributes to the cytoplasm with

dysferlin during skeletal muscle regeneration. *FASEB journal : official publication of the Federation of American Societies for Experimental Biology* 21: 732-42

Hutten S, Dormann D. 2016. hnRNPA2/B1 Function in Neurodegeneration: It's a Gain, Not a Loss. *Neuron* 92: 672-74

Huynh DP, Figueroa K, Hoang N, Pulst SM. 2000. Nuclear localization or inclusion body formation of ataxin-2 are not necessary for SCA2 pathogenesis in mouse or human. *Nature genetics* 26: 44-50

Huynh DP, Yang HT, Vakharia H, Nguyen D, Pulst SM. 2003. Expansion of the polyQ repeat in ataxin-2 alters its Golgi localization, disrupts the Golgi complex and causes cell death. *Human molecular genetics* 12: 1485-96

Igaz LM, Kwong LK, Xu Y, Truax AC, Uryu K, et al. 2008. Enrichment of C-terminal fragments in TAR DNA-binding protein-43 cytoplasmic inclusions in brain but not in spinal cord of frontotemporal lobar degeneration and amyotrophic lateral sclerosis. *The American journal of pathology* 173: 182-94

Ikeda Y, Daughters RS, Ranum LP. 2008. Bidirectional expression of the SCA8 expansion mutation: one mutation, two genes. *Cerebellum* 7: 150-8

Imbert G, Saudou F, Yvert G, Devys D, Trottier Y, et al. 1996. Cloning of the gene for spinocerebellar ataxia 2 reveals a locus with high sensitivity to expanded CAG/glutamine repeats. *Nature genetics* 14: 285-91

Ingelfinger D, Arndt-Jovin DJ, Luhrmann R, Achsel T. 2002. The human LSm1-7 proteins colocalize with the mRNA-degrading enzymes Dcp1/2 and Xrnl in distinct cytoplasmic foci. *RNA* 8: 1489-501

Ishiguro T, Taketa K, Gatti RA. 1986. Tissue of origin of elevated alpha-fetoprotein in ataxia-telangiectasia. *Disease markers* 4: 293-7

Ishii T, Sekiguchi M. 2019. Two ways of escaping from oxidative RNA damage: Selective degradation and cell death. *DNA repair*: 102666

Ito Y, Ofengeim D, Najafov A, Das S, Saberi S, et al. 2016. RIPK1 mediates axonal degeneration by promoting inflammation and necroptosis in ALS. *Science* 353: 603-8

Iyer RR, Pluciennik A, Napierala M, Wells RD. 2015. DNA triplet repeat expansion and mismatch repair. *Annual review of biochemistry* 84: 199-226

Jackson SP, Bartek J. 2009. The DNA-damage response in human biology and disease. *Nature* 461: 1071-8

Jagdeo JM, Dufour A, Klein T, Solis N, Kleifeld O, et al. 2018. N-Terminomics TAILS Identifies Host Cell Substrates of Poliovirus and Coxsackievirus B3 3C Proteinases That Modulate Virus Infection. *Journal of virology* 92

Jain S, Wheeler JR, Walters RW, Agrawal A, Barsic A, Parker R. 2016. ATPase-Modulated Stress Granules Contain a Diverse Proteome and Substructure. *Cell* 164: 487-98

Jeske DJ, Dietschy JM. 1980. Regulation of rates of cholesterol synthesis in vivo in the liver and carcass of the rat measured using [3H]water. *J Lipid Res* 21: 364-76

Ji YJ, Ugolino J, Brady NR, Hamacher-Brady A, Wang J. 2017. Systemic deregulation of autophagy upon loss of ALS- and FTD-linked C9orf72. *Autophagy* 13: 1254-55

Jian J, Konopka J, Liu C. 2013. Insights into the role of progranulin in immunity, infection, and inflammation. *Journal of leukocyte biology* 93: 199-208

Jiménez-López D, Guzmán P. 2014. Insights into the evolution and domain structure of ataxin-2 proteins across eukaryotes. *BMC Research Notes*

Jin J, Bhatti DL, Lee KW, Medrihan L, Cheng J, et al. 2019. Ahnak scaffolds p11/Anxa2 complex and L-type voltage-gated calcium channel and modulates depressive behavior. *Molecular psychiatry*

Johansen T, Lamark T. 2011. Selective autophagy mediated by autophagic adapter proteins. *Autophagy* 7: 279-96

Jones BJ, Roberts DJ. 1968. The quantiative measurement of motor inco-ordination in naive mice using an acelerating rotarod. *The Journal of pharmacy and pharmacology* 20: 302-4

Jung J, Xu K, Lessing D, Bonini NM. 2009. Preventing Ataxin-3 protein cleavage mitigates degeneration in a Drosophila model of SCA3. *Human molecular genetics* 18: 4843-52

Jung M, Kondratyev A, Lee SA, Dimtchev A, Dritschilo A. 1997. ATM gene product phosphorylates I kappa B-alpha. *Cancer research* 57: 24-7

Kakegawa W, Mitakidis N, Miura E, Abe M, Matsuda K, et al. 2015. Anterograde C1ql1 signaling is required in order to determine and maintain a single-winner climbing fiber in the mouse cerebellum. *Neuron* 85: 316-29

Kamsler A, Daily D, Hochman A, Stern N, Shiloh Y, et al. 2001. Increased oxidative stress in ataxia telangiectasia evidenced by alterations in redox state of brains from Atm-deficient mice. *Cancer research* 61: 1849-54

Kao AW, Eisenhut RJ, Martens LH, Nakamura A, Huang A, et al. 2011. A neurodegenerative disease mutation that accelerates the clearance of apoptotic cells. *Proceedings of the National Academy of Sciences of the United States of America* 108: 4441-6

Kattuah W, Rogelj B, King A, Shaw CE, Hortobagyi T, Troakes C. 2019. Heterogeneous Nuclear Ribonucleoprotein E2 (hnRNP E2) Is a Component of TDP-43 Aggregates Specifically in the A and C Pathological Subtypes of Frontotemporal Lobar Degeneration. *Frontiers in neuroscience* 13: 551

Kawaguchi Y, Okamoto T, Taniwaki M, Aizawa M, Inoue M, et al. 1994. CAG expansions in a novel gene for Machado-Joseph disease at chromosome 14q32.1. *Nature genetics* 8: 221-8

Kawai T, Akira S. 2010. The role of pattern-recognition receptors in innate immunity: update on Toll-like receptors. *Nature immunology* 11: 373-84

Kedersha N, Cho MR, Li W, Yacono PW, Chen S, et al. 2000. Dynamic shuttling of TIA-1 accompanies the recruitment of mRNA to mammalian stress granules. *J Cell Biol* 151: 1257-68

Kedersha N, Ivanov P, Anderson P. 2013. Stress granules and cell signaling: more than just a passing phase? *Trends in biochemical sciences* 38: 494-506

Kedersha N, Stoecklin G, Ayodele M, Yacono P, Lykke-Andersen J, et al. 2005. Stress granules and processing bodies are dynamically linked sites of mRNP remodeling. *J Cell Biol* 169: 871-84

Kedersha NL, Gupta M, Li W, Miller I, Anderson P. 1999. RNA-binding proteins TIA-1 and TIAR link the phosphorylation of eIF-2 alpha to the assembly of mammalian stress granules. *J Cell Biol* 147: 1431-42

Khong A, Matheny T, Jain S, Mitchell SF, Wheeler JR, Parker R. 2017. The Stress Granule Transcriptome Reveals Principles of mRNA Accumulation in Stress Granules. *Molecular cell* 68: 808-20 e5

Kiehl TR, Nechiporuk A, Figueroa KP, Keating MT, Huynh DP, Pulst SM. 2006. Generation and characterization of Sca2 (ataxin-2) knockout mice. *Biochemical and biophysical research communications* 339: 17-24

Kiehl TR, Shibata H, Pulst SM. 2000. The ortholog of human ataxin-2 is essential for early embryonic patterning in C. elegans. *Journal of molecular neuroscience : MN* 15: 231-41

Kim HJ, Cho MH, Shim WH, Kim JK, Jeon EY, et al. 2017. Deficient autophagy in microglia impairs synaptic pruning and causes social behavioral defects. *Molecular psychiatry* 22: 1576-84

Kim HJ, Kim NC, Wang YD, Scarborough EA, Moore J, et al. 2013. Mutations in prion-like domains in hnRNPA2B1 and hnRNPA1 cause multisystem proteinopathy and ALS. *Nature* 495: 467-73

Kim TS, Kawaguchi M, Suzuki M, Jung CG, Asai K, et al. 2010. The ZFHX3 (ATBF1) transcription factor induces PDGFRB, which activates ATM in the cytoplasm to protect cerebellar neurons from oxidative stress. *Dis Model Mech* 3: 752-62

Kitamura K, Kano M. 2013. Dendritic calcium signaling in cerebellar Purkinje cell. *Neural networks : the official journal of the International Neural Network Society* 47: 11-7

Klett H, Fuellgraf H, Levit-Zerdoun E, Hussung S, Kowar S, et al. 2018. Identification and Validation of a Diagnostic and Prognostic Multi-Gene Biomarker Panel for Pancreatic Ductal Adenocarcinoma. *Frontiers in genetics* 9: 108

Klionsky DJ. 2008. Autophagy revisited: a conversation with Christian de Duve. *Autophagy* 4: 740-3

Klionsky DJ, Abdelmohsen K, Abe A, Abedin MJ, Abeliovich H, et al. 2016. Guidelines for the use and interpretation of assays for monitoring autophagy (3rd edition). *Autophagy* 12: 1-222

Kobayashi K, Oka K, Forte T, Ishida B, Teng B, et al. 1996. Reversal of hypercholesterolemia in low density lipoprotein receptor knockout mice by adenovirus-mediated gene transfer of the very low density lipoprotein receptor. *The Journal of biological chemistry* 271: 6852-60

Kobayashi S. 2015. Choose Delicately and Reuse Adequately: The Newly Revealed Process of Autophagy. *Biological & pharmaceutical bulletin* 38: 1098-103

Koeppen AH. 2005. The pathogenesis of spinocerebellar ataxia. *Cerebellum* 4: 62-73

Koide R, Ikeuchi T, Onodera O, Tanaka H, Igarashi S, et al. 1994. Unstable expansion of CAG repeat in hereditary dentatorubral-pallidoluysian atrophy (DRPLA). *Nature genetics* 6: 9-13

Kole AJ, Annis RP, Deshmukh M. 2013. Mature neurons: equipped for survival. *Cell death & disease* 4: e689

Komuro A, Masuda Y, Kobayashi K, Babbitt R, Gunel M, et al. 2004. The AHNAKs are a class of giant propeller-like proteins that associate with calcium channel proteins of cardiomyocytes and other cells. *Proceedings of the National Academy of Sciences of the United States of America* 101: 4053-8

Kong J, Tung VW, Aghajanian J, Xu Z. 1998. Antagonistic roles of neurofilament subunits NF-H and NF-M against NF-L in shaping dendritic arborization in spinal motor neurons. *J Cell Biol* 140: 1167-76

Koob MD, Moseley ML, Schut LJ, Benzow KA, Bird TD, et al. 1999. An untranslated CTG expansion causes a novel form of spinocerebellar ataxia (SCA8). *Nature genetics* 21: 379-84

Kozlov A, Nagoshi E. 2019. Decoding Drosophila circadian pacemaker circuit. *Current opinion in insect science* 36: 33-38

Kozlov G, Menade M, Rosenauer A, Nguyen L, Gehring K. 2010. Molecular determinants of PAM2 recognition by the MLLE domain of poly(A)-binding protein. *J Mol Biol* 397: 397-407

Krygier M, Kwarciany M, Wasilewska K, Pienkowski VM, Krawczynska N, et al. 2019. A study in a Polish ataxia cohort indicates genetic heterogeneity and points to MTCL1 as a novel candidate gene. *Clinical genetics* 95: 415-19

Kuhle J, Lindberg RL, Regeniter A, Mehling M, Steck AJ, et al. 2009. Increased levels of inflammatory chemokines in amyotrophic lateral sclerosis. *European journal of neurology* 16: 771-4

Kuljis RO, Chen G, Lee EY, Aguila MC, Xu Y. 1999. ATM immunolocalization in mouse neuronal endosomes: implications for ataxia-telangiectasia. *Brain research* 842: 351-8

Kumar R, Corbett MA, Smith NJ, Jolly LA, Tan C, et al. 2015. Homozygous mutation of STXBP5L explains an autosomal recessive infantile-onset neurodegenerative disorder. *Human molecular genetics* 24: 2000-10

Kuo SH. 2019. Ataxia. *Continuum (Minneap Minn)* 25: 1036-54

Kwiatkowski TJ, Jr., Bosco DA, Leclerc AL, Tamrazian E, Vanderburg CR, et al. 2009. Mutations in the FUS/TLS gene on chromosome 16 cause familial amyotrophic lateral sclerosis. *Science* 323: 1205-8

La Spada AR, Wilson EM, Lubahn DB, Harding AE, Fischbeck KH. 1991. Androgen receptor gene mutations in X-linked spinal and bulbar muscular atrophy. *Nature* 352: 77-9

Labauge P, Renard D, Castelnovo G, Sabourdy F, de Champfleur N, Levade T. 2009. Beta-mannosidosis: a new cause of spinocerebellar ataxia. *Clinical neurology and neurosurgery* 111: 109-10

Lagier-Tourenne C, Tazir M, Lopez LC, Quinzii CM, Assoum M, et al. 2008. ADCK3, an ancestral kinase, is mutated in a form of recessive ataxia associated with coenzyme Q10 deficiency. *American journal of human genetics* 82: 661-72

Lambert JC, Ibrahim-Verbaas CA, Harold D, Naj AC, Sims R, et al. 2013. Meta-analysis of 74,046 individuals identifies 11 new susceptibility loci for Alzheimer's disease. *Nature genetics* 45: 1452-8

Lamont MG, Weber JT. 2015. Mice deficient in carbonic anhydrase type 8 exhibit motor dysfunctions and abnormal calcium dynamics in the somatic region of cerebellar granule cells. *Behavioural brain research* 286: 11-6

Lastres-Becker I, Brodesser S, Lutjohann D, Azizov M, Buchmann J, et al. 2008a. Insulin receptor and lipid metabolism pathology in ataxin-2 knock-out mice. *Human molecular genetics* 17: 1465-81

Lastres-Becker I, Nonis D, Eich F, Klinkenberg M, Gorospe M, et al. 2016. Mammalian ataxin-2 modulates translation control at the pre-initiation complex via PI3K/mTOR and is induced by starvation. *Biochimica et biophysica acta* 1862: 1558-69

Lastres-Becker I, Rub U, Auburger G. 2008b. Spinocerebellar ataxia 2 (SCA2). *Cerebellum* 7: 115-24

Lattante S, Millecamps S, Stevanin G, Rivaud-Pechoux S, Moigneu C, et al. 2014. Contribution of ATXN2 intermediary polyQ expansions in a spectrum of neurodegenerative disorders. *Neurology* 83: 990-5

Lawson LJ, Perry VH, Dri P, Gordon S. 1990. Heterogeneity in the distribution and morphology of microglia in the normal adult mouse brain

. *Neuroscience* 39

Lee IH, Sohn M, Lim HJ, Yoon S, Oh H, et al. 2014. Ahnak functions as a tumor suppressor via modulation of TGFbeta/Smad signaling pathway. *Oncogene* 33: 4675-84

Lee J, Yoo E, Lee H, Park K, Hur JH, Lim C. 2017. LSM12 and ME31B/DDX6 Define Distinct Modes of Posttranscriptional Regulation by ATAXIN-2 Protein Complex in Drosophila Circadian Pacemaker Neurons. *Molecular cell* 66: 129-40 e7

Lee J-H, Mand MR, Kao C-H, Zhou Y, Ryu SW, et al. 2018. ATM directs DNA damage responses and proteostasis via genetically separable pathways. *SCIENCE SIGNALING* 11

Lee JH, Paull TT. 2005. ATM activation by DNA double-strand breaks through the Mre11-Rad50-Nbs1 complex. *Science* 308: 551-4

Lee KH, Mathews PJ, Reeves AM, Choe KY, Jami SA, et al. 2015. Circuit mechanisms underlying motor memory formation in the cerebellum. *Neuron* 86: 529-40

Leeb C, Eresheim C, Nimpf J. 2014. Clusterin is a ligand for apolipoprotein E receptor 2 (ApoER2) and very low density lipoprotein receptor (VLDLR) and signals via the Reelin-signaling pathway. *The Journal of biological chemistry* 289: 4161-72

Lehre KP, Levy LM, Ottersen OP, Storm-Mathisen J, Danbolt NC. 1995. Differential expression of two glial glutamate transporters in the rat brain: quantitative and immunocytochemical observations. *The Journal of neuroscience : the official journal of the Society for Neuroscience* 15: 1835-53

Lenzken SC, Achsel T, Carri MT, Barabino SM. 2014. Neuronal RNA-binding proteins in health and disease. *Wiley interdisciplinary reviews. RNA* 5: 565-76

Levitan I, Singh DK, Rosenhouse-Dantsker A. 2014. Cholesterol binding to ion channels. *Frontiers in physiology* 5: 65

Li D, Zhang J, Yang W, He Y, Ru Y, et al. 2019a. Poly (rC) binding protein 2 interacts with VP0 and increases the replication of the foot-and-mouth disease virus. *Cell death & disease* 10: 516

Li J, Han YR, Plummer MR, Herrup K. 2009. Cytoplasmic ATM in neurons modulates synaptic function. *Current biology : CB* 19: 2091-6

Li Y, Fuhrer M, Bahrami E, Socha P, Klaudel-Dreszler M, et al. 2019b. Human RIPK1 deficiency causes combined immunodeficiency and inflammatory bowel diseases. *Proceedings of the National Academy of Sciences of the United States of America* 116: 970-75

Lian H, Roy E, Zheng H. 2016. Protocol for Primary Microglial Culture Preparation. *Bio-protocol* 6

Liguz-Lecznar M, Skangiel-Kramska J. 2007. Vesicular glutamate transporters (VGLUTs): the three musketeers of glutamatergic system. *Acta neurobiologiae experimentalis* 67: 207-18

Lill CM, Rengmark A, Pihlstrom L, Fogh I, Shatunov A, et al. 2015. The role of TREM2 R47H as a risk factor for Alzheimer's disease, frontotemporal lobar degeneration, amyotrophic lateral sclerosis, and Parkinson's disease. *Alzheimer's & dementia : the journal of the Alzheimer's Association* 11: 1407-16

Lim C, Allada R. 2013. ATAXIN-2 activates PERIOD translation to sustain circadian rhythms in Drosophila. *Science* 340: 875-9

Lim DS, Kirsch DG, Canman CE, Ahn JH, Ziv Y, et al. 1998. ATM binds to beta-adaptin in cytoplasmic vesicles. *Proceedings of the National Academy of Sciences of the United States of America* 95: 10146-51

Lim HJ, Kang DH, Lim JM, Kang DM, Seong JK, et al. 2013. Function of Ahnak protein in aortic smooth muscle cell migration through Rac activation. *Cardiovascular research* 97: 302-10

Lim J, Hao T, Shaw C, Patel AJ, Szabo G, et al. 2006. A protein-protein interaction network for human inherited ataxias and disorders of Purkinje cell degeneration. *Cell* 125: 801-14

Lippincott-Schwartz J, Phair RD. 2010. Lipids and cholesterol as regulators of traffic in the endomembrane system. *Annual review of biophysics* 39: 559-78

Liu W, Otkur W, Zhang Y, Li Q, Ye Y, et al. 2013. Silibinin protects murine fibroblast L929 cells from UVB-induced apoptosis through the simultaneous inhibition of ATM-p53 pathway and autophagy. *The FEBS journal* 280: 4572-84

Liu XY, Li HL, Su JB, Ding FH, Zhao JJ, et al. 2015. Regulation of RAGE splicing by hnRNP A1 and Tra2beta-1 and its potential role in AD pathogenesis. *J Neurochem* 133: 187-98

Lodi R, Cooper JM, Bradley JL, Manners D, Styles P, et al. 1999. Deficit of in vivo mitochondrial ATP production in patients with Friedreich ataxia. *Proceedings of the National Academy of Sciences of the United States of America* 96: 11492-5

Lohmann E, Kruger S, Hauser AK, Hanagasi H, Guven G, et al. 2015. Clinical variability in ataxia-telangiectasia. *Journal of neurology* 262: 1724-7

Lou Z, Minter-Dykhouse K, Franco S, Gostissa M, Rivera MA, et al. 2006. MDC1 maintains genomic stability by participating in the amplification of ATM-dependent DNA damage signals. *Molecular cell* 21: 187-200

Lu D, Wang J, Shi X, Yue B, Hao J. 2017. AHNAK2 is a potential prognostic biomarker in patients with PDAC. *Oncotarget* 8: 31775-84

Lui H, Zhang J, Makinson SR, Cahill MK, Kelley KW, et al. 2016. Progranulin Deficiency Promotes Circuit-Specific Synaptic Pruning by Microglia via Complement Activation. *Cell* 165: 921-35

Luo X, Suzuki M, Ghandhi SA, Amundson SA, Boothman DA. 2014. ATM regulates insulin-like growth factor 1-secretory clusterin (IGF-1-sCLU) expression that protects cells against senescence. *PloS one* 9: e99983

Machtens JP, Kortzak D, Lansche C, Leinenweber A, Kilian P, et al. 2015. Mechanisms of anion conduction by coupled glutamate transporters. *Cell* 160: 542-53

Mahemuti L, Chen Q, Coughlan MC, Qiao C, Chepelev NL, et al. 2018. Bisphenol A induces DSB-ATM-p53 signaling leading to cell cycle arrest, senescence, autophagy, stress response, and estrogen release in human fetal lung fibroblasts. *Archives of toxicology* 92: 1453-69

Majmundar AJ, Wong WJ, Simon MC. 2010. Hypoxia-inducible factors and the response to hypoxic stress. *Molecular cell* 40: 294-309

Makeyev AV, Chkheidze AN, Liebhaber SA. 1999. A set of highly conserved RNA-binding proteins, alphaCP-1 and alphaCP-2, implicated in mRNA stabilization, are coexpressed from an intronless gene and its intron-containing paralog. *The Journal of biological chemistry* 274: 24849-57

Manes S, Martinez AC. 2004. Cholesterol domains regulate the actin cytoskeleton at the leading edge of moving cells. *Trends in cell biology* 14: 275-8

Mangus DA, Amrani N, Jacobson A. 1998. Pbp1p, a factor interacting with Saccharomyces cerevisiae poly(A)-binding protein, regulates polyadenylation. *Mol Cell Biol* 18: 7383-96

Mao R, Aylsworth AS, Potter N, Wilson WG, Breningstall G, et al. 2002. Childhood-onset ataxia: testing for large CAG-repeats in SCA2 and SCA7. *American journal of medical genetics* 110: 338-45

Marmolino D, Manto M. 2010. Past, present and future therapeutics for cerebellar ataxias. *Curr Neuropharmacol* 8: 41-61

Martens LH, Zhang J, Barmada SJ, Zhou P, Kamiya S, et al. 2012. Progranulin deficiency promotes neuroinflammation and neuron loss following toxin-induced injury. *The Journal of clinical investigation* 122: 3955-9

Martin MG, Pfrieger F, Dotti CG. 2014. Cholesterol in brain disease: sometimes determinant and frequently implicated. *EMBO reports* 15: 1036-52

Masunaga T, Shimizu H, Ishiko A, Fujiwara T, Hashimoto T, Nishikawa T. 1995. Desmoyokin/AHNAK protein localizes to the non-desmosomal keratinocyte cell surface of human epidermis. *The Journal of investigative dermatology* 104: 941-5

Matcovitch-Natan O, Winter DR, Giladi A, Aguilar SV, Spinrad A, et al. 2016. Microglia development follows a stepwise program to regulate brain homeostasis. *Science* 353

Matilla-Duenas A, Ashizawa T, Brice A, Magri S, McFarland KN, et al. 2014. Consensus paper: pathological mechanisms underlying neurodegeneration in spinocerebellar ataxias. *Cerebellum* 13: 269-302

Matsuoka S, Ballif BA, Smogorzewska A, McDonald ER, 3rd, Hurov KE, et al. 2007. ATM and ATR substrate analysis reveals extensive protein networks responsive to DNA damage. *Science* 316: 1160-6

Matthews KW, Mueller-Ortiz SL, Wetsel RA. 2004. Carboxypeptidase N: a pleiotropic regulator of inflammation. *Molecular immunology* 40: 785-93

Mattsson N, Cullen NC, Andreasson U, Zetterberg H, Blennow K. 2019. Association Between Longitudinal Plasma Neurofilament Light and Neurodegeneration in Patients With Alzheimer Disease. *JAMA neurology*

Matza D, Badou A, Jha MK, Willinger T, Antov A, et al. 2009. Requirement for AHNAK1-mediated calcium signaling during T lymphocyte cytolysis. *Proceedings of the National Academy of Sciences of the United States of America* 106: 9785-90

Matza D, Badou A, Kobayashi KS, Goldsmith-Pestana K, Masuda Y, et al. 2008. A scaffold protein, AHNAK1, is required for calcium signaling during T cell activation. *Immunity* 28: 64-74

Mayeli M, Mirshahvalad SM, Aghamollaii V, Tafakhori A, Abdolalizadeh A, Rahmani F. 2019. Plasma Neurofilament Light Chain Levels Are Associated With Cortical Hypometabolism in Alzheimer Disease Signature Regions. *J Neuropathol Exp Neurol*

McCann C, Holohan EE, Das S, Dervan A, Larkin A, et al. 2011. The Ataxin-2 protein is required for microRNA function and synapse-specific long-term olfactory habituation. *Proceedings of the National Academy of Sciences of the United States of America* 108: E655-62

Meierhofer D, Halbach M, Sen NE, Gispert S, Auburger G. 2016. Ataxin-2 (Atxn2)-Knock-Out Mice Show Branched Chain Amino Acids and Fatty Acids Pathway Alterations. *Molecular & Cellular Proteomics*

Meneret A, Ahmar-Beaugendre Y, Rieunier G, Mahlaoui N, Gaymard B, et al. 2014. The pleiotropic movement disorders phenotype of adult ataxia-telangiectasia. *Neurology* 83: 1087-95

Meng H, Liu Z, Li X, Wang H, Jin T, et al. 2018. Death-domain dimerization-mediated activation of RIPK1 controls necroptosis and RIPK1-dependent apoptosis. *Proceedings of the National Academy of Sciences of the United States of America* 115: E2001-E09

Menzies FM, Fleming A, Rubinsztein DC. 2015. Compromised autophagy and neurodegenerative diseases. *Nature reviews. Neuroscience* 16: 345-57

Meyer OA, Tilson HA, Byrd WC, Riley MT. 1979. A method for the routine assessment of fore- and hindlimb grip strength of rats and mice. *Neurobehavioral toxicology* 1: 233-6

Michaud JP, Halle M, Lampron A, Theriault P, Prefontaine P, et al. 2013. Toll-like receptor 4 stimulation with the detoxified ligand monophosphoryl lipid A improves Alzheimer's disease-related pathology. *Proceedings of the National Academy of Sciences of the United States of America* 110: 1941-6

Micol R, Ben Slama L, Suarez F, Le Mignot L, Beaute J, et al. 2011. Morbidity and mortality from ataxia-telangiectasia are associated with ATM genotype. *The Journal of allergy and clinical immunology* 128: 382-9 e1

Miyata T, Ono Y, Okamoto M, Masaoka M, Sakakibara A, et al. 2010. Migration, early axonogenesis, and Reelin-dependent layer-forming behavior of early/posterior-born Purkinje cells in the developing mouse lateral cerebellum. *Neural development* 5: 23

Mohagheghi F, Prudencio M, Stuani C, Cook C, Jansen-West K, et al. 2016. TDP-43 functions within a network of hnRNP proteins to inhibit the production of a truncated human SORT1 receptor. *Human molecular genetics* 25: 534-45

Moisse K, Volkening K, Leystra-Lantz C, Welch I, Hill T, Strong MJ. 2009. Divergent patterns of cytosolic TDP-43 and neuronal progranulin expression following axotomy: implications for TDP-43 in the physiological response to neuronal injury. *Brain research* 1249: 202-11

Mollet J, Delahodde A, Serre V, Chretien D, Schlemmer D, et al. 2008. CABC1 gene mutations cause ubiquinone deficiency with cerebellar ataxia and seizures. *American journal of human genetics* 82: 623-30

Moreira MC, Barbot C, Tachi N, Kozuka N, Mendonca P, et al. 2001. Homozygosity mapping of Portuguese and Japanese forms of ataxia-oculomotor apraxia to 9p13, and evidence for genetic heterogeneity. *American journal of human genetics* 68: 501-8

Moreira MC, Klur S, Watanabe M, Nemeth AH, Le Ber I, et al. 2004. Senataxin, the ortholog of a yeast RNA helicase, is mutant in ataxia-ocular apraxia 2. *Nature genetics* 36: 225-7

Moutinho M, Nunes MJ, Rodrigues E. 2016. Cholesterol 24-hydroxylase: Brain cholesterol metabolism and beyond. *Biochimica et biophysica acta* 1861: 1911-20

Nagase T, Kikuno R, Nakayama M, Hirosawa M, Ohara O. 2000. Prediction of the coding sequences of unidentified human genes. XVIII. The complete sequences of 100 new cDNA clones from brain which code for large proteins in vitro. *DNA research*

: an international journal for rapid publication of reports on genes and genomes 7: 273-81

Nakamura K, Beppu M, Sakai K, Yagyu H, Matsumaru S, et al. 2016. The C-terminal region of Reelin is necessary for proper positioning of a subset of Purkinje cells in the postnatal cerebellum. *Neuroscience* 336: 20-29

Nakamura K, Jeong SY, Uchihara T, Anno M, Nagashima K, et al. 2001. SCA17, a novel autosomal dominant cerebellar ataxia caused by an expanded polyglutamine in TATA-binding protein. *Human molecular genetics* 10: 1441-8

Nakayama M, Nakajima D, Yoshimura R, Endo Y, Ohara O. 2002. MEGF1/fat2 proteins containing extraordinarily large extracellular domains are localized to thin parallel fibers of cerebellar granule cells. *Molecular and cellular neurosciences* 20: 563-78

Naphade SB, Kigerl KA, Jakeman LB, Kostyk SK, Popovich PG, Kuret J. 2010. Progranulin expression is upregulated after spinal contusion in mice. *Acta neuropathologica* 119: 123-33

Napolitano G, Ballabio A. 2016. TFEB at a glance. *Journal of cell science* 129: 2475-81

Narain P, Gomes J, Bhatia R, Singh I, Vivekanandan P. 2017. C9orf72 hexanucleotide repeat expansions and Ataxin 2 intermediate length repeat expansions in Indian patients with amyotrophic lateral sclerosis. *Neurobiology of aging* 56: 211 e9-11 e14

Naureckiene S, Sleat DE, Lackland H, Fensom A, Vanier MT, et al. 2000. Identification of HE1 as the second gene of Niemann-Pick C disease. *Science* 290: 2298-301

Nazarov IB, Bakhmet EI, Tomilin AN. 2019. KH-Domain Poly(C)-Binding Proteins as Versatile Regulators of Multiple Biological Processes. *Biochemistry. Biokhimiia* 84: 205-19

Nedergaard M, Ransom B, Goldman SA. 2003. New roles for astrocytes: redefining the functional architecture of the brain. *Trends in neurosciences* 26: 523-30

Neumann M, Sampathu DM, Kwong LK, Truax AC, Micsenyi MC, et al. 2006. Ubiquitinated TDP-43 in frontotemporal lobar degeneration and amyotrophic lateral sclerosis. *Science* 314: 130-3

Nibbeling EAR, Duarri A, Verschuuren-Bemelmans CC, Fokkens MR, Karjalainen JM, et al. 2017. Exome sequencing and network analysis identifies shared mechanisms underlying spinocerebellar ataxia. *Brain : a journal of neurology* 140: 2860-78

Nishimoto Y, Ito D, Yagi T, Nihei Y, Tsunoda Y, Suzuki N. 2010. Characterization of alternative isoforms and inclusion body of the TAR DNA-binding protein-43. *The Journal of biological chemistry* 285: 608-19

Nissenkorn A, Ben-Zeev B. 2015. Ataxia telangiectasia. *Handbook of clinical neurology* 132: 199-214

Nissenkorn A, Levy-Shraga Y, Banet-Levi Y, Lahad A, Sarouk I, Modan-Moses D. 2016. Endocrine abnormalities in ataxia telangiectasia: findings from a national cohort. *Pediatric research* 79: 889-94

Nobrega C, Carmo-Silva S, Albuquerque D, Vasconcelos-Ferreira A, Vijayakumar UG, et al. 2015. Re-establishing ataxin-2 downregulates translation of mutant ataxin-3 and alleviates Machado-Joseph disease. *Brain : a journal of neurology* 138: 3537-54

Nobrega C, Mendonca L, Marcelo A, Lamaziere A, Tome S, et al. 2019. Restoring brain cholesterol turnover improves autophagy and has therapeutic potential in mouse models of spinocerebellar ataxia. *Acta neuropathologica*

Nonhoff U, Ralser M, Welzel F, Piccini I, Balzereit D, et al. 2007. Ataxin-2 interacts with the DEAD/H-box RNA helicase DDX6 and interferes with P-bodies and stress granules. *Molecular biology of the cell* 18: 1385-96

Nonis D, Schmidt MHH, van de Loo S, Eich F, Dikic I, et al. 2008. Ataxin-2 associates with the endocytosis complex and affects EGF receptor trafficking. *Cellular signalling* 20: 1725-39

Nunes C, Mestre I, Marcelo A, Koppenol R, Matos CA, Nobrega C. 2019. MSGP: the first database of the protein components of the mammalian stress granules. *Database : the journal of biological databases and curation* 2019

Obayashi E, Luna RE, Nagata T, Martin-Marcos P, Hiraishi H, et al. 2017. Molecular Landscape of the Ribosome Pre-initiation Complex during mRNA Scanning: Structural Role for eIF3c and Its Control by eIF5. *Cell reports* 18: 2651-63

Ofengeim D, Mazzitelli S, Ito Y, DeWitt JP, Mifflin L, et al. 2017. RIPK1 mediates a disease-associated microglial response in Alzheimer's disease. *Proceedings of the National Academy of Sciences of the United States of America* 114: E8788-E97

Oka A, Takashima S. 1998. Expression of the ataxia-telangiectasia gene (ATM) product in human cerebellar neurons during development. *Neuroscience letters* 252: 195-8

Orr HT, Chung MY, Banfi S, Kwiatkowski TJ, Jr., Servadio A, et al. 1993. Expansion of an unstable trinucleotide CAG repeat in spinocerebellar ataxia type 1. *Nature genetics* 4: 221-6

Ostrowski LA, Hall AC, Szafranski KJ, Oshidari R, Abraham KJ, et al. 2018. Conserved Pbp1/Ataxin-2 regulates retrotransposon activity and connects polyglutamine expansion-driven protein aggregation to lifespan-controlling rDNA repeats. *Communications biology* 1: 187

Paciorkowski AR, Shafrir Y, Hrivnak J, Patterson MC, Tennison MB, et al. 2011. Massive expansion of SCA2 with autonomic dysfunction, retinitis pigmentosa, and infantile spasms. *Neurology* 77: 1055-60

Palau F, Espinos C. 2006. Autosomal recessive cerebellar ataxias. *Orphanet journal of rare diseases* 1: 47

Palfree RG, Bennett HP, Bateman A. 2015. The Evolution of the Secreted Regulatory Protein Progranulin. *PloS one* 10: e0133749

Palmer AL, Ousman SS. 2018. Astrocytes and Aging. *Frontiers in aging neuroscience* 10: 337

Paolicelli RC, Bolasco G, Pagani F, Maggi L, Scianni M, et al. 2011. Synaptic pruning by microglia is necessary for normal brain development. *Science* 333: 1456-8

Paolicelli RC, Jawaid A, Henstridge CM, Valeri A, Merlini M, et al. 2017. TDP-43 Depletion in Microglia Promotes Amyloid Clearance but Also Induces Synapse Loss. *Neuron* 95: 297-308 e6

Park B, Buti L, Lee S, Matsuwaki T, Spooner E, et al. 2011. Granulin is a soluble cofactor for toll-like receptor 9 signaling. *Immunity* 34: 505-13

Parker R, Sheth U. 2007. P bodies and the control of mRNA translation and degradation. *Molecular cell* 25: 635-46

Paull TT. 2015. Mechanisms of ATM Activation. *Annual review of biochemistry* 84: 711-38

Perkins EM, Clarkson YL, Suminaite D, Lyndon AR, Tanaka K, et al. 2018. Loss of cerebellar glutamate transporters EAAT4 and GLAST differentially affects the spontaneous firing pattern and survival of Purkinje cells. *Human molecular genetics*

Perlman SL, Boder Deceased E, Sedgewick RP, Gatti RA. 2012. Ataxia-telangiectasia. *Handbook of clinical neurology* 103: 307-32

Pesold C, Impagnatiello F, Pisu MG, Uzunov DP, Costa E, et al. 1998. Reelin is preferentially expressed in neurons synthesizing gamma-aminobutyric acid in cortex and hippocampus of adult rats. *Proceedings of the National Academy of Sciences of the United States of America* 95: 3221-6

Pfeffer M, Gispert S, Auburger G, Wicht H, Korf HW. 2017. Impact of Ataxin-2 knock out on circadian locomotor behavior and PER immunoreaction in the SCN of mice. *Chronobiology international* 34: 129-37

Philips T, De Muynck L, Thu HN, Weynants B, Vanacker P, et al. 2010. Microglial upregulation of progranulin as a marker of motor neuron degeneration. *J Neuropathol Exp Neurol* 69: 1191-200

Pickford F, Marcus J, Camargo LM, Xiao Q, Graham D, et al. 2011. Progranulin is a chemoattractant for microglia and stimulates their endocytic activity. *The American journal of pathology* 178: 284-95

Pietzner J, Baer PC, Duecker RP, Merscher MB, Satzger-Prodinger C, et al. 2013. Bone marrow transplantation improves the outcome of Atm-deficient mice through the migration of ATM-competent cells. *Human molecular genetics* 22: 493-507

Protter DSW, Parker R. 2016. Principles and Properties of Stress Granules. *Trends in cell biology* 26: 668-79

Puckelwartz MJ, Kessler E, Zhang Y, Hodzic D, Randles KN, et al. 2009. Disruption of nesprin-1 produces an Emery Dreifuss muscular dystrophy-like phenotype in mice. *Human molecular genetics* 18: 607-20

Pulst SM, Nechiporuk A, Nechiporuk T, Gispert S, Chen XN, et al. 1996. Moderate expansion of a normally biallelic trinucleotide repeat in spinocerebellar ataxia type 2. *Nature genetics* 14: 269-76

Pulst SM, Santos N, Wang D, Yang H, Huynh D, et al. 2005. Spinocerebellar ataxia type 2: polyQ repeat variation in the CACNA1A calcium channel modifies age of onset. *Brain : a journal of neurology* 128: 2297-303

Purves D. 2004. *Neuroscience*. Sunderland, Mass.: Sinauer Associates, Publishers.

Putcha GV, Deshmukh M, Johnson EM, Jr. 2000. Inhibition of apoptotic signaling cascades causes loss of trophic factor dependence during neuronal maturation. *J Cell Biol* 149: 1011-8

Qi Y, Qiu Q, Gu X, Tian Y, Zhang Y. 2016. ATM mediates spermidine-induced mitophagy via PINK1 and Parkin regulation in human fibroblasts. *Sci Rep* 6: 24700

Rabbitts TH, Forster A, Larson R, Nathan P. 1993. Fusion of the dominant negative transcription regulator CHOP with a novel gene FUS by translocation t(12;16) in malignant liposarcoma. *Nature genetics* 4: 175-80

Ralser M, Albrecht M, Nonhoff U, Lengauer T, Lehrach H, Krobitsch S. 2005. An integrative approach to gain insights into the cellular function of human ataxin-2. *J Mol Biol* 346: 203-14

Ramirez DM, Andersson S, Russell DW. 2008. Neuronal expression and subcellular localization of cholesterol 24-hydroxylase in the mouse brain. *The Journal of comparative neurology* 507: 1676-93

Reeves SA, Helman LJ, Allison A, Israel MA. 1989. Molecular cloning and primary structure of human glial fibrillary acidic protein. *Proceedings of the National Academy of Sciences of the United States of America* 86: 5178-82

Reichenbach J, Schubert R, Schwan C, Muller K, Bohles HJ, Zielen S. 1999. Anti-oxidative capacity in patients with ataxia telangiectasia. *Clinical and experimental immunology* 117: 535-9

Reiling JH, Sabatini DM. 2006. Stress and mTORture signaling. *Oncogene* 25: 6373-83

Reineke LC, Cheema SA, Dubrulle J, Neilson JR. 2018a. Chronic starvation induces non-canonical pro-death stress granules. *Journal of cell science*

Reineke LC, Cheema SA, Dubrulle J, Neilson JR. 2018b. Chronic starvation induces non-canonical pro-death stress granules. *The Company of Biologists*

Renton AE, Majounie E, Waite A, Simon-Sanchez J, Rollinson S, et al. 2011. A hexanucleotide repeat expansion in C9ORF72 is the cause of chromosome 9p21-linked ALS-FTD. *Neuron* 72: 257-68

Rodriguez F, Duran E, Gomez A, Ocana FM, Alvarez E, et al. 2005. Cognitive and emotional functions of the teleost fish cerebellum. *Brain Res Bull* 66: 365-70

Rodriguez-Calvo R, Tajes M, Vazquez-Carrera M. 2017. The NR4A subfamily of nuclear receptors: potential new therapeutic targets for the treatment of inflammatory diseases. *Expert opinion on therapeutic targets* 21: 291-304

Rogov V, Dotsch V, Johansen T, Kirkin V. 2014. Interactions between autophagy receptors and ubiquitin-like proteins form the molecular basis for selective autophagy. *Molecular cell* 53: 167-78

Rong Y, Bansal PK, Wei P, Guo H, Correia K, et al. 2018. Glycosylation of Cblns attenuates their receptor binding. *Brain research* 1694: 129-39

Rosen DR, Siddique T, Patterson D, Figlewicz DA, Sapp P, et al. 1993. Mutations in Cu/Zn superoxide dismutase gene are associated with familial amyotrophic lateral sclerosis. *Nature* 362: 59-62

Ross OA, Rutherford NJ, Baker M, Soto-Ortolaza AI, Carrasquillo MM, et al. 2011. Ataxin-2 repeat-length variation and neurodegeneration. *Human molecular genetics* 20: 3207-12

Rothblum-Oviatt C, Wright J, Lefton-Greif MA, McGrath-Morrow SA, Crawford TO, Lederman HM. 2016. Ataxia telangiectasia: a review. *Orphanet journal of rare diseases* 11: 159

Rub U, Schols L, Paulson H, Auburger G, Kermer P, et al. 2013. Clinical features, neurogenetics and neuropathology of the polyglutamine spinocerebellar ataxias type 1, 2, 3, 6 and 7. *Progress in neurobiology* 104: 38-66

Rub U, Seidel K, Ozerden I, Gierga K, Brunt ER, et al. 2007. Consistent affection of the central somatosensory system in spinocerebellar ataxia type 2 and type 3 and its significance for clinical symptoms and rehabilitative therapy. *Brain research reviews* 53: 235-49

Rudenko A, Seo J, Hu J, Su SC, de Anda FC, et al. 2015. Loss of cyclin-dependent kinase 5 from parvalbumin interneurons leads to hyperinhibition, decreased anxiety, and memory impairment. *The Journal of neuroscience : the official journal of the Society for Neuroscience* 35: 2372-83

Russell DW, Halford RW, Ramirez DM, Shah R, Kotti T. 2009. Cholesterol 24-hydroxylase: an enzyme of cholesterol turnover in the brain. *Annual review of biochemistry* 78: 1017-40

Ruvinsky I, Sharon N, Lerer T, Cohen H, Stolovich-Rain M, et al. 2005. Ribosomal protein S6 phosphorylation is a determinant of cell size and glucose homeostasis. *Genes & development* 19: 2199-211

Sadakata T, Washida M, Iwayama Y, Shoji S, Sato Y, et al. 2007. Autistic-like phenotypes in Cadps2-knockout mice and aberrant CADPS2 splicing in autistic patients. *The Journal of clinical investigation* 117: 931-43

Saez-Valero J, Costell M, Sjogren M, Andreasen N, Blennow K, Luque JM. 2003. Altered levels of cerebrospinal fluid reelin in frontotemporal dementia and Alzheimer's disease. *Journal of neuroscience research* 72: 132-6

Sahama I, Sinclair K, Fiori S, Doecke J, Pannek K, et al. 2015. Motor pathway degeneration in young ataxia telangiectasia patients: A diffusion tractography study. *NeuroImage. Clinical* 9: 206-15

Saini P, Eyler DE, Green R, Dever TE. 2009. Hypusine-containing protein eIF5A promotes translation elongation. *Nature* 459: 118-21

Sakae N, Roemer SF, Bieniek KF, Murray ME, Baker MC, et al. 2019. Microglia in frontotemporal lobar degeneration with progranulin or C9ORF72 mutations. *Annals of clinical and translational neurology*

Salmela MJ, Weinig C. 2019. The fitness benefits of genetic variation in circadian clock regulation. *Current opinion in plant biology* 49: 86-93

Salta E, De Strooper B. 2012. Non-coding RNAs with essential roles in neurodegenerative disorders. *The Lancet. Neurology* 11: 189-200

Salter MW, Stevens B. 2017. Microglia emerge as central players in brain disease. *Nature medicine* 23: 1018-27

Sanjurjo L, Aran G, Roher N, Valledor AF, Sarrias MR. 2015. AIM/CD5L: a key protein in the control of immune homeostasis and inflammatory disease. *Journal of leukocyte biology* 98: 173-84

Sanpei K, Takano H, Igarashi S, Sato T, Oyake M, et al. 1996. Identification of the spinocerebellar ataxia type 2 gene using a direct identification of repeat expansion and cloning technique, DIRECT. *Nature genetics* 14: 277-84

Sardiello M, Palmieri M, di Ronza A, Medina DL, Valenza M, et al. 2009. A gene network regulating lysosomal biogenesis and function. *Science* 325: 473-7

Satake T, Yamashita K, Hayashi K, Miyatake S, Tamura-Nakano M, et al. 2017. MTCL1 plays an essential role in maintaining Purkinje neuron axon initial segment. *EMBO J* 36: 1227-42

Sathyanesan A, Zhou J, Scafidi J, Heck DH, Sillitoe RV, Gallo V. 2019. Emerging connections between cerebellar development, behaviour and complex brain disorders. *Nature reviews. Neuroscience* 20: 298-313

Satterfield TF, Pallanck LJ. 2006. Ataxin-2 and its Drosophila homolog, ATX2, physically assemble with polyribosomes. *Human molecular genetics* 15: 2523-32

Savitsky K, Bar-Shira A, Gilad S, Rotman G, Ziv Y, et al. 1995. A single ataxia telangiectasia gene with a product similar to PI-3 kinase. *Science* 268: 1749-53

Schaaf CP, Koster J, Katsonis P, Kratz L, Shchelochkov OA, et al. 2011. Desmosterolosis-phenotypic and molecular characterization of a third case and review of the literature. *American journal of medical genetics. Part A* 155A: 1597-604

Schafer DP, Lehrman EK, Kautzman AG, Koyama R, Mardinly AR, et al. 2012. Microglia sculpt postnatal neural circuits in an activity and complement-dependent manner. *Neuron* 74: 691-705

Schieving JH, de Vries M, van Vugt JM, Weemaes C, van Deuren M, et al. 2014. Alpha-fetoprotein, a fascinating protein and biomarker in neurology. *European journal of paediatric neurology : EJPN : official journal of the European Paediatric Neurology Society* 18: 243-8

Schindelin J, Arganda-Carreras I, Frise E, Kaynig V, Longair M, et al. 2012. Fiji: an open-source platform for biological-image analysis. *Nature methods* 9: 676-82

Schmittgen TD, Livak KJ. 2008. Analyzing real-time PCR data by the comparative CT method. *Nature Protocols* 3: 1101-08

Sellier C, Campanari ML, Julie Corbier C, Gaucherot A, Kolb-Cheynel I, et al. 2016. Loss of C9ORF72 impairs autophagy and synergizes with polyQ Ataxin-2 to induce motor neuron dysfunction and cell death. *EMBO J* 35: 1276-97

Sen NE, Canet-Pons J, Halbach MV, Arsovic A, Pilatus U, et al. 2019. Generation of an Atxn2-CAG100 knock-in mouse reveals N-acetylaspartate production deficit due to early Nat8l dysregulation. *Neurobiology of disease*: 104559

Sen NE, Drost J, Gispert S, Torres-Odio S, Damrath E, et al. 2016. Search for SCA2 blood RNA biomarkers highlights Ataxin-2 as strong modifier of the mitochondrial factor PINK1 levels. *Neurobiology of disease* 96: 115-26

Sephton CF, Yu G. 2015. The function of RNA-binding proteins at the synapse: implications for neurodegeneration. *Cellular and molecular life sciences : CMLS* 72: 3621-35

Seyrantepe V, Poupetova H, Froissart R, Zabot MT, Maire I, Pshezhetsky AV. 2003. Molecular pathology of NEU1 gene in sialidosis. *Human mutation* 22: 343-52

Shaikh AG, Zee DS, Mandir AS, Lederman HM, Crawford TO. 2013. Disorders of Upper Limb Movements in Ataxia-Telangiectasia. *PloS one* 8: e67042

Shakkottai VG, Xiao M, Xu L, Wong M, Nerbonne JM, et al. 2009. FGF14 regulates the intrinsic excitability of cerebellar Purkinje neurons. *Neurobiology of disease* 33: 81-8

Shalini S, Dorstyn L, Dawar S, Kumar S. 2015. Old, new and emerging functions of caspases. *Cell death and differentiation* 22: 526-39

Shan J, Munro TP, Barbarese E, Carson JH, Smith R. 2003. A molecular mechanism for mRNA trafficking in neuronal dendrites. *The Journal of neuroscience : the official journal of the Society for Neuroscience* 23: 8859-66

Shankaran SS, Capell A, Hruscha AT, Fellerer K, Neumann M, et al. 2008. Missense mutations in the progranulin gene linked to frontotemporal lobar degeneration with ubiquitin-immunoreactive inclusions reduce progranulin production and secretion. *The Journal of biological chemistry* 283: 1744-53

Shen X, Chen J, Li J, Kofler J, Herrup K. 2016. Neurons in Vulnerable Regions of the Alzheimer's Disease Brain Display Reduced ATM Signaling. *eNeuro* 3

Sheth U, Parker R. 2003. Decapping and decay of messenger RNA occur in cytoplasmic processing bodies. *Science* 300: 805-8

Shiloh Y, Lederman HM. 2017. Ataxia-telangiectasia (A-T): An emerging dimension of premature ageing. *Ageing research reviews* 33: 76-88

Shimobayashi E, Kapfhammer JP. 2018. Calcium Signaling, PKC Gamma, IP3R1 and CAR8 Link Spinocerebellar Ataxias and Purkinje Cell Dendritic Development. *Curr Neuropharmacol* 16: 151-59

Shtivelman E, Cohen FE, Bishop JM. 1992. A human gene (AHNAK) encoding an unusually large protein with a 1.2-microns polyionic rod structure. *Proceedings of the National Academy of Sciences of the United States of America* 89: 5472-6

Sierra A, Encinas JM, Deudero JJ, Chancey JH, Enikolopov G, et al. 2010. Microglia shape adult hippocampal neurogenesis through apoptosis-coupled phagocytosis. *Cell stem cell* 7: 483-95

Sierra A, Gottfried-Blackmore AC, McEwen BS, Bulloch K. 2007. Microglia derived from aging mice exhibit an altered inflammatory profile. *Glia* 55: 412-24

Sinagra M, Verrier D, Frankova D, Korwek KM, Blahos J, et al. 2005. Reelin, very-low-density lipoprotein receptor, and apolipoprotein E receptor 2 control somatic NMDA receptor composition during hippocampal maturation in vitro. *The Journal of neuroscience : the official journal of the Society for Neuroscience* 25: 6127-36

Siomi H, Matunis MJ, Michael WM, Dreyfuss G. 1993. The pre-mRNA binding K protein contains a novel evolutionarily conserved motif. *Nucleic acids research* 21: 1193-8

Slemmer JE, De Zeeuw CI, Weber JT. 2005. Don't get too excited: mechanisms of glutamate-mediated Purkinje cell death. *Progress in brain research* 148: 367-90

Smeets CJ, Verbeek DS. 2016. Climbing fibers in spinocerebellar ataxia: A mechanism for the loss of motor control. *Neurobiology of disease* 88: 96-106

Smith KR, Damiano J, Franceschetti S, Carpenter S, Canafoglia L, et al. 2012. Strikingly different clinicopathological phenotypes determined by progranulin-mutation dosage. *American journal of human genetics* 90: 1102-7

Smolders S, Kessels S, Smolders SM, Poulhes F, Zelphati O, et al. 2018. Magnetofection is superior to other chemical transfection methods in a microglial cell line. *Journal of neuroscience methods* 293: 169-73

Snel B, Lehmann G, Bork P, Huynen MA. 2000. STRING: a web-server to retrieve and display the repeatedly occurring neighbourhood of a gene. *Nucleic acids research* 28: 3442-4

Sodero AO, Vriens J, Ghosh D, Stegner D, Brachet A, et al. 2012. Cholesterol loss during glutamate-mediated excitotoxicity. *EMBO J* 31: 1764-73

Sofroniew MV, Vinters HV. 2010. Astrocytes: biology and pathology. *Acta neuropathologica* 119: 7-35

Spiller KJ, Restrepo CR, Khan T, Dominique MA, Fang TC, et al. 2018. Microglia-mediated recovery from ALS-relevant motor neuron degeneration in a mouse model of TDP-43 proteinopathy. *Nature neuroscience* 21: 329-40

Stern N, Hochman A, Zemach N, Weizman N, Hammel I, et al. 2002. Accumulation of DNA damage and reduced levels of nicotine adenine dinucleotide in the brains of Atm-deficient mice. *The Journal of biological chemistry* 277: 602-8

Stevens B, Allen NJ, Vazquez LE, Howell GR, Christopherson KS, et al. 2007. The classical complement cascade mediates CNS synapse elimination. *Cell* 131: 1164-78

Sthoeger Z, Zinger H, Sharabi A, Asher I, Mozes E. 2013. The tolerogenic peptide, hCDR1, down-regulates the expression of interferon-alpha in murine and human systemic lupus erythematosus. *PloS one* 8: e60394

Stowell RD, Wong EL, Batchelor HN, Mendes MS, Lamantia CE, et al. 2018. Cerebellar microglia are dynamically unique and survey Purkinje neurons in vivo. *Developmental neurobiology* 78: 627-44

Stray-Pedersen A, Borresen-Dale AL, Paus E, Lindman CR, Burgers T, Abrahamsen TG. 2007. Alpha fetoprotein is increasing with age in ataxia-telangiectasia. *European journal of paediatric neurology : EJPN : official journal of the European Paediatric Neurology Society* 11: 375-80

Streit WJ, Braak H, Xue QS, Bechmann I. 2009. Dystrophic (senescent) rather than activated microglial cells are associated with tau pathology and likely precede neurodegeneration in Alzheimer's disease. *Acta neuropathologica* 118: 475-85

Strohm L, Behrends C. 2019. Glia-specific autophagy dysfunction in ALS. *Seminars in cell & developmental biology*

Sudhakaran IP, Hillebrand J, Dervan A, Das S, Holohan EE, et al. 2014. FMRP and Ataxin-2 function together in long-term olfactory habituation and neuronal translational control. *Proceedings of the National Academy of Sciences of the United States of America* 111: E99-E108

Sussman J, Stokoe D, Ossina N, Shtivelman E. 2001. Protein kinase B phosphorylates AHNAK and regulates its subcellular localization. *J Cell Biol* 154: 1019-30

Swarup V, Srivastava AK, Padma MV, Moganty RR. 2013. Quantitative profiling and identification of plasma proteins of spinocerebellar ataxia type 2 patients. *Neuro-degenerative diseases* 12: 199-206

Swisher KD, Parker R. 2010. Localization to, and effects of Pbp1, Pbp4, Lsm12, Dhh1, and Pab1 on stress granules in Saccharomyces cerevisiae. *PloS one* 5: e10006

Synofzik M, Smets K, Mallaret M, Di Bella D, Gallenmuller C, et al. 2016. SYNE1 ataxia is a common recessive ataxia with major non-cerebellar features: a large multi-centre study. *Brain : a journal of neurology* 139: 1378-93

Szklarczyk D, Franceschini A, Wyder S, Forslund K, Heller D, et al. 2015. STRING v10: protein-protein interaction networks, integrated over the tree of life. *Nucleic acids research* 43: D447-52

Tadauchi T, Inada T, Matsumoto K, Irie K. 2004. Posttranscriptional regulation of HO expression by the Mkt1-Pbp1 complex. *Mol Cell Biol* 24: 3670-81

Takahara T, Maeda T. 2012. Transient sequestration of TORC1 into stress granules during heat stress. *Molecular cell* 47: 242-52

Takeda Y, Akasaka K, Lee S, Kobayashi S, Kawano H, et al. 2003. Impaired motor coordination in mice lacking neural recognition molecule NB-3 of the contactin/F3 subgroup. *Journal of neurobiology* 56: 252-65

Tanaka Y, Chambers JK, Matsuwaki T, Yamanouchi K, Nishihara M. 2014. Possible involvement of lysosomal dysfunction in pathological changes of the brain in aged progranulin-deficient mice. *Acta neuropathologica communications* 2: 78

Tarkowski E, Andreasen N, Tarkowski A, Blennow K. 2003. Intrathecal inflammation precedes development of Alzheimer's disease. *Journal of neurology, neurosurgery, and psychiatry* 74: 1200-5

Tarkowski E, Blennow K, Wallin A, Tarkowski A. 1999. Intracerebral production of tumor necrosis factor-alpha, a local neuroprotective agent, in Alzheimer disease and vascular dementia. *Journal of clinical immunology* 19: 223-30

Tateishi T, Yamasaki R, Tanaka M, Matsushita T, Kikuchi H, et al. 2010. CSF chemokine alterations related to the clinical course of amyotrophic lateral sclerosis. *J Neuroimmunol* 222: 76-81

Taylor JP, Brown RH, Jr., Cleveland DW. 2016. Decoding ALS: from genes to mechanism. *Nature* 539: 197-206

Tey S, Shahrizaila N, Drew AP, Samulong S, Goh KJ, et al. 2019. Linkage analysis and whole exome sequencing reveals AHNAK2 as a novel genetic cause for autosomal recessive CMT in a Malaysian family. *Neurogenetics*

Tezenas du Montcel S, Durr A, Bauer P, Figueroa KP, Ichikawa Y, et al. 2014. Modulation of the age at onset in spinocerebellar ataxia by CAG tracts in various genes. *Brain : a journal of neurology* 137: 2444-55

Thambisetty M, An Y, Kinsey A, Koka D, Saleem M, et al. 2012. Plasma clusterin concentration is associated with longitudinal brain atrophy in mild cognitive impairment. *NeuroImage* 59: 212-7

Tharun S. 2009. Roles of eukaryotic Lsm proteins in the regulation of mRNA function. *International review of cell and molecular biology* 272: 149-89

Tolkatchev D, Malik S, Vinogradova A, Wang P, Chen Z, et al. 2008. Structure dissection of human progranulin identifies well-folded granulin/epithelin modules with unique functional activities. *Protein science : a publication of the Protein Society* 17: 711-24

Tremblay ME, Stevens B, Sierra A, Wake H, Bessis A, Nimmerjahn A. 2011. The role of microglia in the healthy brain. *The Journal of neuroscience : the official journal of the Society for Neuroscience* 31: 16064-9

Tripathi DN, Chowdhury R, Trudel LJ, Tee AR, Slack RS, et al. 2013. Reactive nitrogen species regulate autophagy through ATM-AMPK-TSC2-mediated suppression of mTORC1. *Proceedings of the National Academy of Sciences of the United States of America* 110: E2950-7

Trouw LA, Nilsson SC, Goncalves I, Landberg G, Blom AM. 2005. C4b-binding protein binds to necrotic cells and DNA, limiting DNA release and inhibiting complement activation. *J Exp Med* 201: 1937-48

Tsukiyama-Kohara K, Poulin F, Kohara M, DeMaria CT, Cheng A, et al. 2001. Adipose tissue reduction in mice lacking the translational inhibitor 4E-BP1. *Nature medicine* 7: 1128-32

Tuin I, Voss U, Kang JS, Kessler K, Rub U, et al. 2006. Stages of sleep pathology in spinocerebellar ataxia type 2 (SCA2). *Neurology* 67: 1966-72

Uchiyama Y, Kim CA, Pastorino AC, Ceroni J, Lima PP, et al. 2019. Primary immunodeficiency with chronic enteropathy and developmental delay in a boy arising from a novel homozygous RIPK1 variant. *Journal of human genetics*

Uesaka N, Kano M. 2018. Presynaptic Mechanisms Mediating Retrograde Semaphorin Signals for Climbing Fiber Synapse Elimination During Postnatal Cerebellar Development. 17: 17-22

Uesaka N, Uchigashima M, Mikuni T, Nakazawa T, Nakao H, et al. 2014. Retrograde semaphorin signaling regulates synapse elimination in the developing mouse brain. *Science* 344: 1020-3

Ugolino J, Ji YJ, Conchina K, Chu J, Nirujogi RS, et al. 2016. Loss of C9orf72 Enhances Autophagic Activity via Deregulated mTOR and TFEB Signaling. *PLoS genetics* 12: e1006443

Valentin-Vega YA, Kastan MB. 2012. A new role for ATM: regulating mitochondrial function and mitophagy. *Autophagy* 8: 840-1

Valverde R, Edwards L, Regan L. 2008. Structure and function of KH domains. *The FEBS journal* 275: 2712-26

van de Leemput J, Chandran J, Knight MA, Holtzclaw LA, Scholz S, et al. 2007. Deletion at ITPR1 underlies ataxia in mice and spinocerebellar ataxia 15 in humans. *PLoS genetics* 3: e108

Van Goethem G, Martin JJ, Dermaut B, Lofgren A, Wibail A, et al. 2003. Recessive POLG mutations presenting with sensory and ataxic neuropathy in compound heterozygote patients with progressive external ophthalmoplegia. *Neuromuscular disorders : NMD* 13: 133-42

van Swieten JC, Brusse E, de Graaf BM, Krieger E, van de Graaf R, et al. 2003. A mutation in the fibroblast growth factor 14 gene is associated with autosomal dominant cerebellar ataxia [corrected]. *American journal of human genetics* 72: 191-9

Vance C, Rogelj B, Hortobagyi T, De Vos KJ, Nishimura AL, et al. 2009. Mutations in FUS, an RNA processing protein, cause familial amyotrophic lateral sclerosis type 6. *Science* 323: 1208-11

Vance C, Scotter EL, Nishimura AL, Troakes C, Mitchell JC, et al. 2013. ALS mutant FUS disrupts nuclear localization and sequesters wild-type FUS within cytoplasmic stress granules. *Human molecular genetics* 22: 2676-88

Velazquez-Perez L, Rodriguez-Labrada R, Canales-Ochoa N, Montero JM, Sanchez-Cruz G, et al. 2014. Progression of early features of spinocerebellar ataxia type 2 in individuals at risk: a longitudinal study. *The Lancet. Neurology* 13: 482-9

Velazquez-Perez L, Rodriguez-Labrada R, Garcia-Rodriguez JC, Almaguer-Mederos LE, Cruz-Marino T, Laffita-Mesa JM. 2011. A comprehensive review of spinocerebellar ataxia type 2 in Cuba. *Cerebellum* 10: 184-98

Velazquez-Perez L, Rodriguez-Labrada R, Torres-Vega R, Ortega-Sanchez R, Medrano-Montero J, et al. 2018. Progression of corticospinal tract dysfunction in pre-ataxic spinocerebellar ataxia type 2: A two-years follow-up TMS study. *Clinical neurophysiology : official journal of the International Federation of Clinical Neurophysiology* 129: 895-900

Velazquez-Perez L, Tunnerhoff J, Rodriguez-Labrada R, Torres-Vega R, Ruiz-Gonzalez Y, et al. 2017. Early corticospinal tract damage in prodromal SCA2 revealed by EEG-EMG and EMG-EMG coherence. *Clinical neurophysiology : official journal of the International Federation of Clinical Neurophysiology* 128: 2493-502

Verma R, Bharti K. 2017. Toll like receptor 3 and viral infections of nervous system. *Journal of the neurological sciences* 372: 40-48

Verney C, Monier A, Fallet-Bianco C, Gressens P. 2010. Early microglial colonization of the human forebrain and possible involvement in periventricular white-matter injury of preterm infants. *Journal of anatomy* 217: 436-48

Villegas-Llerena C, Phillips A, Garcia-Reitboeck P, Hardy J, Pocock JM. 2016. Microglial genes regulating neuroinflammation in the progression of Alzheimer's disease. *Current opinion in neurobiology* 36: 74-81

Von Boxberg Y, Salim C, Soares S, Baloui H, Alterio J, et al. 2006. Spinal cord injury-induced up-regulation of AHNAK, expressed in cells delineating cystic cavities, and associated with neoangiogenesis. *The European journal of neuroscience* 24: 1031-41

Vucic S, Rothstein JD, Kiernan MC. 2014. Advances in treating amyotrophic lateral sclerosis: insights from pathophysiological studies. *Trends in neurosciences* 37: 433-42

Wahl S, Engelhardt M, Schaupp P, Lappe C, Ivanov IV. 2019. The inner clock - blue light sets the human rhythm. *Journal of biophotonics*: e201900102

Waldmann TA, McIntire KR. 1972. Serum-alpha-fetoprotein levels in patients with ataxia-telangiectasia. *Lancet* 2: 1112-5

Walker DA, Harper PS, Wells CE, Tyler A, Davies K, Newcombe RG. 1981. Huntington's Chorea in South Wales. A genetic and epidemiological study. *Clinical genetics* 19: 213-21

Wallquist W, Plantman S, Thams S, Thyboll J, Kortesmaa J, et al. 2005. Impeded interaction between Schwann cells and axons in the absence of laminin alpha4. *The Journal of neuroscience : the official journal of the Society for Neuroscience* 25: 3692-700

Walter BL, Parsley TB, Ehrenfeld E, Semler BL. 2002. Distinct Poly(rC) Binding Protein KH Domain Determinants for Poliovirus Translation Initiation and Viral RNA Replication. *Journal of virology* 76: 12008-22

Ward AJ, Olive PL, Burr AH, Rosin MP. 1994. Response of fibroblast cultures from ataxia-telangiectasia patients to reactive oxygen species generated during inflammatory reactions. *Environmental and molecular mutagenesis* 24: 103-11

Watanabe M, Kano M. 2011. Climbing fiber synapse elimination in cerebellar Purkinje cells. *The European journal of neuroscience* 34: 1697-710

Watters D, Kedar P, Spring K, Bjorkman J, Chen P, et al. 1999. Localization of a portion of extranuclear ATM to peroxisomes. *The Journal of biological chemistry* 274: 34277-82

Wei CW, Luo T, Zou SS, Wu AS. 2018. The Role of Long Noncoding RNAs in Central Nervous System and Neurodegenerative Diseases. *Frontiers in behavioral neuroscience* 12: 175

Wei Y, An Z, Zou Z, Sumpter R, Su M, et al. 2015. The stress-responsive kinases MAPKAPK2/MAPKAPK3 activate starvation-induced autophagy through Beclin 1 phosphorylation. *eLife* 4

Whitney ER, Kemper TL, Rosene DL, Bauman ML, Blatt GJ. 2008. Calbindin-D28k is a more reliable marker of human Purkinje cells than standard Nissl stains: a stereological experiment. *Journal of neuroscience methods* 168: 42-7

Wiedemeyer R, Westermann F, Wittke I, Nowock J, Schwab M. 2003. Ataxin-2 promotes apoptosis of human neuroblastoma cells. *Oncogene* 22: 401-11

Wilusz CJ, Wilusz J. 2005. Eukaryotic Lsm proteins: lessons from bacteria. *Nature structural & molecular biology* 12: 1031-6

Woods CG, Taylor AM. 1992. Ataxia telangiectasia in the British Isles: the clinical and laboratory features of 70 affected individuals. *The Quarterly journal of medicine* 82: 169-79

Woolaway K, Asai K, Emili A, Cochrane A. 2007. hnRNP E1 and E2 have distinct roles in modulating HIV-1 gene expression. *Retrovirology* 4: 28

Wu D, Yang H, Xiang W, Zhou L, Shi M, et al. 2005. Heterozygous mutation of ataxia-telangiectasia mutated gene aggravates hypercholesterolemia in apoE-deficient mice. *J Lipid Res* 46: 1380-7

Wu J, Xiao Y, Liu J, Yang H, Dong X, et al. 2014. Potential role of ATM in hepatocyte endocytosis of ApoE-deficient, ApoB48-containing lipoprotein in ApoE-deficient mice. *International journal of molecular medicine* 33: 462-8

Wullschleger S, Loewith R, Hall MN. 2006. TOR signaling in growth and metabolism. *Cell* 124: 471-84

Xia G, McFarland KN, Wang K, Sarkar PS, Yachnis AT, Ashizawa T. 2013. Purkinje cell loss is the major brain pathology of spinocerebellar ataxia type 10. *Journal of neurology, neurosurgery, and psychiatry* 84: 1409-11

Xie J, Kozlov G, Gehring K. 2014. The "tale" of poly(A) binding protein: the MLLE domain and PAM2-containing proteins. *Biochimica et biophysica acta* 1839: 1062-8

Xu D, Jin T, Zhu H, Chen H, Ofengeim D, et al. 2018. TBK1 Suppresses RIPK1-Driven Apoptosis and Inflammation during Development and in Aging. *Cell* 174: 1477-91 e19

Xu Y, Ashley T, Brainerd EE, Bronson RT, Meyn MS, Baltimore D. 1996. Targeted disruption of ATM leads to growth retardation, chromosomal fragmentation during meiosis, immune defects, and thymic lymphoma. *Genes & development* 10: 2411-22

Xu Y, Baltimore D. 1996. Dual roles of ATM in the cellular response to radiation and in cell growth control. *Genes & development* 10: 2401-10

Yang DQ, Kastan MB. 2000. Participation of ATM in insulin signalling through phosphorylation of eIF-4E-binding protein 1. *Nature cell biology* 2: 893-8

Yi M, Rosin MP, Anderson CK. 1990. Response of fibroblast cultures from ataxia-telangiectasia patients to oxidative stress. *Cancer letters* 54: 43-50

Yin F, Banerjee R, Thomas B, Zhou P, Qian L, et al. 2010. Exaggerated inflammation, impaired host defense, and neuropathology in progranulin-deficient mice. *J Exp Med* 207: 117-28

Yokoshi M, Li Q, Yamamoto M, Okada H, Suzuki Y, Kawahara Y. 2014. Direct binding of Ataxin-2 to distinct elements in 3' UTRs promotes mRNA stability and protein expression. *Molecular cell* 55: 186-98

Young JE, Gouw L, Propp S, Sopher BL, Taylor J, et al. 2007. Proteolytic cleavage of ataxin-7 by caspase-7 modulates cellular toxicity and transcriptional dysregulation. *The Journal of biological chemistry* 282: 30150-60

Yu CE, Bird TD, Bekris LM, Montine TJ, Leverenz JB, et al. 2010. The spectrum of mutations in progranulin: a collaborative study screening 545 cases of neurodegeneration. *Archives of neurology* 67: 161-70

Yuan A, Veeranna, Sershen H, Basavarajappa BS, Smiley JF, et al. 2018. Neurofilament light interaction with GluN1 modulates neurotransmission and schizophrenia-associated behaviors. *Translational psychiatry* 8: 167

Yuan J, Yankner BA. 2000. Apoptosis in the nervous system. *Nature* 407: 802-9

Zhan Y, Paolicelli RC, Sforazzini F, Weinhard L, Bolasco G, et al. 2014. Deficient neuron-microglia signaling results in impaired functional brain connectivity and social behavior. *Nature neuroscience* 17: 400-6

Zhang B, Gaiteri C, Bodea LG, Wang Z, McElwee J, et al. 2013a. Integrated systems approach identifies genetic nodes and networks in late-onset Alzheimer's disease. *Cell* 153: 707-20

Zhang J, Liu Q. 2015. Cholesterol metabolism and homeostasis in the brain. *Protein Cell* 6: 254–64

Zhang J, Tripathi DN, Jing J, Alexander A, Kim J, et al. 2015. ATM functions at the peroxisome to induce pexophagy in response to ROS. *Nature cell biology* 17: 1259-69

Zhang Q, Sharma NR, Zheng ZM, Chen M. 2019. Viral Regulation of RNA Granules in Infected Cells. *Virologica Sinica* 34: 175-91

Zhang Y, Chen K, Sloan SA, Bennett ML, Scholze AR, et al. 2014. An RNA-sequencing transcriptome and splicing database of glia, neurons, and vascular cells of the cerebral cortex. *The Journal of neuroscience : the official journal of the Society for Neuroscience* 34: 11929-47

Zhang Y, Lee JH, Paull TT, Gehrke S, D'Alessandro A, et al. 2018. Mitochondrial redox sensing by the kinase ATM maintains cellular antioxidant capacity. *Sci Signal* 11

Zhang Y, Ling J, Yuan C, Dubruille R, Emery P. 2013b. A role for Drosophila ATX2 in activation of PER translation and circadian behavior. *Science* 340: 879-82

Zhang YJ, Xu YF, Dickey CA, Buratti E, Baralle F, et al. 2007. Progranulin mediates caspase-dependent cleavage of TAR DNA binding protein-43. *The Journal of neuroscience : the official journal of the Society for Neuroscience* 27: 10530-4

Zhang Z, Casey DM, Julien JP, Xu Z. 2002. Normal dendritic arborization in spinal motoneurons requires neurofilament subunit L. *The Journal of comparative neurology* 450: 144-52

Zheng TS, Flavell RA. 2000. Divinations and surprises: genetic analysis of caspase function in mice. *Experimental cell research* 256: 67-73

Zhuchenko O, Bailey J, Bonnen P, Ashizawa T, Stockton DW, et al. 1997. Autosomal dominant cerebellar ataxia (SCA6) associated with small polyglutamine expansions in the alpha 1A-voltage-dependent calcium channel. *Nature genetics* 15: 62-9

Zoghbi HY. 2000. Spinocerebellar ataxias. *Neurobiology of disease* 7: 523-7

Zoghbi HY, Orr HT. 2000. Glutamine repeats and neurodegeneration. *Annual review of neuroscience* 23: 217-47

Zrzavy T, Hametner S, Wimmer I, Butovsky O, Weiner HL, Lassmann H. 2017. Loss of 'homeostatic' microglia and patterns of their activation in active multiple sclerosis. *Brain : a journal of neurology* 140: 1900-13

Zu L, Figueroa KP, Grewal R, Pulst SM. 1999. Mapping of a new autosomal dominant spinocerebellar ataxia to chromosome 22. *American journal of human genetics* 64: 594-9

8 APPENDIX

8.2 List of Figures

8.2 List of Tables

8.3 Abbreviations

4E-BP	Eukaryotic initiation factor 4E-binding protein
A-T	Ataxia telangiectasia
AA/BA	Acrylamide/Bisacrylamide
ACTB	Actin beta
AD	Alzheimer's disease
ADCA	Autosomal dominant cerebellar ataxia
AFP	Alpha-fetoprotein

AHNAK	AHNAK Nucleoprotein/ Desmoyokin
AHNAK2	AHNAK Nucleoprotein 2/ PLD4
AKT	Protein kinase B
ALS	Amyotrophic lateral sclerosis
AMPK	AMP-activated protein kinase
AR	Androgen receptor
ARCA	Autosomal recessive cerebellar ataxia
ATBF1	AT Motif-Binding Factor 1
ATM	Ataxia telangiectasia mutated
ATR	Ataxia-telangiectasia and Rad3-related
ATX2	Ataxin2 ortholog in *C. elegans*
ATXN2	Ataxin2
BAC	Bacterial artificial chromosome
bp	Base pare
BSA	Albumin fraction V
BV2	Murine microglia cell line
C9ORF72	Chromosome 9 Open Reading Frame 72
CALB1	Calbindin
CASP3	Caspase3
CB	Cerebellum
cDNA	coding DNA
CF	Climbing fibers
cm	centimeter
CNS	Central nervous system
dATP	Deoxyadenosine triphosphate
dATX2	Ataxin2 ortholog in *D. melanogaster*
dCTP	Deoxycytidine triphosphate
DDR	DNA damage response
DDX6	DEAD/H-box RNA helicase
dGTP	Deoxyguanosine triphosphate
DNA	Deoxyribonucleic acid
DNA-PK	DNA-dependent protein kinase catalytic subunit
dNTP	Nucleoside triphosphate
DPBS	Dulbecco's phosphate-buffered saline
dPER	PERIOD
DRPLA	Denatorubral-pallidoluysian atrophy
DSBs	DNA double-strand breaks
dTTP	Deoxythymidine triphosphate
E/I	Excitatory/Inhibitory
EDTA	Ethylenediamine tetraacetic acid
eIF-4E	Eukaryotic initiation factor 4E
ETC/OXPHOS system	Electron transport chain/oxidative phosphorylation system
EtOH	Ethanol
FAT	FRAP-ATM-TRRAP domain
FATC	FAT C-terminal domain

FC	Fold change
FOXO3a	Forkhead box O3
FRDA	Friedrich ataxia
FRT	Flippase recognition target
FTD	Frontotemporal dementia
FTLD	Frontotemporal lobar dementia
FUS	Fus in sarcoma
FXN	Frataxin
GC	Granule cells
GFAP	Glial fibrillary acidic protein
GLD1	Female germline-specific tumor suppressor gld-1, *C. elegans*
GLUT4	Glucose transporter 4
GN	Granule neurons
GO	Gene ontology
HD	Huntington's disease
HeLA	Immortal cell line derived from cervical cancer cells taken from Henrietta Lacks
HIF-1α	Hypoxia-inducible factor 1-alpha
HIV	Human immunodeficiency viruses
HR	Homologous recombination
HRE	Hexanucleotide expanded repeat
hRNP	Heterogeneous nuclear ribonucleoprotein
HTT	Huntingtin
IBA1	Ionized calcium-binding adapter molecule 1/ Allograft inflammatory factor 1
IO	Inferior olive
IR	Ionizing radiation
KD	Knock-down
KD	Kinase domain
kDA	Kilo Dalton
KEGG	Kyoto Encyclopedia of Genes and Genomes
KH-domain	K Homology domain
KIN	Knock-in
KO	Knock-out
Lipo	Lipofectamine
loxP	Locus of X-over P1
LPS	Lipopolysaccharide
LSm	Like-Sm
LSm-AD	LSm-associated domain
LTP	Long term potentiation
M	Molar
Mdc1	Mediator of DNA damage checkpoint 1
MEF	Mouse embryonic fibroblasts
MEX3	Muscle EXcess, *C. elegans*
mg	Mili gram
min	Minute
mL	Mili liter

mM	mili molar
MnSOD	Mitochondria superoxide dismutase
mo	Month
MRN	Mre11, Rad50, Nbs1 complex
mRNA	Messenger RNA
mRNP	Messenger ribonucleoprotein
mTOR	Mammalian target of rapamycin
mTORC1	mTOR complex 1
mTORC2	mTOR complex 2
NaArs	Sodium Arsenite
NeuN	Hexaribonucleotide Binding Protein 3
NF-H	High molecular weight NF
NF-L	Low molecular weight NF
NF-M	Medium molecular weight NF
NFs	Neurofilaments
ng	Nano gram
NHEJ	Non-homologous end joining
NMDR	N-methyl-D-aspartate receptor
ºC	Celsius
OTC	Organotypic cell cultures
P-bodies/PBs	Processing bodies
P0	Postnatal day 0
P3	Postnatal day 3
PABP1	Poly(A)-binding protein
PAM2	PABP-interacting motif
PAR-CLIP	Photoactivatable-ribonucleoside-enhanced crosslinking and Immunoprecipitation
PARK	Parkin
PASK	PAS kinase
PBP1	Pab1-binding protein 1
PBS	Phosphate-buffered saline
PCBP	Poly(C)-binding protein
PCBP1	Poly(C) Binding Protein 1
PCBP2	Poly (C) Binding Protein 2
Pcp2	Purkinje cell protein 2
PCR	Polymerase chain reaction
PD	Parkinson's disease
PDGFRB	Platelet-derived growth factor receptor beta
PEX5	Peroxisomal Biogenesis Factor 5
PFA	Paraformaldehyde
PGRN	Progranulin
PI3	Phosphatidylinositol 3
PI3Ks	PI3 kinases
PIKK	PI3K-like protein kinase
PINK1	PTEN Induced Kinase 1
PN	Purkinje neurons

poly(A)	Polyadenylated
polyQ	Polyglutamine
PSK1	PASK ortholog in yeast
Q	Glutamine
Q-PCR	Quantitative polymerase chain reaction
RBD	RNA binding domain
RBP	RNA binding proteins
REDD1	Regulated in development and DNA-damage response 1
RIPK1	Receptor-interacting serine/threonine-protein kinase 1
RNA	Ribonucleic acid
RNP	Ribonucleoprotein complex
ROS	Reactive oxygen species
rpm	Revolution per minute
RPS6	Ribosomal protein 6
RRM	RNA recognition motif
RT	Room temperature
RT-PCR	Reverse transcription polymerase chain reaction
SBMA	Spinal and bulbar muscular atrophy
SCA	Spinocerebellar ataxia
SCA1	Spinocerebellar ataxia type 1
SCA2	Spinocerebellar ataxia type 2
SCA3	Spinocerebellar ataxia type 3
SDS-PAGE	Sodium dodecyl sulphate-polyacrylamide gel electrophoresis
sec	Second
SG	Stress granules
SH-SY5Y	Human neuroblastoma derived cell line
shRNA	Short hairpin RNA
SMG1	Suppressor of morphogenesis in genitalia 1
SNF1	Carbon carabolite-derepressing protein kinase, *S. Cerevisiae*
SOD1	Superoxide dismutase
Sp Cord	Spinal Cord
SQSTM1/p62	Sequestrosome 1
ss-cDNA	Single stranded cDNA
STRING	Search tool for the retrieval of interacting genes/proteins
TAC	Transcriptome Analysis Console
TDP43	TAR DNA-binding protein 43
TIA1	T-cell-restricted intracellular antigen-1
TNF	Tumour necrosis factor
TREM2	Triggering receptor expressed on myeloid cells 2
TRRAP	Transformation/transcription domain-associated protein
TSC2	Tuberous slcerosis2
TYROBP	TYRO protein tyrosine kinase-binding protein
UTR	Untransleted region
UVR	Ultraviolet radiation
V	Volts
VAMP2	Synaptobrevin

VGAT	Vesicular GABA transporter
VGLUT1	Vesicular glutamate transporter 1
WB	Western blot
WT	Wild type
xG	Times gravity (unit of relative centrifugal force, RCF)
µg	Micro gram
µL	Micro liter
µm	Micro meter

9 Acknowledgments

10 Publications

Sen NE*, Canet-Pons J*, Halbach MV*, Arsovic A, Pilatus U, Chae WH, Kaya ZE, Seidel K, Rollmann E, Mittelbronn M, Meierhofer D, De Zeeuw CI, Bosman LWJ, Gispert S, Auburger G (2019). **Generation of an Atxn2-CAG100 knock-in mouse reveals N-acetylaspartate production deficit due to early Nat8l dysregulation.** Neurobiol Dis 132: 104559.

Auburger G, Gispert S, Torres-Odio S, Jendrach M, Brehm N, Canet-Pons J, Key J, Sen NE (2019). **SerThr-PhosphoProteome of Brain from Aged PINK1-KO+A53T-SNCA Mice Reveals pT1928-MAP1B and pS3781-ANK2 Deficits, as Hub between Autophagy and Synapse Changes.** Int J Mol Sci 20(13).

Canet-Pons J, Schubert R, Duecker RP, Schrewe R, Wölke S, Kieslich M, Schnölzer M, Chiocchetti A, Auburger G, Zielen S, Warnken U (2018). **Ataxia telangiectasia alters the ApoB and reelin pathway.** Neurogenetics 19(4): 237-255.

Moreno E, Canet-Pons J, Garcia E, Lluis C, Mallol J, Canela EI, Cortes A, Casado V (2018). **Molecular Evidence of Adenosine Deaminase Linking Adenosine A_{2A} Receptor and CD26 Proteins.** Front Pharmacol 9: 106.

Gámez-Valero A, Canet-Pons J, Urbizu A, Anillo A, Santos C, Ariza A, Beyer K (2018). **INDEL Length and Haplotypes in the β-Synuclein Gene: A Key to Differentiate Dementia with Lewy Bodies?** J Alzheimers Dis 65(1):207-219.

Torres-Odio S, Key J, Hoepken HH, Canet-Pons J, Valek L, Roller B, Walter M, Morales-Gordo B, Meierhofer D, Harter PN, Mittelbronn M, Tegeder I, Gispert S, Auburger G (2017). **Progression of pathology in PINK1-deficient mouse brain from splicing via Ubiquitination, ER stress, and mitophagy changes to neuroinflammation.** J Neuroinflammation 14(1): 154.

Farré D, Muñoz A, Moreno Guillén E, Reyes-Resina I, Canet-Pons J, Gonzalez-Dopeso I, Rico AJ, Lluis C, Mallol J, Navarro G, Canela E, Cortés A, Labandeira-Garcia J, Casadó V, Lanciego J, Franco R (2014). **Stronger Dopamine D1 Receptor-Mediated Neurotransmission in Dyskinesia.** Mol Neurobiol 52(3): 1408-1420.

Urbizu A, Canet-Pons J, Muñoz-Mármol AM, Aldecoa I, Lopez M, Compta Y, Alvarez R, Ispierto L, Tolosa E, Ariza A, Beyer K (2014). **Cystatin C is differentially involved in multiple system atrophy phenotypes: Cystatin C in MSA.** Neuropathol Appl Neurobiol 41(4): 507-19.

11 Curriculum Vitae